HAL
open science

Les mutations d'IDH2 dans la leucémie aigue myéloïde confèrent une sensibilité spécifique à l'inhibition du métabolisme des acides aminés branchés (BCAA)

Maël Heiblig

To cite this version:

Maël Heiblig. Les mutations d'IDH2 dans la leucémie aigue myéloïde confèrent une sensibilité spécifique à l'inhibition du métabolisme des acides aminés branchés (BCAA). Cancer. Université Paris-Saclay, 2022. Français. NNT : 2022UPASL018 . tel-04108390

HAL Id: tel-04108390

https://theses.hal.science/tel-04108390v1

Submitted on 27 May 2023

HAL is a multi-disciplinary open access archive for the deposit and dissemination of scientific research documents, whether they are published or not. The documents may come from teaching and research institutions in France or abroad, or from public or private research centers.

L'archive ouverte pluridisciplinaire **HAL**, est destinée au dépôt et à la diffusion de documents scientifiques de niveau recherche, publiés ou non, émanant des établissements d'enseignement et de recherche français ou étrangers, des laboratoires publics ou privés.

université PARIS-SACLAY

IDH2 mutations in acute myeloid leukemia confer specific sensitivity to BCAA metabolism inhibition

Les mutations IDH2 dans la leucémie aiguë myéloïde confèrent une sensibilité spécifique à l'inhibition du métabolisme des acides aminés branchés (BCAA)

Thèse de doctorat de l'université Paris-Saclay

École doctorale n° 582, Cancérologie : biologie - médecine - santé
Spécialité de doctorat : Aspects moléculaires et cellulaires de la biologie
Graduate School : Sciences de la vie et santé. Référent : Faculté de médecine

Thèse préparée dans la (ou les) unité(s) de recherche **U1170 INSERM**
Unité de recherche : Dynamique moléculaire de la transformati hématopoïétique (Université Paris-Saclay, Inserm, Institut Gustave Roussy)
sous la direction du Dr. **Virginie PENARD-LACRONIQUE**

Thèse soutenue à Lyon, le 22 Mars 2022, par

Maël HEIBLIG

Composition du Jury

Jérôme TAMBURINI PU-PH, INSERM	Président
Jean Emmanuel SARRY DR1, INSERM	Rapporteur
Véronique MAGUER-SATTA DR1, CNRS	Rapporteur
Melania TESIO CR1, INSERM	Examinatrice
Virginie PENARD-LACRONIQUE DR1, INSERM	Directrice de thèse

THESE DE DOCTORAT

NNT : 2022UPASL018

ÉCOLE DOCTORALE
Agriculture, alimentation, biologie, environnement, santé (ABIES)

Titre : Les mutations affectant le gène *IDH2* dans la leucémie aiguë myéloïde confèrent une sensibilité spécifique à l'inhibition du métabolisme des acides aminés branchés

Mots clés : Isocitrate dehydrogenase, leucémie aigue myéloïde, acides aminés branchés, BCAT1

Résumé : La leucémie aiguë myéloïde (LAM) est une hémopathie maligne caractérisée par la présence de mutations récurrentes dont celles affectant les gènes *isocitrate deshydrogénase 1* et *2* (*IDH1/2*). Ces mutations induisent une néo-activité enzymatique et la production d'un oncométabolite, le D-2-hydroxyglutarate (D-2HG). L'impact des anomalies *IDH* sur le métabolisme des cellules leucémiques reste mal défini.

Nous avons identifié une activité anormale de la voie des acides aminés branchés (ou branched-chain amino acid, BCAA, correspondant aux acides aminés essentiels valine, leucine et isoleucine) dans les blastes leucémiques de patients atteints de LAM avec anomalie *IDH2,* favorisant la synthèse de leucine (sens anabolique) alors que cette voie est d'ordinaire catabolique dans les cellules tumorales. Dans les blastes primaires, nous avons observé une surexpression du gène *BCAT1* responsable du métabolisme de ces acides aminés et l'utilisation privilégiée d'un promoteur alternatif, associé à un remodelage de marques épigénétiques lié à la présence de la mutation.

L'inhibition pharmacologique (gabapentine, inhibiteur BCAT1) et génomique (shRNA) de BCAT1 dans les cellules leucémiques effondre la croissance cellulaire et induit un excès d'apoptose dans différents modèles cellulaires, blastes primaires et modèles murins PDX comparativement au contexte *IDH* non muté. L'inhibition de BCAT1 est également associée à un engagement de la différentiation myéloïde, privilégiée dans les cellules portant une anomalie *IDH2*.

Notre travail révèle une reprogrammation métabolique spécifique des cellules leucémiques portant une anomalie *IDH2*, caractérisée par une activité anabolique de la voie BCAA. L'inhibition de cette voie métabolique représente une approche thérapeutique intéressante dans les LAM avec anomalie *IDH2,* par son lien avec les processus de prolifération et de différenciation.

Title : IDH2 mutations in acute myeloid leukemia confer specific sensitivity to BCAA metabolism inhibition

Keywords : Isocitrate dehydrogenase, acute myeloid leukemia, branched chain amino acids, BCAT1

Abstract : Acute myeloid leukemia (AML) is a hematological malignancy characterized by the presence of recurrent mutations including those affecting the *isocitrate dehydrogenase 1* and *2* (*IDH1/2*) genes. These mutations induce a neomorphic activity and the production of an oncometabolite, D-2-hydroxyglutarate (D-2HG). The impact of *IDH* mutations on leukemia cell metabolism remains poorly defined.

We have identified an abnormal activity of the branched-chain amino acid (BCAA) pathway in primary *IDH2* mutant AML cells, favoring leucine synthesis (anabolic direction) whereas this pathway is usually catabolic in tumor cells. In primary blasts, we observed an overexpression of the *BCAT1* gene associated with a remodeling of epigenetic marks at the *BCAT1* locus and leading to the use of an alternate promoter.

Pharmacological (gabapentin, BCAT inhibitor) and genomic (shRNA) inhibition of BCAT1 in leukemic cells collapses cell growth and induces apoptosis in different mutant *IDH2* cellular models, primary blasts and PDX mouse models compared to the wild type *IDH2* context. Inhibition of BCAT1 is also associated with an engagement of myeloid differentiation, which is favored in mutant *IDH2* cells.

Our work reveals a specific metabolic reprogramming of leukemic cells harboring a *IDH2* mutation, characterized by anabolic activity of the BCAA pathway. Inhibition of BCAT1 activity could represents an interesting therapeutic approach.

1 RESUME/ABSTRACT 5

2 ACKNOWLEDGMENTS 9

3 LIST OF ABBREVIATIONS 11

4 INTRODUCTION 15

4.1 Metabolism in hematopoietic stem cells: from quiescence to commitment 15
4.1.1 Hematopoietic stem cells characteristics and hierarchy 15
4.1.2 HSC metabolism 17
4.1.2.1 Energy-producing metabolic pathways 18
4.1.2.2 The TCA cycle is a signaling hub 19
4.1.2.3 Nutrient sensing pathway: the mTORC1 signaling network 25

4.2 Isocitrate dehydrogenase (IDH) enzymes 30
4.2.1 IDH metabolic properties 30
4.2.2 Transcriptional and post-transcriptional regulation 36
4.2.3 IDH in hematopoiesis 37

4.3 Acute myeloid leukemia 41
4.3.1 Epidemiology and classification 41
4.3.2 From clonal hematopoiesis to overt leukemia 43
4.3.2.1 Leukemic stem cells initiate and maintain the disease 43
4.3.2.2 Premalignancy 44
4.3.2.3 CH increases all-cause mortality and the risk of cardiovascular disease 48

4.4 Isocitrate dehydrogenase mutations in AML 52
4.4.1 Mutations in *IDH* enable conversion of ·KG to D-2HG 54
4.4.2 D-2HG accumulation triggers leukemogenesis through multiple mechanisms 58
4.4.3 D-2HG-mediated metabolic rewiring 62

4.5 Metabolism in AML 63
4.5.1 General aspects in AML metabolism 64
4.5.2 Metabolic reprogramming and metabolic vulnerabilities in AML 65
4.5.2.1 Glycolysis 65
4.5.2.2 Fatty acid metabolism 67
4.5.2.3 Amino acids 69
4.5.2.4 Mitochondrial metabolism 71
4.5.3 Influence of the genomic context on metabolism in AML cells 75

4.6 Branched chain amino acids (BCAA) metabolism 78
4.6.1 BCAA metabolism 78
4.6.2 BCAA metabolism in HSC and progenitors 80
4.6.3 BCAA metabolism in leukemia 82
4.6.4 BCAA metabolism in glioma 83

4.7 Working hypothesis 84

5 METHODOLOGY 86

5.1 Metabolites assessment and mass spectrometry 86
5.1.1 2HG measurement 86
5.1.2 Liquid-chromatography/mass spectrometry (LC-MS) 86
5.1.3 GC-MS based metabolic analysis: BCAA tracing 87

5.2 Cell Culture 87
5.2.1 Cell lines and reagents 87
5.2.2 Human primary samples 87

5.3 Viral constructs and production 88

5.4 Molecular biology assay 89

5.4.1 Primary cells analysis 89
5.4.2 DNA extraction, Real-time qPCR analysis 89
5.4.3 HpaII tiny fragment Enrichment by Ligation-mediated PCR assay (HELP) 89
5.4.4 Chromatin immunoprecipitation sequencing (CHIP-Seq) 90

5.5 Western blot analysis 90

5.6 Flow Cytometry 91
5.6.1 Annexin V 91
5.6.2 Differentiation assay in human primary samples 91

5.7 Murine experiments 91
5.7.1 Patient derived xenograft (PDX) model 91
5.7.2 *In vitro* imaging system (IVIS) 92

5.8 Survival analysis 92

6 RESULTS 93

6.1 PART I: IDH2 mutations and BCAA metabolism 93
6.1.1 Metabolic profile distinguishes mutant and wild type *IDH2* AML cells 93
6.1.1.1 Altered metabolism of BCAAs in primary mutant IDH2 AML cells 93
6.1.1.2 Leucine anabolism is favored in primary mutant IDH2 AML cells 94
6.1.2 Epigenetic marks regulate *BCAT1* expression in mutant *IDH2* AML blasts 97
6.1.2.1 BCAT1 is overexpressed in mutant IDH2 AML blasts 97
6.1.2.2 Epigenetic changes in the BCAT1 locus are associated to the IDH2 mutation in primary AML blasts 100
6.1.3 Mutant *IDH2* AML blasts are strictly dependent on BCAT1 activity for their growth and survival 103
6.1.4 IDH2 mutational context impairs α-ketoacids metabolism (preliminary results) 109
6.1.5 Metabolic rewiring appears as a consequence of impaired mTORC1 activity 112
6.1.6 IDH mutation and D-2HG is associated with proliferation 117

6.2 PART II : Mechanisms of response and acquired of resistance to enasidenib 121
6.2.1 Introduction 121
6.2.2 Results 123
6.2.3 Discussion 125
6.2.4 Clinical update 126
6.2.5 Published manuscript 128

7 DISCUSSION 141

8 CONCLUSION AND PERSPECTIVES 151

9 REFERENCES 153

10 ANNEXES 185

1 RESUME/ABSTRACT

Introduction

La leucémie aiguë myéloïde (LAM) est une maladie complexe et hétérogène sur le plan moléculaire qui se caractérise par l'accumulation de progéniteurs myéloïdes immatures. Les mutations somatiques affectant les gènes *isocitrate déshydrogénase* (*IDH*) *1* et *2* sont présentes dans ~20-25% des cas. Les gènes *IDH* codent pour une même fonction du cycle de Krebs, i.e., l'oxydation de l'isocitrate en alpha-cétoglutarate (αKG). Sous leur forme mutées, les enzymes IDH induisent l'accumulation d'un métabolite, le stéréoisomère D du 2-hydroxyglutarate (D-2HG) responsable de dérégulations énergétiques et de l'inhibition fonctionnelle de dioxygénases cellulaires dépendantes de l'αKG parmi lesquelles des acteurs majeurs de l'épigenèse. La réversion du blocage de différenciation des blastes leucémiques est un paradigme thérapeutique important de la LAM. L'enasidenib et l'ivosidenib (inhibiteurs des enzymes IDH mutées) représentent aujourd'hui une stratégie de traitement innovante pour les patients atteints de LAM avec anomalie *IDH*. De nombreuses réactions enzymatiques utilisent l'αKG comme co-substrat, notamment les réactions de biosynthèse/dégradation des acides aminés (AA) par transamination. Nos études ont identifié une activité anormale de la voie métabolique des AA branchés (ou branched-chain amino acid, BCAA), plus particulièrement de la leucine, dans les blastes leucémiques avec anomalie *IDH2*.

Méthodes

Au cours de ce travail, nous avons :

- étudié la production de leucine et d'alpha-cétoisocaproate (▪KIC) issu de la transamination de la leucine, sur une cohorte indépendante d'échantillons primaires de patient LAM avec mutation *IDH2* et en modèle cellulaire.
- analysé le métabolisme de la leucine, de l'▪KIC et d'autres métabolites, par des méthodes d'analyse de flux métaboliques basées sur l'analyse de radioisotopes marqués sur des blastes primaires de patients et en lignée cellulaire.
- étudié la régulation transcriptionnelle du gène *branched chain amino-transaminase 1* (*BCAT1*) dont l'activité contrôle le métabolisme de la leucine et de l'▪KIC, sur des blastes primaires de patients et en modèle cellulaire (RT-qPCR, CHIP-qPCR).
- étudié les conséquences sur la leucémogénèse d'une inhibition pharmacologique et génétique de *BCAT1*, en lignées cellulaires et dans des modèles murins de type patient-derived xenograft (PDX).
- étudié les liens entre l'activité de la voie BCAA, la production de leucine et l'activité de la voie mTOR.

Résultats

Nous avons observé un sens anabolique de la voie BCAA (habituellement catabolique dans les cellules cancéreuses et catabolique dans les cellules de LAM sans anomalie *IDH*) ainsi que l'accumulation de leucine de façon spécifique au sein des blastes primaires avec anomalie *IDH2* et dans des modèles cellulaires. Dans ces cellules, nous avons observé

une surexpression du gène *BCAT1* incluant l'utilisation privilégiée d'un promoteur alternatif, associé à un remodelage de marques épigénétiques lié à la présence de la mutation *IDH2*. L'inhibition pharmacologique (gabapentine, inhibiteur BCAT) et génomique (shRNA) de BCAT1 dans les cellules leucémiques effondre la croissance cellulaire et induit un excès d'apoptose dans différents modèles cellulaires, blastes primaires et modèle murins PDX avec anomalie *IDH2*, comparativement au contexte *IDH2* non muté. L'inhibition de *BCAT1* est également associée à un engagement de la différentiation myéloïde, privilégiée dans les cellules portant une anomalie *IDH2*. Nous avons montré que la mutation *IDH2* est associée à une augmentation de l'activité de mTORC2 et une diminution de l'activité de mTORC1.

Conclusions

Notre travail révèle une reprogrammation métabolique spécifique des cellules leucémiques portant une anomalie *IDH2*, caractérisée par une activité anabolique de la voie BCAA. L'inhibition de cette voie métabolique représente une approche thérapeutique intéressante dans les LAM avec anomalie *IDH2,* par ses liens avec les processus de prolifération et de différenciation.

Mots clefs : Isocitrate déshydrogénase, leucémie aigue myéloïde, acides aminés branchés, BCAT1

Introduction

Acute myeloid leukemia (AML) is a complex and molecularly heterogeneous disease characterized by the accumulation of immature myeloid progenitors. Somatic mutations affecting the *isocitrate dehydrogenase* (*IDH*) *1* and *2* genes are present in ~20-25% of cases. The *IDH* genes code for a reaction of the Krebs cycle, i.e., the oxidation of isocitrate into alpha-ketoglutarate (αKG). In their mutated form, IDH enzymes induce the accumulation of an oncometabolite, the D-stereoisomer of 2-hydroxyglutarate (D-2HG) responsible for energetic deregulations and functional inhibition of αKG-dependent cellular dioxygenases among which are major actors of epigenesis. Reversal of the leukemic blast differentiation blockade is an important therapeutic paradigm in AML. Enasidenib and ivosidenib (allosteric inhibitors of mutant IDH) now represent an innovative treatment strategy for patients with mutant *IDH* AML. A variety of enzymatic reactions use αKG as a co-substrate, including amino acid (AA) biosynthesis/degradation reactions via transamination. Our studies identified abnormal activity of the branch-chain amino acid (BCAA) metabolic pathway, specifically leucine, in leukemic blasts mutated for *IDH2*.

Methods

In this study, we have:

- investigated the production of leucine and alpha ketoisocaproate (・KIC) the keto acif from leucine, in an independent cohort of primary AML patient samples with *IDH2* mutation and in cellular models.
- analyzed the metabolism of leucine, aKIC and other metabolites, using metabolic flux methods based on the analysis of labeled radioisotopes on primary patient blasts and in cell lines.
- studied the transcriptional regulation of the *branched chain amino-transaminase 1* (*BCAT1*) gene whose activity controls the metabolism of leucine and ・KIC, on primary blasts from AML patients and in cell lines (RT-qPCR, CHIP-qPCR).
- studied the consequences on leukemogenesis of pharmacological and genetic inhibition of BCAT1, in cell lines and in mouse models of patient-derived xenograft (PDX).
- investigated the relationship between BCAA pathway activity, leucine production and mTOR pathway activity.

Results

We observed an anabolic direction of the BCAA pathway (usually catabolic in cancer cells as in AML cells devoid of *IDH* mutation) as well as leucine accumulation specifically in primary blasts with *IDH2* mutation and in cellular models. In mutated *IDH2* cells, we observed an overexpression of the *BCAT1* gene and the preferential use of an alternative promoter, associated with a remodeling of epigenetic marks linked to the presence of

the *IDH2* mutation. Pharmacological (gabapentin, BCAT inhibitor) and genomic (shRNA) inhibition of BCAT1 in mutant *IDH2* leukemic cells inhibits cell growth and induces apoptosis in cellular models, primary blasts and in PDX mice models, compared to the wild type *IDH2* context. Inhibition of BCAT1 is also associated with an engagement of myeloid differentiation, favored in cells with *IDH2* mutation. We showed that *IDH2* mutation leads to increased mTORC2 activity and decreased mTORC1 activity.

Conclusion

Our study identifies a metabolic reprogramming of leukemic cells expressing a mutant *IDH2*, characterized by the anabolic activity of the BCAA pathway. Inhibition of this pathway represents an interesting therapeutic approach in AML with *IDH2* mutation, as it affects proliferation and differentiation processes.

Keywords : Isocitrate dehydrogenase, acute myeloid leukemia, branched chain amino acids, BCAT1

2 ACKNOWLEDGMENTS

Il me sera très difficile de remercier tout le monde car c'est grâce au soutient de nombreuses personnes que j'ai pu mener cette thèse, fruit de 3 ans de travail sur Paris. Je garderai un souvenir ému et éprouvé. Trois ans, c'est long… surtout après tout ce chemin parcouru. Enfin, reprendre l'activité clinique sans avoir finalisé/soutenu ce travail n'était pas la plus brillante des idées…Je me rappele encore Gabriel me dire : « Surtout, ne part pas de ton labo sans avoir soutenu » … Je pensais qu'il exagerait et que je ferais front. Il avait raison…

J'aimerai d'abord dédicacer cette thèse à ma maman, pour qui ces nombreuses années qui ont séparé la naissance de ce projet à son accomplissement auront été presque aussi éprouvantes que pour moi. C'est chose faite !

J'aimerai également dédicer ce travail à toute mon équipe d'acceuil à Gustave Roussy. Un mot très spéciale à Muriel et Cyril qui ont été d'un précieux secours. Merci encore Muriel pour toutes ces explications « concises » qui ont permi d'élucider tant de problème. Merci à Amaury qui a pris « ma suite » dans ce projet difficile. Merci Virginie pour m'avoir laissé m'épanouir dans ce projet atypique, né d'une idée folle. Merci à Laure, Yanis, Chloé et tant d'autres que j'oublie certainement.

Une pensée toute particulière à toute l'équipe d'hématologie du centre hospitalier de Lyon Sud, et plus particulièrement l'équipe du secteur myéloïde qui m'a permi de me dégager du temps pour finaliser ma thèse ainsi que toutes les contraintes de ce début d'année 2022.

Un mot pour Florent (et Carole également)… Je vais enfin pouvoir signer ton cahier … d'ici quelques mois !

Enfin, j'aimerai remercier Sabrina. Tu as pris le train en cours de route mais tu m'as quand même supporté. Ces dernière semaines auront été épiques, et je n'y serai pas arrivé sans toi.

J'aimerai remercier également le COVID19 pour nous m'avoir facilité la tache.

Pour finir, j'aimerai conclure en citant un « homme sage », qui dans un excès d'engouement lors d'une réunion de laboratoire pendant mon Master 2, dit :

« Science is a bitch »
Pr Thaunat Olivier, MD, PhD, Hospices civils de Lyon

Il a sans doute raison, mais malgré tout, on continue à chercher.

3 LIST OF ABBREVIATIONS

ACC : acetyl-CoA carboxylase

ACO : aconitate hydratase

ACLY : ATP-citrate lyase

ACSS2 : acyl-CoA synthetase short-chain family member 2

Ara-C : cytarabine

αKA : α-ketoacids

αKG : alpha-kétoglutarate

αKIC : α-ketoisocaproate

αKIV : α-keotisovalerate

αKMV : alpha-ketomethylvalerate

AMPK : AMP-activated protein kinase

ALL : acute lymphoblastic leukemia

ARCH : Age related clonal hematopoiesis

ATM : ataxia telangiectasia mutated

ADP : adenosine diphosphate

AML : acute myeloid leukemia

ATP : adenosine triphosphate

ASXL1 : additional sex combs like 1

BCAT1 : branched chain amino transferase 1

BCAT2 : branched chain amino transferase 2

BCL2 : B Cell Leukemia/Lymphoma 2

BCOR : BCL6 corepressor

BM : bone marrow

CEBPA : CCAAT/enhancer-binding protein alpha

CH : clonal hematopoiesis

CLP : common lymphoid progenitor

CMP : common myeloid progenitor

CR : complete response

DHODH : dihydro-orotate dehydrogenase

DCA : dichloroacetate

DCK : deoxycytidine kinase

DDR : DNA damage repair

DNA: desoxyribonucleic acid

DNMT : DNA methyltransferase

ELN : European LeukemiaNet

ETC : electron transport chain

ETS2 : E26 oncogene homolog 2

EZH2 : enhancer of zeste homolog 2

FAO : fatty acids oxidation

FCM: flow cytometry

FLT3 : fms-like tyrosine kinase 3 with internal tandem duplication

G6PD : glucose 6 phosphate dehydrogenase

GLUT1 : glucose transporter 1

HSC : hematopoietic stem cell

HMT : histone methyltransferases

IDH1 : isocitrate deshydrogenase 1

IDH2 : isocitrate deshydrogenase 2

IDH3 : isocitrate deshydrogenase 3

FABP4 : fatty acid-binding protein 4

FIS1 : mitochondrial fission 1

FLCN : Folliculin

GDH : glutamate dehydrogenase

GLS : glutaminase

GMP : granulocyte/monocyte progenitor

GOT : glutamate-oxaloacetate transaminase

GPT : glutamate-pyruvate transaminases

HIF1 : hypoxia inducible factor 1

HPC : hematopietic progenitor cell

HSC : hematopoietic stem cell

LAT1 : L-type / large neutral amino acid transporter 1

LDHA : lactate dehydrogenase A

LMPP : lymphoid-primed multipotent progenitor

LSC : leukemic stem cell

KGDH : αKG dehydrogenase

KMT2A : lysine N-méthyltransférase 2A

MCL1 : myeloid cell leukemia sequence 1

NAD : nicotinamide adenine dinucleotide

NADH : nicotinamide adenine dinucleotide

NADPH : nicotinamide adenine dinucleotide phosphate

NPM1 : nucleophosmin 1

MDH1 : malate dehydrogenase 1

MECOM1 : MDS1 And EVI1 Complex Locus

MEP : megakaryocyte/erythrocyte progenitor

MY : myelocyte

NAPMT : nicotinamide phosphoribosyltransferase

NGS : Next generation sequencing

OXPHOS : oxidative phosphorylation

PPARγ : peroxisome proliferator-activated receptor-γ

PB : peripheral blood

PDX : patient-derived xenografts

PDK1 : pyruvate dehydrogenase kinase 1

PEP : phosphoenolpyruvate

PI3K : phosphoinositide 3-kinase

PHF6 : PHD finger protein 6

PKM2 : pyruvate kinase M2

PM : promyelocyte

PMN : polymorphonuclear neutrophil

PPM1D : protein phosphatase Mg2+/Mn2+ dependent 1D

PTPMT1 : Protein Tyrosine Phosphatase Mitochondrial 1

RNA : ribonucleic acid

ROS : reactive oxygen species

RRM2b: ribonucleotide reductase regulatory TP53 inducible subunit M2B

SIRT3 : sirtuine 3

SIRT5 : sirtuine 5

SRSF2 : Serine And Arginine Rich Splicing Factor 2

SREBPs : sterol regulatory element-binding proteins

STAG2 : stromal antigen2

TCA : tricarboxylic acid cycle

TET : Ten-eleven-translocation hydroxylase

TK1 : thymidine kinase 1

TNF- α : tumor necrosis factor-α

TP53 : tumor protein 53

U2AF1 : U2 small nuclear RNA auxiliary factor

VLCAD: very-long-chain acyl-CoA dehydrogenase

ZRSR2 : zinc finger CCCH-Type, RNA binding motif and serine/arginine rich 2

4 INTRODUCTION

4.1 METABOLISM IN HEMATOPOIETIC STEM CELLS: FROM QUIESCENCE TO COMMITMENT

4.1.1 Hematopoietic stem cells characteristics and hierarchy

In the era of Darwinism theory, Ernst Haeckel was the first to use the word stem cell in 1868. Since the initial concept referring to the primordial unicellular organism from which all multicellular life descended has evolved. Despite extensive exploration on hematopoietic system ontogenesis, the genuine origin of pre-hematopoietic stem cells (HSCs), which give rise to the definitive HSC line, is still rather unclear. Initially thought coming from the yolk sac, there is now increasing evidence that HSC originate from the embryonic aorta (aorta gonad mesonephros, AGM) and more specifically from an endothelial intermediate (hemogenic endothelium)[1]. Next, HSCs migrate to the fetal liver and spleen to ultimately reside in the bone marrow[2]. Embryonic and neonatal HSCs rapidly proliferate to constitute the HSC pool that will sustain all lifelong. In contrast, adult HSCs rarely divide[3]. These transitions from embryonic/neonatal stage to adult hematopoiesis require drastic alterations in metabolic state, which will not be developed in this manuscript.

HSCs are characterized by pluripotency, self-renewal, and a specific phenotype, as well as engraftment into the hematopoietic organs. HSC hierarchy is still a matter of debate since the first model have been hypothesized in the early's 2000. In this model, the first branch point segregates lymphoid potential to the common myeloid progenitor (CMP) that give rise to myeloid, erythroid, and megakaryocytic lineage, followed by several further branching steps on either side of the tree progressing from multi- to bi- and finally unipotent progenitor cells (**Figure 1A**). Unraveling new surface markers by flow cytometry (FCM) suggested several modifications of this classical tree, including common lymphoid and myeloid fates (through the lymphoid-primed multipotential progenitors (LMPP)) remaining possible until further down the tree, an early megakaryocyte commitment, as well as subdivision of the multipotent progenitor (MPP) compartment into distinct subpopulations (**Figure 1B**). There are several limits in these models. First, most of the studies assessing these concepts have been realized in mice models that might not be similar in humans. Second, most of the HSC subpopulation and progeny have been historically defined by FCM. However, it is now clear that the HSC pool itself is functionally

and molecularly heterogeneous. In addition, the differentiation state is defined by a collection of metabolic and molecular properties. Around 70% of all expression changes between HSCs and early progenitors occur independently of lineage choice, with a similar observations at methylation and chromatin accessibility levels (reviewed in [4]). Sustained by single cell transcriptomic analysis, these results combined with more stochastic pattern of differentiation by FCM, defined HSC fate more as a continuum of differentiation. Velten and colleagues have investigated the fate decisions made during human adult hematopoiesis by presenting combined analysis of single-cell transcriptional and functional data and found that whilst multipotent cells exist in the adult stem cell compartment, the majority of blood progenitor cells are in fact unipotent (**Figure 1C**)[5]; these data are in agreement with a previous report[6]. The hierarchical or non-hierarchical relationship between multipotent HSCs that adopt distinct lineage-restricted fates remains however a debate topic, with recent revised roadmaps suggesting that the megakaryocyte/platelet-biased lineage arises independently of other hematopoietic fates[7].

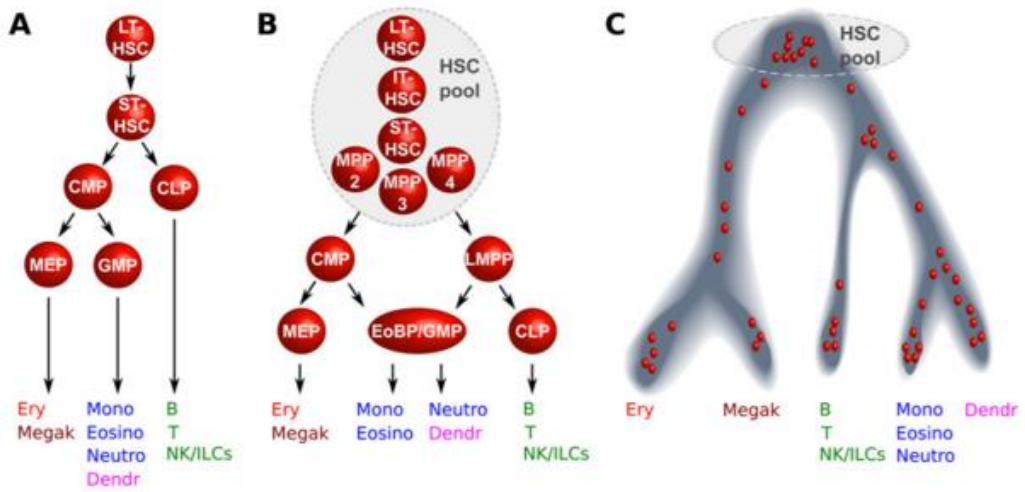

Figure 1: Evolution of hematopoiesis models (from [4]). In contrast to the traditional branching model with its stepwise progression from stem cells via multipotent to bipotent and finally unipotent progenitors (A, B) acquisition of lineage specific fates appear as a continuous process where unilineage-restricted cells emerge directly from a continuum of undifferentiated HSCs, without any transitional state through multi- and bipotent stages (C). A) HSC hierarchy state-of-the-art around the year 2000. B) Incorporation of new surface markers identifies HSC pool as a more heterogeneous entity. As a hallmark, the myeloid and lymphoid branches remain common further down in the hierarchy via the LMPP and MPP populations. C) Single cell transcriptomics studies suggest a continuum of differentiation more than a temporal fixed state.

This evolutionary concept allows to depict more precisely pathophysiology, especially in acute leukemia. However, as initiating cells of acute leukemia, defined as leukemic stem cells (LSC), are thought to arise from HSC and/or their progeny, identifying their normal counterparts could be detrimental for treatment decision as leukemic cells from different lineage do not have the same chemosensitivity profile. As an example, transcriptomic studies identify that some acute myeloid leukemias (AML) were more closed to T-cell acute lymphoblastic leukemias (T-ALL) due to T-cells transcriptional enrichment or that some Ph^+ ALL may in fact arise from a common myeloid progenitor despite B-cell engagement of the leukemic progeny[8].

4.1.2 HSC metabolism

HSCs reside in a hypoxic bone marrow environment as their metabolic requirements and adaptations to their niches evolved during development. These metabolic adaptations confer them distinct status from their differentiated progeny. At steady state, HSCs are non-proliferative cells maintained in a quiescent state, the G0 phase of the cell cycle. As HSC reside in a relatively reduced condition, they are termed reactive oxygen species (ROS)-low. They are mainly using anaerobic glycolysis and fatty acids oxidation (FAO) as source of energy while differentiated cells primarily rely on mitochondrial oxidative phosphorylation (OXPHOS). Upon response to cell-intrinsic or cell-extrinsic stimuli (stress, infection, injury, inflammatory signals, regenerative context...), quiescent HSCs switch from glycolysis (their conversion of pyruvate to acetyl coenzyme A (acetyl-CoA) required to fuel the TCA cycle, is blocked) to OXPHOS to produce energy and metabolic substrates. Indeed, active proliferation cannot be sustained by the limited flux of glucose-derived intermediates to the TCA cycle. Therefore, regulation of TCA cycle flux by limiting substrate/oxygen availability represents a level of control for determining HSC fate, i.e. decision between quiescence, self-renewal or differentiation. This metabolic switch results in increasing amounts of TCA products, including acetyl-CoA and alpha-ketoglutarate (αKG); this switch also incudes an increase in NAD^+ and S-adenosylmethionine (SAM) metabolites, that are essential to epigenetic modifiers such as the NAD^+-dependent deacetylases sirtuins (SIR) and the histone methyltransferases (HMT). The activity of metabolic pathways, metabolic variation, and the environmental inputs (such as nutrient availability, hypoxia) impact the engagement of signaling pathways and the

concentration of substrates used to modify nucleic acids (including various RNAs species) and chromatin. Many of the chemical modifications that decorate RNA, DNA and histones are adducts derived from intermediates of cellular metabolic pathways. In addition, numerous enzymes removing such genomic marks use metabolites as part of their enzymatic reaction. Thus, cellular metabolism constitutes a fundamental component of chromatin status and thereby of genome regulation.

4.1.2.1 Energy-producing metabolic pathways

Glycolysis is the process by which one molecule of glucose is converted into two molecules of pyruvate and two hydrogen ions. Pyruvate is converted to acetyl coenzyme A (acetyl-CoA) which enters the tricarboxylic acid cycle (TCA) cycle, also called the Krebs cycle, enabling the production of ATP and nicotinamide adenine dinucleotide (NAD^+) reduced (NADH), a critical coenzyme for enzymes that fuel multiple reduction-oxidation reactions. Under hypoxic conditions, glycolysis is a way for HSC to sustain low levels of energy as only 2 ATP molecules per glucose molecule are generated (mitochondrial respiration produces 36 ATP molecules per glucose molecule). This process is sustained by the serine-threonine kinase AKT that act primarily as a downstream target of the phosphoinositide 3-kinase (PI3K), the mechanistic target of rapamycin (mTOR, that belongs to the family of PI3K-related kinases, and that can participate into two distinct complexes, mTORC1 and mTORC2, *cf. infra*) and the hypoxia inducible factor 1 subunit alpha (HIF1α) which individually increase glycolysis through transcriptional upregulation or phosphorylation of glucose transporters (such as the glucose transporter 1, GLUT1), glycolytic enzymes (as the lactate dehydrogenase A, LDHA) and metabolic regulatory enzymes (as the pyruvate dehydrogenase kinase 1, PDK1). HIF1α, together with HIF1β, also known as ARNT, forms the HIF1 activity and mediates an active switch from glycolytic to oxidative metabolism and vice versa[9]. Under normoxic conditions, HIF1α is hydroxylated by oxygen (O_2)- and αKG-dependent prolyl hydroxylases (PHDs), then recognized by the von Hippel-Lindau (VHL) tumor suppressor protein which recruits a specific ubiquitination complex, and degraded by the proteasome. Under hypoxic conditions, HIF1α prolyl hydroxylation is suppressed, stabilizing HIF1α protein. HIF1α is regulated by myeloid ecotropic viral integration site 1 homolog (MEIS1), a homeodomain transcription factor which is a critical regulator of adult bone marrow hematopoiesis. Compared to mature bone

marrow cells, HSCs have elevated levels of HIF1α and increased expression of hypoxia-inducible genes, including those controlling glycolysis[10]. HSC-specific deletion of HIF1α or MEIS1 results in an increased mitochondrial respiration, decreased glycolytic flux, increased ROS production and apoptosis of HSCs, indicating that mitochondrial metabolism and apoptotic pathways are linked in HSC[11]. Self-renewing HSCs cannot properly work when they are unable to engage mitochondrial OXPHOS to generate energy. Indeed, deletion of phosphatase and tensin homolog (PTEN)-like mitochondrial phosphatase (PTPMT1) induces a pyruvate influx block into mitochondria. This metabolic rewiring leads to a large expansion of the HSC pool in the mouse while preventing HSC differentiation into downstream lineages; these observations indicate that interference with pyruvate entry into mitochondria deeply impacts HSC fate[12].

Despite low pyruvate income, mitochondria biogenesis remains active to provide enough acetyl-CoA which is necessary for HSC epigenetic regulation. Acetyl-CoA is generated in the mitochondria through the catabolism of glucose and amino acids and mainly by FAO; it is the acetyl donor for lysine acetylation reactions in mammalian cells, notably on histone. Acetyl-CoA enters the TCA cycle where it combines with oxaloacetate to generate citrate. Citrate travels from the mitochondria and gets converted in both the cytosol and the nucleus to acetyl-CoA again by the ATP-citrate lyase (ACLY). The abundance of acetyl-CoA correlates with the levels of global histone acetylation and is thus highly dependent on glucose availability, FAO, and mitochondrial respiratory function. Coupling of these processes has a functional significance; for instance, the decrease in intracellular acetyl-CoA abundance that occurs during glucose deprivation induces histone redistribution to rewire transcriptional activity to favor pathways that produce acetyl-CoA for oxidation[13]. When sources of acetyl-CoA, such as glucose and acetate, are limited (metabolic stress), acetyl-CoA levels are maintained by acyl-CoA synthetase short-chain family member 2 (ACSS2), which generates acetyl-CoA from acetate; nuclear ACSS2 forms complexes with transcription activators at the promoter regions of different sets of genes to locally support histone acetylation and activate gene expression programs[14,15].

4.1.2.2 The TCA cycle is a signaling hub

Mitochondria and the nucleus maintain a bidirectional regulation and mitochondria constantly communicate with the cytosol to initiate biological events under homeostatic and

stress conditions[16]. Indeed, cells check whether mitochondrial metabolism is fit before they engage in complex and highly demanding cellular functions, including differentiation or adaptation to stress and reversely, mitochondria regulate the expression of genes to facilitate cellular functions (**Figure 2**).

Isocitrate oxidation by NADP-dependent isocitrate dehydrogenases (IDH) enzymes lead to αKG production, a metabolite at the center of a wide range of physiological processes besides cellular metabolism (**Figures 2 and 3**). Indeed, αKG is the co-substrate of Fe(II)/aKG-dependent dioxygenases, a family of enzymes that catalyze the oxidative decarboxylation of αKG producing succinate and CO_2 from O_2. αKG is notably a substrate of dioxygenase enzymes involved in DNA repair as the AlkB family of enzymes, in the regulation of histone as the jumonjiC domain-containing histone lysine demethylases (KDM2-7) which are the major histone demethylases, and the members of the ten eleven translocation hydroxylases (TET1-3) family involved in DNA demethylation **(Figure 3**). Low activity of IDH enzymes leads to high density chromatin structure, hypermethylated phenotype and, therefore, gene repression. Specifically, histone acetylation by histone acetyltransferases relies on the availability of acetyl-CoA[14]. Other TCA cycle metabolites have diverse non-metabolic signaling roles. For example, acetyl-CoA, itaconate, succinate, fumarate, and L-2 hydroxyglutarate (L-2HG, a metabolite produce from αKG, *cf. infra*) can alter the response of both the innate and adaptive immune systems by rewiring the epigenetic landscape of the cells through inhibition of histone and DNA demethylases[17,18].

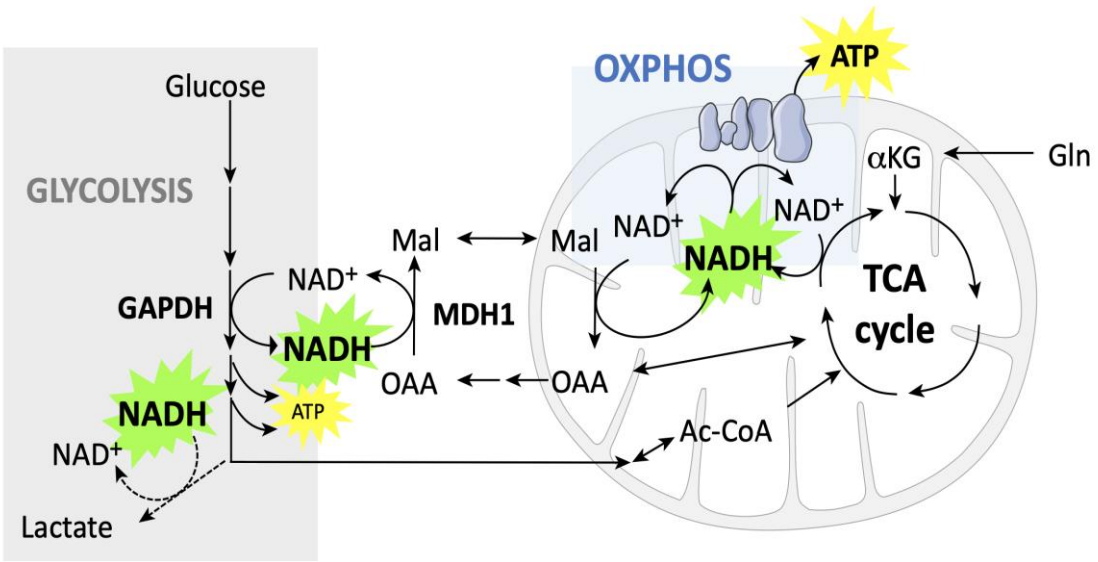

Figure 2 : Cellular energy generation pathways (from [19]). In a cell with normal mitochondrial function, ATP is generated in the cytosol through glycolysis and in the mitochondria through the coupling of the TCA cycle and OXPHOS. OXPHOS is driven by NADH, which is produced in the TCA cycle and shuttled into the mitochondria from glycolysis. The glyceraldehyde-3-phosphate dehydrogenase (GAPDH) reaction in glycolysis consumes cytosolic NAD^+, which is regenerated by the malate dehydrogenase 1 (MDH1) reaction.

Another energy-producing metabolic pathway providing αKG is glutaminolysis, in which deamination of glutamine (a nutritionally semi-essential amino acid) by glutaminase (GLS) gives rise to glutamate; subsequent deamination of glutamate by glutamate dehydrogenase (GDH) produces αKG and ammonia. αKG is also produced through glutamine transamination into α-ketoglutaramate, which after an ω-amidase-catalyzed hydrolysis (active both in cytosol and mitochondria), releases αKG and ammonia. α-ketoglutaramate, that is a ketoacid, is involved in amino acids metabolism (**Figure 3A**). Other enzymes, including glutamate-pyruvate transaminases (GPT1/2) and glutamate-oxaloacetate transaminase (GOT1/2), can also produce αKG, allowing parallel synthesis of alanine and aspartate respectively, that can also be used as precursors for TCA cycle intermediates and protein synthesis.

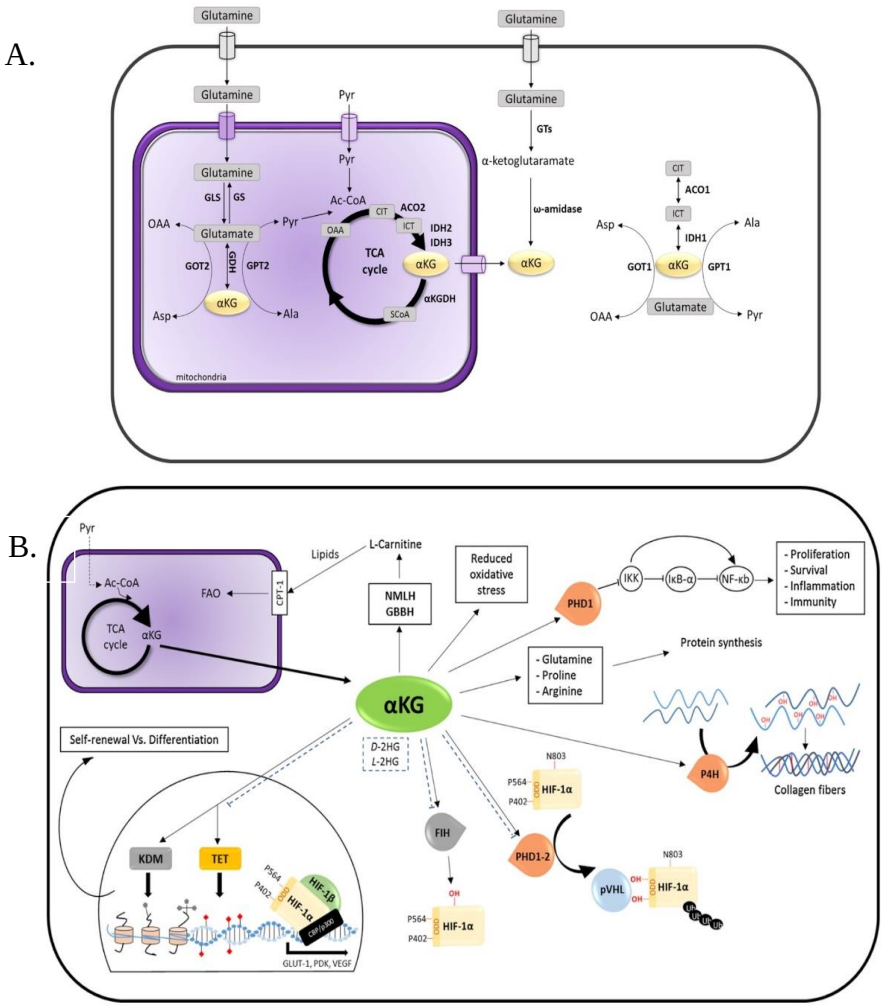

Figure 3: The metabolite αKG is involved in a plethora of physiological reactions besides fueling TCA cycle and OXPHOS (from [20]). A) αKG biosynthetic pathways; αKG originates from transamination of glutamine by glutamine transaminases (GTs) or glutamate by glutamate-pyruvate transaminase 1 (GPT1)/glutamic-oxaloacetic transaminase 1 (GOT1), in the presence of pyruvate (Pyr)/oxaloacetate (OAA) respectively; inside the mitochondria, GPT2 and GOT2 isoforms catalyze the same reactions. B) αKG is involved in multiple cellular processes. For examples, αKG induces global histone and DNA demethylation; abundance of αKG regulates PHDs activity thus controls the response to hypoxic environment; αKG activates PHD1 to induce nuclear factor-kappa B (NF-κB) degradation; collagen fibers hydroxylation at proline residues by αKG-dependent proline 4-hydroxylase allows collagen monomers stabilization.

The survival of quiescent HSCs in the anaerobic bone marrow niche is dependent on an active glycolysis. The use of anaerobic glycolysis has a protective advantage for resting HSCs, given that the alternative metabolic pathway, mitochondrial OXPHOS (OXPHOS refers to the redox reactions involving the flow of electrons along a series of membrane-bound proteins, coupled with the generation of ATP, oxidative phosphorylation is the fourth and final step in cellular respiration), is associated with the production of DNA-

damaging ROS. However, anaerobic glycolysis is a relatively inefficient method of ATP production and HSCs undergoing self-renewal or differentiation-associated divisions have robust energy demands. Active proliferation cannot be sustained by the limited flux of glucose-derived intermediates to the TCA cycle. In line, disrupting mitochondrial OXPHOS upon the loss of protein tyrosine phosphatase mitochondrial 1 (PTPMT1), a mitochondrial phosphatase targeting phosphatidylinositol phosphates (PtdIns3P/PI(3)P) blocks early HSC differentiation[21].

This metabolic switch results in increasing amounts of TCA products, including acetyl-CoA and αKG; this switch also includes an increase in NAD^+ and S-adenosylmethionine (SAM) metabolites, that are essential to epigenetic modifiers such as the NAD^+-dependent deacetylases sirtuins (SIR) and enzymes that use SAM as a methyl-group donor as the histone methyltransferases (HMT), DNA methyltransferases (DNMT), TET and JmjC proteins (**Figure 4A**). These enzymatic reactions are critical for the dynamic regulation of gene expression in response to commitment and differentiation and the reaction rates of these enzymes are highly responsive to substrate availability. Thus, regulation of TCA cycle flux (by limiting substrate/oxygen availability) represents a level of control for determining HSC fate, i.e., decision between quiescence, self-renewal, or differentiation. In line, the maintenance of stem cells pluripotency has been associated with αKG levels[22,23] and modification of αKG levels is sufficient to regulate chromatin modifications such as $H3K9me^3$, $H3K27me^3$, $H4K20me^3$ (repressive chromatin marks) and TET-mediated DNA demethylation[22] (**Figure 4B**).

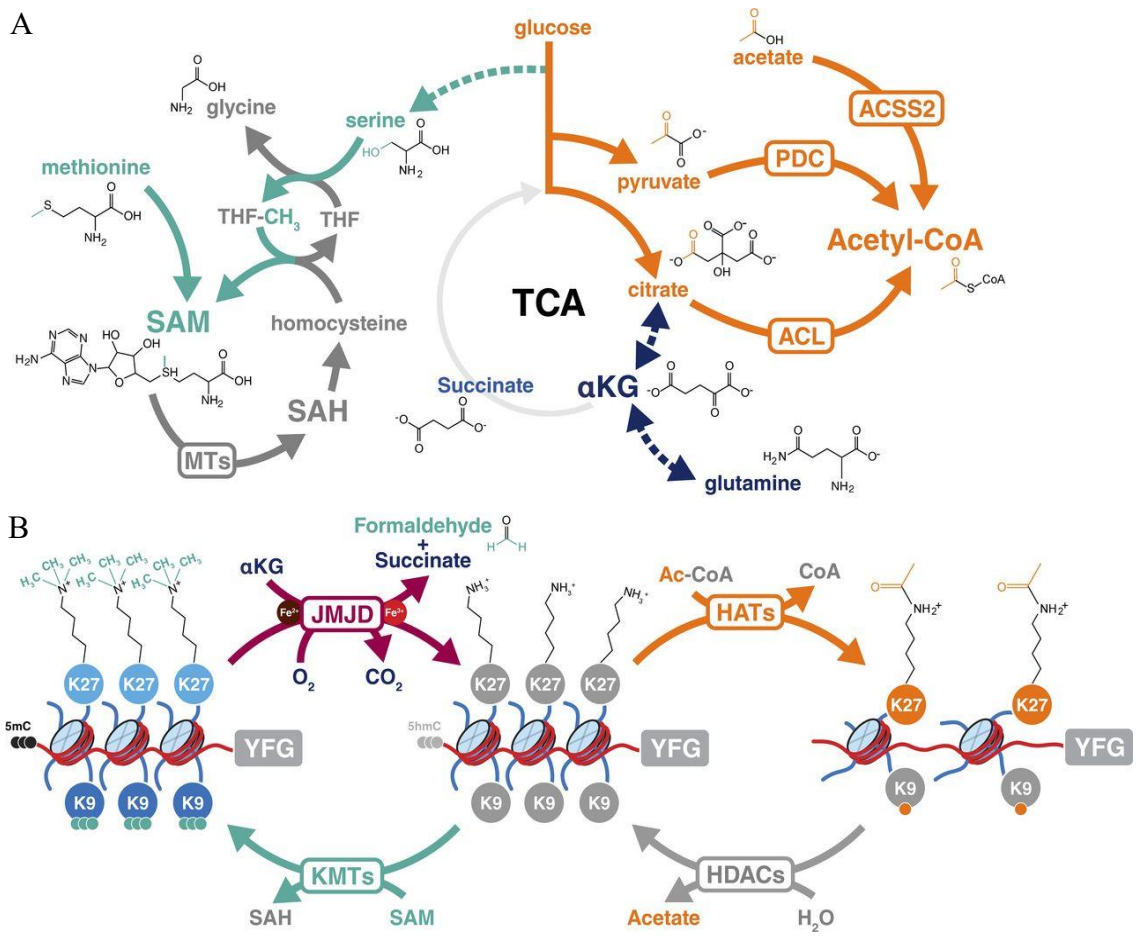

Figure 4: Metabolic pathways provide substrates for enzymes that modify chromatin (from [24]). A) Metabolic pathways implicated in the generation of carbon groups required for methylation (turquoise), acetylation (orange), or demethylation (dark blue) of chromatin. Tetrahydrofolate (THF); S-adenosylhomocysteine (SAH); methyltransferases (MT); pyruvate dehydrogenase complex (PDC) (B) Chromatin modification reactions that require intermediary metabolites. 5-methylcytosine (5mC); 5-hydroxymethylcytosine (5hmC); histone acetyltransferases (HATs); Jumonji-domain containing histone demethylases (JMJD); histone lysine methyltransferases (KMT); YFG, your favorite gene. SAM is the major methyl donor for methylation of cytosine bases in DNA and histone residues by DNA methyltransferases (DNMTs) and histone methyltransferase (HMTs), respectively. Acetyl-CoA is an essential substrate for acetylation of histone residues carried out by HATs.

As shown **Figure 5**, the glycolytic metabolism and TCA cycle in HSCs are interlinked with numerous metabolic pathways as glutamine metabolism, branched-chain amino acid (BCAA) catabolism (IDH-derived αKG can be transaminated to glutamate through the BCA transaminase-1 or 2 (BCAT1/2); *cf. infra*) or FAO[25, 26]. Notably, fatty acids are transported into the cells and are activated in the cytoplasm to Acyl-CoA. Fatty acyl-CoA enters the mitochondria where it is a substrate for FAO, generating acetyl-CoA that, like glucose, fuels the TCA cycle. FAO is utilized as an energy source by both HSCs and more-

committed progenitors to aid self-renewal and differentiation. Inhibiting FAO has been shown to reduce HSCs capability; the peroxisome proliferator-activated receptor delta (PPARδ), a transcriptional nutrient sensor and regulator and the FAO pathway, both downstream of PML, provide the required energy to allow for the proper execution of asymmetric (HSC-preserving) versus symmetric (HSC-exhausting) division[27].

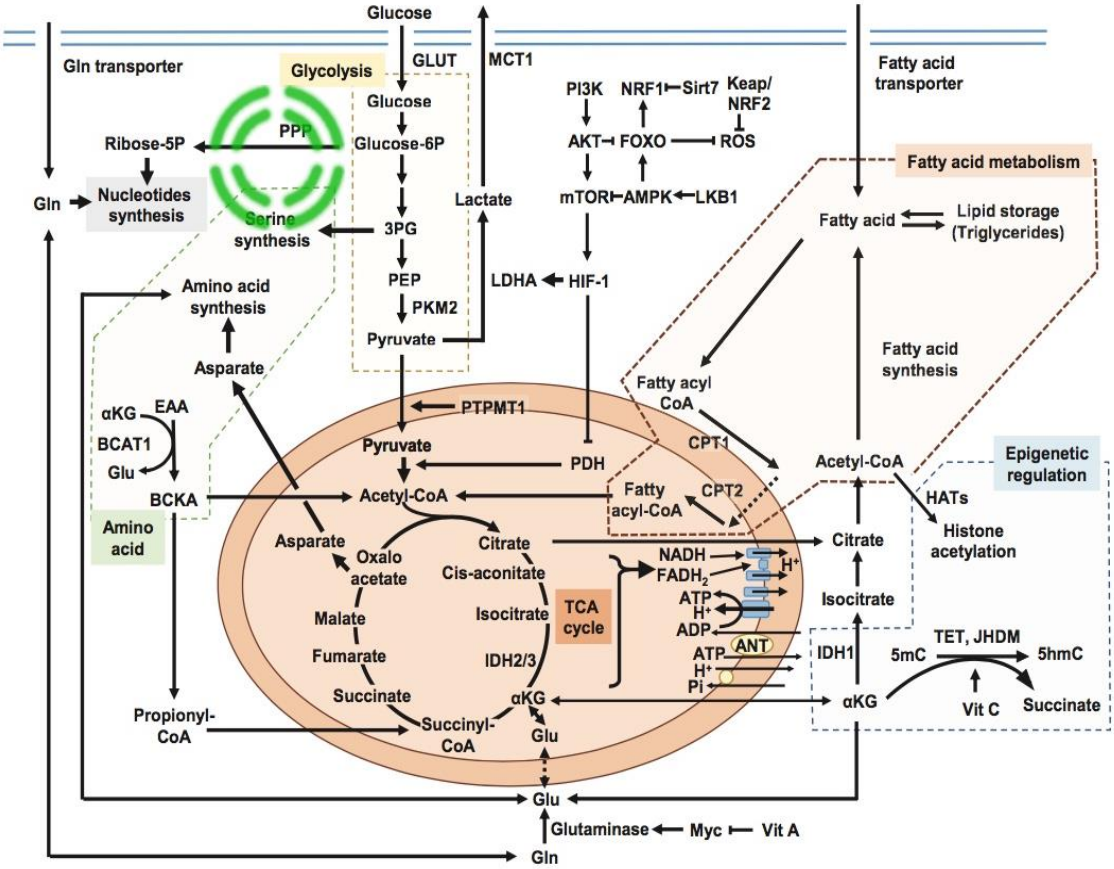

Figure 5: Overview of metabolic pathways contributing to HSC homeostasis and differentiation (from [28]). Metabolic pathways regulate various stem cell behaviors (e.g., self-renewal, migration, and differentiation) by modulating energy production through glycolysis or oxidative phosphorylation and by regulating the generation of metabolites, which can modulate multiple signaling pathways.

4.1.2.3 Nutrient sensing pathway: the mTORC1 signaling network

To respond to the status of energy and/or nutrient availability in the extracellular environment, HSC have several sensors responsible for maintaining cell homeostasis with the extracellular environment, such as the serine/threonine kinase AMP-activated protein kinase (AMPK), which senses cellular AMP levels and coordinates a metabolic switch from anabolism toward catabolism under energy deprivation conditions (as hypoxia or hypoglycemia). Compared to mature bone marrow cells, HSCs exhibit increased rates of

glucose consumption and lactate production, and decreased rates of OXPHOS and O_2 consumption[10]. The serine/threonine kinase LKB1 also balances proliferation and quiescence in HSCs by regulating cell survival, cell cycle progression and mitochondrial function[29]. Although LKB1 is known to limit cell growth in the absence of nutrients by phosphorylating AMPK, thereby inhibiting mTORC1 signaling (*cf. infra*), most of the effects of LKB1 on HSC homeostasis are independent of AMPK and mTORC1, but downstream effectors of LKB1 signaling include AMPK-related kinases.

Another important sensor is the mTORC1 complex (AMPK is one of the key regulators of mTORC1 activity in response to glucose) and is essential for HSC homeostasis. mTORC1 plays a central role in regulating the production of proteins, lipids, and nucleotides while also in suppressing catabolic pathways such as autophagy (reviewed in [30]); therefore mTORC1 controls the balance between anabolism and catabolism in response to environmental conditions, and coordinates cell growth and metabolism with environmental inputs including nutrients and growth factors (**Figure 6A**). mTORC1 also regulates mitochondrial functions as mitochondrial biogenesis, mitophagy, mitochondrial fission and/or fusion. The activity of mTORC1 is coordinated with the activity of the other amino acid-sensing kinase, i.e., the general control nonderepressible 2 (GCN2), whose function in HSC is not well defined.

While mTORC1 regulates cell growth and metabolism, mTORC2 instead controls proliferation and survival. The most important role of mTORC2 is likely the phosphorylation and activation of serine-threonine kinase AKT, a key effector of insulin/ PI3K signaling. AKT activation notably regulates the activity of FOXO transcription factors (FOXO1, FOXO3, FOXO4, and FOXO6) that participate in the transcription of genes involved in cell-cycle arrest, apoptosis, and detoxification of ROS (e.g., *p21*, *p27*, *BIM*, *PUMA*, *SESTRIN3*) which are detrimental for HSC[31]. AKT directly regulates the activity of glycogen synthase kinase 3 beta (GSK-3β), a kinase that modulates proliferation in response to various stimuli, and that is one of the subtypes of the serine/threonine kinase GSK3; AKT phosphorylates GSK-3β to an inactive form. Unexpectedly, mTORC2 signaling is regulated by mTORC1, due to the presence of a negative feedback loop between mTORC1 and insulin/PI3K signaling.

HSCs have a relatively low PI3K-AKT-mTOR activity compared to more mature cells or progenitors. Indeed, mTORC1 hyperactivation in HSC leads to HSC depletion through the

induction of multiple tumor suppressors, including cyclin-dependent kinase inhibitor 2A (CDKN2A/p16Ink4A), *TP53*, ROS production[32, 33]. In line, deletion of mTORC1 negative regulators, as phosphatase and tensin homolog (PTEN), tuberous sclerosis 1 (TSC1), promyelocytic leukemia protein (PML) and F-box/WD repeat-containing protein 7 (Fbxw7), results in similar observation such as HSC depletion through hyperproliferation and defective repopulating potential. Under stress, the AKT-mTOR upregulation is one of the major mechanisms driving dormant HSCs to cycle, thus meeting the demand of hematopoiesis. mTORC1 also responds to intracellular and environmental stresses incompatible with cellular growth (low ATP levels, hypoxia, or DNA damage)[30]. In summary, both hyperactivation and inhibition of the PI3K-AKT-mTOR impair HSC self-renewal and reduce the HSC pool thus resulting in hematopoietic diseases. (**Figures 6A and 6B**).

mTORC1 signaling is also strongly implicated in amino acid sensing (**Figure 6C**). mTORC1 senses both intra-lysosomal and cytosolic amino acids through several mechanisms that are not all coupled to the control of the Rag GTPase-mTORC1 axis. Cytosolic leucine, an essential amino acid, and arginine, signal to mTORC1 through a pathway comprising the GATOR1 and GATOR2 complexes. Under leucine, but not arginine, deprivation conditions, SESTRIN2 (a direct leucine sensor upstream of mTORC1) inhibits GATOR2 whereas leucine stimulation causes SESTRIN2 dissociation from GATOR2. SESTRIN2 is regulated by the stress-responsive activating transcription factor 4 (ATF4), which is activated by long-term amino acid deprivation and other cellular stresses[34]. Cytosolic arginine also activates mTORC1 through the GATOR1/2-Rag pathway by directly binding the arginine sensor CASTOR1 (cellular arginine sensor for mTORC1). Like SESTRIN2, CASTOR1 binds and inhibits GATOR2 in the absence of arginine and dissociates upon arginine binding to allow mTORC1 activation.

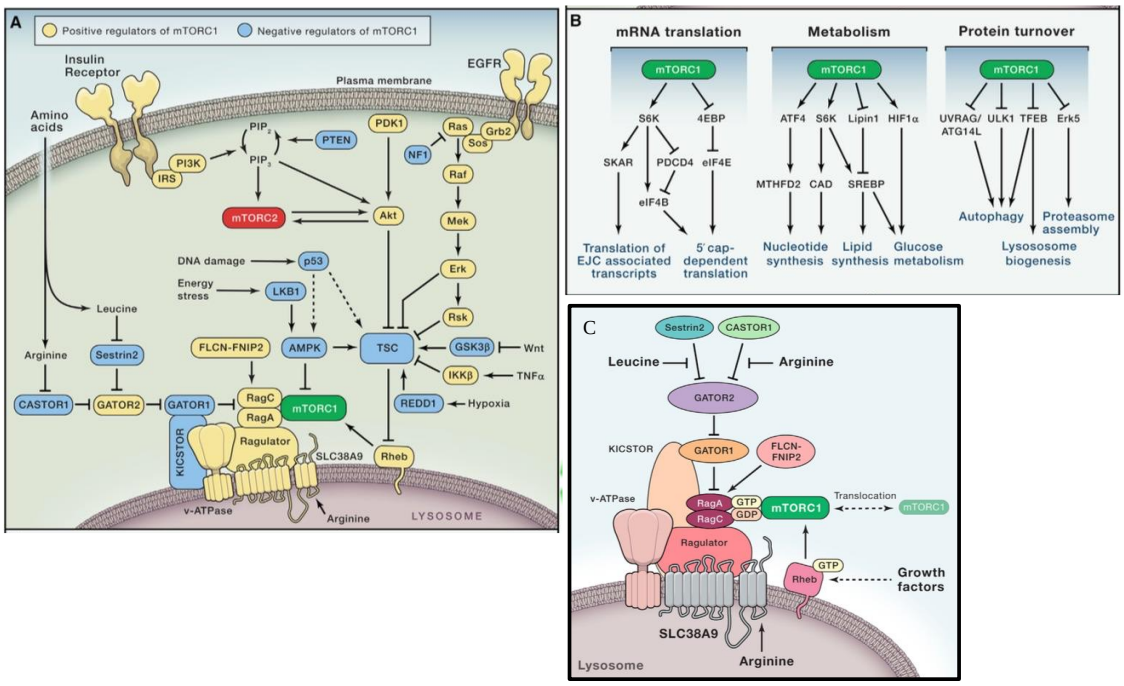

Figure 6: mTORC1 and mTORC2 serve as hubs to regulate many cellular processes and are central in growth factors and nutrients sensing in HSC (from [35]). (A) *Signaling pathways upstream of mTORC1 and mTORC2. Positive regulators of mTORC1 signaling are shown in yellow, negative regulators are shown in blue. The mTORC1 complex includes DEPTOR and PRAS40 (negative regulators) and RAPTOR and mSLT8 (positive regulators). mTORC1 is regulated by a complex of Ras-related GTPases (Rag) that control mTORC1 localization to the lysosomal surface in response to nutrient levels; Rag GTPases mediate also glucose sufficiency[36]. mTORC2 activity is primarily regulated by class IA PI3Ks. Following activation by upstream signals (growth factors, nutrient status, oxygen level) PI3K is recruited to the cell membrane where it converts phosphatidylinositol (4,5)-bisphosphate (PIP2) to phosphatidylinositol (3,4,5)-triphosphate (PIP3). PIP3 recruits 3-phosphoinositide-dependent protein kinase-1 (PDK1) and AKT to the plasma membrane where PDK1 activates AKT. The primary negative regulators of the PI3K-mTOR pathway are PTEN, TSC1 and TSC2. PTEN converts PIP3 to PIP2 and subsequently inhibits the recruitment of PDK1 to the plasma membrane. TSC2 is a GTPase-activating protein, and it is associated with TSC1 for inactivating the small G protein Ras homolog enriched in brain (Rheb). AKT phosphorylates TSC2, which results in binding of TSC2 to 14-3-3 and subsequent reduction in GAP activity of the TSC1/TSC2 complex. GTP-bound Rheb phosphorylates and subsequently activates mTORC1.* (B) *mTORC1 drives ATP-consuming anabolic processes necessaries for proliferation and growth (protein and lipid synthesis), controls ribosome biogenesis and several metabolic processes (for example, the OXPHOS; mTORC1 also increases the ATF4-dependent expression of methylenetetrahydrofolate dehydrogenase (NADP+ dependent) 2 (MTHFD2), a key component of the mitochondrial tetrahydrofolate cycle that provides one-carbon units for purine synthesis; mTORC1-dependent activation of sterol regulatory element-binding protein (SREBP) leads to increased flux through the oxidative pentose phosphate pathway (PPP)) and inhibits autophagy (for example, ULK1 is a kinase that forms a complex with ATG13, FIP2000, and ATG101 and drives autophagosome formation; the*

transcription factor EB (TFEB) drives the expression of genes for lysosomal biogenesis and the autophagy machinery). (C) *The nutrient sensing pathway upstream of mTORC1. mTORC1 activation is coupled to diet-induced changes in amino acid concentrations. Amino acids inside the lysosomal lumen alter the Rag nucleotide state through a mechanism dependent on the lysosomal v-ATPase, which interacts the Ragulator-Rag complex to promote the guanine-nucleotide exchange factor (GEF) activity of Ragulator toward RagA/B. The lysosomal amino acid transporter SLC38A9 interacts with the Rag-Ragulator-v-ATPase complex and is required for arginine to activate mTORC1. GATOR1 consists of DEPDC5, Nprl2, and Nprl3 and inhibits mTORC1 signaling by acting as a GAP for RagA/B. The KICSTOR complex (consisting of Kaptin, ITFG2, C12orf66, and SZT2) tethers GATOR1 to the lysosomal surface and is necessary for the appropriate control of the mTORC1 pathway by nutrients. GATOR2 is a complex comprising Mios, WDR24, WDR59, Seh1L, and Sec13 and is a positive regulator of mTORC1 signaling that interacts with GATOR1 at the lysosomal membrane. In addition to sensing leucine for its activation, CASTOR proteins were identified as a putative arginine sensor for the mTORC1 pathway, which is activated by extracellular arginine and interacts with GATOR2 and activate mTORC1 via promotion of the hetero-dimerization of GTP-RagA and GDP-RagC* [37].

Aminoacyl-tRNA synthetases are critical enzymes for protein synthesis by ligating amino acids to their corresponding tRNAs but also for protein homeostasis by sensing amino acid availability. Han and colleagues pinpointed that leucyl-tRNA synthetase functions as a leucine sensor for mTORC1 by its activity as a GTPase-activating protein (GAP) for RagD[38].

The mTORC1 complex also plays the major role in the regulation of protein translation. mTORC1 phosphorylates the ribosomal protein S6 kinase beta-1 (S6K1), also known as p70S6 kinase (p70S6K, p70-S6K) on its hydrophobic motif site, Thr389, enabling its phosphorylation and activation by PDK1. S6K1 activates several substrates that promote mRNA translation initiation, including eukaryotic translation initiation factor 4B (eIF4B), a positive regulator of the 5'cap binding eIF4F complex. mTORC1 also phosphorylates the eIF4E-binding protein 1 (4E-BP1) and promotes its dissociation from eIF-4E, thereby allowing eIF-4E to interact with eIF-4A and eIF-4G to accelerate the translation of cap-dependent protein. In line, mTORC1 supports mitochondrial biogenesis during erythropoiesis and mTORC1 inhibition leads to reduced red blood cell counts (**Figure 6B**)[39].

Summary points:

- HSC metabolism is regulated during differentiation; this regulation is based on hypoxia condition imposed by the bone marrow microenvironment and nutrients availability.
- HSC glycolytic metabolism is progressively shutdown during differentiation. The switch from aerobic glycolysis to OXPHOS is necessary and sufficient to recruit quiescent HSCs into hematopoiesis, and rapidly abolishes the self-renewal capacity of the cells. This switch allows energy production for biosynthesis proliferation.
- αKG production through IDH activity (TCA cycle) and glutaminolysis is associated to a wide range of physiological processes besides cellular metabolism.
- TCA is at the crossroads between energy metabolism and epigenetics and metabolite availability influence chromatin modifications and gene expression.

4.2 ISOCITRATE DEHYDROGENASE (IDH) ENZYMES

4.2.1 IDH metabolic properties

In all eukaryotic cell types except mature red blood cells, three different IDH paralogs exist. In the cytosol and peroxisomes, IDH1 (the *IDH1* gene is located in 2q33.3) catalyzes the oxidative decarboxylation of isocitrate to αKG with a highly unstable intermediate state (oxalosuccinate), and produces carbon dioxide (CO_2) while reducing cofactors $NAD(P)^+$ (used as electron acceptor) to NAD(P)H. This reaction is bidirectional as the reductive carboxylation of αKG to isocitrate oxidizes nicotinamide adenine dinucleotide phosphate (NADPH) to $NADP^+$ (**Figure 7**). IDH2 (gene located in15q26.1) catalyzes the same reversible reaction within the mitochondria. This reaction requires binding to a divalent metal ion, typically Mn^{2+} or Mg^{2+}.

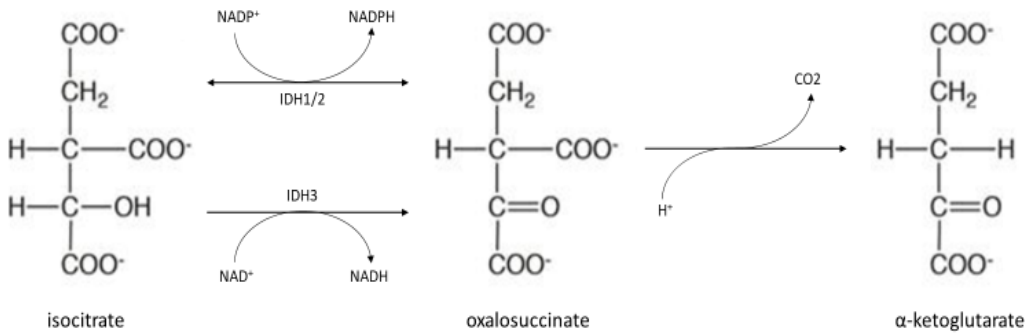

Figure 7: IDH1 and IDH2 enzymes catalyze a two-step reaction. First, isocitrate is oxidized to oxalosuccinate), with concomitant reduction of $NADP^+$ to NADPH. Second, oxalosuccinate losses its beta-carbonyl group, which is released as CO_2, giving rise to the formation of aKG. The IDH3-mediated reaction is unidirectional. The reverse reaction is a reductive carboxylation.

Most of the TCA is sustained inside the mitochondria, thus the contribution of IDH1 is less understood, except that the isoforms may facilitate cofactors accessibility in these different subcellular compartments.

At a protein level, IDH1 and IDH2 are both hetero-tetrameric enzymes with 2α:1β:1γ subunit ratio, that function as homodimers. The IDH1 and IDH2 polypeptides are very similar, with an overall of 42% sequence identity[40]. Despite differences in cofactor specificity and allosteric properties, IDH1 and IDH2 are much more closely related to the *E. coli* $NADP^+$-specific enzyme (approximately 32% residue identity) than are the yeast $NADP^+$-specific enzymes (less than 15% residue identity), suggesting a possible conservation of structure related to function in the TCA cycle[41]. The α and β subunits form a heterodimer (αβ) and the α and γ subunits form another heterodimer (αγ), which are assembled into a hetero-tetramer (α2βγ) and further into a hetero-octamer (the hetero-tetramer and hetero-octamer are sometimes called holoenzyme). The α subunit is essential for the catalytic activity whereas the β and γ subunits play regulatory roles in the α2βγ hetero-tetramer. The activity of the α2βγ hetero-tetramer is positively regulated by citrate and ADP and inhibited by ATP and NADH[42,43]. The active site, formed by the large and small domains of one subunit and a small domain of the other subunit, includes the $NADP^+$-binding and the intramolecular charge transfer (ICT)-metal ion-binding site (**Figure 8**). In order to initiate substrate binding, subunits defining the catalytically active site modify their structure as one transform into an asymmetric open conformation, while the other adopts a quasi-open conformation. The catalytically active enzyme is based upon ICT binding in a closed conformation.

Main IDH regulation is based on self-regulatory mechanisms through hetero-tetrameric interactions. In the inactive enzyme configuration, Asp^{279} occupies the isocitrate-binding site and forms hydrogen bonds with Ser^{94}. Isocitrate allosterically breaks the hydrogen bonds between these residues and enables Asp^{279} to chelate the metal ion which is necessary to reach the active enzyme configuration. However, IDH enzymes are also indirectly regulated by upstream substrates such as citrate; the α2βγ hetero-tetramer and αγ

heterodimer can be allosterically activated by citrate and ADP. Ma and colleagues reported that binding of the citrate induces significant conformational changes at the allosteric site, which are transmitted to the active site through the heterodimer interface, leading to stabilization of the isocitrate binding at the active site and activation of the enzyme[43]. The Lys[256] residue is also important for the catalytic activity, as it keeps the substrate binding pocket accessible for and enables binding of ICT; in line, Lys[256] acetylation reduces IDH2 activity[44].

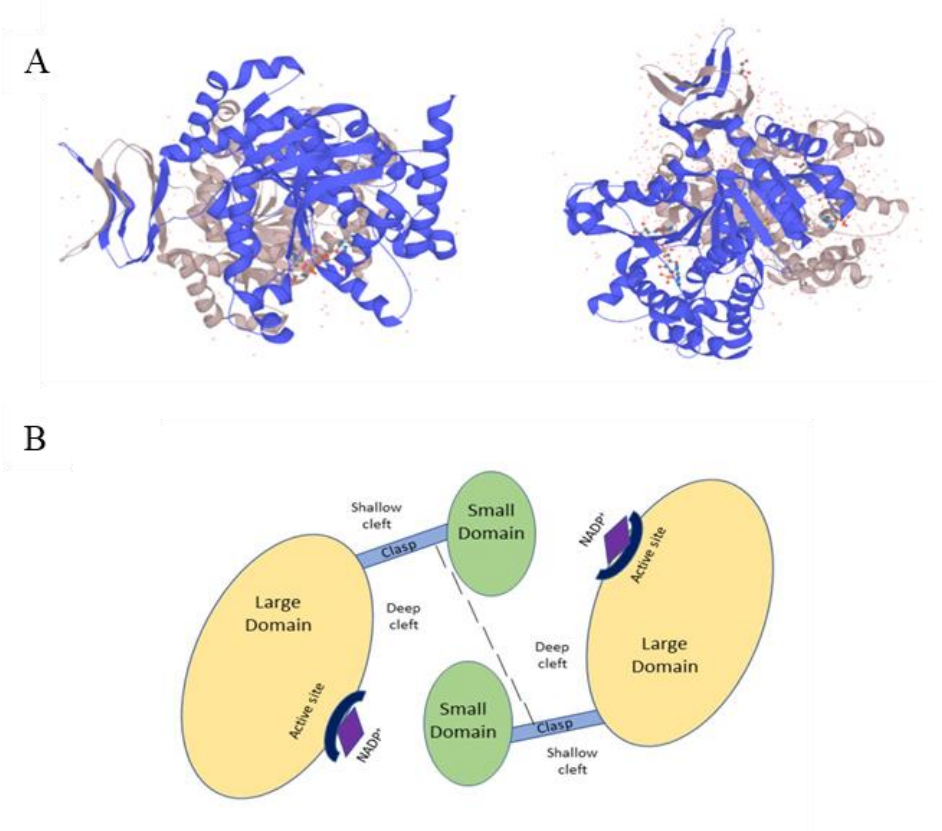

Figure 8: IDH1 protein secondary structure. A) IDH1 has 3 conformation states: an inactive open, an inactive semi-open, and a catalytically active closed conformation. IDH1 comprises two monomers which each consist of a large domain (residues 1–103 and 286–414,), a small domain (104–136 and 186–285) and a clasp domain (137–185). The clasp domain holds the two subunits together and define the catalytic active site. B) (from [45]) Simplified schematic representation of IDH1 in its inactive state (open). Two clefts are present on either side of the clasp domain: a shallow and a deep cleft. The deep cleft lies between the large and small domain of one monomer and the small domain of the second monomer. The deep cleft contains the active binding site for $NADP^+$. The two clasp regions join the two monomers together. In the inactive open conformation, Asp^{279} occupies the position where the isocitrate substrate normally forms hydrogen bonds with Ser^{94}. This steric hindrance is relieved in the active closed conformation.

IDH3 is a hetero-tetramer with two α-subunits (the *IDH3A* gene is located on 15q25.1–q25.2), one β-subunit (*IDH3B* gene on 20p13), and one γ-subunit (*IDH3G* gene on Xq28).

IDH3 is NAD-dependent and catalyzes the irreversible conversion of isocitrate to αKG while reducing NAD^+ to NADH[46]. This isoform is principally regulated by substrate availability (i.e., isocitrate and NAD^+) and inhibited by ATP and its products (i.e., αKG and NADH)[47]. Allosteric effectors are also involved in its activity such as calcium, ADP, and citrate that activate its catalytic activity, whereas ATP, NADH, and NADPH inhibit its activity[48]. Thus, when NADH or αKG levels are elevated (due to high mitochondrial energy level or elevated αKG production from glutamate and glutamine), mitochondrial ICT level increases due to IDH3 inhibition. The αKG produced by IDH3 is metabolized to succinate, and the NADH is used by the electron transport chain (ETC) to generate ATP [49]. When mitochondrial NADH/NAD ratio is high (i.e., due to high energy level), mitochondrial metabolites as citrate are exported to the cytosol to participate in anabolic processes (this process allows to shuttle citrate out of mitochondria instead of utilizing it by TCA cycle). IDHs play important roles in both the occurrence and the regulation of these processes.

The 3 IDH isoforms have overlapping but no redundant roles in metabolism including, but not limited to, mitochondrial OXPHOS, glutamine metabolism, lipogenesis, glucose sensing, and regulation of cellular redox status (**Figure 9**). IDH1 is involved in lipid metabolism (in addition αKG is a key factor in fatty acid production through reductive carboxylation, whereas IDH2 might be more involved in the regulation of oxidative respiration[50]. In addition, IDH1 is involved in glucose sensing. In mammalian pancreatic islets, Ronnebaum and colleagues showed that knockdown of *IDH1* results in impairment of glucose-stimulated insulin secretion and significant modification of lactate metabolism. This knockdown promoted glucose incorporation into fatty acids and glucose-induced increases in $NADPH/NADP^+$[51]. In this cycle, glucose-derived pyruvate enters the TCA cycle through pyruvate carboxylase, that catalyze the ATP– dependent carboxylation of pyruvate to oxaloacetate. Several enzymatic step conduct to isocitrate, that ultimately exits the mitochondria. IDH1 converts this isocitrate to αKG, thus producing NADPH. It is thought that αKG and/or NADPH promote insulin secretion, possibly by modulating αKG hydroxylases or voltage-gated potassium channels, respectively[52]. The potential role for IDH1 in glucose metabolism is also supported by IDH1 overexpression in mice models that induce overactive glucose-stimulated insulin secretion phenotype, fatty liver, hyperlipidemia, and obesity[53].

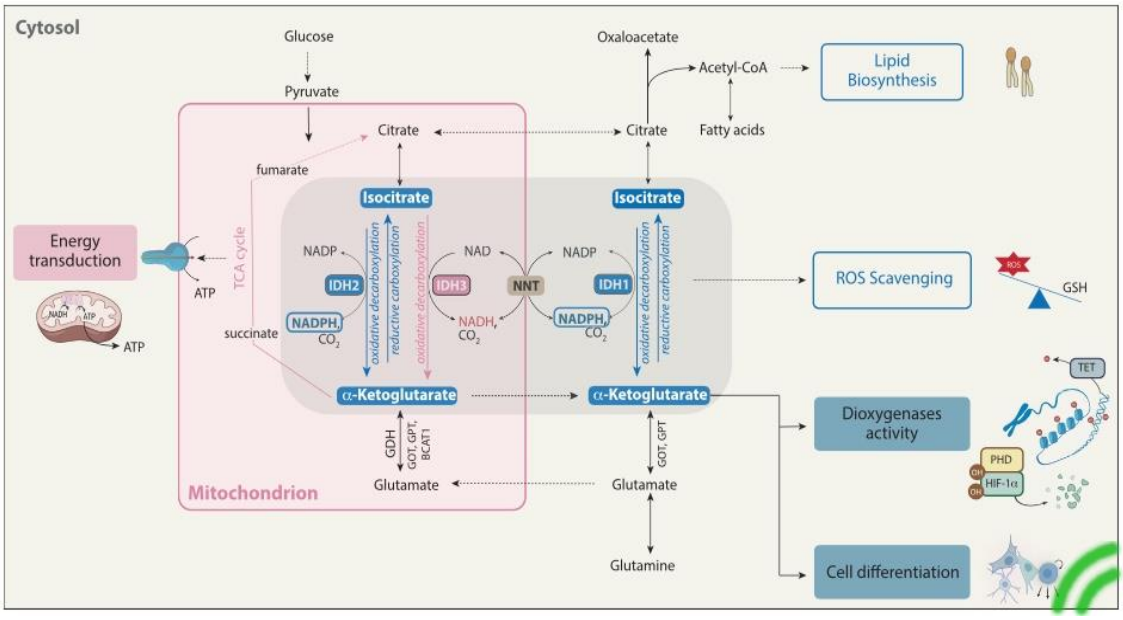

Figure 9: Metabolic properties of wild type IDH enzymes (from [54]). Depending on the isoform, the cofactor, and the localization, IDH enzymes are involved in different cellular processes including mitochondrial energy production, glutamine metabolism, lipogenesis, epigenetic profile, cell responses to hypoxia and cellular redox status. IDH1 and IDH2 are homodimeric $NADP^+$-dependent enzymes and catalyze the ATP-dependent carboxylation of pyruvate to oxaloacetate are localized in different cellular compartments. IDH1 is in the cytoplasm whereas IDH2 is expressed in mitochondria. In contrast, IDH3, also expressed in the mitochondria, uses NAD^+ as cofactor, forms heterodimers or hetero-tetramers composed of αβ and αγ subunits and works in an irreversible manner (which is the opposite for IDH1 and IDH2). Inside the mitochondria, metabolites are processed for energy generation, mostly through TCA and the production of NADH. NADH, rich in reduced electrons, is used by mitochondrial ETC to produce ATP. In the reductive carboxylation reaction, citrate is formed from isocitrate by ACO by reducing αKG and consuming CO_2. This reaction confers a tight regulation of cellular energy thanks to mitochondrial transhydrogenase enzymes. These enzymes are able to regulate mitochondrial NADH and NADPH interconversion for energy homeostasis but are also critical for fatty acids production in the peroxisome. As reactions catalyzed by IDH1 and IDH2 are reversible, the directionality relies the relative Km values of the forward oxidative reaction and the reverse reductive carboxylation reactions. The αKG/citrate ratio is also a critical determinant of glutamine-dependent reductive carboxylation, that is inhibited by $NADP^+$ and isocitrate levels.

The reductive carboxylation retains glutamine as a crucial growth-promoting nutrient when mitochondrial metabolism is impaired[55]; in cells with mitochondrial dysfunction, the malate dehydrogenase 1 (MDH1) reaction directly couples reductive carboxylation to glycolysis (**Figure 10**)[56].

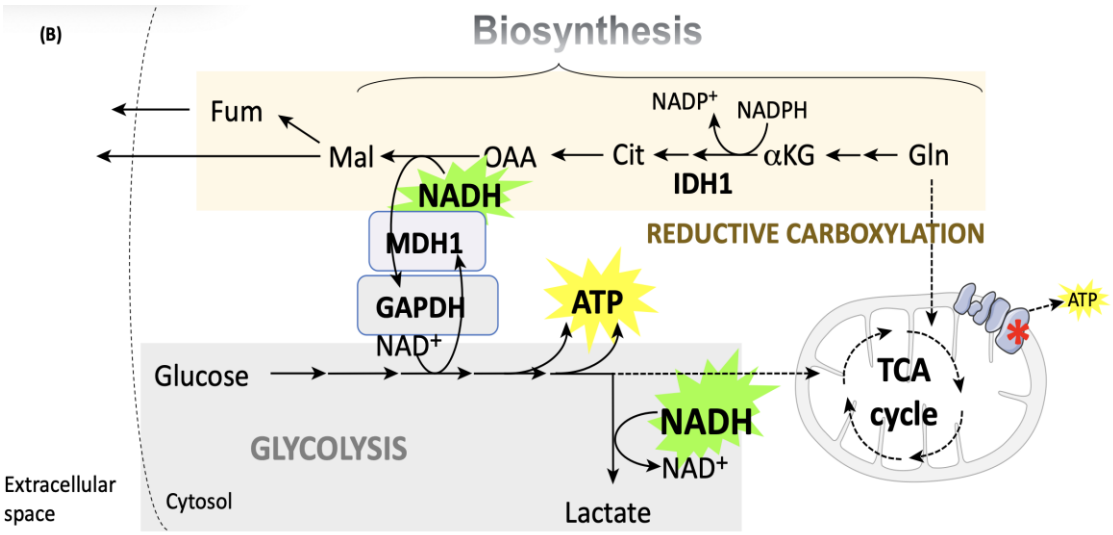

Figure 10: Relationship between mitochondrial function, reductive carboxylation, and glycolysis (from [19]). In the event of mitochondrial dysfunction, glutamine carbon metabolism is shifted to reductive carboxylation in the cytosol, providing oxaloacetate to fuel the MDH1 reaction and thus facilitate glycolysis.

In addition, IDH-dependent reactions produce NADPH, which is necessary for multiple cellular processes. NADPH is a key cellular reducing agent, required for detoxification processes through reduction of glutathione, thioredoxins, activation of catalase and cytochrome P450, which are all involved in the protection against ROS. NADPH is also involved in the breakdown of lipids for energy. By providing mitochondrial NADPH for NADPH-dependent antioxidant enzymes, IDH maintain a pool of reduced glutathione and peroxiredoxin. These molecules protect mitochondria from ROS-mediated oxidative damage (as lipid peroxidation and DNA damage), and from other stresses (heat shock, tumor necrosis factor-α (TNF-α) indicating that IDH are also important for cell stress responses. In line, Mailloux and colleagues have shown that IDH activity increases in response to a variety of oxidative stress, while activity of other TCA cycle enzymes, including αKG dehydrogenase (KGDH) and IDH3, decreases[57]. Park and colleagues have shown that IDH1 or IDH2 deficiency leads to increased lipid peroxidation, oxidative DNA damage, intracellular peroxide generation, and decreased survival after oxidant exposure and that overexpression of either IDH suppress ROS accumulation[58]. However, as the main source of NADPH comes from glucose 6 phosphate dehydrogenase (G6PD, a rate-limiting enzyme of the pentose phosphate pathway) activity in glycolytic state, IDH role in maintaining redox status might be only true in cells with unattenuated OXPHOS.

Although IDH1 and IDH2 play a crucial role in the defense against oxidative stress, they are inactivated by oxidation (i.e., lipid peroxidation products, ROS)[59,60]. This process is likely mediated by enzymatic modifications including glutathionylation in the presence of high levels of oxidized glutathione and non-enzymatic glycation in the presence of high glucose levels, as demonstrated in diabetic human and rat tissue[61,62].

Of note, specific *IDH* mutations cause loss of wild-type IDH functions, resulting in decreased NADPH and GSH levels and increased ROS levels, both in steady-state conditions and after induction of ROS production[63,64].

4.2.2 Transcriptional and post-transcriptional regulation

Transcriptional regulation of *IDH1* and *IDH2* genes is regulated by different sets of transcription factors : sterol regulatory element-binding transcription factor 1a (SREBP1a), activating transcription factor 6 (ATF6), CCAAT/enhancer-binding protein alpha (CEBPA), ectopic viral integration site 1 (EV1/MECOM1), GATA-binding factor 1 (GATA1) and signal transducer and activator of transcription 5B (STAT5B) for *IDH1*, and runt-related transcription factor 1 (RUNX1), myc-associated zinc finger-related factor MAZR/PATZ1, neurofibromin 1 (NF1) and SRY-Box Transcription Factor 9 (SOX9) for *IDH2*. The presence of a SREBP-binding element in the *IDH1* promoter region suggests that IDH1 activity is coordinately regulated with the cholesterol and fatty acid biosynthetic pathways, and that IDH1 may fuel the needs of these pathways in cytosolic NADPH. *IDH1/2* gene expression is also regulated by androgens, at least in prostatic tissue[65,66].

IDH are highly conserved over species. Phosphorylation of Ser^{113} on bacterial IDH directly impacts on enzyme activity (the phosphorylated enzyme is unable to bind isocitrate)[67,68]. Although this residue is conserved in eukaryotic proteins (Ser^{94}), there was no evidence of IDH phosphorylation in humans nor in any mammalian until recently[69]. Chen and colleagues showed that IDH1 functional activation involves phosphorylation at tyrosine residues (Y^{391} and Y^{42}) that implicate separate groups of kinase (**Figure 11**)[70]; this mechanism does not occur at the corresponding residues in IDH2 where tyrosine residues are replaced by phenylalanine. A different mechanism of regulation exist on IDH2, that notably implies acetylation of residue Lys^{413} that reduces IDH2 activity[71]; indeed, deacetylation by the mitochondrial deacetylase SIRT3 promotes IDH2 dimerization. Acetylation/de-

acetylation at residue Lys[256] is also a critical mode of IDH2 regulation. Deacetylation of Lys[256] by the mitochondrial deacetylase SIRT3 in response to caloric restriction activates IDH2 and leads to increased NADPH levels and reduced levels in glutathione in its reduced state (GSH) thus impairing the ability to scavenge ROS and increasing cellular susceptibility to oxidative stress[72]. Similar effects are observed upon IDH2 desuccinylation by SIRT5[73]. Regulation by distinct sirtuins suggests a crosstalk and/or synergy between different post-translational modifications. Glutathionylation of proteins by the reversible glutaredoxin (a thiol group transferase) reaction serves to protect against irreversible oxidation of cysteines; such protection has been demonstrated for IDH2 as oxidized glutathione (GSSG) inactivates IDH2 by forming a mixed disulfide bond with Cys[269] [74].

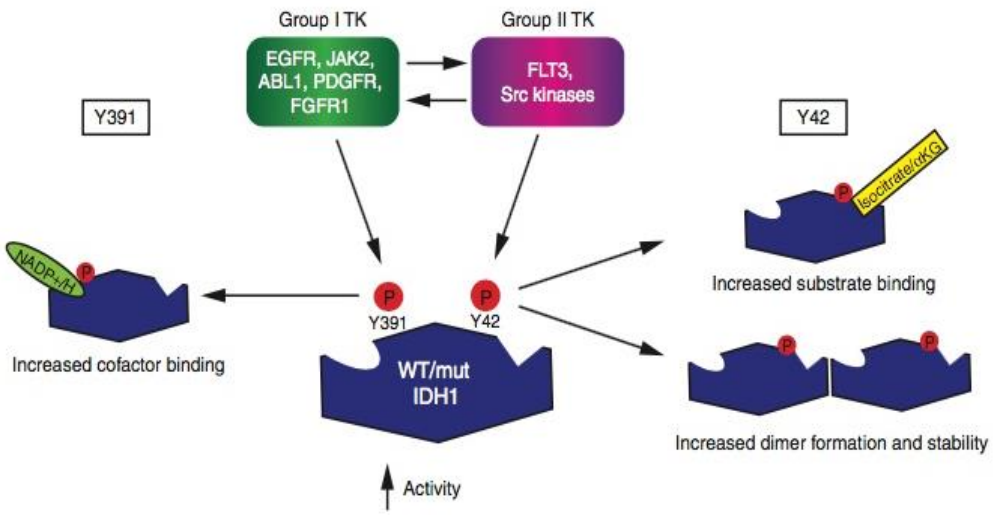

Figure 11: Regulation of IDH1 through phosphorylation (from [75]). Y^{42} phosphorylation occurs in IDH1 monomers, which promotes dimer formation with enhanced substrate (isocitrate or αKG) binding, whereas Y^{42}-phosphorylated dimers show attenuated disruption to monomers. Y^{391} phosphorylation occurs in both monomeric and dimeric IDH1, which enhances cofactor ($NADP^+$ or NADPH) binding. Tyrosine kinases (TKs) phosphorylate IDH1 at Y^{42} and activate Src to phosphorylate IDH1 at Y^{391}, which contributes to reductive carboxylation.

Altogether these observations establish a link between intracellular signaling and central metabolism and thus, couple energy and biomass provision to proliferation.

4.2.3 IDH in hematopoiesis

Self-renewal, lineage specification, and earliest differentiation of HSC are influenced by a variety of intra and extracellular signals (metabolic activity, nutrients, etc.). Metabolically

activated HSCs are poised to undergo lineage priming and produce different lineage-biased multipotent progenitors. Autophagy (that is activated in response to nutrient deprivation and other stressors to generate energy and allow survival) plays an essential role by clearing activated mitochondria to allow OXPHOS-driven HSCs to efficiently revert to a mostly glycolysis-based quiescence metabolism. Without autophagy, HSCs display an overactive OXPHOS-driven metabolism that promotes myeloid-biased differentiation and loss of stemness, likely as a direct consequence of epigenetic reprogramming[76]. These observations link metabolic reprogramming with epigenetic modifications in the control of HSC fate and engagement into myeloid lineages. In addition, one of the main regulators of gene expression during myeloid differentiation is histone and DNA methylation. αKG is an important metabolic intermediate that acts as a cofactor for several chromatin-modifying enzymes such as Fe(II)/αKG-dependent dioxygenase but also other αKG-dependent hydroxylase. Many dioxygenases are mandatory in hematopoiesis and myeloid differentiation such as histone demethylases Jumonji 2 (JMJD2), Jmj C domain-containing histone demethylase-1 (JHDM1), and the DNA demethylase TET2.

TET enzymes oxidize the methyl group of 5-methylcytosine (5mC) to yield 5-hydroxymethylcytosine (5hmC) and other oxidized methylcytosines, facilitating both passive and active demethylation which are detrimental mechanisms for chromatin modifications, gene expression and differentiation[77]. TET proteins, with the co-factors $Fe2^{+}$ and αKG, use oxygen to oxidize 5mC into 5hmC, generating CO^{2} and succinate as by-products (**Figure 12**). The enzymatic activity of TET can be modulated by additional factors. For instance, vitamin C (ascorbate) can enhance TET activity, potentially via reduction of the iron ion. TET proteins and 5hmC were identified/rediscovered almost 15 years ago. Increasing evidence has demonstrated the essential functions of TET enzymes in regulating gene expression, promoting cell differentiation, and suppressing tumor formation (reviewed in [78]). 5hmC in gene bodies and enhancers has been positively correlated with increased gene expression in various cell types. In the hematopoietic system, TET2-mediated demethylation occurs primarily at cell-type–specific enhancer regions; this process modulates enhancer activity and gene expression programs that are important for establishing cell identity and for differentiation. Interestingly, *Tet2* deletion results in global depletion of 5hmC at sequences bound by the insulator binding protein CCCTC-binding factor (CTCF), indicating that TET2 activity shapes the local chromatin environment at

enhancers. Numerous mice models have shown that conditional loss of TET2 activity leads to an expansion of the lineage negative Sca1$^+$ cKit$^+$ (LSK) cells, increased stem cell function such as self-renewal, and development of myeloproliferative neoplasms. Thus αKG availability (and IDH activity) directly impacts on myeloid differentiation by acting on αKG-dependent TET2 proteins. Collectively, these data argue for a direct contribution of IDH-driven signaling in the commitment to HSC differentiation.

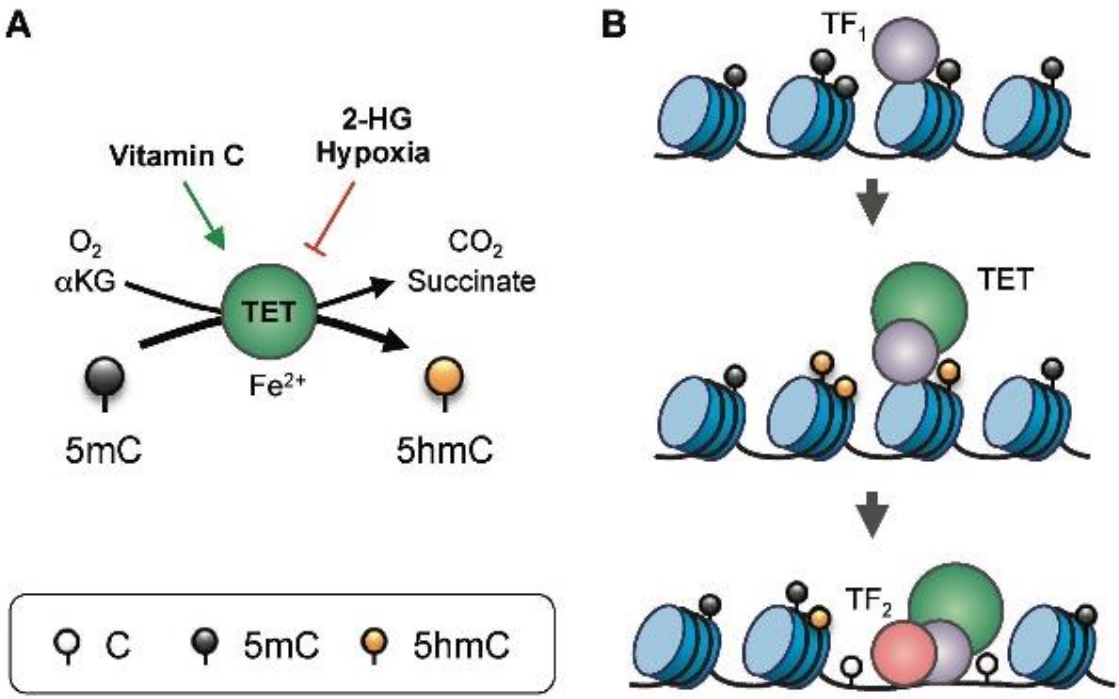

Figure 12: Gene regulation by TET proteins (from [78]). (A) Enzymatic activity of TET. TET proteins, with the co-factors Fe2$^+$ and αKG, use oxygen to oxidize 5mC into 5hmC, generating CO^2 and succinate as by-products ; lack of oxygen in hypoxia inhibits TET function. (B) Model of TET-mediated enhancer regulation. Prior to the commissioning of an enhancer, pioneer transcription factor (indicated as TF$_1$) binds to nucleosomal DNA and recruits TET which oxidizes the surrounding 5mC into 5hmC (and/or other oxi-mCs), facilitating DNA demethylation. TET proteins and TF$_1$ promote enhancer accessibility by recruiting nucleosome remodeling complexes, thus allowing binding of secondary transcription factors (indicated here as TF$_2$) that are otherwise inhibited by DNA methylation or the presence of nucleosomes.

The expression of *IDH1* and *IDH2* genes progressively increases during myeloid differentiation. *IDH* expression reaches a maximum level at the promyelocyte state and then decreases when reaching more mature forms such as polymorphonuclears and monocytes (**Figure 13**). Increase in *IDH* expression thus coordinates with metabolic rewiring from

glycolytic to OXPHOS. The increase of IDH enzyme activity and quantity translates into higher levels of αKG[23].

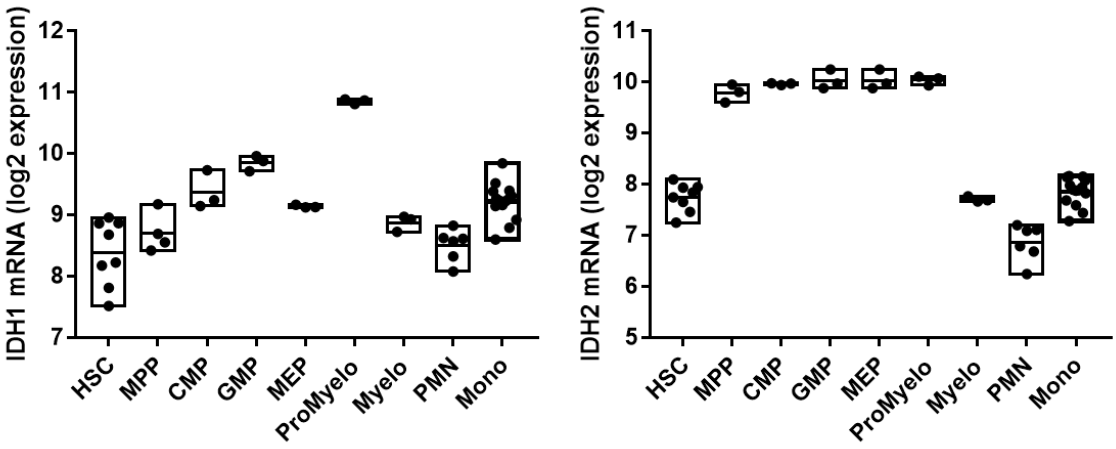

Figure 13: IDH mRNA expression in human hematopoietic different cell types. Gene expressions were from obtained from the Bloodspot database (www.bloodspot.eu). Common myeloid progenitor, CMP; granulocyte-macrophage progenitor, GMP; megakaryocyte/erythroid progenitor, MEP; promyelocytes, ProMyelo; myelocytes, Myelo; polymorphonuclear, PMN; Monocytes, Mono.

In the zebrafish model, *Idh1* knockdown induces blockade in myeloid differentiation, as evident by an increase in transcription factor PU.1/SPI1 expression, a decrease in myeloperoxydase (MPO) and significantly impaired terminal differentiation. However, *Idh2* knockdown also induces a blockade in myeloid differentiation but definitive hematopoiesis is not affected. As the *Idh1* knockdown phenotype is not rescuable by *Idh2* overexpression, non-redundant functions in the myeloid differentiation process are seemingly exert by Idh1 and Idh2 in this model[79].

Summary points:

- Among the canonical functions of IDH enzymes is the production of αKG, a mitochondrial key metabolite with pleiotropic activity

- Besides αKG production, the oxidative decarboxylation catalyzed by IDH enzymes leads to the formation of reducing equivalents, NAD(P)H, involved in ATP production, lipid synthesis, and antioxidant defenses.

- Reductive carboxylation retains glutamine as a crucial growth-promoting nutrient when mitochondrial metabolism is impaired.

- Wild-type enzymes are interesting actionable therapeutic targets.

4.3 ACUTE MYELOID LEUKEMIA

4.3.1 Epidemiology and classification

Acute myeloid leukemia (AML) is a disease marked by abnormal differentiation of the myeloid cell lineage. It is heterogeneous with respect to contributing factors, presentation and clinical outcome. According to data from the Institut de Veille Sanitaire, the frequency of AML is about 3 cases per 100,000 inhabitants, a frequency which increases with age to reach 20 per 100,000 at 70 years[80]. With a median age at diagnosis of 67 years old and an equivalent sex ratio, AML is characterized by recurrent molecular and cytogenetic abnormalities that led to modern clinical classifications[81,82]. These classifications stratify patients in specific prognosis subgroups and are used to decipher treatment strategies for patients eligible for intensive chemotherapy and/or HSC transplantation (HSCT)[83]. The ELN 2017 classification is actually the most commonly classification in clinical practice, which stratifies patients in 3 different risk groups: favorable, intermediate and unfavorable. This classification is essentially based on recurrent karyotypic abnormalities and some molecular markers as *CEBPA*, *nucleophosmin 1* (*NPM1*), *fms-like tyrosine kinase 3 with internal tandem duplication* (*FLT3-ITD*), *additional sex combs like 1* (*ASXL1*), *RUNX1*, or *tumor protein 53* (*TP53*)[84]. There is some limitations to this classification such as the absence of secondary type mutations type in risk stratification (e.g. *DNA* (*cytosine-5-*)*-methyltransferase 3 alpha* (*DNMT3A*), *serine and arginine rich splicing factor 2* (*SRSF2*), *splicing factor 3B subunit 1* (*SF3B1*)) or mutational interaction such as suggested by Papaemmanuil and colleagues[82]. Interestingly, after 60 years old, there are no major modifications among ELN risk group distribution under and beyond 70 years old, which is the same regarding *NPM1* and *FLT3-ITD* mutations distribution and cytogenetics, suggesting that other confounding factors (i.e. immune regulation, metabolism, secondary mutations) may also impact on survival[85]. Integrating secondary AML-like related gene mutations (*stromal antigen 2* (*STAG2*), *BCL6 corepressor* (*BCOR*), *U2 small nuclear RNA auxiliary factor 1* (*U2AF1*), *enhancer of zeste homolog 2* (*EZH2*), *zinc finger CCCH-*

Type, RNA binding motif and serine/arginine rich 2 (*ZRSR2*), *SF3B1, ASXL1* and *SRSF2*) identifies specific subset of high-risk patients ; this may improve the definition of high-risk older AML patients and improve older patients identification who derive survival benefit from HSCT in first remission[86].

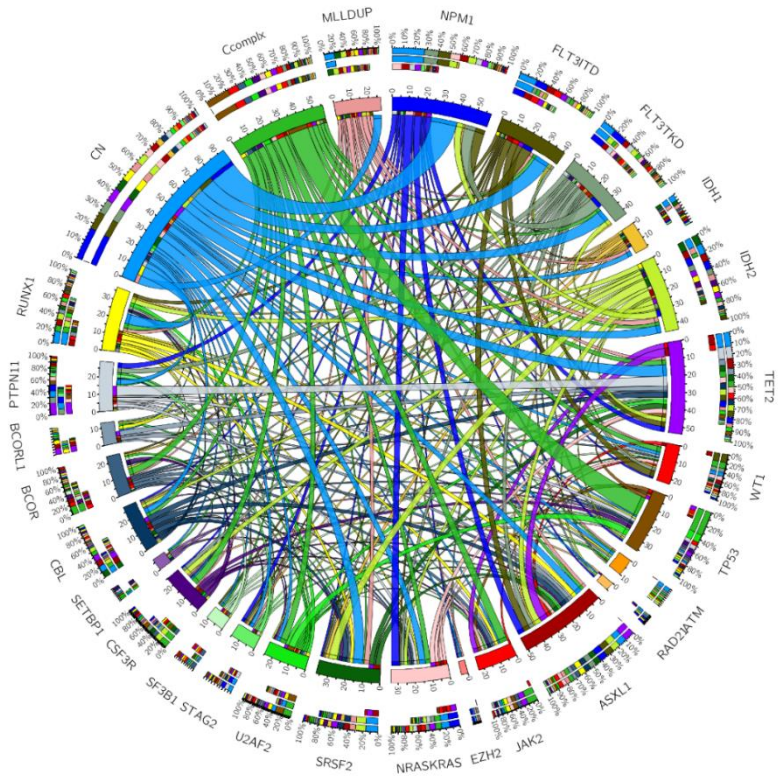

Figure 14: Mutations in AML. Circos plot represent mutation interaction in a cohort of 132 AML patients (median age: 58, range 18-75 years). Data have been collected retrospectively in intensively treated patients in Lyon Hospital center.

Combination of mutation contribute to the etiology of AML. Gene expression profiling identifies 16 transcriptional groups of patients with AML on the basis of their molecular signatures, correlated with the presence of chromosomal abnormalities (e.g., t(8;21), t(15;17) and inv(16)), driver mutations (*FLT3, RUNX1, CEBPA* and lysine methyltransferase 2A (*KMT2A*, formerly mixed lineage leukemia, *MLL*)), abnormal expression of the oncogene *MECOM1* and specimens with normal karyotype (NK)[87]. Furthermore, 11 mutational patterns emerge, each with distinct diagnostic features and clinical outcomes, that highlight the cooperation between somatic mutations. Class-defining lesions include mutations in genes regulating RNA splicing (*SRSF2, SF3B1, U2AF1* and *ZRSR2*) or regulating chromatin (*ASXL1, STAG2, BCOR, EZH2, KMT2A* and *PHD finger protein 6* (*PHF6*)) or both (18% of patients), complex karyotype alterations, cytogenetically visible copy-number alterations (aneuploidies) or a combination (13%) and $IDH2^{R172}$ mutations (1%) co-

associated with *NPM1* mutation[82]. *NPM1*-mutated AML is the largest class (27%), with patients also carrying mutations in DNA methylation or hydroxymethylation genes (*DNMT3A*, *IDH1*, *IDH2* and *TET2*).

Studies assessing the feasibility and benefit of treatment allocation based on cytogenetic and molecular results have been reported[88]. Examples of the successful development of precision medicines, such as targeted inhibitors of FLT3 (such as midostaurin and gilteritinib), IDH1 (ivosidenib), IDH2 (enasidenib), BCL-2 (venetoclax), as the development of monoclonal antibodies and cellular immunotherapies, represent the beginning of a paradigm shift that will reshape the approach to the treatment of patients with AML (reviewed in [84]). A Beat AML study was recently published, applying a precision medicine strategy where patients aged ≥ 60 years are matched to a therapeutic approach based on a full genetic and cytogenetic analysis (within 7 days) ; patients who were treated in a genetically defined subgroup had a lower early-death rate (30-day mortality rate of 3.7% vs. 20.4%) and improved overall survival (median OS, 12.8 vs. 3.9 months) compared with the group that received the standard-of-care treatment approach[88].

4.3.2 From clonal hematopoiesis to overt leukemia

4.3.2.1 Leukemic stem cells initiate and maintain the disease

AML arises through the sequential acquisition of somatic mutations, most initially occurring in the HSC compartment. Next generation sequencing (NGS) have revealed complex patterns of AML clonal organization and evolution during leukemogenesis. Samples from AML patients may show a hierarchical organization of the leukemic clones, with a rare fraction of leukemic stem cells (LSCs, generally defined as $CD34^{+}CD38^{low/-}CD123^{+}$) at the top of the hierarchy. LSCs are functionally defined as cells that are capable of initiating the disease when transplanted into immunodeficient animals. Analogous to how normal HSCs generate progenitors and mature blood cells, LSCs differentiate to give rise to leukemic progenitor cells (blasts) while also retaining some biological properties of HSCs, especially their self-renewal capacity. As an example, LSCs activate an AMPK/mitochondrial fission 1 (FIS1) pathway that inhibit differentiation and support self-renewal. In LCS, this axis drives mitophagy to degrade stressed mitochondria generated from oncogenic transformation while in normal HSCs it maintains stemness and regenerative

potential[76,89]. LSCs also highjack HSCs-specific pro-survival mechanisms to limit programmed cell death. For instance, LSCs rely on an overexpression of BCL-2 and/or myeloid cell leukemia sequence 1 (MCL1) anti-apoptotic proteins or functional inhibition of receptor interacting serine/threonine kinase 3 (RIPK3), a regulator of necroptosis and an inhibitor of inflammasome[90,91]. The overexpression of B-cell lymphoma 2 (BCL2) family members in LSCs represents an important driver of chemoresistance (reviewed in [92]).

Stemness properties are clinically relevant in human AML as stemness transcriptional signatures can predict therapy response; the prognostic significance of stemness transcriptional programs in LSCs has been recently confirmed at the single cell level[93]. In addition, leukemic AML myeloblasts can also adapt their energetic metabolism toward a high OXPHOS (as LSCs) to survive chemotherapy[94].

Upon treatment with conventional therapeutics, leukemic blasts while not LSCs are killed, allowing particular resistant LSCs, as quiescent LSCs located in osteoblast-rich areas of the bone marrow, to re-establish the disease. Quiescence is one of the main contributors to LSC drug resistance as conventional chemotherapeutics predominantly target dividing cells[95,96]. LSCs also aberrantly overexpress BCL-2 that positively regulates OXPHOS; in line, BCL-2 inhibition reduces OXPHOS and selectively eradicates quiescent LSCs[97]. In another hand, leukemic AML myeloblasts (bulk tumor) can also become LSCs if not eradicated by the therapy, by acquiring mutations conferring self-renewal capacity.

4.3.2.2 Premalignancy

Deep sequencing studies have evidenced that LSCs often emerge from a pool of "pre-leukemic" mutated HSCs or from their progeny, upon acquisition of additional mutations. Pre-leukemic HSCs are functionally defined by their ability to reconstitute a normal hematopoietic hierarchy in *in vivo* transplantation studies without obvious change in the lineage output of the hematopoietic system. In patient-derived xenografts (PDX), pre-leukemic mutated HSCs have a competitive repopulation advantage over normal HSCs. The fitness advantage relative to other clonal lineages is the defining feature of clonal hematopoiesis (CH). It has been demonstrated that part of the population (3% before age 50, up to 15% after age 70) develops CH. During the course of human ageing, gain mutations in HSCs could be driven by erroneous DNA repair and age-associated single-base

substitutions; this finding has been termed age-related clonal hematopoiesis (ARCH). CH is very common in the elderly, trending toward inevitability[98]. CH can be subcategorized according to the gene and mutation subtype involved, etiology and clinical features, including age, blood-count effects and associated comorbidities. A recent analysis of non-cancer cohorts has identified CH at both hotspots and non-hotspots in children, indicating a need to also explore CH in younger-age cohorts[99].

Since HSC accumulate mutations by cell-cycle independent mechanisms, founder mutations might also arise in quiescent HSCs (reviewed in [100]). It is assumed that mutations that promote self-renewal, proliferation, and/or reduced cell death will lead to the expansion of a mutated HSC clone at a disproportionate rate compared to other clones. For instance, the *TET2* and *DNMT3A* mutations known to disrupt HCS self-renewal programs in mice models, are among the most common early lesions found in pre-leukemic HSCs. From recent data, *DNMT3A*, which encodes a *de novo* DNA methyltransferase that catalyzes the methylation of cytosine bases in CpG dinucleotides, is the most frequently mutated gene in CH. Pre-leukemic HSC exist at diagnosis, can survive chemotherapy and can be present at clinical remission, and accumulating evidence indicate that refractoriness to chemotherapy and disease relapse can occur as a result of *bona fide* pre-leukemic HSC clones having acquired additional driver mutations and having been transformed into new LSC clones[99,101,102].

Individuals with CH are at greater risk for progression to blood cancers, response to chemotherapies[103,104], bone marrow transplant[105–107], and increased mortality from non-hematological cancers through cell-non-autonomous effect[108,109] and cardiovascular disease (atherosclerosis and myocardial infarction; *cf. infra*). The association of CH with the subsequent development of diseases has led to the use of term "clonal hematopoiesis of undetermined potential (CHIP)" [110]. ARCH and CHIP are technical findings, not diseases, characterized at the molecular level by the presence of a low-variant allele fraction (VAF) of above 2% ; they constitute an at-risk clinical entity (reviewed in [110–116]). CHs associated with chromosomal alterations have also been studied and shown to be associated with the development of hematologic diseases , including lymphoid malignancies, with distinct categories of genetic abnormalities enabling to stratify the risk of incident myeloid and lymphoid malignancies[111,112].

Individuals with CH are at greater risk for hematological malignancies such as AML, myeloproliferative neoplasms (MPN), or myelodysplastic syndrome(MDS)), at an estimated rate of 0.5%-1.0% per year compared to <0.1% for non-CH controls. The risk of AML in CHIP/ARCH patients is mutations specific, i.e., defined by the nature of the lesion, the subclonal abundance, and the VAF (reviewed in [113]). This risk is not the same for all patients with CH and increases with the size of the clone and clonal complexity; this latter can be assessed by the number of mutations[108,109]. CH-associated *DNMT3A*, *TET2* or *ASXL1* mutations are linked to a low risk of progression to AML and their persistence during complete remission after induction therapy does not have prognostic value for relapse[114–116]. By contrast, CH lesions such as mutations in *TP33, U2AF1*, *IDH1* or *IDH2* impart a relatively high risk of subsequent AML (although there are some differences between the above mentioned studies mainly because risk is related to both nature of the lesion and VAF), allowing the identification of high-risk mutational signatures that can predict with high confidence CH progression to AML with a median of 6 to 10 years prior to disease onset[113,114]. Both conditions, clonal hematopoiesis and myeloid malignancies, are strongly associated with age, further supporting a mechanistic link.

Recently, Watson and colleagues investigate the clonal architecture and evolutionary dynamics of healthy blood by analyzing targeted DNA sequences of ~50,000 blood cancer–free individuals and positive selection for beneficial mutations, rather than neutral genetic drift, was found to dictate the genetic diversity of normal blood[117]. Moreover, this study has defined the fitness of key CH driver genes (**Figure 15**) and has also showed that highly fit variants confer an increased risk of AML. In the future, combining this framework with studies that will track individuals over time will shed light on how CH lesions acquire further mutations that drive overt disease.

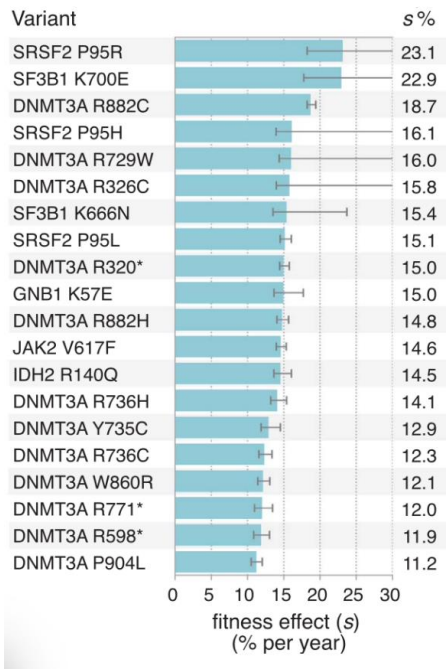

Figure 15 : The fitness landscape of CH variants (from [117]). *Inferred fitness effects and mutation rates for the top 20 most commonly observed CH variants. Error bars represent 95% confidence intervals.*

Interestingly, the recent (yet unpublished) examination of the molecular consequences of *DNMT3A*^{R882} mutation in primary CD34^{+} cells in human CH at the single cell level reveals differentiation skewing, even before clinically observable changes in blood counts, and notably a myeloid over lymphoid bias, in line with the strong association of this genotype with myeloid versus lymphoid neoplasms, and the preferential hypomethylation of PRC2 targets[118].

When using 0.0003% VAF lower threshold, almost 95% of healthy individuals over 50-60 years old possess AML-related mutations[119]; as ARCH /CHIP mutations collectively are "weak drivers", progression from ARCH to MPN or MDS/AML is probably selected upon specific conditions (bone marrow niche degradation, decline in HSC functions for instance, immune anergy). As examples, a tumor necrosis factor (TNF)a-driven inflammatory context favors *Tet2* mutant CH and chemotherapy drives protein phosphatase $Mg2^{+}$/$Mn2^{+}$ dependent 1D (PPM1D) mutant CH[119,120]. In addition, as disease phenotypes differ upon CH, the subsequent mutations acquired by the CH clone might play an instructive role in dictating disease phenotype. In AML, activation of emergency hematopoiesis pathways and inhibition of differentiation drive disease development [122]. The

microbiome may also impact ; in *Tet2*-deficient mice, microbial systemic inflammation through increased IL-6 production leads to severe myeloproliferation, extramedullary hematopoiesis and splenomegaly that mimic a pre-leukemic myeloproliferation[123].

CH is also a strong risk factor for therapy-related (t-) myeloid neoplasms. The highest risk of therapy-induced expansion is seen in CH with damage repair (DDR) variants, specially *TP53*, *PPM1D* (which is part of a regulatory feedback loop with *TP53*) and *CHEK2*, and in patients receiving radiation, platinum, or topoisomerase II inhibitor therapy for unrelated malignancies[124]. In line, Wong TN and colleagues also showed that preexisting mutant HSC clones carrying *TP53* mutations seemingly selectively expand under the pressure of cytotoxic therapy and cause t-AML and t-MDS several years later with the acquisition of subsequent mutations[105]. Another study has shown that in patients treated for solid cancers, CHIP mutations are more prevalent than in populations not selected for cancers[125]. The mechanism of selection for *TP53*- and *PPM1D*-associated clones differs from *DNMT3A*- and *TET2*-associated clones, as *TP53* and *PPM1D* mutants are at particularly high risk of expansion and progression in patients receiving radiotherapy or chemotherapy.

4.3.2.3 CH increases all-cause mortality and the risk of cardiovascular disease

The link between CHIP, cancer treatment and specific gene mutations has been defined in a seminal study by Coombs and colleagues where data of paired tumor and blood samples from 8810 individuals were used to dissect the role of CHIP in patients with solid tumors[125]; different patterns of clonal evolution have been now identified in case of therapy related-myeloid neoplasms development after anti-cancer treatment exposure[126].

In the case of atherosclerosis, carriers of CH have about a 2-fold increased risk of coronary heart disease[127]. *TET2*-associated CHIP represents a vascular risk driven by interactions between clonal monocytes-macrophages and the endothelium, as *TET2*-mutant monocytes promote inflammation (the pro-inflammatory effects of *Tet2* loss-of-function mutations have been established in mice[128]. Mice models have shown that *Tet2*-deficient macrophages exhibit an increase in NOD-like receptor family pyrin domain containing 3 (NLRP3) inflammasome-mediated interleukin-1b (IL-1β) secretion through a mechanism that is independent of Tet2 catalytic activity infiltrate myocardium and traffic to atherosclerotic plaques leading to cardiovascular injury (**Figure 16**)[109,128]. Moreover, recent

studies have also shown that in both atherosclerotic mice and patients with atherosclerosis harboring *TET2* or *DNMT3* mutation, HSC proliferation rates are increased (evidenced by HSC shorter telomeres) driving leukocytosis (elevated levels monocytes, neutrophils and platelets), a factor associated with atherosclerosis[130]. Together, these interactions potentiate themselves to generate more atherosclerosis and enforce CHIP evolution. Designing strategies to target *TET2* loss-of-function mutations could potentially be considered for attenuate cardiovascular disease[129].

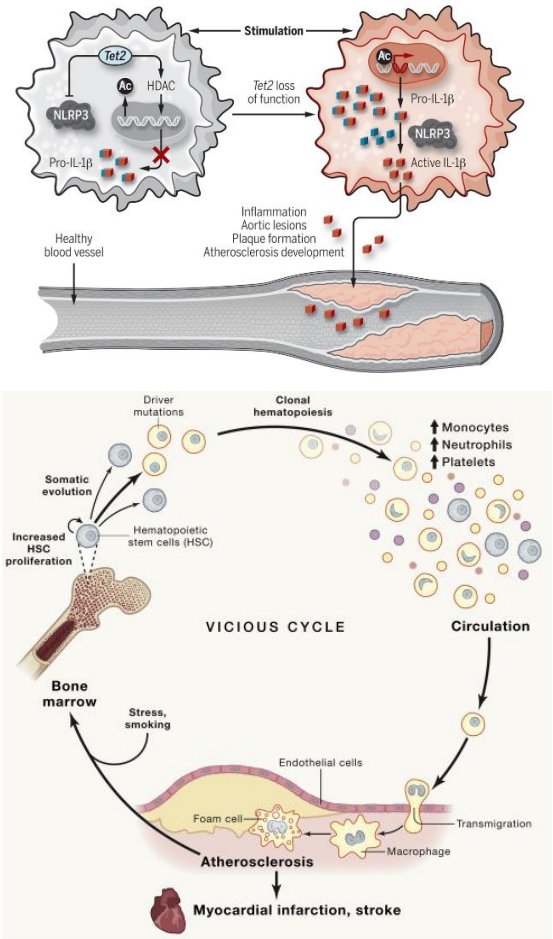

Figure 16: TET2-associated CHIP promotes atherosclerosis. Upper panel: TET2 influences IL-1β production in multiple ways that are independent of its catalytic abilities [131]. Lower panel : A model linking atherosclerosis, increased hematopoiesis, clonal proliferation, and leukocytosis (from [132]).

Mutation causing ARCH are not necessarily identical to those present in pre-leukemic HSCs, driving leukemia and/or relapse[101,132]. Even though ARCH/CHIP cases are characterized by the association at high significance with mutations that have previously been seen mutated in myeloid neoplasia (i.e. *TET2, DNMT3A, ASXL1, SF3B1, PPM1D* and *TP53*), they could also exist in the absence of any mutations in candidate drivers or in the presence of mutations yet not referenced in the COSMIC catalog[98,108]. Recently, germline genetic variations within the *TERT* and *TET2* loci have been identified, that shape HSCs function, leading to CHIP through mechanisms that are specific to CH ; these data and others highlight the importance of the germline context[133,134].

Understanding the phenotypic consequences of ARCH/CHIP-related lesions and of CH expansion remains an intense area of investigation. Multiple mechanisms and factors account for the etiology of CH, for its expansion and for progression to overt malignant hematopoietic diseases, such as genetic predispositions (reviewed in [134]), intrinsic pathogenic effects of the somatic lesions, metabolic reprogramming of pre-leukemic HSCs by stromal niche cells (reviewed in [136]), factors as inflammation exposure providing genomic instability, anergic immune system and chronic systemic inflammation (reviewed in [136,137]), cellular states, epigenetic profiles, spatial distributions and interactions with the microenvironment (**Figure 17**)[139]. As an example, Fennelle and colleagues recently evidenced two non-genetic transcriptional signatures that participate in malignant clonal dominance: the repression of antigen presentation (downregulation of $\beta_2$microglobulin (*B2m*)) which suggests that clonal fitness might be related to the capacity of the cells to remain hidden from the immune system, and the increased expression of secretory leukocyte peptidase inhibitor (*Slpi*) that has anti-inflammatory functions. These signatures are present both in leukemia-initiating cells and in overt AML disease, indicating that they are mitotically heritable and not acquired during disease progression. In addition, some of the fittest clones have a gene-expression signature reminiscent of LSC, providing a clue to how these heritable identities provide an advantage[140].

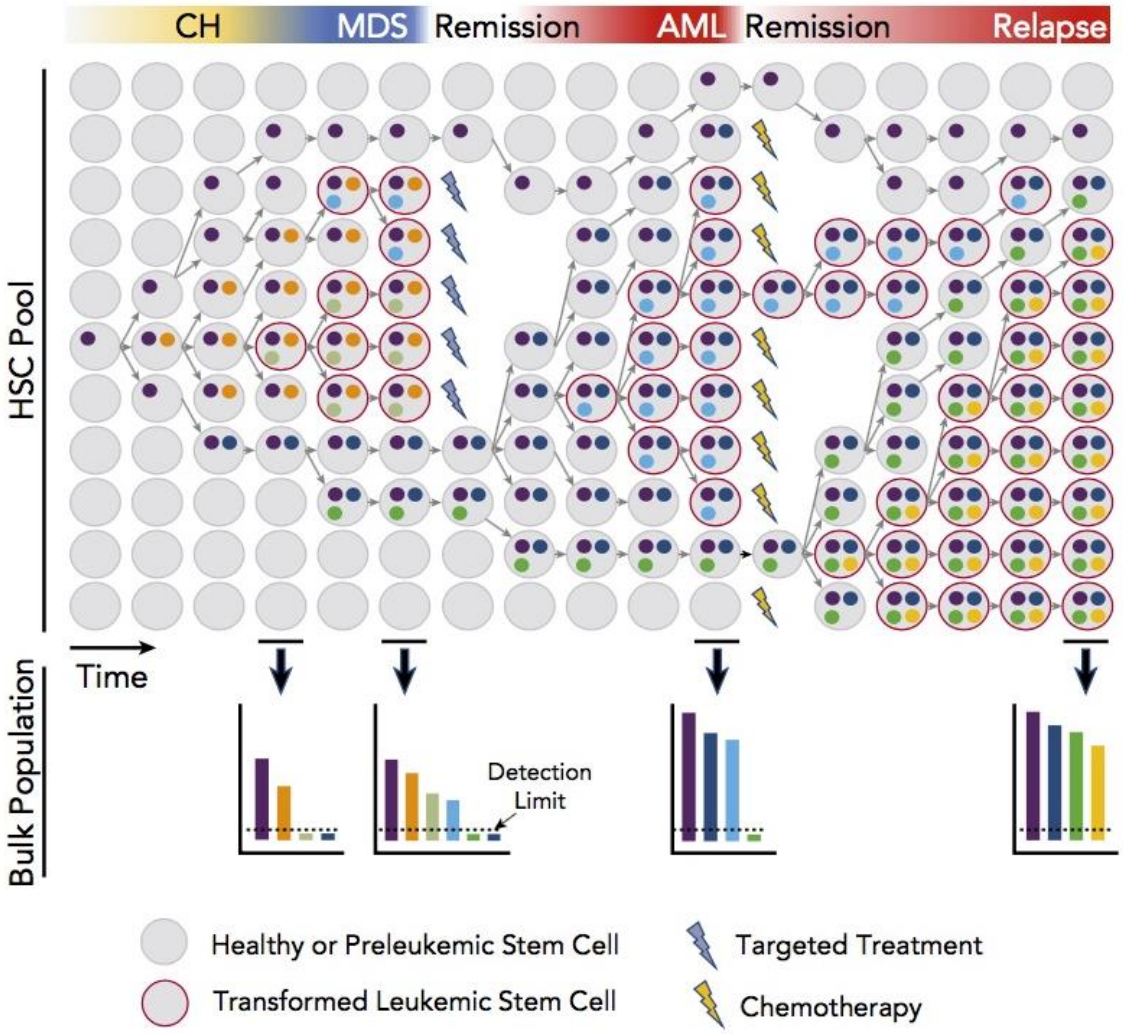

Figure 17 : Model of clonal evolution leading to AML pathogenesis and progression (from [113]). The presence of CHIP/ARCH and/or pre-leukemic HSCs is established in a proportion of AML patients. Besides TP53- or post-CH-driven AML, other AML subtypes (defined as pan-AML/de novo AML) might arise from more punctual oncogenic events such as translocations (e.g. KMT2A translocations) or selective mutations (e.g. NPM1/FLT3-ITD mutations)[141].

The presence of CHIP/ARCH and/or pre-leukemic HSCs confers a new paradigm for the management of AML relapse as the characterization of disease molecular features will also impact the choice of post-induction or post-consolidation therapy[141,142]. The increasing frequency with which people with CH are identified and the need for counseling these patients is driving many institutions to create specialized clinics[144].

4.4 ISOCITRATE DEHYDROGENASE MUTATIONS IN AML

The biology of cancer-associated isocitrate dehydrogenase mutations have been extensively reported[145–148]; an extensive bibliography on the development of small molecule targeted inhibitors, which inhibit the D-2HG oncometabolite is also included in the attached review.

Together with the mutations *in succinate dehydrogenase* (*SD*) and *fumarate hydratase* (*FH*), *IDH* mutations link deregulation in central carbon metabolism to tumorigenesis. *IDH* mutations are prevalent in grade II and III gliomas (>70%) and secondary glioblastomas (55%-88%), in cartilaginous and bone tumors (20%-80%), intrahepatic cholangiocarcinoma (6%-30%) and are also found in myeloid malignancies i.e., in a minority of myelodysplastic syndromes (MDS) and accelerated myeloproliferative neoplasms (MPN), in AML (15%-20% *de novo* AML), and peripheral T-cell lymphomas (AITL) (**Figure 18**).

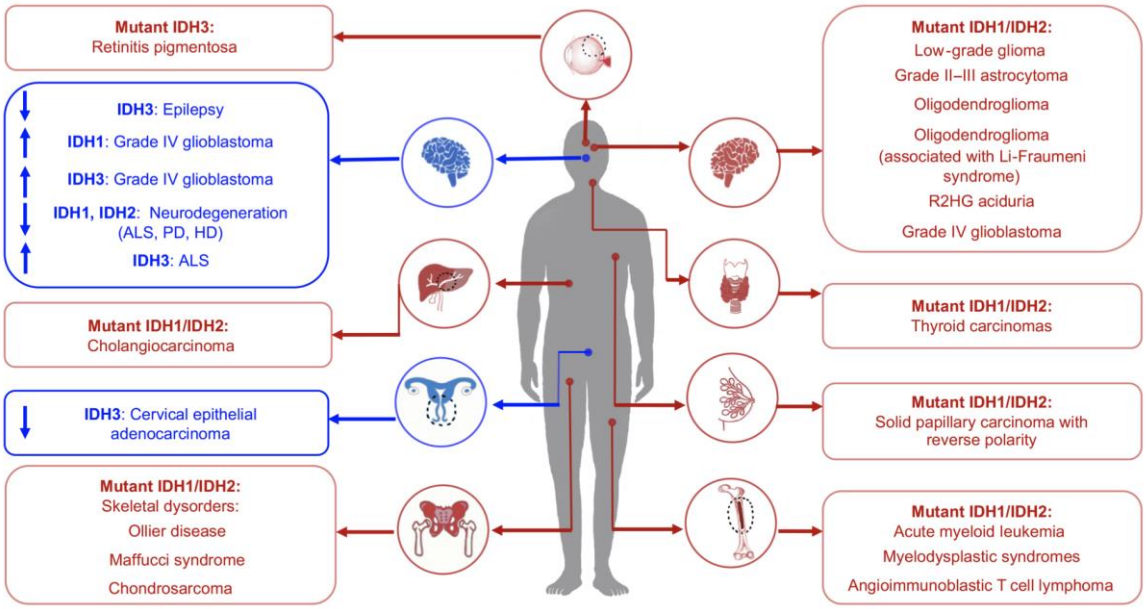

Figure 18: Mutations in IDH genes have been identified in more than 20 different neoplasms (from [145]). Overexpression or downregulation of wild-type IDHs (shown in blue) have also been observed.

The impact of *IDH* mutations on AML prognosis remains controversial, although a generally inferior outcome is seen with *IDH1* mutations and a relatively favorable prognosis may be seen with *IDH2* mutations, particularly $IDH2^{R172K}$ mutations, in the setting of standard intensive chemotherapy. *IDH* mutations are associated with specific patient and

disease characteristics notably an older age at presentation (**Figure 19**), diploid, or other intermediate-risk cytogenetics (i.e., trisomy 8), genetic lesions (*SRSF2*, *DNMT3A*, *NPM1*, *MLL* partial tandem duplications, *FLT3-ITD*) and a sustained platelet count at presentation. The impact of *IDH* mutations is thus context dependent, with *IDH* mutations that occur in the setting of *NPM1* mutations (without *FLT3-ITD*) appearing to confer more favorable outcomes.

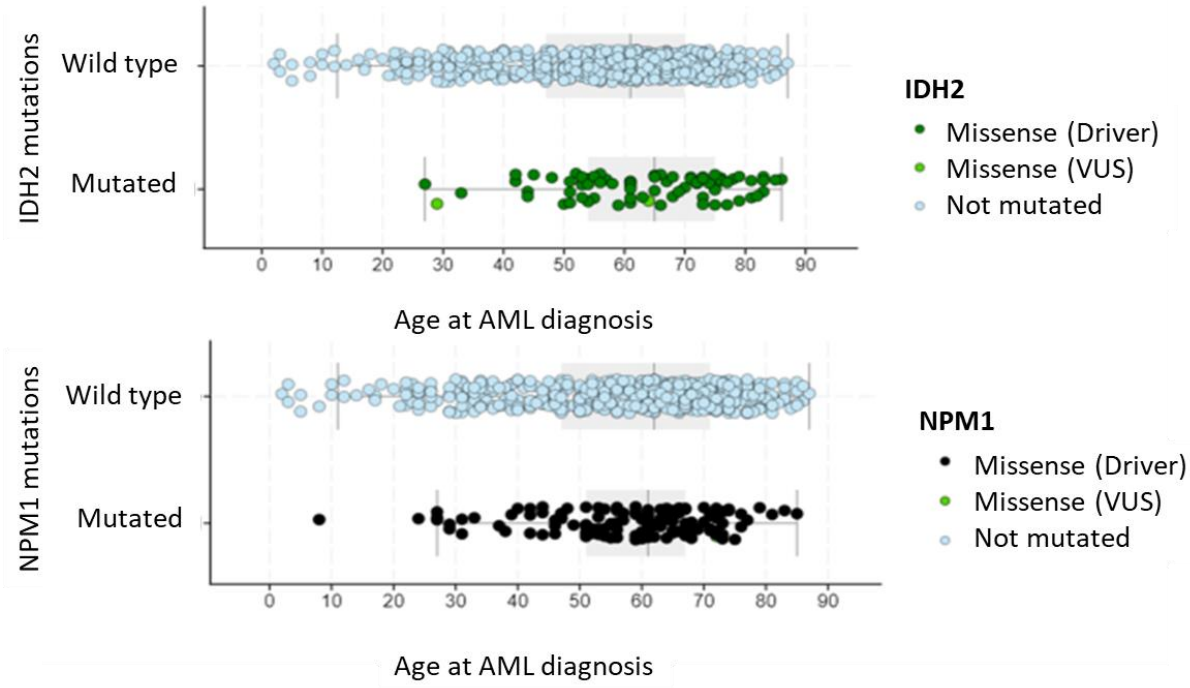

Figure 19: Median age at AML diagnosis of patients with IDH2^{R140} or IDH2^{R172} mutation (median: 66.1 years old; P=0.003, compared to wild type IDH) and NPM1 mutation (median: 60.2 years old, P=0.32). Data were extracted from the TCGA database. Legend: VUS = variant of undermined significance.

IDH mutations are drivers of clonal hematopoiesis in aging (however less frequent than mutations in *DNMT3A or TET2)*. Whereas most individuals with clonal hematopoiesis mutations in *DNMT3A* and *TET2* will rarely develop AML, individuals with *IDH1/2* mutations at the time of baseline sampling, are at very high risk of AML progression. Interestingly, *IDH* mutated context is associated with a long latency of up to 20 years prior to the development of AML, although rising VAF is associated with faster time to overt disease[115,149]. It is also clear that *IDH* mutant clones persist in long-term clinical remission[150]; what is their natural history, clinical fate, multilineage differentiation potential and relationship to other mutations is currently investigated. It has been recently reported that

mutation in *IDH* predisposes to cardiovascular disease in AML patients, because R-2HG exacerbates doxorubicin-mediated cardiotoxicity[151]. As previously mentioned, CHIP has been associated with all-cause mortality due to an increased risk of coronary artery disease and mutations in CHIP drivers *DNMT3A* and *TET2* are also significantly associated with the progression of degenerative aortic valve stenosis[152].

4.4.1 Mutations in *IDH* enable conversion of aKG to D-2HG

IDH mutations are heterozygous, missense mutations, leading to the substitution of the amino acids that play key role in substrate binding in the enzyme active site (Arg^{140} or Arg^{172} in IDH2*;* Arg^{132} in IDH1 analogous codon of Arg^{172} of IDH2*)*. Mutations are neomorphic gain of function, which affect cofactor binding affinity (increased affinity to NADPH) and affect conformation of the enzyme's active site. These mutations abrogate the IDH forward reaction (i.e., the oxidative decarboxylation of isocitrate to aKG), and results in a partial reverse reaction leading to the reduction αKG to D-2HG (and conversion of NADPH to $NADP^+$). Less abundant level of αKG in the cytosol seemingly results in lower D-2HG level production by $IDH1^{R132}$ mutations; D-2HG serum levels in AML patients with mutant *IDH1* or *IDH2* agree with this observation[153]. It is still rather unclear if mutant *IDH* cells have normal αKG levels or if the mutational context alters αKG availability regarding cellular needs[144].

At diagnosis, D-2HG is a biomarker predictive of the presence of *IDH* mutations in AML[145,153]. In isolated myeloid sarcomas, a situation in which molecular characterization is not routinely performed due to technical difficulties, D-2HG elevation is also predictive of the presence of an *IDH* mutation[155,146]. Prospective evaluation of D-2HG levels during treatment of newly diagnosed AML treated with standard chemotherapy reveals that both D-2HG level and mutated *IDH* allele burden decreased with response to treatment. Failure to normalize D-2HG levels is associated with treatment failure whereas elevated D-2HG levels at CR are associated with poorer outcome suggesting that D-2HG is a biomarker predictive of clinical response to intensive chemotherapy in AML patients with *IDH* mutations[153,156].

In physiological conditions, D-2HG is produced at very low levels in the cytoplasm by the promiscuous activity of phosphoglycerate dehydrogenase (PHGDH), an enzyme that catalyze the first step in *de novo* serine biosynthesis pathway and that is frequently overexpressed in cancer[157]; it seems thus plausible that D-2HG elevation in wild type *IDH* tumor cells may have a pathological effect. In the mitochondria, D-2HG is produced by the D-2-hydroxyglutarate dehydrogenase (D2HGDH) (**Figure 20**). In addition, malate dehydrogenases (MDH) 1 or 2 and lactate dehydrogenase A (LDHA) can generate L-2HG, the levogyre form of D-2HG. L-2HG accumulates in hypoxic conditions through LDHA, or acidic pH/environment resulting from lactate accumulation, a situation reminiscent of the Warburg effect. Consequently, L-2HG sustains the activity of HIF pathway when cells must adapt to hypoxia. L-2HG is also implicated in maintaining the redox balance (reviewed in [158]). Interestingly, L-2-HG is five- to tenfold more potent than D-2-HG in inhibition of some α-KG-dependent dioxygenases. Thienpont and colleagues showed that tumor hypoxia broadly reduces the activity of TET and causes DNA hypermethylation[159]. TET activity is limited by oxygen supply, but TET is also a target of L-2HG[160]; those two mechanisms may thus contribute to epigenetic landscape modifications in hypoxic tumors.

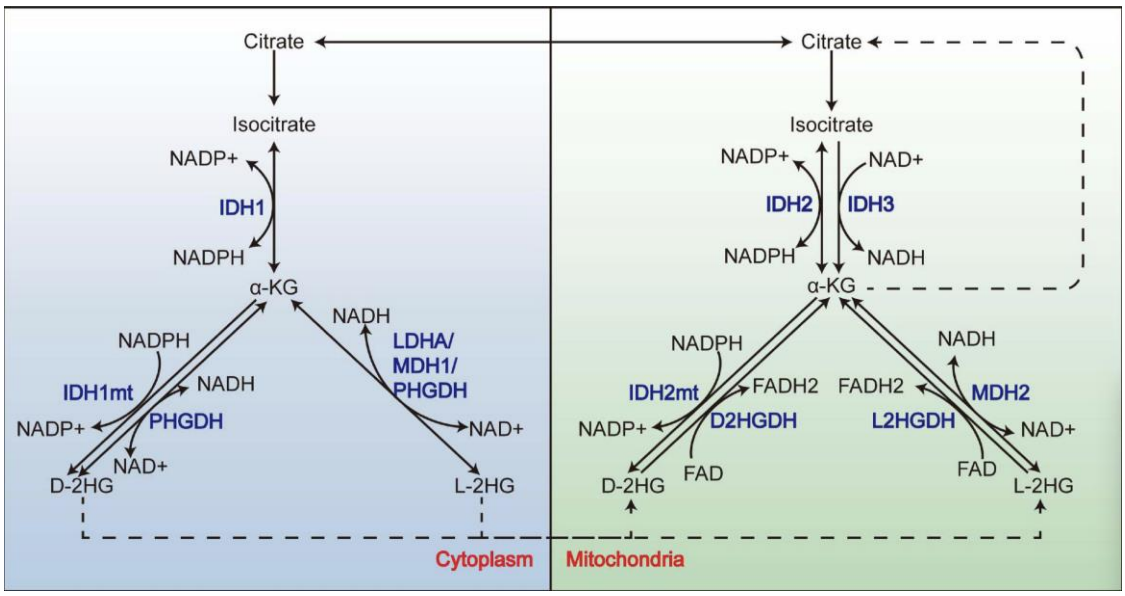

Figure 20: Production cycle of 2HG (from [158]).

2HG also contributes T cell differentiation and tumor immunity (**Figure 21**). 2HG is found to be five- to tenfold higher in T-helper 17 cells (T_H17, involved in the promotion of inflammation) compared with T regulatory cells (T_{reg}, involved in the suppression of inflammation) and elevated 2HG is associated with transcriptional inhibition of fork head box P3 (FOXP3), the master regulatory transcription factor of T_{reg} cells. The origin of 2-HG in T_H17 cells was traced to glutamate, which can be converted to α-KG by glutamic-oxaloacetic transaminase (GOT) (**Figure 21A)**[161]. In addition, in human gliomas, D-2HG exerts a direct effect on tumor-infiltrating T cells by disturbing T cell metabolism and shapes the glioma immune microenvironment[162]. In those tumors, differentiation of infiltrating myeloid cells is also blocked by the presence of D-2HG, resulting in an immature phenotype and preventing T cell response. Interestingly, infiltrating monocytes-derived macrophages show a complex re-orchestration of tryptophan metabolism; in this model R-2HG is taken up by myeloid cells to enzymatically induce tryptophan 2,3-dioxygenase (TDO2)-dependent activation of the kynurenine pathway (and not the indoleamine 2,3-dioxygenases (IDO)1 and IDO2) and, subsequently, the AhR[163]. This pathological tryptophan degradation results in an amino acid starvation-like response that triggers the expression of LAT1/CD98, a key transporter for tryptophan linked to T cell activation and differentiation (**Figure 21B**).

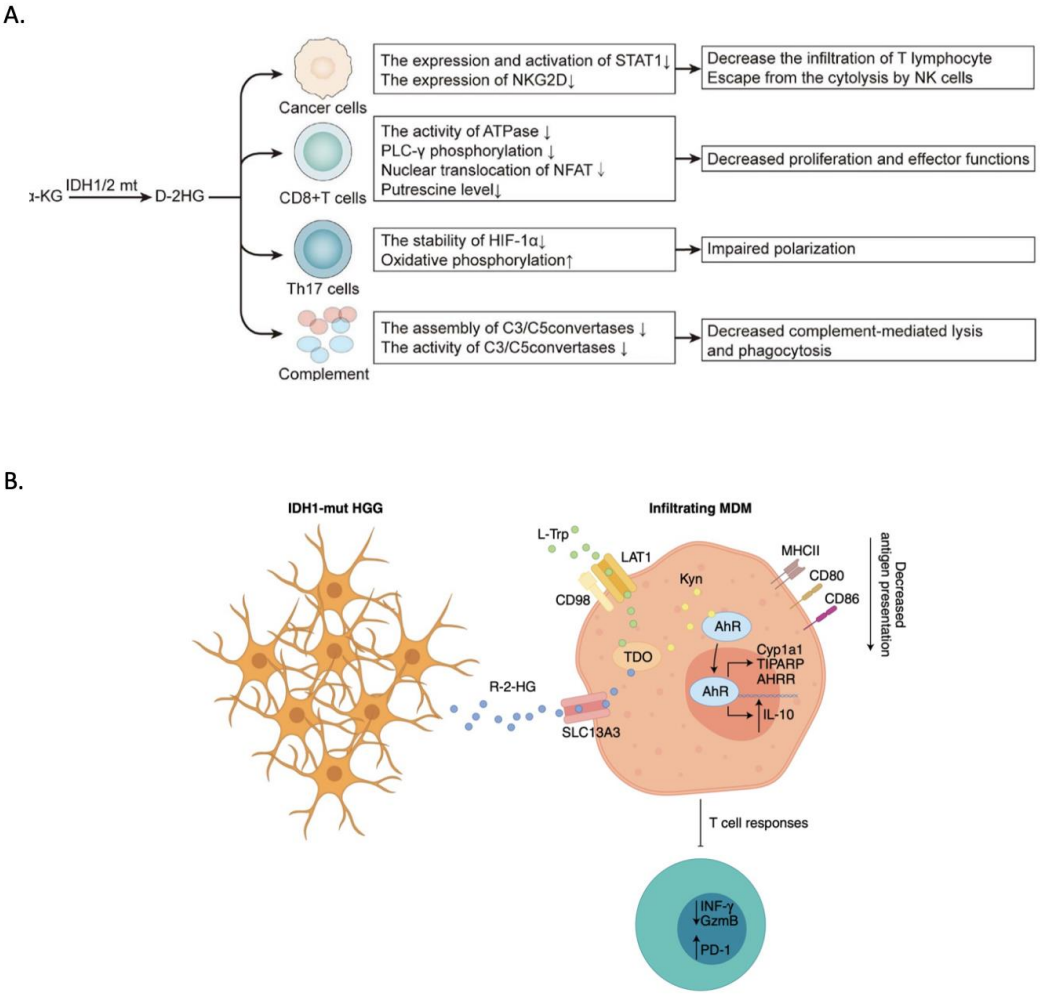

Figure 21: 2HG is a direct and indirect immunosuppressive metabolite. A) The D-2HG is poorly cell-penetrative but the transporter solute carrier family 13 member 3 (SLC13A3) can import the oncometabolite into T lymphocytes. Increased D-2-HG altered the gene expression and differentiation pathway of CD8^{+} T cells, leading to decreased antitumor capacity (from [158]). B) D-2HG increases the activity of TDO; this drives metabolism of l-tryptophan (L-Trp) to the AhR ligand kynurenine (Kyn). Kynurenine induces the translocation of AhR to the nucleus, where it increases production of IL-10 and decreases expression of the co-stimulatory molecules CD86 and CD80 and of major histocompatibility complex class II (MHCII). This results in decreased antigen presentation and increased T cell suppression, which drives a more immunosuppressive tumor microenvironment. Cyp1a1, aryl hydrocarbon hydroxylase and cytochrome P450 enzyme; TIPARP, transcriptional repressor of AhR; AHRR, AhR receptor; Gzmb, granzyme B (from [164]).

As mentioned in section 4.2 of the manuscript, IDH2 enzymatic activity is restricted through Lys^{413} acetylation[71]. Chen and colleagues recently reported that in AML cells, inhibitory Lys^{413} acetylation optimizes mutant *IDH2*-driven transformation, by producing sufficient D-2HG for transformation and avoiding cytotoxic accumulation of intracellular

D-2HG[165]. This mechanism is isoform specific as the acetyl-CoA acetyltransferase 1 (ACAT1) and deacetylase SIRT3 involved in this process (see **Figure 22**) are mitochondrial and cannot modify cytosolic mutant *IDH1*.

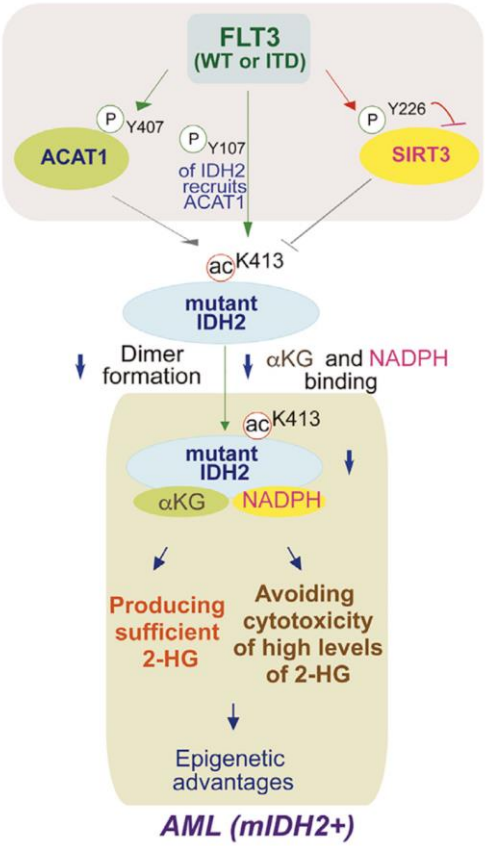

Figure 22: Identification of post-translational modifications on mutant IDH2 enzyme that act in concert to provide precise regulation of D-2HG production (from [165]). Flt3 kinase promotes Lys[413] acetylation by phosphorylating mutant IDH2 on Tyr[107], which enhances ACAT1 recruitment to mutant IDH2. FLT3 simultaneously activates ACAT1 but inhibits deacetylase SIRT3 through direct tyrosine phosphorylation, which also contributes to mutant IDH2 lysine acetylation.

4.4.2 D-2HG accumulation triggers leukemogenesis through multiple mechanisms

At the cellular level, the tumorigenic effect of D-2HG relies on its capacity to behave as a weak antagonist of aKG (reviewed in [158,166]). For a clear inhibition on aKG-dependent dioxygenases, a 100-fold molar excess of D-2HG over aKG is required.

High D-2HG levels affect the activity of αKG-dependent dioxygenases (more than 60 are known) involved in a wide range of cellular processes such as DNA repair (AlkB homolog 2 (ALKBH2) and 3 (ALKBH3), belonging to a family of demethylases that catalyze demethylation on ssDNA, dsDNA, mRNA, tRNA and proteins), hypoxia (EGLN prolyl 4-

hydroxylases), angiogenesis, maturation of collagens of the extracellular matrix (collagen hydroxylases) or regulation of epigenetics (histone demethylases; TET proteins, FTO RNA demethylase among others).

Notably D-2HG inhibits demethylation at several histone sites (H3K9, H3K27, H3K36, H3K79) leading to the accumulation of methylation on chromatin. H3K9 methylation is one of the changes induced by mutant IDH that may be mechanistically important as aberrant retention of H3K9 methylation is known to restrict access of lineage-specific transcription factors on the chromatin. In addition, 2-HG-driven increase in H3K9 methylation was recently demonstrated to impair recruitment of DNA damage repair factors to sites of double-stranded DNA breaks, resulting in vulnerability to therapies targeting DNA damage pathways, and conferring a "BRCAness" phenotype and sensitivity to poly (ADP-ribose) polymerase (PARP) inhibitors[167,168].

Through inhibition of the TET demethylases, D-2HG induces accumulation of DNA methylation at CpG islands, leading to a characteristic epigenomic phenotype called CpG island methylator phenotype (G-CIMP). Such wide epigenetic modifications are associated with altered expression of genes involved in cellular differentiation. However, the molecular pathways by which *IDH* mutation and consequently TET2 inhibition affect the self-renewal process and block the differentiation of hematopoietic stem/progenitor cells, remain largely elusive. Single-cell RNA-sequencing (scRNA-seq) to HSC from mice with somatic deletion of *Tet2* or expression of $Idh2^{R140Q}$, show that $Idh2^{R140Q}$ do not phenocopies *Tet2* deletion and that $Idh2^{R140Q}$ does not induce major changes in gene expression[169] (**Figure 23**). In $Idh2^{R140Q}$ HSC, disruption appears less pronounced than in *Tet2*-deleted HSC, which could be consistent with the fact that in clonal hematopoiesis

IDH2 mutations are less frequently observed.

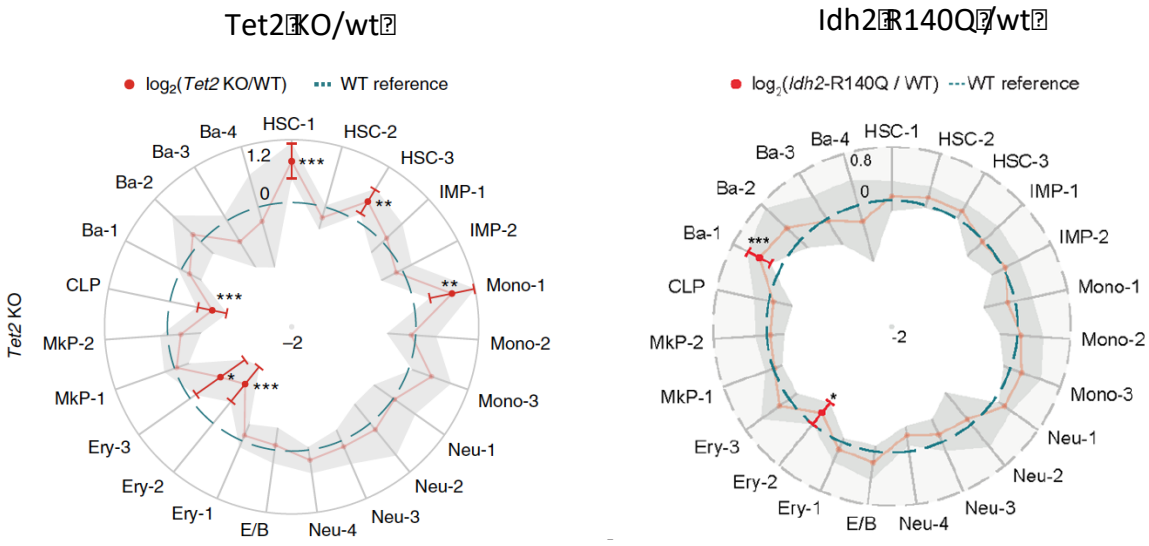

Figure 23: Cell cluster frequency changes in Idh2^{R140Q} mutant mice and Tet2 KO mice (from [169]).

From this study, another interesting mechanism emerges. Comparing the effects of the methyltransferase DNMT3A and of TET2, that have opposing biochemical activities but paradoxically result in similar phenotypic outcomes (CH, hematological malignancies), the authors found that *Dnmt3a* and *Tet2* mutations in murine HSC led to divergent differentiation biases through opposing changes in DNA methylation at transcription factor-binding sites (**Figure 24**). Most patients with *IDH* mutations (>95%) had ≥1 co-mutation, primarily in *DNMT3A,* and *IDH* and *TET2* mutations are usually mutually exclusive in AML. Mouse models suggest an epigenetic cooperation between *Idh* and *Dnmt3a* alterations, leading to activation of a stem cell-like gene signature[170]. It remains to be determined how methylation changes due to *DNMT3A* mutation combine with methylation changes induced by mutant *IDH* in human pre-leukemic cells.

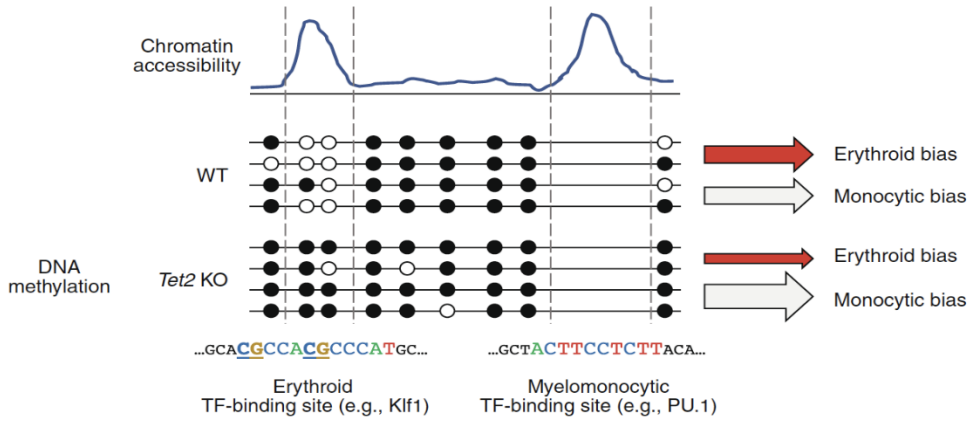

Figure 24: Tet2 loss leads to divergent differentiation biases through opposing changes in DNA methylation at transcription factor-binding sites (from [171]). Key lineage-determining transcription factors (as kruppel like factor 1 (KLF1) implied in erythroid differentiation or PU.1/SPI1 involved in the myelomonocytic engagement) are susceptible to changes in DNA methylation, particularly those with CpG-dense DNA-binding motifs; erythroid-related transcription factors have higher CpG content in their binding motifs than myelomonocytic-related transcription factors.

Hypermethylated signature at specific DNA locus is not uniformly related to gene expression downregulation and may affect the structure of the genome into domains called topologically associated domains (TADs), which insulate genes in one domain from activation by enhancers in different domains; thus, other hypermethylation-related mechanisms could be implied in myeloid differentiation block.

m5C and 5hmC are also present on various RNA species including mRNA. TET2 is an RNA-binding protein that play a role in post-transcriptional regulation[172,173]. TET-mediated RNA hydroxymethylation is seemingly predominant at intronic regions within preRNA[174]. Hence, this process represents a novel pathway by which loss of TET2 function and mutant IDH could influence RNA biology, hematopoietic differentiation, and myeloid malignancies. Of note, an increased level of RNA:m5C has been associated to the resistance to 5-aza-2'-deoxycytidine/Decitabine, a DNA hypomethylating agent historically used against MDS and AML[175]. The key epigenetic activities inhibited by D-2HG that drive leukemogenesis remain to be defined.

4.4.3 D-2HG-mediated metabolic rewiring

In addition to its epigenome activities, accumulation of D2-HG rewires metabolic pathways in cancer cells and affects mitochondrial functions, i.e. inhibits ATP synthase β subunit (ATP5B, a subunit of mitochondrial ATP synthase or complex V) [176], induces hypersuccinylation[177], and inhibits the ETC by compromising the activity of cytochrome c oxidase (COX) resulting in a lower mitochondrial threshold to induces apoptosis, thus sensitizing cells to BCL-2 knockdown[177,178]. These metabolic perturbations lead to a specific vulnerability of mutant *IDH* cells[177,178,179], addiction to metabolites[180,181], or decrease in proliferation/viability[176,181,182], a situation that can be exploited therapeutically. For instance, Sabatier and colleagues reported that D2-HG induces vitamin D receptor-related transcriptional changes, priming leukemic cells to differentiate with pharmacologic doses of all-*trans* retinoic acid (ATRA) and/or vitamin D, in a CEBPA-dependent manner [183]. This result and previous[184,185] further illustrate that CEBPA is a key effector of mutant *IDH* AML biology. There are also preclinical advances in restoring TE2 function by vitamin C; two studies showed that vitamin C supplementation reduce HSC self-renewal and partially reverse the block in HSC differentiation seen in *Tet2*-deficient animals[186,187]; similar treatment and changes in a *Tet2*$^{-/-}$*FLT3-ITD* AML mice model alters the progression of leukemia[186].

Metabolic changes reported in the most common mutant *IDH* cancers (i.e., gliomas) have been extensively described and included altered redox homeostasis, altered cholesterol metabolism and reliance on glutaminolysis; in addition, cells are less glycolytic and rely more on OXPHOS; in contrast, there are conflicting results regarding the impact of *IDH* mutations on PI3K/AKT/mTOR activity (reviewed in [188]).

Little is known about the metabolic changes in mutant *IDH* AML. Mutant *IDH1* AML cells are characterized by a profound vulnerability to depletion of the coenzyme NAD^+ and nicotinamide phosphoribosyltransferase (NAMPT) inhibition[181]; Interestingly, NAMPT expression and NAD levels are controlled by epigenetic marks at a NAMPT enhancer region in tumors[189], opening opportunities for targeting epigenetic remodeling to target NAD metabolism.

Baccelli and colleagues showed that a subset of AMLs including mutated *IDH* AML showed OXPHOS hyperactivity and are addicted to ETC complex I activity[190]. Stuani and

colleagues recently confirmed an enhanced OXPHOS activity in *IDH1* mutated cells lines and primary human AML samples; OXPHOS maintenance is mediated by FAO in a CPT1a- and CEBPα- dependent manner. This phenotype is dependent, but not only, on D-2HG. In keeping, enrichment in FAO and OXPHOS gene signatures was associated to relapse and absence of response to ivosidenib in mutant *IDH1* AML patients[185].

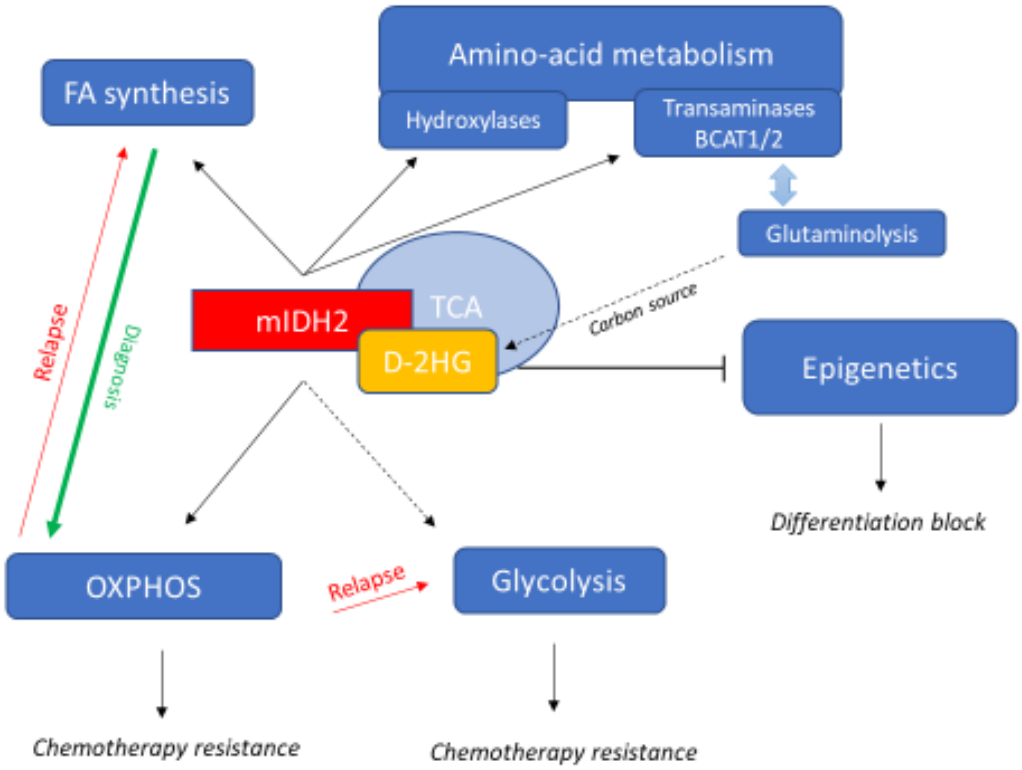

Figure 25: Various metabolic pathways are altered in mutant IDH cells and contribute to their phenotype.

4.5 METABOLISM IN AML

LSCs share metabolic features with normal HSCs and deregulation of metabolic processes supports LSC emergence and leukemogenesis. Leukemogenic genetic and epigenetic lesions fundamentally change the way how LCSs and leukemic progenitor cells (blasts) proliferate, differentiate, and interact with the bone marrow microenvironment, but also their general energetic metabolism. Reciprocally, tumor microenvironment drives metabolic changes and impacts on how leukemic cells satisfy energetic and anabolic demands (biosynthesis of molecules).

4.5.1 General aspects in AML metabolism

Like most cancer cells, AML cells are characterized by uncontrolled proliferation requiring large amount of energy. One key alteration in cancer metabolism is the increased glucose uptake and dependence on aerobic glycolysis, not so much for energy production which can be provided by other pathways (such as the pentose-phosphate pathway, a metabolic pathway parallel to glycolysis) but rather as a platform to increase the biomass required to rapidly provide a new cell (e.g., cellular membrane, ribosome biogenesis, DNA synthesis). High proliferating cells have important metabolic demands that extend beyond ATP production and need anabolic carbons, acetyl-CoA and NAD phosphate (NADP), reduced (NADPH) for macromolecular synthesis (fatty acids, nucleotides, amino acids).

Deregulation of biomass accumulation creates an addiction of tumor cells to an adequate anabolic supply. A way to sustain this, described by Otto Warburg, is named the 'Warburg effect' (reviewed in [191,192]). In the Warburg reaction, regardless of whether oxygen is present, glucose is converted into lactate by the glycolytic enzyme lactate dehydrogenase A (LDHA; the cofactor for LDHA is NADH which is converted to NAD^+) while generating 4 molecules of ATP per glucose molecule, which results in lower yields of ATP than OXPHOS. In the Warburg effect, the bulk of the glucose is not committed to carbon catabolism for ATP production; for instance, this reaction serves to provide anabolic carbons for fatty acid synthesis. It has been recently shown that the Warburg effect is driven by an hyperactivity of the LDHA seemingly due to a loss of interaction between LDHA dimers and/or tetramers and the tumor suppressor folliculin (FLCN), a protein implicated in multiple cellular processes which acts as *a bona fide* endogenous uncompetitive inhibitor of LDHA[193]; as the *FLCN* mutation rate is low across cancers, this suggests an epigenetic and/or post-translational inactivation. More recently, it has been shown that lactate production in tumor cells must also result from the metabolism of non-glucose substrates, as glutamine can be converted into lactate by the TCA cycle ; this reaction produces NADPH for lipid biosynthesis and oxaloacetate for the refueling of the TCA intermediates (reviewed in [192]).

Key components of the Warburg effect (increased glucose consumption, decreased OXPHOS and lactate production) are distinguishing features of oncogene activation ; these effects can also be caused by oncogenes that hijack signaling pathways, such as

PI3K (**Figure 26**)[194]. In addition tumoral cells use diversions from glycolysis, most importantly the pentose-phosphate pathway (PPP), a highly energetic pathway that pursue nucleotides, amino acids, and electron carriers necessary for cancer progression[195].

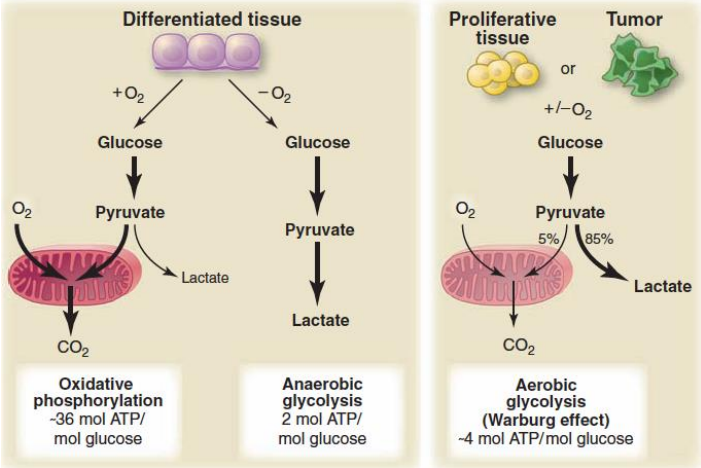

Figure 26: Differences between OXPHOS, anaerobic glycolysis, and aerobic glycolysis (Warburg effect) (from [191]). Generation of lactate (anaerobic glycolysis) by LDHA allows glycolysis but results in minimal ATP production when compared with OXPHOS.

4.5.2 Metabolic reprogramming and metabolic vulnerabilities in AML

The reprogramming of metabolic pathways allows the maintenance of AML growth and survival by altering bioenergetics, biosynthetic and redox functions to meet the higher demands of AML cells; therapies targeting different aspects of AML cells metabolism have demonstrated efficacy (reviewed in [196–199]).

4.5.2.1 Glycolysis

Glycolysis is increased in most cases of primary AML myeloblasts compared to normal myeloid progenitors (reviewed in [149, 151, 153]) and leukemic cells induce complex variations of the metabolic homeostasis of the host to ensure high glucose concentrations in the bone marrow (e.g., increase of insulin resistance and inhibition of insulin secretion by tissues). Increased glycolysis has been associated with drug resistance, notably through the cytosolic export of the proliferating cell nuclear antigen (PCNA), a scaffolding protein involved in DNA replication which interacts with the nicotinamide phosphoribosyltransferase (NAMPT) involved in NAD biosynthesis[201].

The glycolytic flux is partly mediated by AMPK activation[96]; a high glycolytic flux seems to correlate with a decreased level of autophagy leading to a more aggressive leukemias

in vivo[202]. In glycolytic settings, oxidative PPP through G6PD activity is the major contributor to NADPH that is essential for the synthesis of various organic molecules; overexpression of *G6PD* has been reported in AML and associated with overall poor prognosis[203]. Sensitivity to G6PD inhibition seems to be linked to the activity of mTORC1; indeed, in AML cells mTORC1 signaling promotes glycolysis and leads to glucose addiction through PPP, a phenomenon that is not found in normal HPCs. Thus, level of mTORC1 activity determines the sensitivity of AML cells to glycolysis inhibition as switch-off mTORC1 activity leads to glucose-independent cell survival that is sustained by an increase in OXPHOS[203]. Inhibition of G6PD activity leads to leukemic growth arrest and synergize with cytarabine, also known as cytosine arabinoside (ara-C). While glycolysis is increased in AML blasts, quiescent LSCs, unlike quiescent HSCs, are less reliant on glycolysis and instead utilize OXPHOS to meet their energy requirements; this is due to the fact that OXPHOS utilizes the available nutrients more efficiently[97].

Several studies provide evidence that at least some hematopoietic malignancies use the Warburg effect. The pyruvate kinase M2 (PKM2) which converts phosphoenolpyruvate (PEP) to pyruvate (the third irreversible reaction of glycolysis) and HIF1a, both inducers of the Warburg effect, have been implicated in hematopoietic diseases (reviewed in [36]). PKM2 is overexpressed in proliferating tissues and tumor cells and favors aerobic glycolysis (production of pyruvate) compared with the alternative splicing form PKM1[204]. Deletion of the two glycolytic enzymes PKM2, and LDHA, inhibits BCR-ABL- and MLL-AF9-driven AML in mice models while preserving normal HSC functions[205]. Short-term treatment by echinomycin, a peptide blocking HIF1a activity, prevents serial transplantation of AML by the induction of apoptosis of LSC ($CD34^{+}CD38^{-}$) in a xenogeneic model of human AML[206]. The possible involvement of HIF1a in *IDH*-mutant AML cells has not been studied yet. However, in neural tumors (gliomas, glioblastomas), the phenotype of *IDH*-mutant cancer cells is partly related to HIF1a activity[207]. As the observed metabolic effects of mutant *IDH* greatly vary between primary patient-derived materials and established experimentally (neural cell lines), the Warburg effect appears to be dependent on the intrinsic metabolic context.

Despite AML seems to rely on glycolysis, several studies highlighted that AML cells had higher mitochondrial biogenesis and an increased oxygen consumption rate compared to normal hematopoietic progenitors[208]. Increased mitochondrial mass in AML did not

translate into an increase in ETC complex I, III, IV, and V activities indicating that AML have low spare reserve capacity compared with normal cells [209].

4.5.2.2 Fatty acid metabolism

De novo lipid biosynthesis sustains cell proliferation by providing signaling molecules and molecules for synthesis of membranes (reviewed in [163, 164]). AML cells, but not HSCs, are metabolically dependent on FAO (and OXPHOS) for survival [212].

Bone marrow adipocytes represent an extracellular source of long chain fatty acids for leukemic cells (**Figure 27**) that could be internalized via the leukemia cell scavenger receptor CD36 and transferred to the nucleus by an intracellular lipid chaperone fatty acid-binding protein 4 (FABP4) followed by ligation of peroxisome proliferator-activated receptor-γ (PPARγ), a member of the nuclear hormone receptor family. Activated PPARγ then induces downstream target genes, including *CD36, FABP4*, and *BCL2*. In this process, the intramitochondrial FAO enzyme very-long-chain acyl-CoA dehydrogenase (VLCAD) catalyzes the first intramitochondrial step of long-chain FAO ; VLCAD activity is required for AML cells survival[213]. The increase of bone marrow adipocytes in elderly patients may contribute to the worst overall survival in this subset of population; in line, Behan and colleagues demonstrated that bone marrow adipocyte markedly impaired the antileukemia efficacy of chemotherapeutic agents, and that the rate of relapse after chemotherapy is higher in obese mice compared to their normal-weight counterparts [214].

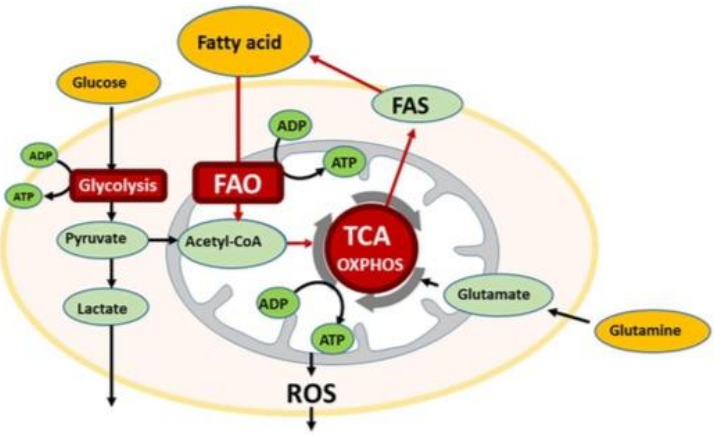

Figure 27: Medullar microenvironment reprograms energy metabolism in AML (from [211]. AML cells undergo FAO, a major source of energy production, if fatty acid is available. In the oxidative stressed bone marrow microenvironment, AML cells are supplied for free fatty acids by abundant bone marrow adipocytes. Mitochondrial FAO generates the reducing compounds NADH and flavin adenine dinucleotide 2 (FADH2) for ECT and provides acetyl-CoA to TCA cycle to produce ATP.

FAO is an important source of cytosolic NADPH ad the production of FAO-derived NADPH is key to counteract the oxidative stress in the context of metabolic stress[215]. FAO is associated with quiescence and drug-resistance in LSC, suggesting that eradication of chemoresistant cells might be achieved by targeting FAO dependency of LSC. In this context, several strategies have been developed[216]. Pharmacological inhibition of carnitine palmitoyltransferase 1 (CPT1) responsible for the translocation of fatty acids from the cytosol to the mitochondrial matrix, with etomoxir enhanced AML sensitivity towards apoptosis-inducing agents that interfere with the mitochondrial apoptosis machinery. These data indicated that this may be due to a specialized function of FAO that is not related to ATP production. Rather, FAO may serve to regulate the BCL2 homologous antagonist/killer (BAK)-dependent mitochondrial permeability transition, a core function in cytochrome c-dependent apoptosis regulation[212]. FAO is also a key catabolic pathway involved in the generation of NADH and FADH2, which are the electron donors of complex I and complex II of the ETC, respectively, and leading to the production of acetyl-CoA (**Figure 28**). In AML cells co-cultured with bone marrow adipocytes, FAO inhibition with avocatin B (a FAO inhibitor derived from avocado), caused adaptive stimulation of free fatty acid uptake through upregulation of fatty acid-binding protein 4 (FABP4) mRNA, enhanced glucose uptake and switch to glycolysis ; however, its combination with cytarabine shows highly synergistic efficacy in apoptosis induction[170,171].

Inhibition of other key lipogenic enzymes such as stearoyl CoA desaturase 1 (SCD1) revealed to be of interest in AML. Based on applied mass spectrometry-based lipidomics, Southam and colleagues have shown that BaP, a combined treatment with the lipid-regulating drug bezafibrate (BEZ) and the sex hormone medroxyprogesterone acetate (MPA), caused redirection of pyruvate utilization, leading to αKG conversion to succinate and conversion of oxaloacetate into malonate, to deal with oxidative stress in AML cell lines[219].

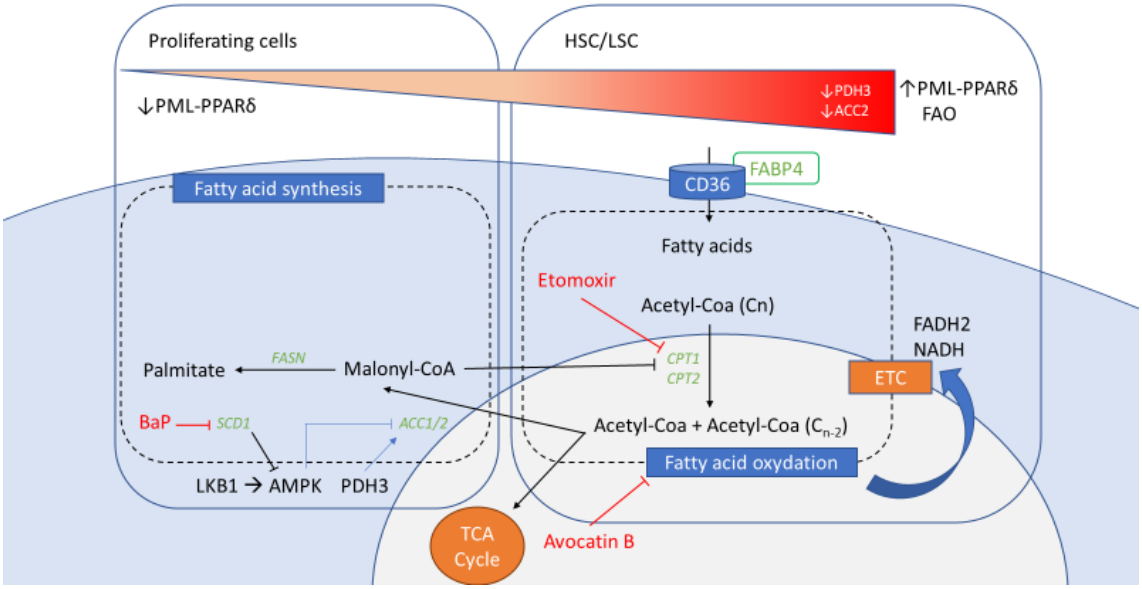

Figure 28: Fatty acid synthesis and oxidation in HSC/LSC and proliferating cells. FAO is activated by PML that regulates the PPAR signaling ; the PML-PPARδ-FAO pathway controls notably the asymmetric division of HSC[27]. FAO can contribute to the accumulation of acetyl CoA in the cytoplasm that is needed to initiate fatty acid synthesis, (fatty acid synthesis and FAO can support each other). It seems that in quiescent and undifferentiated cells (HSC) the competition between fatty acid synthesis and FAO is less prominent, as these cells display a lower membrane synthesis rate. ACC: acetyl-CoA carboxylase; AMPK: AMP-activated kinase; CoA: Coenzyme A; CPT: carnitine palmitoyltransferase; FABP: fatty acid binding protein; FADH2: flavin adenine dinucleotide; FASN, fatty acid synthase; PDH3, Prolyl hydroxylase 3.

4.5.2.3 Amino acids

The multiple roles of amino acid metabolism in leukemia growth and survival have been described in details in[196–198,200]. AML cells are particularly dependent on glutamine. Glutamine supplies nitrogen for purine and pyrimidine synthesis, as well as for the generation of non-essential amino acids and protein synthesis. It is imported via the glutamine importer SLC1A5 **(**glutamine is required for leucine uptake as import of one molecule leucine by the amino acid transporter LAT1/SLC7A5 requires the export of one molecule of glutamine) or is produced intracellularly by lysosomal degradation of proteins obtained from autophagy, endocytosis or macropinocytosis. Glutamine occupies a central role in cell metabolism from various metabolic pathways that can convert it into αKG. As a first step, glutamine is directly converted to αKG via glutamate dehydrogenase (GDH) or converted to glutamate through glutaminase (GLS); inhibition of GLS C, a glutaminase isoform that is most abundantly expressed in AML, leads to reduced OXPHOS,

proliferation arrest and apoptosis without any activity against normal HSC (as glutamine controls OXPHOS in AML cells, removal of glutamine leads to apoptosis and it has been shown that glutaminolysis inhibition efficacy relies on mitochondrial depolarization, intrinsic caspase-dependent apoptosis). Glutaminolysis inhibition also sensitizes leukemic cells to priming with venetoclax, a "BH3-mimetic" antagonist of BCL2[220]. Glutamine availability is a limiting step for mTORC1 activation[221]; indeed, intracellular glutamine concentration controls the uptake of leucine, and leucine is required for Rheb-mediated mTORC1 activation[222].

In addition, glutamine deprivation in AML cells results in the up-regulation of 3-phosphoglycerate dehydrogenase (PHGDH) and phosphoglycerate aminotransferase (PSAT), two enzymes involved in the biosynthesis of serine.

AML blast cells also frequently show defects in enzymes of the arginine-recycling pathway, i.e., argininosuccinate synthase-1 or synthetase (ASS1, involved in intracellular synthesis of arginine) and ornithine transcarbamylase (OCT), which makes AML cells auxotrophic for arginine and dependent on exogenous sources[223]. Plasma arginine levels of AML patients are significantly decreased compared to those of healthy volunteers[224]. Arginine is a conditionally non-essential amino acid (cells can synthesize arginine but under certain circumstances this amino acid is imported) important for the supply of metabolites including nitric acid and polyamines. The arginine deiminases BCT-100 and ADI-PEG 20 showed potent anti-leukemic activity by depleting rapidly intracellular arginine, prompting their clinical development [225].

The roles of amino acid metabolism in leukemia growth and survival are also supported by the use of cysteine as a precursor for the biosynthesis of glutathione (GSH) required for the maintaining of intracellular redox potential.

In chronic myeloid leukemia (CML) blast crisis cells, defined by an enhanced proliferation and survival and a differentiation arrest, the synthesis of essential branched-chain amino acids (BCAA) leucine, valine, and isoleucine is enhanced by the up-regulation of *branched chain amino acid transaminase 1* (*BCAT1*), encoding an αKG-dependent transaminase catalyzing the amination of branched-chain keto acids (BCKA) (**Figure 29**)[226]. In this setting, BCAT1 inhibition impairs CML blast crisis propagation, supporting an essential role for BCAA production in this disease. BCAT1 has been shown to be enriched and activated

in LSCs in human AML linking BCAA catabolism to HIF1α stability and regulation of the epigenomic landscape through TET2 activity[227].

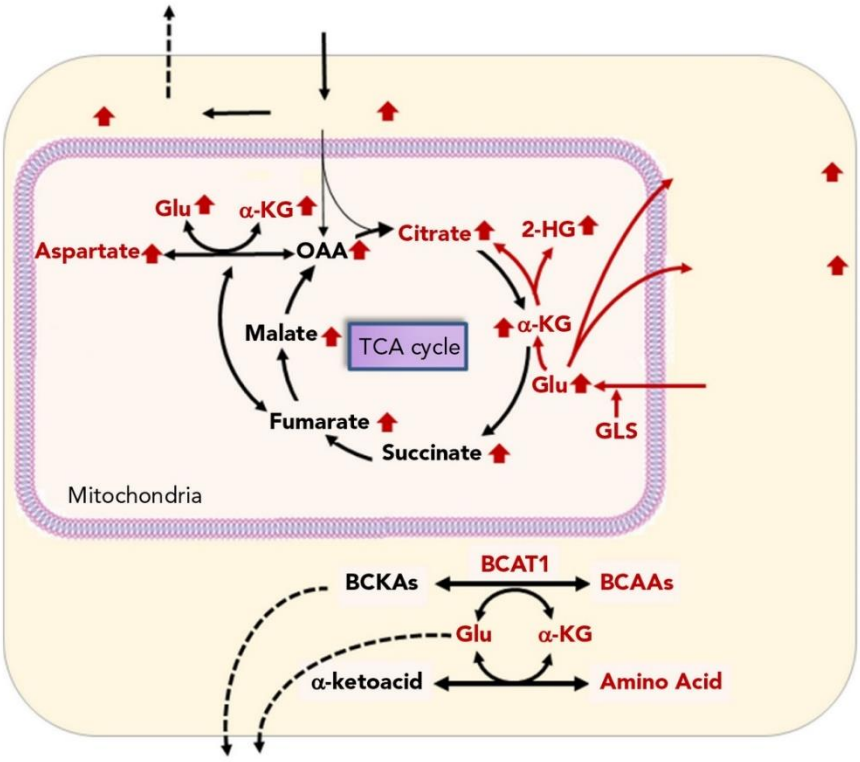

Figure 29: Glutamine metabolism in AML (from [197]). GLS converts glutamine (Gln) to glutamate (Glu), which is a necessary step for Gln to enter the TCA cycle. In the cytosol, BCAT1 initiates the catabolism of BCAAs (reversible transamination of BCKAs to BCAAs valine, leucine and isoleucine, which are essential for cell growth) and results in the production of Glu.

Recently, a pan-metabolome analysis revealed that in human LSC amino acid uptake, steady-state levels, and catabolism were all increased compared to more mature AML blasts (amino acid depletion did not either affect normal HSC in terms of diversity, colony-forming potential or engraftment). OXPHOS in LSCs, and not in AML blasts, is selectively sensitive to amino acids loss and inhibition of amino acid metabolism reduces OXPHOS and induces cell death[228]. This lack of metabolic flexibility is therefore an attractive target for developing therapies against LSCs. However, at relapse, LSCs usually develop a compensatory ability to overcome the loss of amino acid metabolism by increasing FAO[228].

4.5.2.4 Mitochondrial metabolism

Various studies have focused on mitochondrial metabolism and its inhibition (reviewed in [149, 151]). It appears that targeting OXPHOS without considering the metabolic

background might be inefficient as the glycolysis is negatively controlled by OXPHOS and is induced by TCA-mediated allosteric inhibition of glycolytic enzymes (the "Pasteur effect"). Therefore, OXPHOS inhibition should result in compensatory upregulation of glycolysis to maintain ATP levels and redox balance, resulting in modest antiproliferation effects. In this context, Molina and colleagues reported that AML cells with a reduced capacity for compensatory glycolysis are more sensitive to OXPHOS inhibition (ETC complex I inhibitor IACS-010759) and undergo apoptosis. Interestingly, IACS-010759 also induces signs of myeloid differentiation through CD14 expression[229].

The dihydroorotate dehydrogenase (DHODH) protein is a mitochondrial enzyme that catalyzes the ubiquinone-mediated conversion of dihydroorotate dihydroorotate (DHO) to orotate, and provides electrons to the ETC via ubiquinone ; DHODH links mitochondrial bioenergetics to de novo pyrimidine synthesis[230]. Sykes and colleagues recently reported that inhibiting DHODH activity shows anti-leukemic activity and induces a partial differentiation of AML cells in murine models and human cell lines[231]; similar results have been reported with the BAY-2402234, which is actually in clinical development[232].

Devimistat (CPI-613®) is a novel lipoate analog that inhibits the TCA cycle at two key carbon entry points, through inhibition of pyruvate dehydrogenase (PDH) and αKG dehydrogenase complexes (KGDH). Devimistat inhibits the entry of glucose and glutamine derived carbons[233,234]. PDH inactivation contributes to the collapse of mitochondrial function and leads to specific apoptosis[235]. CPI-613 also induces massive increase in mitochondrial ROS, a signal that inhibits KGDH activity[234]. CPI-613 has demonstrated clinical efficacy and is actually in phase III development in AML settings (NCT03504410)[236].

Inhibition of mitochondrial translation (and not nuclear translation) by tigecycline also shows antileukemic activity in mouse models of human leukemia[208].

Inhibition of mitochondrial metabolism could also be an effective approach to overcome resistance to treatment. As an example, Farge and colleagues have shown that AraC-resistant AML cells harbor metabolic features and gene signatures consistent with a high OXPHOS status. Targeting/lowering OXPHOS via the CD36-FAO-OXPHOS axis with metformin sensitizes the cells to Ara-C and abrogates Ara-C resistance[94]. In line, enrichment in genes relevant for mitochondrial function is negatively correlated with the sensitivity to Ara-C and associated with a poor prognosis[237].

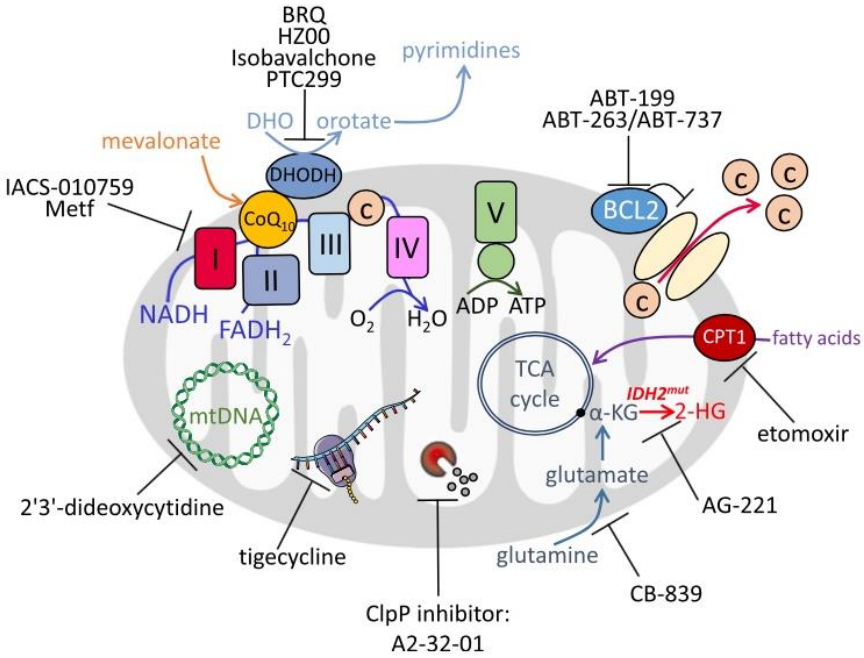

Figure 30 : Pharmacological inhibitors in clinical development and used to inhibit mitochondrial activities in AML (from [198]). Due to increased mass of mitochondria with lower ETC capacity, AML cells are at the brink of a failing respiratory system. There seems to be a delicate balance between the requirement for OXPHOS-dependent energy supply, glycolysis, ROS induced stress, ETC reserve and other mitochondrial functions that are important for proliferation, survival, and cell fate decisions in AML. Impacting on OXPHOS may also be a trigger for AML differentiation.

BCL2 and venetoclax

Venetoclax, a highly specific BH3 mimetic, is an orally administered inhibitor of BCL2 (formerly ABT-199, GDC-0199) ; venetoclax also inhibits the anti-apoptotic BCL2L2/BCL-w protein (reviewed in [238,239]). When used alone, venetoclax has a modest activity in patients with AML, although Jordan and colleagues previously showed that inhibition of the BCL2 family proteins with navitoclax (ABT-263) impaired OXPHOS in LSCs (LSCs overexpress BCL2), leading to cell death[97, 193]. As documented by numerous preclinical and clinical studies, combination therapy with venetoclax and hypomethylating agents or low-dose cytarabine (LDAC) demonstrates superior anti-leukemic activity in comparison to single agents[241–243]. Notably the randomized, double-blind study VIALE-A compared azacytidine (aza) in combination with venetoclax (ven) versus azacitidine + placebo in patients not eligible for intensive chemotherapy with AML at diagnosis; this combination was highly efficient in *IDH* mutated patients with 70-80% complete response rates reaching and long-lasting responses[196]. Combination of venetoclax with azacitidine (ven/aza)

inhibits amino acid uptake and catabolism[241]; the combination has been shown to be effective against LSCs which depend on amino acid metabolism for OXPHOS and survival[228]. However, ven/aza fails to eradicate LSCs in relapsed/refractory (R/R) patients, probably because of various altered metabolic properties in LSCs. Conversely, Jones and colleagues showed that resistance to the combination ven/aza can be overcome by targeting fatty acid transport in R/R LSCs as R/R LSCs depend on both amino acid and fatty acid metabolism for OXPHOS and survival[181, 197]. R/R LSCs observed upon ven/aza treatment can also be eradicated by inhibiting the activity of the nicotinamide phosphoribosyltransferase (NAMPT), a rate-limiting enzyme in nicotinamide metabolism, because R/R LSCs demonstrate elevated nicotinamide metabolism [245]. Recently, Bosc and colleagues also showed that venetoclax enhances the efficacy of cytarabine (AraC) by reversing the hyperactivation of OXPHOS upon AraC treatment ; accordingly, treatment of ven/AraC-resistant AML cells with inhibitors blocking ECT function and activity, substantially delayed relapse[246].

It has also be reported that venetoclax preferentially targets mutated *IDH* AML cells ; in a phase II clinical trial of venetoclax monotherapy, mutated *IDH* relapsed/refractory AML patients had a response rate of 33% compared to 10% in wild type *IDH* patients [240]. This result was unexpected given that the mechanism by which *IDH* mutations increase BCL2 dependence is via the production of the oncometabolite D-2-hydroxyglutarate (D-2HG) ([247] and *cf. infra*), and that reduction of D-2HG with enasidenib may antagonize venetoclax activity. Cathelin S and colleagues recently provided some answers by showing that enasidenib monotherapy results in a significant decrease in *BCL2* expression in enasidenib-responders ; the reduction in *BCL2* expression thus potentiates mitochondrial priming and sensitization to venetoclax[248]. A clinical trial of ivosidenib + venetoclax ± azacytidine is ongoing; interim trial results have been presented at American Society of Clinical Oncology meeting in 2020 and demonstrated a composite remission rate of 80% in patients with both newly diagnosed and relapsed mutated *IDH1* myeloid malignancies, with 50% of patients attaining minimal or measurable residual disease (MRD) negativity[249]. Updated trial results with longer follow-up are anticipated in 2022. In addition, a trial of enasidenib in combination with venetoclax (NCT04092179) is actually enrolling.

As most of targeted therapies, mechanisms of resistance to venetoclax have been described. Resistance to venetoclax results from *BCL2* mutation, failure to engage

apoptosis through BAX loss, decreased expression of *BCL2*, and/or survival bypassing on alternative BCL2 family members such as MCL1 or BCL2L1 (reviewed in [239]). The resistance is also accompanied by changes in mitochondrial homeostasis and cellular metabolism as those linked to *TP53* mutations[250]. Pharmacologic inhibition of mitochondrial protein synthesis with antibiotics that target the ribosome (as tedizolid and doxycycline) overcome venetoclax resistance ; when used in combination, those drugs cooperate to activate the integrated stress response (ISR), which suppresses the glycolytic capacity, resulting in ATP depletion and cell death[251].

4.5.3 Influence of the genomic context on metabolism in AML cells

Genetic alterations closely associated with metabolism seemingly behave as cancer drivers in cancers, rather than genes affiliated to metabolic pathways[252]. In AML, several mutations have been associated with metabolic reprogramming such as *FLT3-ITD, TP53, MYC* and *IDH1/2*.

Human and murine *FLT3-ITD* cell lines exhibit significant decrease of mitochondrial respiration, increase of glycolytic activity and phosphorylated form of mitochondrial hexokinase 2 (HK2). *FLT3-ITD* confers indirectly a protection against cytochrome c release by preventing opening mitochondrial permeability transition pore, and using glycolysis inhibitor restore at least partially cytotoxic activity of sorafenib[253]. Mutant *FLT3* induces severe mitochondrial oxidative stress (impaired production of the antioxidant factor glutathione) that is relayed by the ataxia telangiectasia mutated (ATM) kinase or its downstream effector glucose 6-phosphate dehydrogenase (G6PD)[254]. Finally, glutaminolysis, along with other TCA metabolic pathways, plays an important role in increasing the survival and resistance of quizartinib-treated *FLT3-ITD* AML cells (as the resistance of imatinib-treated BCR-ABL$^+$ cells) ; moreover genes involved in fatty acid synthesis (*MECR*) and phosphatidylinositol metabolism (*PLCH1*) demonstrate a significant synergistic lethality with quizartinib[255].

MYC and TP53 play important roles in metabolic regulation ; *TP53* mutations and deregulation of MYC coordinate multiple metabolic events to fuel metabolic rewiring and sustain unrestrained growth in malignant cells (reviewed in [256–258]).

The frequency of *TP53* mutations in AML is approximately 10%. However, in AML with complex karyotype, the rate of *TP53* mutations and/or deletions is almost 70%. In addition, *TP53* mutations are associated with poor prognosis and decreased survival in AML[259]. Mutant *TP53* regulates metabolism by affecting glycolysis (mutant TP53 can have dramatically different phenotypic effects in terms of glycolysis and enhancing OXPHOS (**Figure 30A**)[260]. In line, whereas doxorubicin (an anthracycline) and dichloroacetate (DCA), an inhibitor of mitochondrial pyruvate dehydrogenase kinase 1 (PDK1) that can shift glycolysis to OXPHOS synergize to enhance p53 activation and AML suppression, this combination has no effect on leukemia cell lines and primary leukemic cells expressing mutant *TP53*[214,215]. Mutant *TP53* also promotes lipid synthesis through the inhibition of AMPK activity, known to inhibit the lipid synthesis through phosphorylation of sterol regulatory element-binding proteins (SREBPs) activation and acetyl-CoA carboxylase (ACC)[216, 217]. Finally, mutant *TP53* promotes nucleotide synthesis through cooperating with the erythroblastosis virus E26 oncogene homolog 2 (ETS2) transcription factor, to transcriptionally activate multiple nucleotide metabolism genes, including *ribonucleotide reductase regulatory TP53 inducible subunit M2B* (*RRM2b*), *deoxycytidine kinase* (*DCK*), and *thymidine kinase 1* (*TK1*) (**Figure 30A**)[265].

The expression of MYC is downstream of multiple control mechanisms that are regulated by nutrient levels and respond to metabolic stress (**Figure 30B)**. In AML, deregulation of *MYC* (chromosome amplification/translocation, super-enhancer activation, aberrant upstream signaling) along with the inactivation of the serine-threonine protein phosphatase 2A (PP2A) which marks MYC for ubiquitin-mediated proteasomal degradation, is persistently found[266]. In a similar way to *TP53* mutation, MYC deregulation rewires multiple metabolic pathways to generate energy and building blocks for the growing of tumor cells. Conversely, tumor cells need to modulate *MYC* expression and/or function for better survival under poor nutrient conditions (increased demands of glucose, glutamine, or essential amino acids).

A.

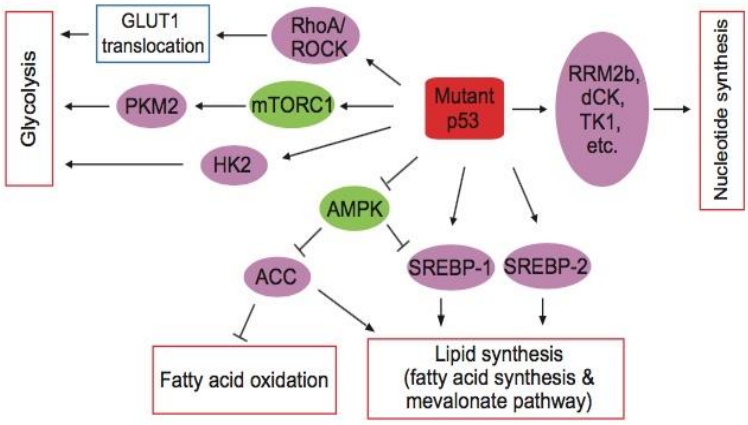

B.

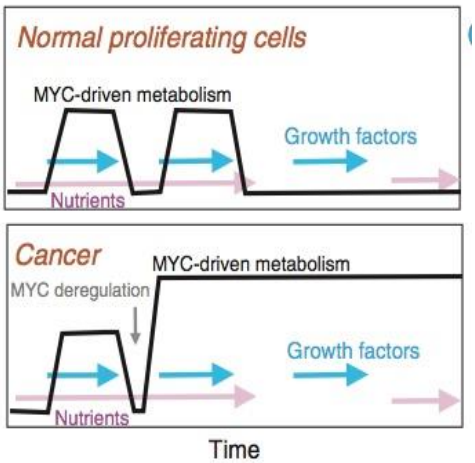

Figure 30: Metabolic rewiring by oncogenic TP53 and MYC. (A) Regulation of metabolism by gain-of-function TP53 mutations (from [267]). TP53 promotes GLUT1 translocation to the plasma membrane through activation of a small GTPase RhoA, thus promoting glycolysis and Warburg effect. Mutant TP53 also promotes glycolysis through inducing the expression of HK2 and enhancing mTORC1-mediated phosphorylation of PKM2. Mutant TP53 induces the expression of gene involved in the mevalonate and fatty acid synthesis pathway through SREBPs activation. (B) *The effect of nutrient and growth factor availability on MYC-driven metabolism (from [257]). In normal proliferating cells, MYC-driven metabolism is activated in the presence of nutrients and growth factors and individual exposure to nutrients or growth factors is not sufficient to activate MYC-driven metabolism, while in cancer cells, MYC deregulation leave cells unable to turn off MYC-driven metabolism independent of growth factors and nutrient availability.*

4.6 BRANCHED CHAIN AMINO ACIDS (BCAA) METABOLISM

Branched chain amino acids (leucine, isoleucine, and valine) have an aliphatic sidechain with a branch (a central carbon atom bound to three or more carbon atoms) (**Figure 31**). The three proteinogenic BCAAs are among the nine essential amino acids for humans, accounting for 35% of the essential amino acids in muscle proteins and 40% of the pre-formed amino acids required by mammals[268].

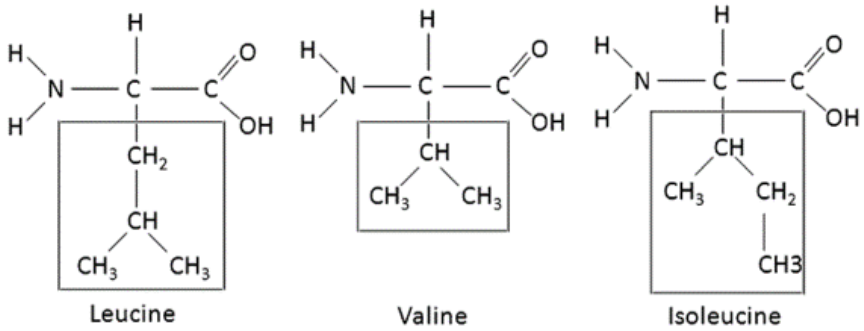

Figure 31: Branched chain amino acids. The side carbon chain is composed of 3-4 carbon atoms branched to the aliphatic core.

BCAA are transported into the cytosol through the L-Type amino acid transporter 1 (LAT1) also known as the solute carrier family 7 member 5 (SLC7A5). LAT1 transports BCAAs into the cell via a bi-transport system that simultaneously exports glutamine. BCAA might also be transported through LAT2 (SLC7A8) and LAT4 (SLC43A2).

The mTORC1 complex regulates BCAA catabolism independently of leucine sensing as rapamycin treatment significantly suppressed the leucine-induced activation of the complex despite similar increases in leucine and αKIC levels[269].

4.6.1 BCAA metabolism

After their absorption in the gut, BCAAs are catabolized in two major steps (**Figure 32**), in the muscle and liver. BCAA catabolism begins with a transamination reaction catalyzed by the branched chain aminotransferase (BCATs). BCAA produce branched chain α-ketoacids (BCKDA), known as α-ketoisocaproate (αKIC), α-ketoisovalerate (αKIV), and α-keto-β-methylvalerate (αKMV), and corresponding to leucine, valine, and isoleucine

transamination respectively. Valine is found at the highest concentration in circulation, followed by leucine and isoleucine. αKIC was reported to have the highest concentration in the human blood suggesting preferential use of leucine in several metabolic processes[270].

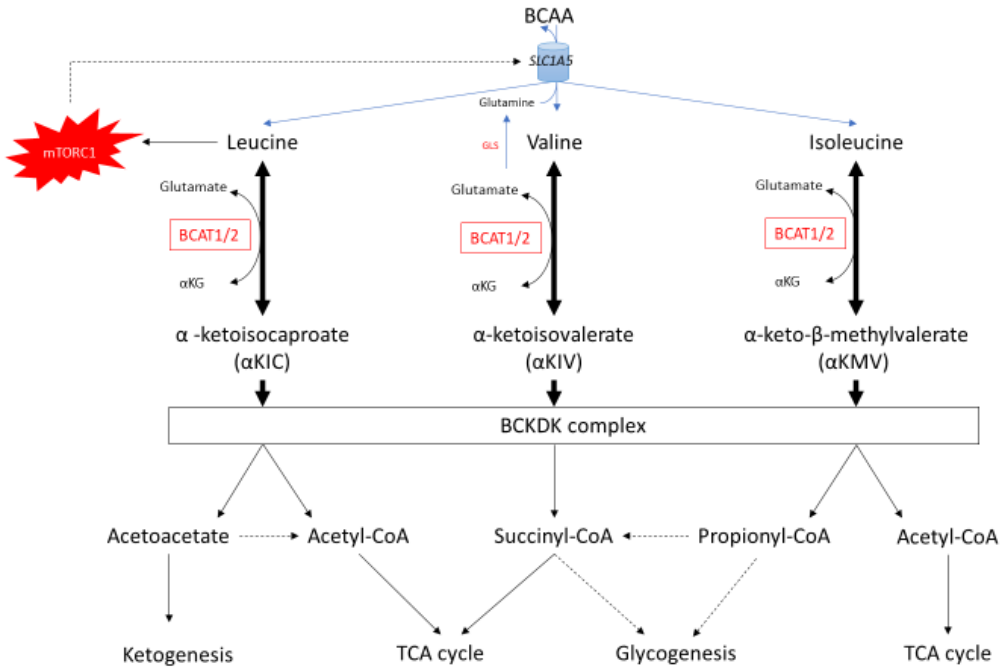

Figure 32: Schematic representation of BCAA catabolism. BCAA are converted into branched-chain α-ketoacids (BCKDA) by removing their amino group; the alpha-keto acids must travel to the liver to undergo oxidation. BCKDA are decarboxylated by the branched-chain α-ketoacid dehydrogenase complex (BCKDC). Finally, they are catabolized by a series of enzyme reactions: acetyl-CoA and acetoacetate from leucine, succinyl-CoA from valine, and both acetyl-CoA and succinyl-CoA from isoleucine. Most of acetyl-CoA enters the TCA cycle. Succinyl-CoA and propyonil CoA are also used for glycogenesis through carnitine metabolism and acetoacetate for ketogenesis.

BCAT1 (cytosolic) and BCAT2 (mitochondrial) are αKG-dependent transaminases. Kruppel like factor 15 (KLF15) and peroxisome proliferator-activated receptor δ (PPARδ) participate in the control of *BCAT1* expression[271]. KLF15 is induced under unfed conditions, which allows it to suppress lipogenesis and increase BCAA catabolism to provide substrates for enhanced glycogenosis[272]. Like other transaminases, BCAT require the cofactor pyridoxal-5'-phosphate (PLP or vitamin B6) to catalyze the reaction.

BCAT transamination is bidirectional. BCAA catabolism is regulated by both allosteric (through vitamin B6 or PLP) and covalent mechanisms (through αKG availability). The

redox-active dithiol/disulfide C315-Xaa-Xaa-C318 (CXXC) *center*, which allow the reversible nature of the transamination plays a major role in catalytic reactions. BCAT2 is more sensitive to the redox environment of the cell and BCAT1 demonstrates a lower redox potential (approximately 30 mV) compared to BCAT2, suggesting that redox status may influence BCAA catabolism[273]. BCAT enzymes operate near equilibrium, with both substrate and BCKA concentrations being at or below their Km values. This equilibrium allows BCAT isozymes to quickly respond to metabolic demand in the tissue concerned.

In the next step, the mitochondrial complex branched chain α-keto acid dehydrogenase (BCKD, also known as BCKDC, for BCKD complex) irreversibly catabolizes BCKA through oxidative decarboxylation. BCKD is found on the mitochondrial inner membrane and is composed of E1α (also known as branched chain keto acid dehydrogenase E1 subunit alpha, BCKDHA) and E1β (BCKDHB), E2 (DLT), and E3 (DLP).

BCKDHC is an important gatekeeping enzyme that is regulated by reversible phosphorylation catalyzed by a specific BCKD kinase (BCKDK); this phosphorylation inhibits BCKDHC activity and blocks BCAA catabolism. On the opposite, dephosphorylation of BCKDHC by the mitochondrial protein phosphatase PP2Cm (encoded by *PPM1K* gene) stimulates BCKDHC activity. The coordinated response between BCKDK and PP2Cm achieves optimal BCKDHC activity to maintain BCAA homeostasis and are directly regulated by BCKDA levels and especially αKIC[274,275].

4.6.2 BCAA metabolism in HSC and progenitors

BCAA metabolism in HSC and progenitors remain largely elusive. Recently, Wilkinson and colleagues showed that BCAA homeostasis is critical for HSC proliferation and survival. BCAA imbalance, and especially high concentration of valine, inhibits HSC growth more strongly than insufficiency of the three BCAAs. Therefore, imbalance of BCAAs may be an essential promoter of dysfunction of HSCs[26].

In the human hematopoietic system, *BCAT1* expression is elevated in HSC and progressively downregulated throughout differentiation, when compared to BCAT2 (**Figure 33**).

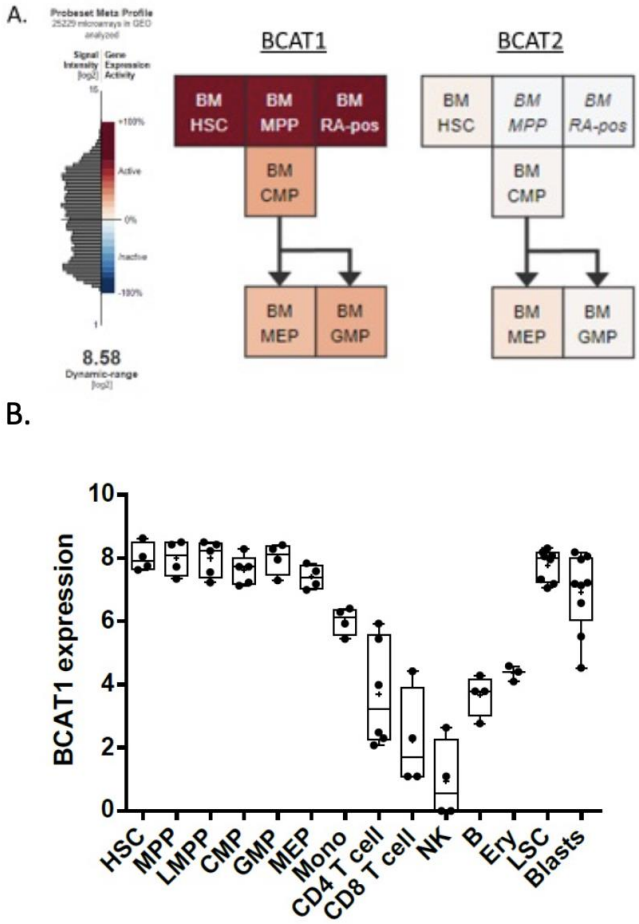

Figure 33: A) BCAT1 and BCAT2 expression in the hematopoietic tree (from https://gexc.riken.jp/). B) human BCAT1 log2 expression. Data sets are GSE17054 (HSC), GSE19599 (GMP, MEP), GSE11864 (monocytes). Common myeloid progenitor, CMP; granulocyte-macrophage progenitor, GMP; hematopoietic progenitor, early HPC; megakaryocyte/erythroid progenitor, MEP; promyelocytes, PM; myelocytes, MY; polymorphonuclear in the bone marrow, PMN_BM; polymorphonuclear in the peripheral blood, PMN_PB.

A similar gene expression profile is observed for other key regulators of BCAA metabolism and especially *PPM1K* and *BCKDHA* (**data not shown**). Liu and colleagues reported a high expression of *PPM1K* in mouse long-term-HSCs compared with short-term HSCs, progenitors (MEP, CMP, CLP, and Lin- cells) and differentiated cells[276]. In murine HSC, PPM1K, which activate BCKDKC, promotes BCAA catabolism and maintains the glycolysis and quiescence of HSCs through the downregulation of the transcription factor MEIS1 and cell cycle regulator p21/CIP[276]. Gu and colleagues showed that *BCAT1* is repressed by EZH2-PRC2 mediated H3K27me3 in normal hematopoietic processes [277].

BCAT1 could also to have regulatory functions in mature myeloid cells. Oral administration of BCAA had stimulatory effects on peripheral blood mononuclear cells (PBMCs) and led to increased IFN-g production[278]. Papathanassiu and colleagues also demonstrated that BCAT1 is critical in human macrophage inflammatory responses; *BCAT1* inhibition reduces oxygen consumption and OXPHOS but also glycolysis, suggesting a pleiotropic function of BCAT1 in cellular metabolism[279].

The role of BCAA metabolism in cancer pathogenesis has been a topic of interest and has recently been extensively reviewed in [26,280,281].

4.6.3 BCAA metabolism in leukemia

Recent studies have illustrated the main contribution of BCAT1 in human leukemia. Hattori and colleagues evidenced a link between altered BCAA metabolism and propagation of blast crisis chronic myeloid leukemia (BC-CML)[226]. These authors showed that BCAT1 is functionally required for CML and up regulated during CML progression. They identified Musashi2 (MSI2), an oncogenic RNA binding protein that physically associates with the *BCAT1* transcript, as a positive regulator of BCAT1 protein accumulation in leukemic cells. Blocking expression or enzymatic activity of BCAT1 induces cellular differentiation and significantly impairs the propagation of BC-CML both *in vitro* and *in vivo*. Metabolic analysis demonstrates intracellular BCAA production by BCAT1; consistently, direct supplementation with BCAA ameliorates the defects caused by *BCAT1* knockdown. They also showed that BCAA anabolism is associated with mTORC1 activation. In addition, the authors evidenced that, *BCAT1* expression also predicts disease outcome in an AML patient cohort.

In another study, Raffel and colleagues showed that high *BCAT1* expression mimics *IDH* mutations in AML[227]. The authors performed high-resolution proteomic analysis of human LSC and non-stem cell populations and found that the BCAA pathway was enriched and BCAT1 protein and transcripts were overexpressed in LSCs. Depletion of BCAT1 suppressed the proliferation and survival of AML cells *in vitro*, and eliminated leukemic initiation i*n vivo*, indicating a requirement for BCAT1 in AML LSCs. BCAT1 depletion also resulted in accumulation of αKG, leading to EGLN1-mediated degradation of HIF1α, and

HIF1α overexpression was sufficient to restore cell growth and survival after *BCAT1* knockdown. Conversely, *BCAT1* overexpression decreased intracellular αKG levels and caused DNA hypermethylation through inhibition of TET2, "mimicking" the effects of *IDH* mutations. As reported, by Hattori and colleagues[226], the authors also found that high *BCAT1* expression is associated with poor survival in patients with AML, but not in *IDH*- or *TET2*-mutant AML, consistent with the redundant role of BCAT1 overexpression and *IDH* mutations in suppressing TET2 activity. High *BCAT1* expression was associated with enrichment of LSC signature genes, and *BCAT1* expression increased upon AML relapse. Thus, BCAT1 activity supports LSC.

More recently, Jin and colleagues showed that *BCAT1* overexpression confers a worst overall prognosis among normal karyotype AML. As *IDH* mutational context has been reported to confer a specific "BRCAness" phenotype[167,168] and that *BCAT1* overexpression might recapitulate *IDH* epigenetic phenotype[227], the authors hypothesized that a "BRCAness" phenotype could also be observed in AML samples overexpressing *BCAT1*. They observed an increase in the base line level of DNA damage marker γ-H2AX and found an excess of cytoxicity when PARP inhibitors were combined with genotoxic agents in BCAT1 overexpressing cells[282].

4.6.4 BCAA metabolism in glioma

BCAT1 expression is especially high in the brain, contributing to cytosolic glutamate generation for neurotransmitter production. Tonjes and colleagues found that a distinct subset of glioblastomas, which have wild type *IDH*, have increased expression of *BCAT1* [283]. The authors found that expression of *BCAT1* is necessary for the progression of gliomas. *BCAT1* expression seems to be controlled by αKG levels suggesting that αKG or D-2HG levels may influence BCAA metabolism. In culture, inhibition of BCAT1 resulted in partial cell cycle arrest and substantial suppression of proliferation. *BCAT1* knockdown also decreased invasiveness and led to decreased secretion of glutamate, an excitatory brain neurotransmitter. This indicates that increased glutamate secretion mediated by cancer cells with increased *BCAT1* levels may be involved in the pathogenesis of neurotoxicity to tumor-adjacent normal brain tissue and may contribute to the propensity of patients with glioma to have seizures.

IDH mutant tumoral cells are also dependent on glutaminolysis even though the molecular mechanism underlying this selectivity remains[284]. Interestingly, glutamine reliance seems to be related to BCAT complexes as BCAT1 loss increases reliance on glutaminase for glutamate and glutathione synthesis in mutant *IDH* glioblastomas[179].

4.7 WORKING HYPOTHESIS

IDH is at the corner stone between metabolism and epigenetic. Comprehensive studies reporting metabolic changes with respect to mutant *IDH* have mainly focused on glioma, but little is known about mutant *IDH*-induced specific alterations in metabolism in primary AML cells (reviewed in [188]).

It remains important to explore these metabolic changes for leukemogenesis and to explore their potential for therapeutic exploitation and notably to identify therapies that may exploit D-2HG-driven molecular effects. For instance, D2-HG induces vitamin D receptor-related transcriptional changes, priming leukemic cells to differentiate with pharmacologic doses of all-*trans* retinoic acid (ATRA) and/or vitamin D[183]. D-2HG as a metabolite itself (in wildtype *IDH* cellular context) primarily suppresses glycolysis in leukemia cells and thereby rewires leukemic metabolism[285]. Stuani and colleagues also recently reported that OXPHOS plays a crucial role in mutant *IDH* biology and in response to IDH inhibitors[185]. In *IDH1* mutated glioblastomas, McBrayer showed that D-2HG inhibit αKG-dependent transaminases BCAT1 and BCAT2, thereby decreasing glutamate levels, increasing BCAA levels and more specifically leucine amino-acid. By using this metabolic specificity, the authors identify that glutaminase inhibition specifically sensitized IDH mutant glioma cells to oxidative stress and radiation [286]. Raffel et al showed in AML settings that BCAT1 links BCAA catabolism to HIF1α stability and regulation of the epigenomic landscape, thus mimicking the effects of IDH mutations[227].

Previous results of our team and others have shown that the differentiation block induced by IDH mutants is reversible using a specific allosteric inhibitor, enasidenib[287–289]. Clinical results have been now reported[290,291]. Although the survival benefit provided by mutant IDH2 inhibition is clear, primary resistance have been described and relapse

remains of major concern. An essential question for the implementation of every targeted or metabolic-driven therapy is the determination of the escape mechanism and also their diversity.

<u>The major aims of the project are:</u>

1. **Identify deregulated metabolic pathways in IDH^{mut} human primary leukemic cells by pan-metabolome approach, decipher functional consequences of metabolism alteration, and evaluate if this metabolic pathway might represent a potential metabolic vulnerability.**
2. **Evaluate the molecular bases of response and acquired resistance to enasidenib on paired diagnosis/relapse samples obtained from the AG-221/CC90007/enasidenib clinical trial**

5 METHODOLOGY

5.1 METABOLITES ASSESSMENT AND MASS SPECTROMETRY

5.1.1 2HG measurement

2HG metabolites levels were determined by ion-paired reverse-phase LC coupled to negative mode electrospray triple-quadrupole mass spectrometry using multiple reactions monitoring, and integrated elution peaks were compared with metabolite standard curves for absolute quantification as previously reported[292].

5.1.2 Liquid-chromatography/mass spectrometry (LC-MS)

Liquid chromatography coupled to a mass spectrometer analyses were performed at the CEA (Commissariat à l'énergie atomique et aux énergies alternatives) in Saclay (France) in collaboration with Dr. Christophe Junot (director of the Laboratoire d'étude du métabolisme des médicaments, LEMM) and under the supervision of Drs Sandrine Aros-Calt and Florence Castelli. Sample preparation consisted essentially in the removal of proteins by methanol precipitation (initial steps). Two 150 µL volumes of each sample were transferred to clean, labeled Eppendorf tubes before being dried in a Speed Vacuum. In addition, 100 µL of each sample was transferred into a 5 mL Eppendorf tube (30 samples x 100 µL = 3 mL total). This volume was vortexed and then separated into 4 x 1.5 mL Eppendorf tubes (750µL in each). These 4 tubes were used for the development of the analysis of AML extracts on LC-MS (choice of the optimal concentration mainly). The mass spectrometry analyzer was an Exactive (Thermo). Different columns were used, for the broadest possible metabolomic analysis. Finally, we chose to run these samples on a first ZIC-HILIC column (Hydrophilic Interaction Liquid Chromatography; SeQuant) allowing, by the weak interactions between the charged metabolites and the neutral zwitterionic stationary phase, a good selectivity for polar and hydrophilic compounds: sugars, small metabolites, organic acids and bases, amino acids, peptides among others. Both negative and positive modes were used to increase the total number of compounds identified. Metabolites heatmap was realized by BRB-arrray Tool 4.5.0.2.

5.1.3 GC-MS based metabolic analysis: BCAA tracing

Cells were cultured and labeled in media supplemented with either 170 µM [(U)-13^C]-L-Leucine, 30 or 170 µM [(U)-13^C]- KIC sodium salt (for 13C tracer experiments; Cambridge Isotope Laboratories). The concentrations are based on the standard RPMI-1640 media formulation. At the time of collection (0, 30 and 60 minutes respectively), cells were washed twice with ice-cold PBS and iced shocked in liquid azote. After thawing, insoluble particles by centrifugation were removed by centrifugation the supernatants were collected and dried using a SpeedVac at 30°C. The cell extracts were dissolved. Calibration samples (150–250 mM) were prepared from 98% 15^N-enriched leucine (Isotec Inc.) and 13^C-enriched KIC and 13^C,15^N-enriched leucine. All signals were identified either with authentic samples or by reference to literature values. These analysis were realized by Pr Ottolenghi Christopher (Hopital Necker, service de biochimie analytique, Paris).

5.2 CELL CULTURE

5.2.1 Cell lines and reagents

PLB-985 and K562, cell lines were cultured in non-treated culture dishes, plates, or flasks at 37°C in 5% CO2 with Fisher Scientific RPMI 1640 Medium (Gibco, 11340892) supplemented with 10% fetal bovine serum (FBS, Sigma Aldrich, F2442), 1% Glutamine, 100 UI/ml Penicillin. HEK 293T cells used for lentiviral production were grown in Dulbecco's Modified Eagle Medium (DMEM, glucose 4.5 g/L, and sodium pyruvate) supplemented with 10% FBS, 1% Glutamine and 100 UI/ml Penicillin. BCAT1 inhibitors were BCATc inhibitor 2 (Cayman Chemical, 9002002) and gabapentin (Tokyo Chemical Industry Co.). mTORC1 and mTORC2 inhibitors were purchased from Selleckchem (GSK458 (S2658), PP242 (S2218) and rapamycin (S1039)).

5.2.2 Human primary samples

All samples were obtained from the department of Hematology, Gustave Roussy (Villejuif, France) in a collaboration with Dr. Stéphane DeBotton. Peripheral blood and/or bone marrow aspirates samples were obtained at time of diagnosis or relapse. Informed consents were obtained from all patients in accordance with the Declaration of Helsinki. AML diagnosis was morphologically proven according to the French-American–British (FAB)

classification. Immunophenotyping and cytogenetic analyses were done locally. Description of the karyotypes followed the International System for Human Cytogenetic Nomenclature. Patients with AML provided a written informed consent in accordance with the declaration of Helsinki. Bone marrow samples were enriched in AML blast cells using Ficoll gradient density centrifugation. Characteristics of the patients are provided in table below.

	Patient number	Age	IDH status	Karyotype	NPM1	FLT3-ITD
IDH2m	#1	77,6	IDH2 R140Q	Normal	mut	wt
	#2	60,5	IDH2 R172H	Normal	wt	wt
	#3	73,9	IDH2 R140Q	Trisomy 8	wt	wt
	#4	47,7	IDH2 R140Q	-7	wt	wt
	#5	47,0	IDH2 R140Q	Normal	mut	mut
	#6	58,2	IDH2 R172K	Normal	wt	wt
	#7	73,3	IDH2 R140Q	Normal	wt	mut
IDHwt	#1	65.2	wt	MK	mut	wt
	#2	66.4	wt	MK	wt	wt
	#3	59.1	wt	-7	wt	wt
	#4	75	wt	Iso6p	wt	wt
	#5	71.3	wt	Normal	mut	mut
	#6	49.6	wt	Normal	wt	mut

Cells were cultured in serum-free conditions Stemspan medium (StemCell Technologies) in the presence of recombinant human cytokines (25ng/ml hSCF, 10ng/ml hFLT3-L, 10ng/ml hTPO, hIL6 10ng/ml, 10ng/ml hIL3, 1UI/ml hEPO, 1ng/ml hGCSF and 5ng/ml human GM-CSF). All cytokines were from PeproTech France (Neuilly s/Seine, France).

5.3 VIRAL CONSTRUCTS AND PRODUCTION

We used pRRL lentivirus expressing wild type *IDH2* or *IDH2*^{R140Q} as previously reported in [287]. *BCAT1* lentiviral short hairpin RNA (shRNA) constructs were obtained from Hattori and colleagues [226]. Virus was produced in HEK cells transfected using polyethylenimine with viral constructs along with VSV-G and gag-pol. For lentivirus production Rev was also co-transfected. Viral supernatants were collected for two days followed by ultracentrifugal concentration at 50.000×g for 2h. For lentiviral infections, cells were seeded at 2x10^6/ml with 10µl of lentiviral supernatant, and then GFP$^+$-sorted on Influx -UV (BD Biosciences) flow cytometer.

5.4 MOLECULAR BIOLOGY ASSAY

5.4.1 Primary cells analysis

Mice were sacrificed when marrow or blood infiltration reach at least 80% or at any sign of clinical deterioration. Primary AML cells or PDX samples were incubated with SYTOX blue (Life Technologies SAS, Saint Aubin, France) to label dead cells prior to flow cytometry sorting based on hCD45 expression. Cells were gathered and sorted based on human (PeCy7) and murine (APC) CD45 (Becton Dickinson France SAS, Le Pont-De-Claix, France) expression.

5.4.2 DNA extraction, Real-time qPCR analysis

Cells were processed for DNA extraction with the All Prep DNA/RNA Microkit (Qiagen) and DNA was quantified with the Nano-Drop ND-1000 spectrophotometer (Nano-Drop technology). cDNA was synthesized from total RNA purified (using the RNeasy microkit, QIAgen) from GFP+-sorted or sorted primary leukemic samples using the Superscript II reverse transcriptase (Invitrogen). The expression level of each gene was assessed by qRT-PCR with an ABI PRISM 7500. The 2-ΔΔCt method was used to normalize expression to B2M for cell lines and primary AML samples.

	Forward (5'-3')	Reverse (5'-3')
BCAT1	CAACTATGGAGAATGGTCCTAAGCT	TGTCCAGTCGCTCTCTTCTCTTC
transcript 201	GCTACGACCCTTGGGATCT	AAGTCCCCACCACCTCTTTT
transcript 202	GTGCCACTGCCGCTCTCT	AAGTCCCCACCACCTCTTTT
transcript 204	CGGTATCATGGATTGCAGTA	CTATTAGGTCTTTAGCCT
BCAT2	TTCATTCGTCAGAGCCTGGATA	ACTACTCCAGGCAAGATGACGC
BCKDK	CAAGACCGTCACCTCCTTTT	CTTTCATCATTGGCTGCAAC
BCKDHA	CAGTCCCGCAGGAAGGTGA	TAGTGCTCCCCGTAGGTCTGC
PPM1K	GTCAGAAGTGGTGGGAACC	GAATTGGCTTGCCATACTTA
B2M	ACTGAATTCACCCCCACTGA	CCTCCATGATGCTGCTTACA

5.4.3 HpaII tiny fragment Enrichment by Ligation-mediated PCR assay (HELP)

Specific cytosine methylation on BCAT1 promotors 1 and 2 was assessed by Thermo Scientific EpiJET DNA Methylation Analysis Kit (MspI/HpaII). Digestion and PCR was realized according to manufacturer instruction. 5-mC percentage was then calculated as % of 5-

mC =100 / (1 + E)$^{Cq2-Cq1}$. Primer sequences used for HELP assay are summarized in table below.

Cytosine	Promotor	Forward (5'-3')	Reverse (4-3')
c.211	P1	AAATCTGGAGTCCCAGCCT	TCAGAGCGAGTCCATAGCT
c.340	P1	AATATCTGCGCTTGGAAAGG	AACCCCTCCAGCATCCCTT
c.138	P2	ACTCGGATACGCACCCACAGT	CGAAGATTCGGAGCCAGCG

5.4.4 Chromatin immunoprecipitation sequencing (CHIP-Seq)

Chromatin immunoprecipitation (ChIP) was performed at the Centre de recherche en cancérologie de Marseille, under the supervision of Dr Syvain Garciaz and Estelle Duprez as previously described [293]. Mutant and wild type *IDH2* samples were obtained from Drs Syvain Garciaz and Estelle Duprez.

5.5 WESTERN BLOT ANALYSIS

Primary samples or cell lines were rinsed with ice-cold PBS, lysed in 10µl/10^6 cells in RIPA buffer, and were shock-frozen in ice. Samples were vortexed and centrifuged at 14,000 rpm for 10min. The upper phase was removed and quantified with BCA Protein Assay Kit (Pierce -Thermo Scientific). Proteins were resolved on 4–12% TGX gels (Criterion, Bio-Rad) with TGS (Tris-GlycineSDS) running buffer (Bio-Rad) and blotted on PVDF membranes (Trans-Blot TURBO, Bio-Rad). Membranes were blocked for 1h in TBS containing 0.3% (v/v) Tween-20, with 5% (w/v) BSA powder. Primary antibodies against BCAT1 (1/1000; Cell Signaling Technologies, 12822), BCAT2 (1/1000; ThermoFisher, PA5-21549), AKt (1/1000; Cell Signaling Technologies, 4685), pAkt Ser473 (1/1000; Cell Signaling Technologies, 4060), S6K (1/1000; Cell Signaling Technologies, 2708), pS6K Thr389 (1/1000; Cell Signaling Technologies, 9205), 4EBP1 (1/500; Santa Cruz Biotechnology, sc-9977), p4EBP1 (1/10000; Santa Cruz Biotechnology, sc-18091-R), hsc70 (1/10000; Santa Cruz Biotechnology, sc-1059), were incubated overnight at 4°C in blocking solution. Phospho-antibodies were incubated in 5% w/v BSA, 1X TBS, 0.1% Tween-20 at 4°C with gentle shaking, overnight. Secondary antibodies (anti-rabbit-IgG peroxidase-linked antibody or anti-goat-IgG horseradish peroxidase-linked antibody were incubated for 1h at room temperature. Membranes were washed in TBS-Tween 0.3% and immunocomplexes

were detected using an ECL Kit (ThermoFisher, 32106) and acquired with an Image Quant LAS-4000 (Bio-Rad).

5.6 FLOW CYTOMETRY

Flow cytometry assays were analyzed using flowjo (BD biosciences) software.

5.6.1 Annexin V

Cells were washed in annexin V binding buffer, incubated with PE-coupled annexin V (BD biosciences).

5.6.2 Differentiation assay in human primary samples

Cells were washed with PBS, supplemented with 0.5% SVF (flow cytometry washing buffer) and Fcblocked with 0.1µl of human IgG/10^5 cells for 15 min at room temperature (Human TruStain FcX Fc Receptor Blocking Solution, BioLegend) prior to staining. After washing, cells were transferred to a 5ml tube and incubated with 1 µl/10^6 cells of antibody for 30- 45 minutes at 2° - 8° C. As a control for this analysis, cells (in a separate tube) were treated with equivalent IgG1 isotype antibodies (BD biosciences). Cells were then analyzed on a BD LSRFortessa™ (BD biosciences). Cytometric analysis was performed using phycoerythrin (PE)-conjugated anti-human CD11b (BD biosciences, clone ICRF44), FITC-conjugated anti-human CD14 (BD biosciences, clone 61D) APC-conjugated anti-human CD15 (BD biosciences, VIMC15), PerCP-Cy5-conjugated anti-human CD24 antibodies (BD biosciences, clone ML05), PeCy7-conjugated anti-human CD34 (BD biosciences, clone 8G12).

5.7 MURINE EXPERIMENTS

5.7.1 Patient derived xenograft (PDX) model

All animal studies were conducted with approval of the local ethics committee. Sorted mutant *IDH2* and wild type *IDH2* primary samples (0.5-1x10^6 cells) were transplanted in NOD SCID IL2Rgammanull (NSG) mice after sublethal irradiation (1.5 Gy). After transplantation, recipient mice were evaluated every week for signs of morbidity and weight loss, failure to groom. Mice were monthly evaluated by marrow biopsy to assess PDX

engraftment. Premorbid animals were sacrificed, and relevant tissues were harvested and analyzed by flow cytometry and histopathology. For *BCAT1* knockdown by retroviral shRNA transduction, primary AML cells were transduced with either shRNACtrl or shRNA-Bcat1c/d retrovirus for 48 h. Infected cells were sorted based on GFP expression, and 0.5-1x10^6 cells tractor were transplanted in sublethally irradiated NSG recipients. At sacrifice, sorted GPF positive and negative blood cells were cytospin and stained with MGG stain solution for cytopathologic evaluation. Marrow and spleen were fixed in and histology assessed by a board-certified veterinary pathologist.

For *in vivo* mTOR inhibition, human primary samples were transduced with mCherry pFuw-luciferase lentivirus and mCherry$^+$ FACS-sorted cells were transplanted in NSG recipients as previously. Engraftment was assessed by hCD45 flow cytometry staining in peripheral blood or bone marrow. Mice received by daily oral gavage 3mg/kg/d GSK428 or vehicle for a month. AML cells burden was assessed with *in vitro* imaging system (IVIS) every week (see below). After 1 month or in case of morbidity signs, mice were sacrificed and AML cell burden was measured by flow cytometry and sorted based on hCD45 staining.

5.7.2 *In vitro* imaging system (IVIS)

Luciferin at 15mg/mL was intra-peritoneally injected in pFuw-PDX mice recipients, treated with GSK458 or vehicle, 10-15 minutes before imaging on IVIS 50 (Perkin Elmer).

5.8 SURVIVAL ANALYSIS

BEAT AML and TCGA datasets were used to assess *BCAT1* expression on overall survival. Samples were stratified according to genotype and *BCAT1* expression (high, above median; low, below median). Survival analysis used a Mantel-Cox log-rank test and a hazard-ratio (log-rank) test using GraphPad Prism 7 software.

6 RESULTS

6.1 PART I: IDH2 MUTATIONS AND BCAA METABOLISM

6.1.1 Metabolic profile distinguishes mutant and wild type *IDH2* AML cells

In order to clarify the metabolic abnormalities caused by the expression of mutant *IDH* in the context of primary AML cells, the team has undertaken an untargeted metabolism analysis of clinical samples (sera and plasma) from patients with AML harboring (N=17) or not (N=7) an *IDH2* mutation, by LC-MS (high resolution liquid chromatography-mass spectrometry, LC qExactive). This analysis was performed by Dr. Florence Castelli and Pr Christophe Junot, LEMM, CEA. Clinical samples included baseline/diagnosis samples and obtained at different time points during treatment (frontline intensive chemotherapy). Four analytic procedure/sample (HILIC pos/neg and C18 pos/neg columns) were realized in order to potentiate metabolites identification. Alignment of detected peaks was performed according to the mass-to-charge ratio (m/z) value and normalized migration time. The detected peaks were compared with all substances registered on the Human Metabolome Technologies Metabolic Substance Database based on the m/z and MT or RT values, including home-made data bases (Drs Castelli and Junot). Obtained peak area were converted to aera under the curve (AUC); data processing and analysis will be described later on.

6.1.1.1 Altered metabolism of BCAAs in primary mutant IDH2 AML cells

Results presented here were obtained from the HILIC-neg dataset. Hilic-negative indicates the dataset obtained by hydrophilic interaction liquid chromatography (HILIC)-electrospray ionization (ESI) in negative mode. Overall, 2757 substance peaks were identified. 289 annotated metabolites were identified at baseline (minimal value > 0.1%) and unsupervised clustering identified 33 metabolites that were differentially expressed and clearly separate samples with or without *IDH2* mutation (**Figure 34A**). Beside D-2-HG, the marked difference in the metabolic profile involved metabolites associated to the prostaglandin pathway, glutamine metabolism, fatty-acid metabolism and branched-chain amino acids (BCAA, consisting of valine, leucine and isoleucine) metabolism. Zhang and colleagues recently reported the overproduction of prostaglandin E2 (PGE2) in a

Dnmt3a KO-*Idh2*^{R140Q} mouse model of leukemia ; PGE2 has been implicated in promoting stem cell self-renewal and cancer stem cell maintenance[170].

Interestingly, two derivatives of the BCAA metabolic pathway were present at lower levels in mutant *IDH2* samples: the 2-hydroxy-3-methylbutyric acid, that mainly originates from the terminal ketogenesis of valine, leucine, and isoleucine, and the α-ketoisocaproic acid (αKIC) that is the branched chain α-keto acid (BCKA) of leucine (**Figure 34B**). For αKIC, median AUC was $3.2x10^7$ (range: $9.9x10^5$-$5.3x10^7$) in mutated *IDH2* samples compared to $6.1x10^8$ (range: $3.7x10^7$-$5.8x10^8$) in wild type *IDH2* samples ($P<0.001$). Interestingly, there was also a trend toward higher isoleucine and leucine levels in mutant *IDH2* samples, although the differences were not statistically significant (not shown); the keto analog of valine, α-ketoisovalerate (αKIV), and the keto analog of isoleucine, α-keto-β-methyl-valerate (αKMV), were not identified/annotated in our datasets. We confirmed by GC-MS on an independent cohort of mutated (N=21) and wild type (N=10) *IDH2* samples, a lower serum level of αKIC in mutated *IDH2* samples compared to wild type (0.7 vs 9.7 µmol/l, $P=0.0008$) (**Figure 34C**). We also observed a significant negative correlation between D-2 HG and αKIC levels ($R^2= 0.47$, $P=0.006$) (**Figure 34D**).

We investigated αKIC levels during intensive chemotherapy course and observed that αKIC level distinguishes patients with distinct clinical characteristics (**Figure 34E**). High and stable αKIC levels identify patients who attain complete response (CR) (100% vs 50%, $P=0.13$) and show a better disease free survival (DFS) (not reached vs 3.3 months, $P=0.03$), when compared to others patients. In contrast, primary refractory patients and patients with early relapse (relapse within 12 months following CR1) showed lower αKIC levels (two way RM ANOVA: $P=0.03$ for interaction). These preliminary data suggest that αKIC levels might represent a predictive factor for chemo-resistance and/or poor outcome in this clinical context. Patients characteristics are summarized in **Figure 34F**.

6.1.1.2 Leucine anabolism is favored in primary mutant IDH2 AML cells

The catabolic pathway of BCAAs is the predominant direction in most tumor types and involves a first reversible transamination step performed by BCAT enzymes, who transfer the BCAA amino group to αKG to produce glutamate and a branched chain α-ketoacid (BCKA). BCKAs are converted back to BCAAs or oxidized to TCA cycle intermediates

through a series of additional enzymatic steps, initiated by an irreversible oxidative decarboxylation by the BCKDH complex. The overproduction of D2-HG in mutant *IDH*2 AML cells and the α-KG dependance of transaminases involved in the BCAA metabolism that support cancer progression, prompt us to investigate this metabolic pathway in primary mutant *IDH* AML cells. Interestingly, impaired leucine catabolism and inhibition of BCAT1 and BCAT2 by D-2HG hallmark mutant *IDH1* glioma cells[179].

To track the fate of leucine and αKIC in mutant and wild-type *IDH2* AML bulks, primary $SSC^{low}CD45^{int}$ blasts were purified by FACS and BCAA- and BCKA-tracing experiments were performed with [^{13}C]-labeled leucine or [^{13}C]-αKIC respectively. Samples were collected after 1 hour of tracing and metabolite measurement was performed by gas chromatography (GC)-MS. BCAA oxidation flux using [^{13}C]leucine established a significant labeling of αKIC in wild-type *IDH2* blasts, indicating a contribution of transamination to BCAA in those cells ([^{13}C]-αKIC conversion to leucine: mutant *IDH2* =39.13 ± 6.313; wild-type *IDH2* = 3.967 ± 1.686; P=0.0058). In contrast, a clear enrichment of labeled leucine was observed in mutant *IDH2* samples, showing the formation of leucine from αKIC but not the breakdown of leucine to αKIC. Stable isotope tracer experiments performed in the hematopoietic PLB-985 cells (a derivative of the human HL-60 cell line) engineered to express either human $IDH2^{R140Q}$ or the wild type allele confirmed a BCAA oxidation in the wild type context at 2 h after labeling; in contrast, [^{13}C]-αKIC formation was barely detectable in $IDH2^{R140Q}$ cells, while again an efficient production of leucine from αKIC was observed (**Figures 34G** and **34H**). Therefore, AML cells with *IDH2* mutation show decreased levels of αKIC compared to control cells, a situation reminiscent of mutant *IDH1* glioma cells where a BCKA depletion is observed[179,294].

A.

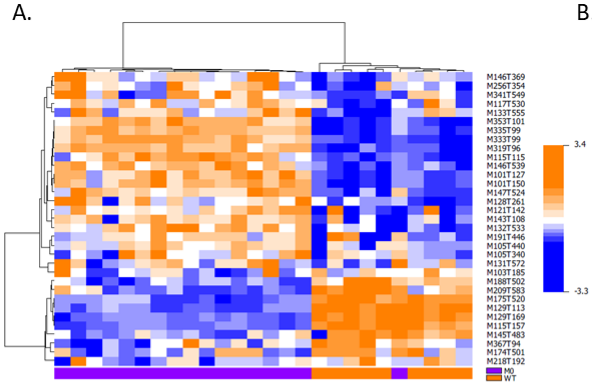

B.

Compound name	Compound family	KEGG-id	Fold-change (mIDH/WT)	p-value
Prostaglandin E1	Prostaglandin pathway	C04741	45.3	< 1e-07
Prostaglandin A2		C05953	22.34	< 1e-07
Prostaglandin B1		C00959	22.34	< 1e-07
D-2-Hydroxyglutaric acid	IDH2m consequence	C03196	11.48	< 1e-07
8S-hydroxy-eicosatetraenoic acid	Fatty acids metabolism	C14823	27.68	< 1e-07
Caproic acid		C01585	4.82	< 1e-07
Arabinose		C00259	2.40	0.004
Octanoic acid		NA	2.30	0.02
Mevalonic acid		C00418	0.21	< 1e-07
L-glutaminic acid	Glutamine metabolism	C00025	3.44	< 1e-07
N-acetyl-L-glutaminic acid		C00624	0.34	< 1e-04
L-glutamine		C00064	0.25	0.004
2-hydroxy-3-methylbutyric acid	BCAA metabolism	NA	0.24	< 1e-07
2-ketahexanoic acid (αKIC)		C00902	0.01	< 1e-07

C.

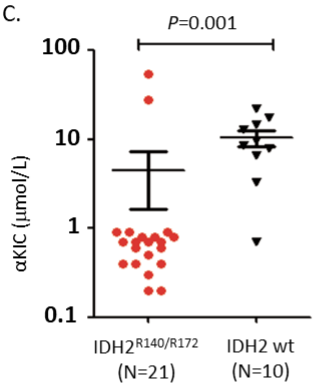

D.

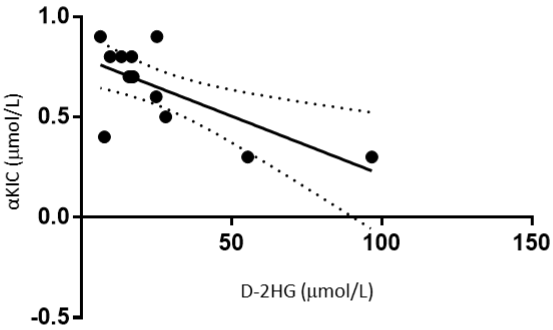

E.

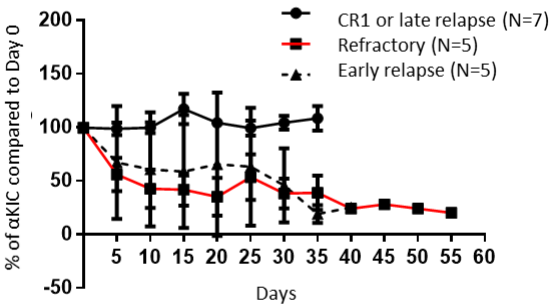

F.

	Stable αKIC kinetic (n=7)	Decreasing αKIC kinetic (n=10)
Median age, years (range)	59.2 (32-69)	59.8 (45-70)
D-2HG median, µM	12.2	12.7
IDH2 type of mutation		
IDH1 R132, n	3/7	1/7
IDH2 R140, n	4/7	7/9
IDH2 R172, n	0/7	2/9
Median marrow blasts, % (range)	73 (20-100)	70.5 (32-95)
ELN 2013 Classification		
Favorable, % (n)	42 (3/7)	40 (4/10)
Intermediate I/II, % (n)	58 (4/7)	50 (5/10)
Unfavorable, % (n)	0	10 (1/10)
Treatment response		
Complete remission, % (n)	100% (7/7)	50% (5/10)
Relapse incidence, % (n)	42% (3/7)	80% (4/5)

G.

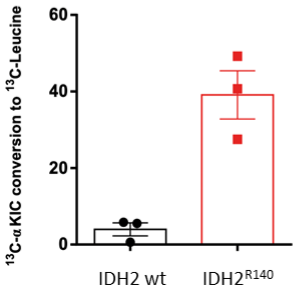

H.

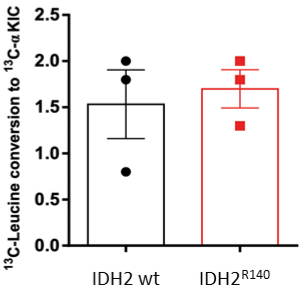

I.

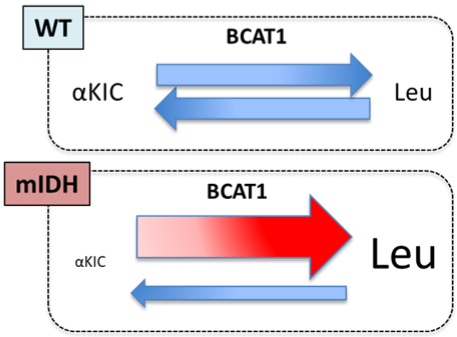

Figure 34 : A) Heatmap comparison of 33 metabolites in mutant and wild type IDH2 samples. B) Pathway enrichment analysis of metabolites. P-values were evaluated by two-sided

unpaired t test. C) αKIC levels (IDH2^{mut} samples N= 21; IDH2 wt samples N= 10); P-value was assessed by two-sided, unpaired t-test. D) Spearman correlation between αKIC and D-2HG levels in samples at baseline. E) Relative abundance trajectories of αKIC according to patients clinical outcome. CR1 was defined as reached at least < 5% of marrow blasts after intensive chemotherapy. Late relapse was defined as relapse occurring 12 months after CR1. F) Clinical characteristics and outcome of IDH^{mut} and IDH^{wt} patients. G) BCAA- and BCKA-tracing experiments; data were normalized to succinate values as internal control. P-value was assessed by two-sided, unpaired t-test. H) Characteristics of leucine metabolism in wild type IDH2 and IDH2^{R140Q} samples.

6.1.2 Epigenetic marks regulate *BCAT1* expression in mutant *IDH2* AML blasts

6.1.2.1 BCAT1 is overexpressed in mutant IDH2 AML blasts

To address the contribution of mutant *IDH2*-induced epigenetic changes to this phenotype, we determined whether modulation of the BCAA metabolic pathway may rely on altered BCAT expression. No significant change in the expression of the mitochondrial BCAT2 enzyme was found by quantitative RT-PCR (qRT-PCR) between FACS-purified mutant (N=8) or wild-type (N=8) *IDH2* AML blasts, while accumulation of transcripts from the cytosolic BCAT1 was predominant in mutant *IDH2* cells (**Figure 35A**); the *BCAT1* gene also showed upregulation in the Beat AML dataset [295] for AML patients that share (N=114) or not (N=467) *IDH2* mutation (**Figure 35B**); these analyses have been done by Nicolas Poulain, PhD in the team. Consistently, western blot analysis showed that BCAT1 protein expression was high in primary mutant *IDH2* AML blasts while lower or nearly absent in wild type *IDH2* AML controls (**Figure 35C**), suggesting that despite the genetic heterogeneity of human blasts, *IDH2* mutation governs the accumulation of BCAT1.

BCAT1 is the first enzyme involved in the BCKA pathway. BCKA are decarboxylated by branched-chain α-ketoacid dehydrogenase complex (BCKDC); BCKDC activity is tightly controlled notably by the PPM1K phosphatase and the BCKDH kinase (BDK). BCKDK expression has been reported to be negatively controlled by high levels of BCAA[296]. In line, we observed a downregulated expression of *BCKDK* in mutant *IDH2* cells (*P*=0.001) ; this result was confirmed in the Beat AML dataset [295] (**data not shown**).

To assess if D-2HG can recapitulate *BCAT1* expression phenotype observed in human samples, PLB-985 cells were treated for 5 days with (2R)-Octyl-α-hydroxyglutarate (octy(R)-2HG), a cell-permeable derivative of the D-isomer of 2-HG. A faint increased accumulation of BCAT1 proteins levels was observed (**Figure 35D**) that suggests that

BCAT1 expression is sensitive to metabolic and/or epigenetic modifications induced by the oncometabolite.

As alternatively spliced *BCAT1* transcript variants have been reported in tumor cells that originate from two alternative promoters[283], we characterized *BCAT1* transcripts expression by transcript-specific qRT-PCR in primary mutant *IDH2* AML blasts. We observed the expression of specific transcripts initiated at the alternate promoter 1 (P1) and promoter 2 (P2) respectively (**Figure 35E**), 201 being the predominant transcript in primary AML cells (**Figure 35F**). We failed to quantify accumulation of 205 and 206 transcripts due to problems in designing unique primers and there are no commercial probes for the quantification of BCAT1 transcripts by qPCR. Expression of transcript 204 was significantly higher in *IDH2*^{R140Q} cells compared with wild type *IDH2* cells (**Figure 35G**), pointing to a persistent use of P2 in the mutant *IDH2* genetic context. These results indicate that expression of *IDH2*^{R140Q} while globally enhancing *BCAT1* expression, also enforces the accumulation of specific transcripts. Whether expression of these transcripts, which differ in their first exons and generate ~43 kDa protein species, is translated into functional differences in the gene product is yet unknown. In addition, a significant correlation emerges between the upregulation of 204 transcript and amounts of octy(R)-2HG, used to treated human hematopoietic cell lines devoid of mutation on *IDH* genes (PLB-985 and K562) and to "mimic" *IDH2* mutation (**Figure 35G**). Although exogenous 2-HG cannot entirely recapitulate the effects of mutant *IDH* enzymes[297], our data suggest that the oncometabolite elicits the same directionality of metabolic change as *IDH* genetic abnormalities. These results also show the ability of D-2HG to unexpectedly activates transcription of a key metabolic gene.

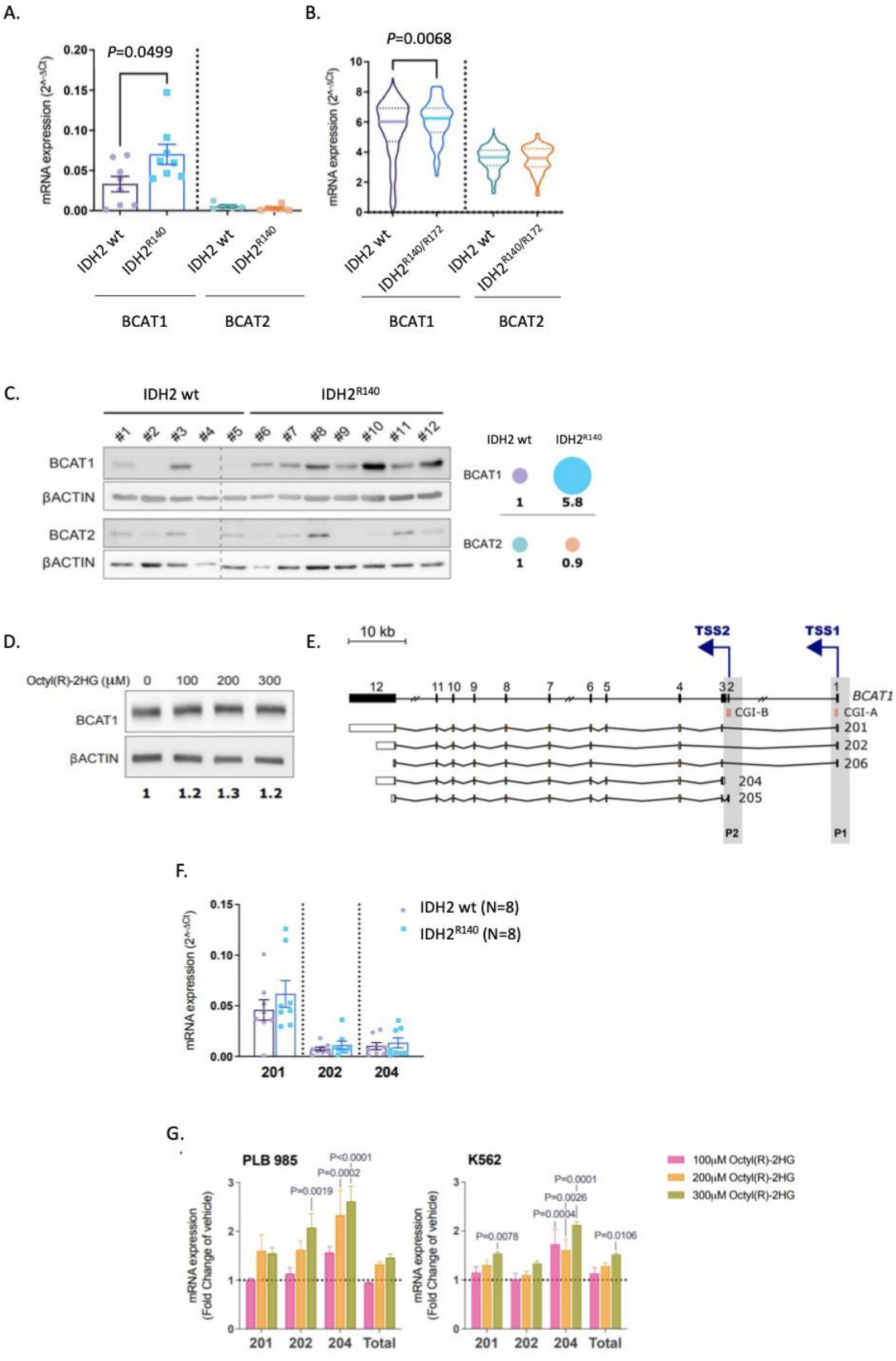
A.
P=0.0499
mRNA expression (2^-ΔCt)
IDH2 wt
IDH2R140
BCAT1
BCAT2
B.
P=0.0068
IDH2R140/R172
C.
IDH2 wt
IDH2R140
#1 #2 #3 #4 #5 #6 #7 #8 #9 #10 #11 #12
BCAT1
βACTIN
BCAT2
1
5.8
0.9
D.
Octyl(R)-2HG (μM) 0 100 200 300
1 1.2 1.3 1.2
E.
10 kb
TSS2
TSS1
BCAT1
CGI-B
CGI-A
201
202
206
204
205
P2
P1
F.
IDH2 wt (N=8)
IDH2R140 (N=8)
G.
PLB 985
K562
100μM Octyl(R)-2HG
200μM Octyl(R)-2HG
300μM Octyl(R)-2HG
mRNA expression (Fold Change of vehicle)
P<0.0001
P=0.0002
P=0.0019
P=0.0078
P=0.0001
P=0.0026
P=0.0004
P=0.0106
Total

Figure 35: The IDH2 mutation causes significant upregulation of BCAT1. A) Accumulation of BCAT1 and BCAT2 transcripts in primary mutant (N=8) and wild type (N=8) IDH2 AML samples; P-value was assessed by two-sided Mann Whitney rank test. B) Expression data from N=174 AML patients available in the TCGA AML database (N=17 mutant IDH2 AML patients); p-value was assessed by two-sided, unpaired t-test. Data are represented as mean ± SEM. C) Western blot analysis of BCAT1 and BCAT2 proteins in whole cell lysates from primary AML samples (blast enrichment in samples was >80%). Fold changes in protein accumulation (ratio of the mutant IDH2 samples to wild type controls) were calculated using the values normalized with actin. D) Western blot analysis of BCAT1 proteins accumulation in whole cell lysates from PLB985 treated with increasing doses of octy(R)-2HG. Fold changes in protein accumulation were calculated using the values normalized with actin. E) Schematic drawing of the human BCAT1 locus. Promoter P1 allows the expression of 201, 202 and 206 transcripts whereas promoter P2 initiates the expression of 204 and 205 transcripts. F) Analysis of 201, 202 and 204 transcripts accumulation in human primary samples by qRT-PCR. Results were normalized relative to the expression of the peptidylprolyl isomerase A (PPIA)used as control. All qRT-PCR samples were assayed in triplicates. P-value was assessed by one way ANOVA test G). Analysis by RT-qPCR of 201, 202 and 204 transcripts accumulation in human PLB-985 and K562 cell lines treated with increasing doses of octyl-2HG for 5 days (technical triplicates). P-value was assessed by two way ANOVA test.

6.1.2.2 Epigenetic changes in the BCAT1 locus are associated to the IDH2 mutation in primary AML blasts

To more directly test the effects of epigenetic changes due to mutant *IDH2* on 204 transcripts expression, we next examined the methylation of P1 and P2 regions, that both localize in CpG-enriched regions known as CpG islands (CGI). By exploiting the TCGA database, we observed that while P1 methylation pattern tended to be relatively stable in the two genetic groups (mean β-value: 0.22 vs. 0.1 in mutant *IDH2* and wild type *IDH2* samples respectively), P2 exhibited a significantly higher level of DNA methylation in mutant *IDH2* AML blasts compared with wild-type *IDH2* 0.42 vs. 0.36) (**Figure 36A,** data from Nicolas Poulain PhD in the team). These observations indicate that P2 hypermethylation unexpectedly allows for 204 transcript upregulation in mutant *IDH2* cells, a situation reminiscent of what was reported in wild type *IDH* human gliomas where BCAT1 controls proliferation and invasiveness [283]. Hypermethylation at promoter P2 in both mutant *IDH2* AML and mutant *IDH1* glioma suggests that hypermethylation is associated with *IDH* genetic lesions. This result correlates with high DNA methylation of CGI located in the promoter regions P1 (CGI-A) and P2 (CGI-B) in mutant *IDH2* AML cells compared to wild type *IDH2* AML cells (**Figure 36B**).

Semi-quantitative HELP (HpaII tiny fragment Enrichment by Ligation-mediated PCR) assays[298] that compare representations generated by methylation-sensitive HpaII and by methylation-insensitive MspI digestions of the genome followed by ligation-mediated PCR, also evidenced a trend to higher degree of methylation at specific cytosine residues within P2 in primary mutant *IDH2* AML blasts compared to wild type *IDH2* controls (**Figure 36C**).

We next looked whether other epigenetic marks might contribute to 204 transcript expression in mutant *IDH2* AML cells by activating highly methylated P2. Recent work has proposed regulation of *BCAT1* expression in leukemic cells through the activity of enhancer of zest homolog-2 (EZH2), the enzymatic subunit of the Polycomb Repressive Complex 2 (PRC2) that catalyzes Histone 3 Lysine 27 (H3K27) methylation[277] PRC2 is commonly located at CGI and high level of DNA methylation may impair PRC2 recruitment at CGI and participates to transcripts de-repression[299]. We thus investigated H3K27me^3 patterns at hypo- (P1) and hyper-methylated (P2) regions by chromatin immunoprecipitation (ChIP)-qPCR assays using samples obtained from primary mutant *IDH2* AML cells (N=6) and wild type *IDH2* AML cells (N=3) and subjected to IP reactions; immunoprecipitated DNAs were kindly provided by Drs Sylvain Garciaz and Estelle Duprez (Cancerology Research Center, Marseille). A significant decrease of H3K27me^3 was observed for both P1 and P2 in mutant *IDH2* cells compared with wild type *IDH2* cells (average decrease of ~3-fold), as compared with the peptidylprolyl isomerase A (*PPIA*) negative target. This result indicates that the strong expression of *BCAT1* in mutant *IDH2* cells occurs by breaking a H3K27me^3-dependent negative regulatory mechanism ; this also indicates that expression of 204 transcripts occurs independently of EZH2 activity on P2 in mutant *IDH2* cells. Unexpectedly, two histone marks associated to active transcription, i.e., H3K27Ac and H3K4me^3, were also found decreased in mutant *IDH2* cells when compared to controls (**Figure 36D**). These analyses have been performed by Amaury Bongers, PhD in the team. Collectivelly, these observations indicate that epigenetic modifications provide a robust way to regulate *BCAT1* isoforms expression in AML cells. However, we failed to correlate specific epigenetic marks and variation in P2 promoter usage in mutant *IDH2* cells.

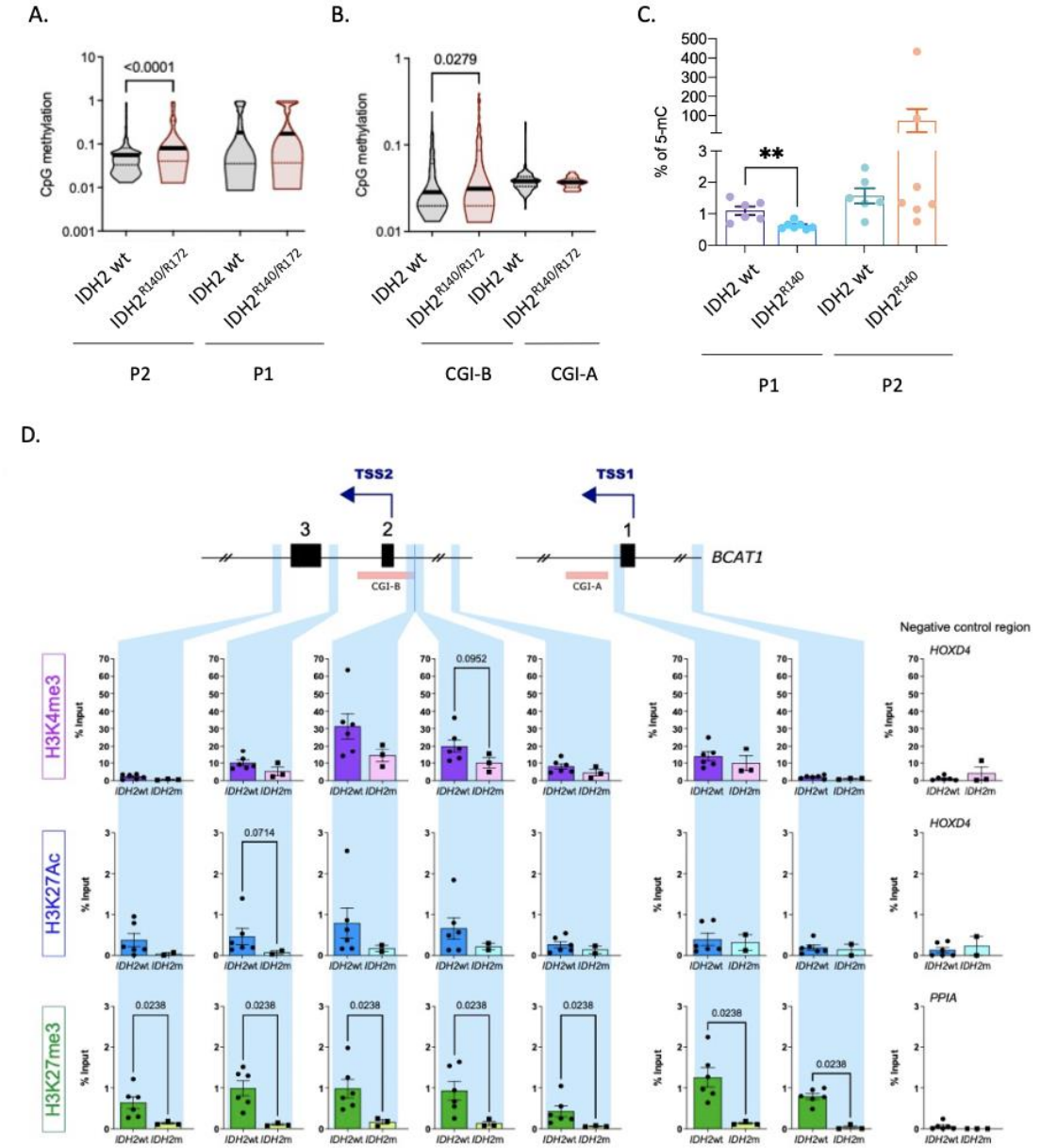

Figure 36: Methylation pattern at human BCAT1 locus. A) Methylation pattern at promoter regions P1 and P2 ; genotypes are indicated; mutant IDH2 affecting the R140 and R172 residues were pooled. P-value was assessed by two-sided unpaired t test. B) DNA methylation of CGI located in P1 (CGI-A) and P2 (CGI-B). P-value was assessed by two-sided unpaired t test. Data in A-B are represented as median ± SEM. C) HELP assay at cytosine residues located within P1 and P2 in primary IDH2^{R10Q} (N=7) and wild type IDH2 (N=5) AML cells. P-value was assessed by Mann Whitney rank test. Data are represented as mean ± SEM (3 biological replicates). D) ChIP-qPCR assays for H3K27me^3 and H3K4me^3 methylation and for H3K27Ac acetylation at promoters P1 and P2 in primary AML samples. Reactions were performed in triplicate on each sample. The fold enrichment of ChIP over input was calculated as 2 to the power of the quantification cycle (Cq) difference between input chromatin and ChIP samples. Negative controls are indicated. Data are represented as mean ± SEM.

6.1.3 Mutant *IDH2* AML blasts are strictly dependent on BCAT1 activity for their growth and survival

We next dissected the effects of *BCAT1* loss during AML evolution in a patient-derived xenograft (PDX) model, and employed retroviral expression of a functionally validated short hairpin RNA BCAT1 (shBCAT1) construct to mediate depletion of *BCAT1*[226]; this construct encodes the GFP protein used as a marker to trace shRNA-expressing transplanted cells. We confirmed a strong reduction in accumulation of all *BCAT1* transcripts relative to a non-targeting negative control shRNA (shCtrl) in the PLB-985 cell line (~80%, **not shown**) and in primary patients samples (~70%, **Figure 37A**) and subsequent decrease of the corresponding protein (**Figure 37B**).

Retroviral shBCAT1 and shCtrl constructs were introduced into *IDH2R*^{140Q} (Patient #3 and #4) or wild type *IDH2* (Patient #1) AML bulk populations ; transduced populations were transplanted by intra-femoral injection (0.1x10^{6} transduced cells per mice) into immunocompromised (NOD scid gamma, NGS) mice after sublethal irradiation (1.5 Gy). Donor bone marrow chimerism monitored over 3 months after transplantation showed a time-dependent increase in transduced AML cells (positive for human CD45, hCD45, and GFP) confirming engraftment in each recipient (**Figure 37C)**; at sacrifice, a marked expansion of hCD45^{+} cells was observed in all engrafted animals (**Figure 37D**). In endpoint studies, we found a marked expansion of both the shCtrl- and shBCAT1-transduced wild type *IDH2* AML cells into bone marrow, demonstrating that *BCAT1* knockdown did not significantly alter the development of the patient-derived xenografts in comparison with wild type *IDH2*-shCtrl engrafted mice (**Figure 37E**). In contrast, the *IDH2*^{R140Q}-shBCAT1 AML transplanted cohort showed delayed AML expansion, indicating a strong disadvantage for the combination of *IDH2*^{R140Q} and shBCAT1, compared with the *IDH2*^{R140Q}-shCtrl control arm (**Figure 37E**). White blood cell counts confirmed the disadvantage of such combination (**Figure 37F**). 2-HG plasma level measured as a marker of engraftment and maintenance of *IDH2*^{R140Q} leukemic cells dropped over time in the *IDH2*^{R140Q}-shBCAT1 AML transplanted mice, confirming blasts disappearance (**not shown**). In keeping with these observations, we found a negative correlation between the % of GFP^{+} *IDH2*^{R140Q}-shBCAT1 AML cells and the % of hCD45^{+} cells in the bone marrow, confirming the negative impact of *BCAT1* loss on AML expansion in a *IDH2*^{R140Q} context (**Figure 37G**). *In*

vitro, we could demonstrate that *BCAT1* inhibition was associated to a decreased viability in *IDH2*^{R140Q}-shBCAT1 primary AML cells as detected in by flow cytometry after staining with Annexin V (**Figure 37H**).

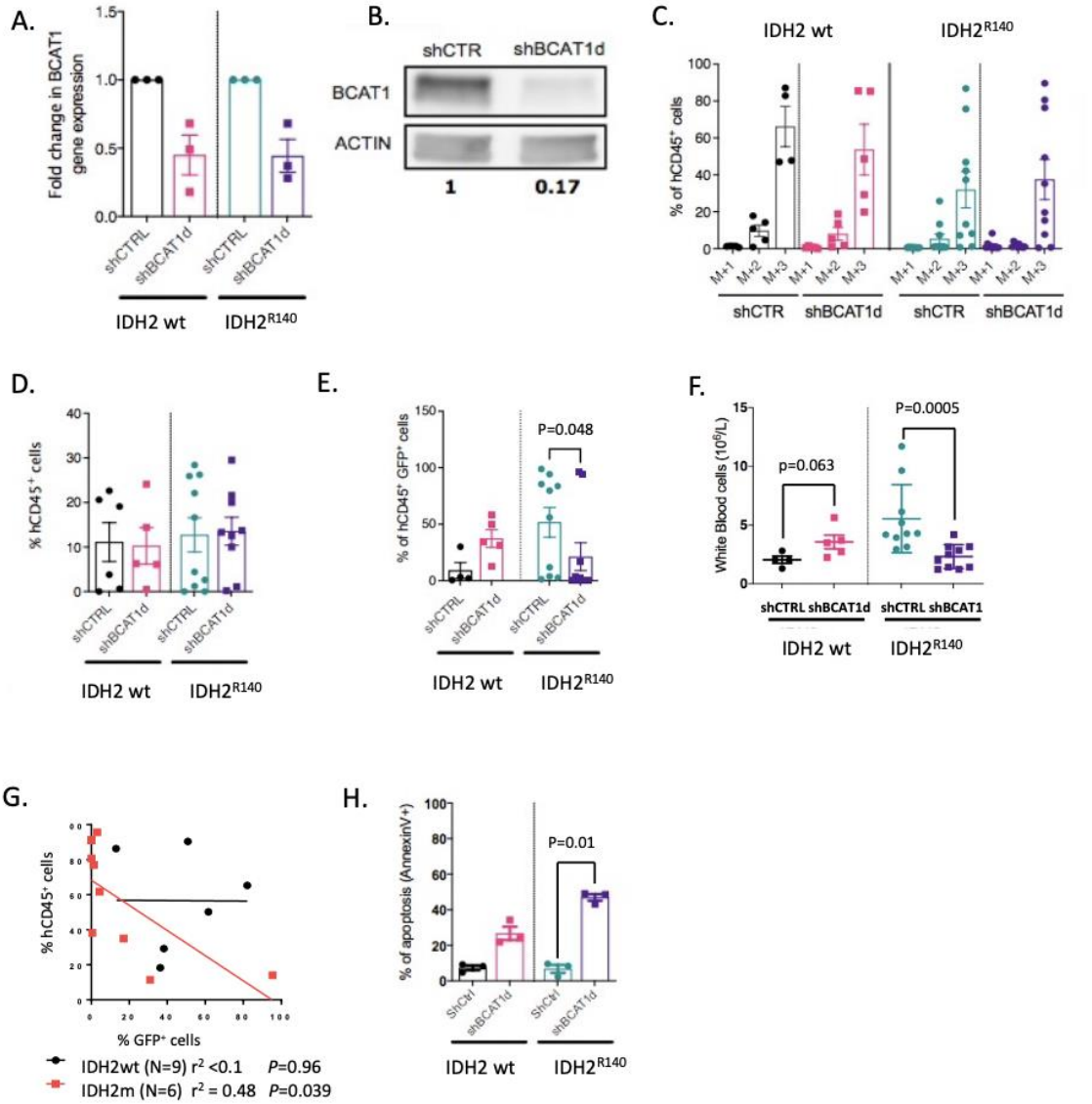

Figure 37: BCAT1 inhibition selectively reduces the growth of primary mutant IDH2 AML cells. A) Fold change in BCAT1 expression in primary blasts (N=6) upon transduction with a lentiviral vector allowing the constitutive expression of an shRNA raised against BCAT1 (N=3) or shRNACtrl (N=3). B) BCAT1 protein level in primary blasts invalidated for BCAT1 expression. C) Percentage of hCD45^{+} *cells in the bone marrow of engrafted mice at one month (M+1), two months (M+2) and 3 months (M+3; endpoint) post-transplant; studied cohorts were : shRNA Ctrl- (N=6) and shRNA-BCAT1-injected (N=5) wild type IDH2 PDX (left panel) and the shRNA Ctrl- (N=10) and shRNA BCAT1-injected (N=9) IDH2*^{R140Q} *PDX (right panel). Chimerism was evaluated every month by bone marrow aspiration. P-value was assessed by Mann Whitney rank test. D) Percentage of hCD45*$^{+}$ *cells in the bone marrow of engrafted mice at sacrifice. P-value was assessed by Mann Whitney rank test. E)*

Percentage of GFP$^+$ cells within the pool of hCD45$^+$ cells in the bone marrow of engrafted mice. P-value was assessed by Krustall-Wallis test. *F) White blood cell counts at sacrifice. P-value was assessed by Mann Whitney rank test. G) Spearman correlation between the % of GFP$^+$ cells and hCD45$^+$ cells in recipient mice. H) Induction of apoptosis upon BCAT1 invalidation in wild type (N=3) and IDH2^{R140Q} (N=3) primary AML cells cultured in vitro (in vitro culture condition was as in [287]). P-value was assessed by two-sided, unpaired t-test. All data are represented as mean ± SEM.*

Altogether these data indicate that BCAT1 function is required for mutant *IDH2* AML cells maintenance and/or expansion in recipients, while less relevant to the proliferation of wild type *IDH2* AML cells. Counter-selection of mutant *IDH2* cells invalidated for *BCAT1 in vivo* highlights the key contribution of BCAA reprogramming in mutant *IDH*-driven leukemogenesis.

Remarkably, we observed that *BCAT1* depletion also promotes partial cellular differentiation of *IDH2^{R140Q}* blasts in the PDX model, as staining for human CD14 (monocytic marker) and CD15 (granulocytic marker) showed a dramatic increase in the MFI in the bone marrow hCD45$^+$ fractions from *IDH2^{R140Q}*-shBCAT1 AML transplanted mice (N=6), compared with the *IDH2^{R140Q}* -shCtrl cohort (N=8) (**Figure 38A**). In line, we observed a faint decrease in the MFI of the CD24 marker, usually used as an aberrant cancer stemness marker [300] and also present on neutrophil early precursors in mice [301]; this observation may indicate a maturation along the granulocytic lineage. We observed a statistically significant decrease in CD11b staining, a myeloid antigen aberrantly expressed in human AML and associated with an unfavorable prognosis. In contrast, immunophenotype of wild type *IDH2*-shBCAT1 AML did not show similar pattern of granulo-monocytic expression (**Figure 38B**).

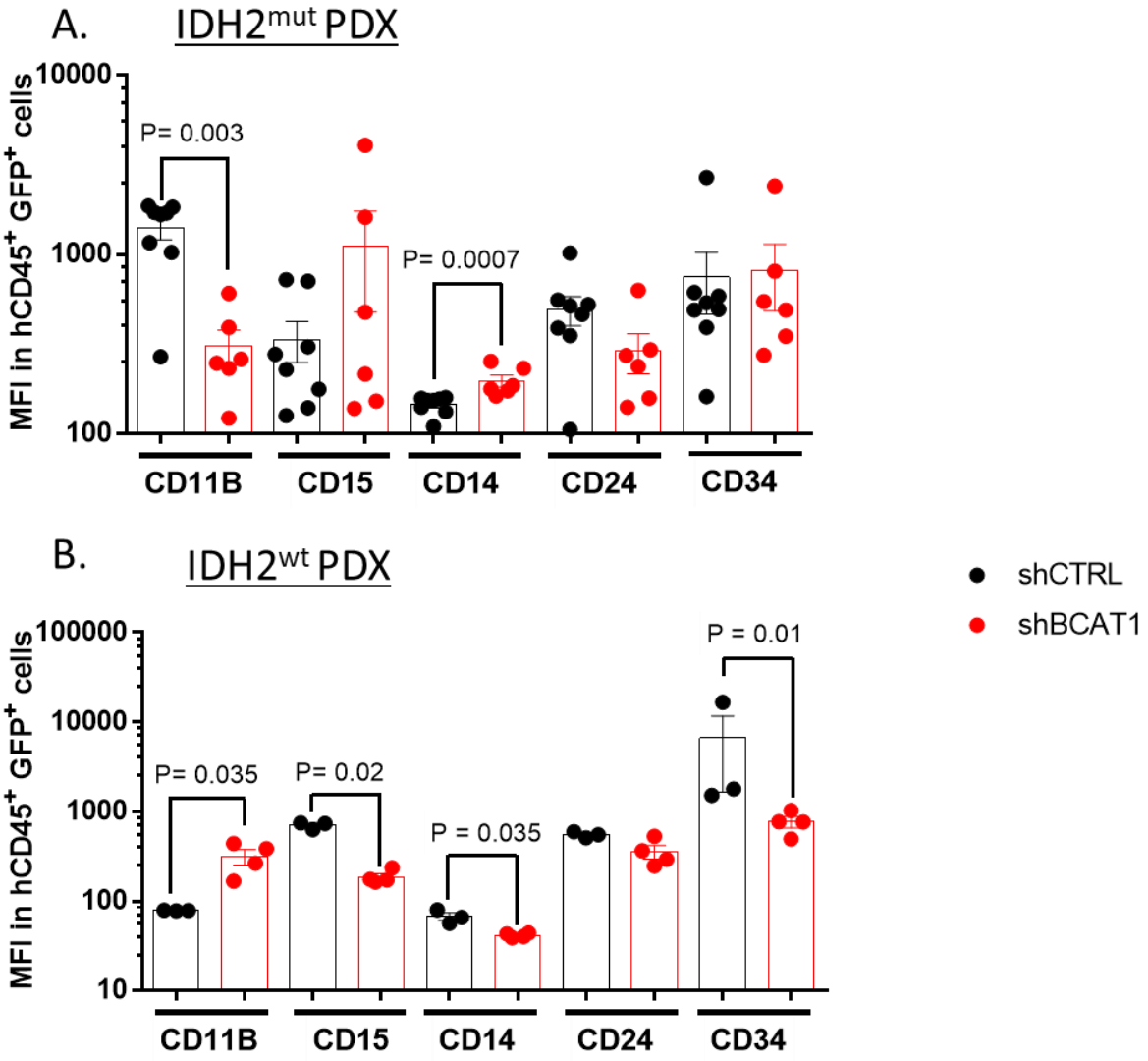

Figure 38: BCAT1 depletion engages a partial differentiation of IDH2^{R140Q} primary blasts in PDX model. MFI indicates the geometric mean fluorescence intensity. P-values were assessed by Mann Whitney rank test. Data are represented as mean ± SEM.

Collectively, these data indicate a link between monocyte and/or granulocyte differentiation and BCAT1-mediated metabolic pathways. In keeping, in an exogenic BCR-ABL1 leukemic mice model, Hattori and colleagues reported that *BCAT1* overexpression induced a highly immature phenotype compared to controls but also that its inhibition led to signs of myeloblastic differentiation[302].

We next interrogated the function of BCAT1 in the proliferation and viability of *IDH2 IDH2^{R140Q}* PLB-985 cells cultured *in vitro* and, as an alternative approach to gene knockdown, we employed a specific inhibitor of BCAT1, the -chloro-2-benzofurancarboxylic

acid (referred as BCATi) and the synthetic amino acid gabapentin, a structural analog of leucine[303]. Anti-leukemic activity of gabapentin has been reported in the progression of BCR-ABL-associated chronic myeloid leukemia[302]. *IDH2*^{R140Q}-PLB-985 cells demonstrated a sensitivity to gabapentin and BCATi with half-maximal inhibitory concentration (IC_{50}; concentration where 50% viability is observed) of ~25 mM and ~50 mM respectively and showed a significant decrease in survival in their presence compared with wild type *IDH2*-PLB-985 isogenic cells (**Figures 39A** and **39B**, left panels). At similar concentrations, both compounds similarly affected the viability of primary *IDH2*^{R140Q} blasts (**Figures 39A** and **39B**, right panels) and the viability of primary wild type *IDH2* blasts treated with increasing doses of octyl-(R)2HG (**Figure 39D)**; a dose-dependent linearity for gabapentin-induced apoptosis was observed.

To validate the inhibitory activity of BCATi, we measured the intracellular levels of αKIC and 3-hydroxyisovaleric acid (HIVA), used as an indirect marker of the BCKDH activity, in PLB-985 cells treated with the inhibitor; as shown **Figure 39C**, a dose dependent increase in the αKIC/HIVA ratio confirms a specific inhibition of BCAT1 by the compound. Moreover, αKIC accumulation upon *BCAT1* inhibition suggests that the BCAA pathway favors leucine anabolism rather than catabolism in mutant *IDH2* cells. Interestingly, untreated *IDH2*^{R140Q} cells show a lower HIVA intracellular level, suggesting that BCKD complex is more active in this genetic context (**Figure 39C**).

BCAT1 utilizes αKG as a substrate and its inhibition in hematopoietic wild type *IDH* cell lines increases intracellular αKG levels[304] (in these cells BCAT1 initiates the catabolism of leucine). We raised the question of whether inhibition of *BCAT1* in *IDH2*^{R140Q} AML cells in which the BCAA pathway runs in reverse, may decrease αKG levels and subsequently reduce D-2HG accumulation. For that, we treated primary *IDH2*^{R140Q} AML cells with increasing doses of gabapentin and measured D-2HG levels in culture media upon 10 days of treatment; as a control we used the IDH2 inhibitor AG-221/enasidenib. We observed that gabapentin decreases D-2HG, yet in a lesser extent than AG-221 (**Figure 39E**); we did not observed signs of terminal differentiation either by flow cytometry or cytology, probably due to early apoptosis. This result suggests that gabapentin may "mimic" the activity of AG-221.

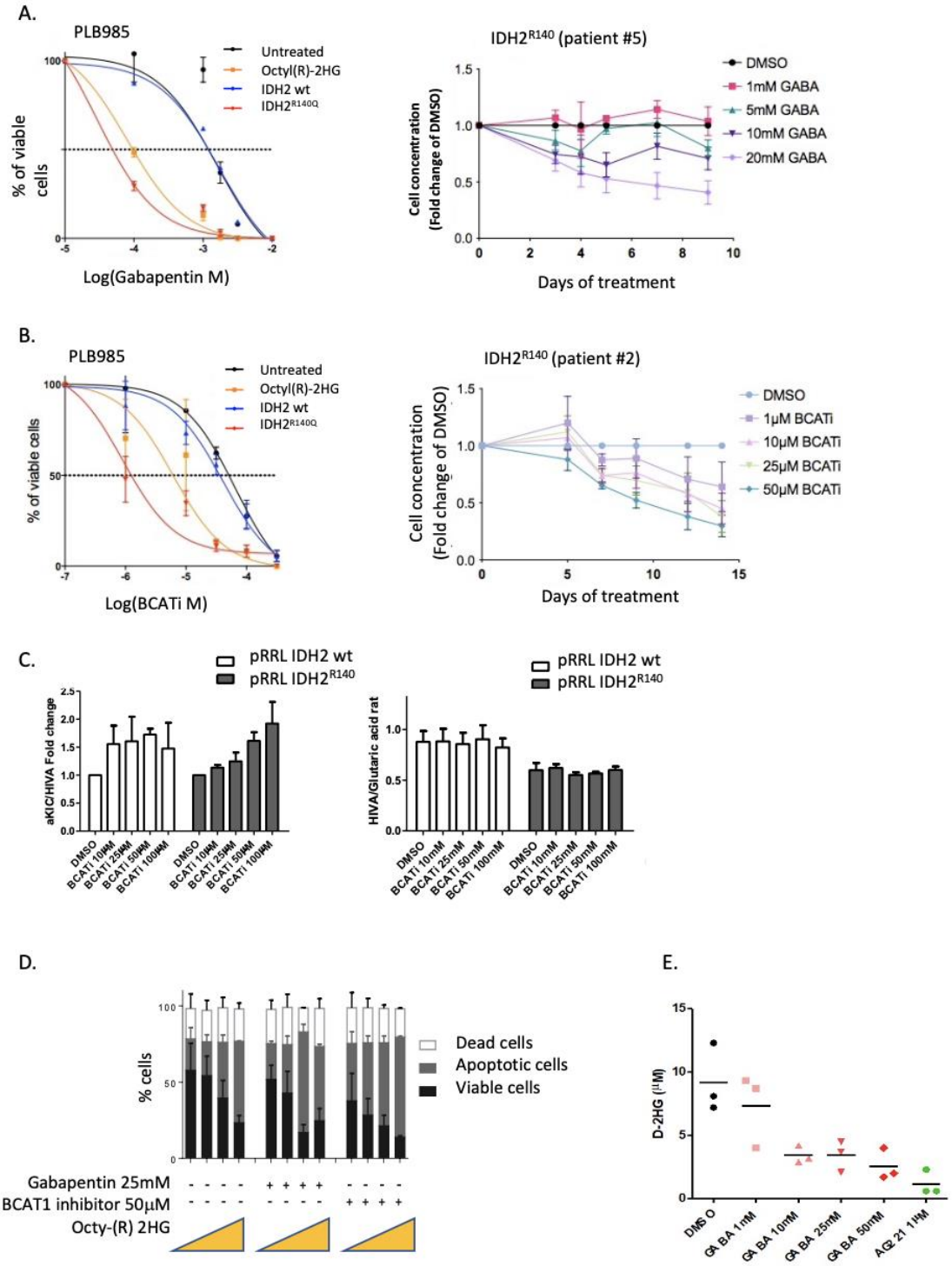

Figure 39: Pharmacological inhibition of BCAT1 selectively affects the growth of IDH2^{R140Q}-expressing cells. IC_{50} of gabapentin (A) and BCATi (B) were determined on PLB-985 cells engineered to express a wild type (wt) or a mutant form (R140Q) of IDH2 (lentiviral delivery). Control corresponds to parental PLB-985 cells treated with PBS. Right panels: experiments performed on primary IDH2 wt and IDH2^{R140Q} AML cells; DMSO was used as excipient. Cell viability was assessed at day 3 by trypan blue exclusion; viability is expressed as the % of viable cells relative to viable DMSO-treated cells (set to 100%), in each condition.

C) Estimation of αKIC (left panel) and HIVA (right panel) levels in culture media upon treatment of IDH2^{R140Q}-and wild type IDH2-expressing PLB985 cells treated with increasing doses of BCAT1i (3 biological replicates); values are expressed as ratio of αKIC/HIVA and HIVA/glutaric acid levels respectively. D) Induction of cell death in primary wild type IDH2 AML (N=3 patients) cells treated with gabapentin or BCAT1 inhibitor, in the presence of octyl-(R)2HG. Data are represented as mean ± SEM. F) Concentration of D-2HG in culture media upon treatment for 10 days with gabapentin of primary AML IDH2^{R140Q} cells; data are represented as mean ± SEM (3 biological replicates for each patient and each condition).

Collectively and consistent with *BCAT1* activation in other models of human leukemia [302,304], *BCAT1* inhibition selectively reduces the growth of primary mutant *IDH2* AML cells and offers a dual mode of action of proliferation inhibition and differentiation induction that points to a therapeutic vulnerability for mutant *IDH2* AML.

6.1.4 IDH2 mutational context impairs α-ketoacids metabolism (preliminary results)

We then tested the hypothesis that rewiring of the BCAA metabolism in mutant *IDH2* cells may correspond to an adaptative process induced by the mutation, in order to limit α-ketoacids accumulation and to protect cells from elevated levels of reactive oxygen species (ROS). Indeed, several pioneer studies have suggested that expression of *IDH* mutants increase ROS levels due to the depletion of NADPH and glutathione (GSH)[64, 246] and GSH, together with NADPH-producing pathways and glutathione reductase, provides a defense system against oxidants. In line, in the maple sirup disease (inherited neurometabolic disorder caused by a deficiency of the branched-chain α-keto acid dehydrogenase complex (BCKD) activity), accumulation of α-ketoacids (αKA) disrupts ROS homeostasis through lipid peroxidation and free radicals production[306,307]. In addition levels of BCAA might regulate the expression of BCKDK[308] that controls the activity of BCKD. We thus investigate the interplay between the BCAA pathway and ROS generation in *IDH2^{R140Q}* cells (**Figure 40A**).

Using the CellROX™ Green Flow Cytometry Assay, we did not detect increase in ROS level in PLB-985 cells upon expression of the IDH2^{R140Q} mutant or upon treatment with octyl-(R)-2HG (**data not shown**). In contrast, we observed a significant increase in ROS level in *IDH2^{R140Q}*-expressing PLB-985 cells, while not in their parental counterparts, upon addition of the α-ketoacid αKIC in the media (**Figure 40B**), indicating a relationship between αKIC and ROS production in the *IDH2^{R140Q}* genetic context. Increasing doses of αKIC

clearly affect the viability of *IDH2*^{R140Q}-expressing or octyl-(R)-2HG-treated PLB-985 cells in a dose-dependent manner (**Figure 40C**). Viability was partly rescued by preliminary treatment of the cells with AG-221/enasidenib (**Figures 40C** and **40D**). Loss of viability induced by the presence of αKA in the media (equimolar mix of αKIC, αKIV and αKMV) was associated to induction of apoptosis (increased proportion of cells stained as annexinV^{+}DAPI^{-}) and we also observed signs of necrosis (cells stained as annexinV^{+}DAPI^{+}) (**Figure 40D**).

Figure 40: Viability of IDH2^{R140Q} *cells, but not wild type IDH2 cells, seemingly relies on αKIC levels. A) Interplay between BCAT1 and BCKDC activities. B) PLB985 cells were treated with octyl(R)-2H for 3 days, then cultured in the presence of increasing doses of αKIC (0, 1, 5mM) for 3 hours; ROS levels were assessed with the CellROX™ Green Flow Cytometry Assay; MFI indicates the geometric mean fluorescence intensity (biological triplicates). Hydrogen peroxide was used as positive control. C) Cellular viability; cells were cultured in medium enriched with α-KA (equimolar amounts of αKIC, αKIV and αKMV). AG-221 was added 5 days prior αKA supplementation. Viability was assessed by bleu trypan exclusion. Data in B and C are represented as mean ± SEM (3 technical triplicates). D) Apoptosis and necrose rates were measured after 3 days of culture. AG-221 was added 5 days prior to αKA supplementation.*

A.

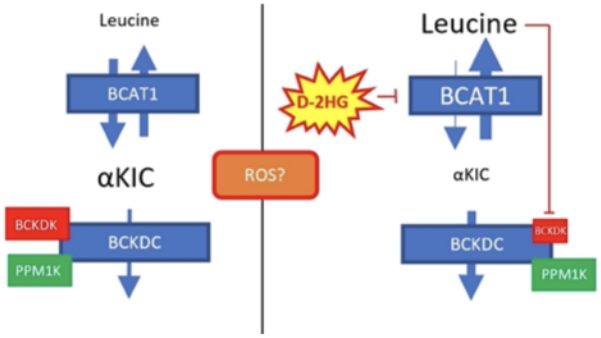
Leucine
BCAT1
αKIC
BCKDK
BCKDC
PPM1K
ROS?
D-2HG
Leucine
BCAT1
αKIC
BCKDK
BCKDC
PPM1K

B.

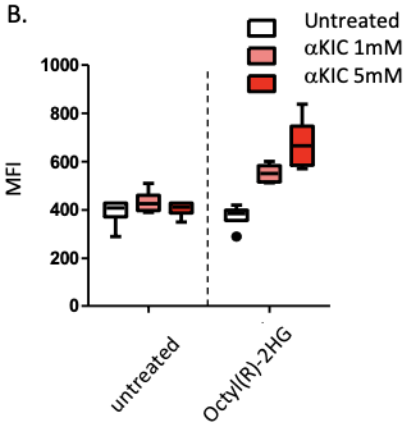
Untreated
αKIC 1mM
αKIC 5mM
MFI
1000
800
600
400
200
0
untreated
Octyl(R)-2HG

C.

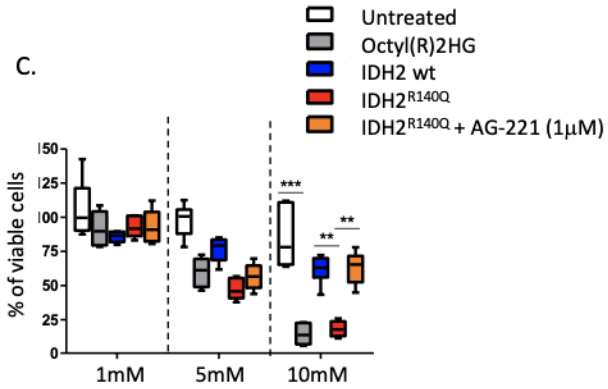
Untreated
Octyl(R)2HG
IDH2 wt
IDH2R140Q
IDH2R140Q + AG-221 (1μM)
% of viable cells
150
125
100
75
50
25
0
***
**
**
1mM
5mM
10mM

D.

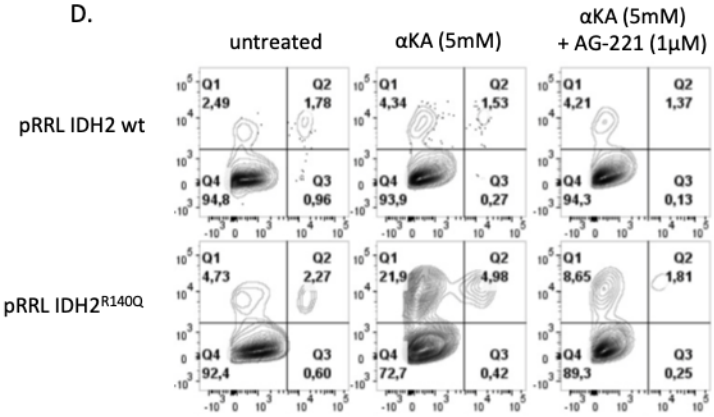
untreated
αKA (5mM)
αKA (5mM) + AG-221 (1μM)
pRRL IDH2 wt
pRRL IDH2R140Q
Q1 2,49
Q2 1,78
Q4 94,8
Q3 0,96
Q1 4,34
Q2 1,53
Q4 93,9
Q3 0,27
Q1 4,21
Q2 1,37
Q4 94,3
Q3 0,13
Q1 4,73
Q2 2,27
Q4 92,4
Q3 0,60
Q1 21,9
Q2 4,98
Q4 72,7
Q3 0,42
Q1 8,65
Q2 1,81
Q4 89,3
Q3 0,25

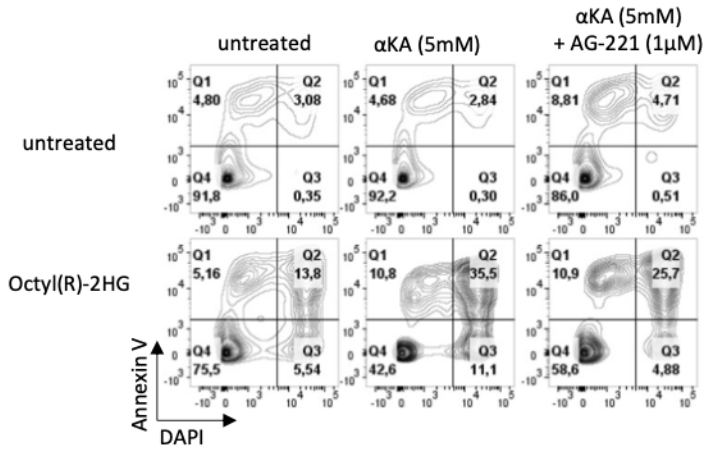
untreated
αKA (5mM)
αKA (5mM) + AG-221 (1μM)
untreated
Octyl(R)-2HG
Q1 4,80
Q2 3,08
Q4 91,8
Q3 0,35
Q1 4,68
Q2 2,84
Q4 92,2
Q3 0,30
Q1 8,81
Q2 4,71
Q4 86,0
Q3 0,51
Q1 5,16
Q2 13,8
Q4 75,5
Q3 5,54
Q1 10,8
Q2 35,5
Q4 42,6
Q3 11,1
Q1 10,9
Q2 25,7
Q4 58,6
Q3 4,88
Annexin V
DAPI

Collectivelly, these data suggest that the viability of *IDH2*^{R140Q} cells is highly sensitive to αKA accumulation and that apoptosis and necrosis contribute to loss of viability in *IDH2*^{R140Q} leukemic cells exposed to high amounts of αKA. Apoptotic death involves the participation of ROS, which have also been implicated in necrotic cell death; it can be presumed that low level of αKIC in *IDH2*^{R140Q}-expressing might help, at least in part, to limit ROS generation.

6.1.5 Metabolic rewiring appears as a consequence of impaired mTORC1 activity

At the molecular level, leucine activates mTORC1[34], a complex which coordinates cell growth with nutritional status. mTORC1, together with mTORC2, participates into the various physiological functions of mTOR in cell growth, motility and metabolism[35] and its constitutive activation in AML cells has been reported[1].

Because 2-DHG inhibits ATP5B and consequently decreases mTOR signaling downstream[176], we asked whether leucine anabolism would compensate for loss of mTOR activity in mutant *IDH2* AML cells. Indeed leucine availability is required for mTORC1 activation[309] [Nicklin et al., 2009]. We thus measured the activation of the mTOR pathway by quantifying the phosphorylated level of its effectors by western blot, i.e. the p70 ribosomal protein S6 kinase 1 (p70^{S6K1} also known as S6K1) that phosphorylates multiple downstream substrates including the ribosomal protein S6 (rpS6), eIF4B, and GSK3 and the eukaryotic initiation factor 4E–binding (eIF4E-binding) protein 1 (4E-BP1) by which mTORC1 controls translation initiation, that are phosphorylated and activated by mTORC1, and the mTORC2 substrate AKT (**Figure 41A-B**). Phosphorylation of S6K1 on threonine (Thr) 389 and phosphorylation of 4E-BP1 on Thr37 and Thr46 residues (both recognized by the antibody used) was consistently reduced in primary *IDH2*^{R140Q} AML cells compared with control wild type *IDH* blasts, suggesting a lower activity of mTORC1 in the former, in agreement with previous report showing that exogenous 2HG and overexpression of mutant *IDH1* inactivate mTOR[176]. Of note, phosphorylation by mTOR of Thr 37 and Thr 46 on 4E-BP1 serves as a priming event, which is followed by Thr 70 phosphorylation and finally serine (Ser) 65 phosphorylation[311,312]; Thr46 is the site that controls eIF4E binding. On the opposite, the phosphorylation level of AKT at Ser 473 was increased

in mutant *IDH2* AML cells compared with wild type *IDH2 cells*, indicating higher mTORC2 activation. Data were obtained in collaboration with Amaury Bongers, PhD in the team.

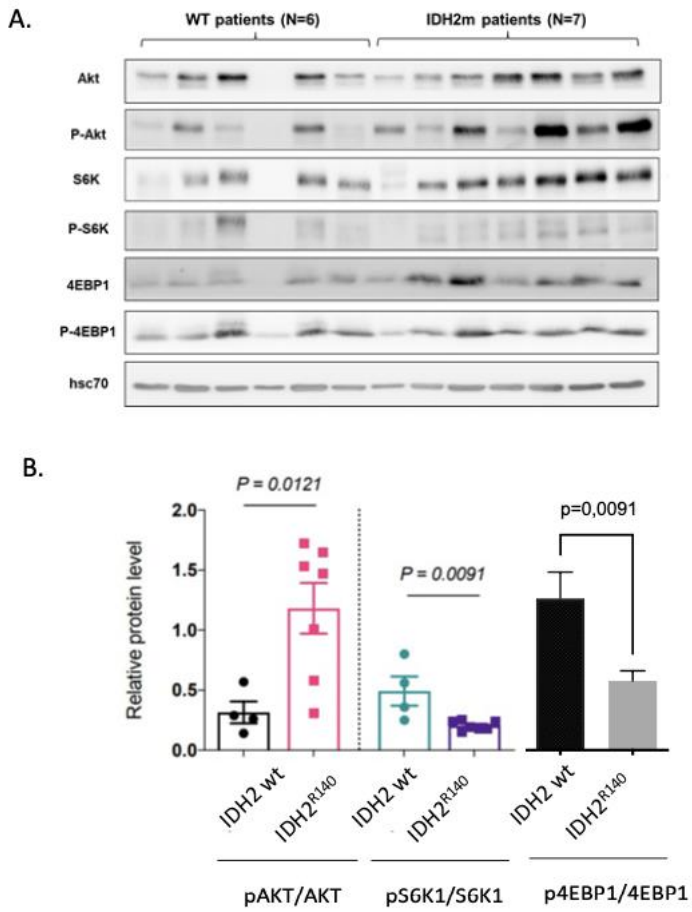

Figure 41: A) Western blot analysis of AKT, pAKT, S6K, pS6K, 4E-BP1 and p4E-BP1 in FACS-sorted IDH2^{R140Q} and wild type IDH2 AML samples. The heat shock protein70 (HSC70) was used as a loading control. B) Quantification of phosphorylated and non-phosphorylated species (Image J® software). Data are represented as mean ± SEM (3 biological replicates).

Using different inhibitors of mTOR, i.e. the rapamycin, the dual inhibitor of mTORC1/2 PP242[313] and the dual pan-PI3K/mTOR inhibitor Omipalisib/GSK2126458 (GSK458), we observed a substantial sensitivity of *IDH2^{R140Q}* expressing or octyl-2HG-treated PLB-985 cells (compared with untreated wild type *IDH2* isogenic genetic background) to PP242 and GSK458, that were significantly more effective than rapamycin in eliciting antileukemic effects *in vitro* (**Figure 42A**). Although mTORC2 was initially identified as a rapamycin-insensitive entity, subsequent studies have shown that a prolonged rapamycin

treatment (≥1 day) also abrogates mTORC2 while not only mTORC1 signaling[314], precluding our viability assay to discriminate between those two complexes in their support of *IDH2* cells viability.

To determine whether inhibition of mTORC1/2 activity influences the maintenance of *IDH2*^{R140} AML cells *in vivo*, we established an aggressive human xenograft mouse model for each genotype. For that we used AML cells serially transplanted into NSG mice (survival rate was significantly reduced between each transplant) and derived from patients with AML harboring or not *IDH2*^{R140}; before engraftment, cells were transduced with the lentivirus pFUW-mCherry-firefly luciferase allowing the monitoring of growth and expansion of transduced cells and a bioluminescent imaging that can be analyzed in an anatomical context. Both recipient groups (N=10 mice per AML sample) developed AML. When hCD45^{+} AML cells became detectable (≥2% of blasts in peripheral blood), animals were randomly allocated to vehicle (N=5) or GSK458 (N=5) at 30 mg/kg once daily until end of treatment (day 30) (**Figure 42B**). While GSK458 treatment did not confer survival advantage to mice transplanted with wild type *IDH2* AML cells, the cohort transplanted with cells derived from *IDH2*^{R140} survived until study termination (**Figure 42C**).

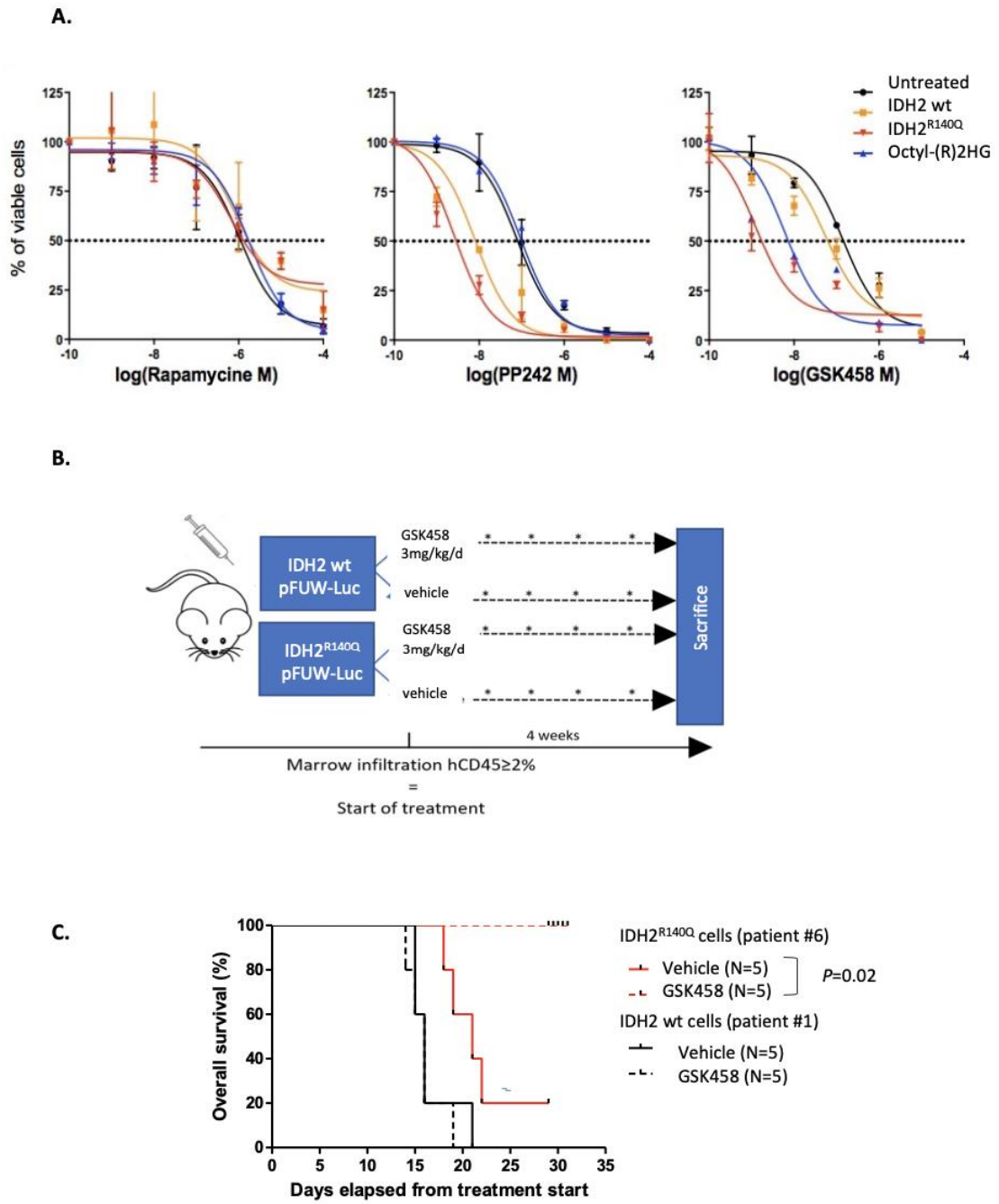

Figure 42: mTOR supports the viability of IDH2^{R140} cells. A) In vitro dose-response studies for rapamycin, PP242 and GSK458 using IDH2^{R140Q}-, wild type IDH2-expressing and octyl-2HG-treated PLB-985 cells. Experiments were performed in triplicates. B) Schematic representation of the PDX model; primary AML cells were transduced with pFUW mCherry+luciferase, sorted by flow cytometry and transplanted (0.1x10^6 cells) in NSG mice after sub-lethal irradiation (1.5Gy). Engraftment was assessed by the presence of hCD45$^+$ cells in the peripheral blood and/or bone marrow. Mice were then orally force feed with GSK458 or vehicle for 28 days. Mice were sacrificed in case of clinical alteration or for the presence of

more than 80% of hCD45⁺ medullar infiltration. C) Kaplan-Meier estimates of overall survival of the cohort.

This survival advantage was accompanied by reduction in cell viability *in vivo* (**Figure 43**). On Day 15 of treatment, there was a a strong increase in the percentage of bone marrow apoptotic cells correlated to a decrease in hCD45⁺ cells, that was not seen in control mice (**Figure 43**). Of note, hematoxylin-eosin-safranin (HES) staining evidenced intramedullary cell death and necrosis upon GSK458 treatment, however rates of cell death/necrosis were not significantly different between the two genetic contexts (**not shown**).

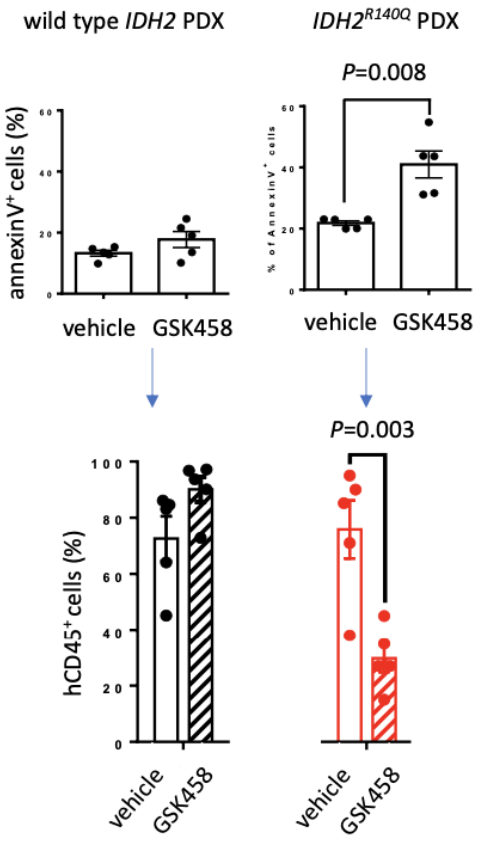

Figure 43: GSK458 treatment specifically affects the viability and differentiation of IDH2^{R140} AML cells in PDX model. Bone marrow aspirates were obtained at day 15 of treatment and analyzed for their content in hCD45⁺cells and annexinV⁺ cells. P-values were assessed by two-way unpaired t test. Data are represented as mean ± SEM.

These data assess that dual targeting of mTORC1/mTORC2 quickly impaired the viability of *IDH2*^{R140} AML cells in recipients while this pathway was seemingly less relevant for the

maintenance and propagation of wild type *IDH2* AML *in vivo*, suggesting that *IDH2*^{R140} confers unique dependence on mTOR metabolic pathways.

It is noteworthy that under energy stress conditions AMPK leads to mTORC1 repression[315]. As *IDH1* mutation could confer resistance to energy stress though AMPK activation[316], it will be necessary to elucidate the whole mechanism acquired by *IDH2* mutation in AML blasts that finally controls relationships between AMPK and mTORC1/2 and the functional consequence of an hyper-activity of mTORC2 in those cells.

6.1.6 IDH mutation and D-2HG is associated with proliferation

As one of the main functions of mTORC1 is to regulate cell growth, we next interrogated the association between growth and mutant *IDH2*-induced accumulation of D2-HG. We transduced *IDH2*^{R140Q}, *IDH2*^{R172K} and wild type *IDH2* lentiviruses into the PLB-985 and K562 cells and determined *in vitro* the relationship between D-2HG intracellular concentrations and cell population doubling times (Td). Accumulation of endogenous D-2HG produced by *IDH2*^{R140Q} and *IDH2*^{R172K} was gradually reduced by treating transduced cells with increasing doses of inhibitor AG-221/enasidenib that reverses the effects of mutant *IDH2*[287]. In both PLB-985 and K562 cellular contexts, treatment with increasing doses of enasidenib led to a substantial decrease in D-2HG levels, and D-2HG levels and Td were linearly related (**Figure 44A**). Similar observation was made in wild type *IDH2* human primary treated with octyl(R)-2HG (**Figure 44B**). *In vivo*, we also observed a correlation between type of *IDH2* mutations (*IDH2*^{R140} vs. *IDH2*^{R172}) and expansion of the disease in PDX models. *IDH2*^{R140} and *IDH2*^{R172} are known to produce different levels of D-2HG (*IDH2*^{R172} variants produce more significant quantities of D-2HG in AML patients[153] and PDX models evidence a slower expansion of *IDH2*^{R172}-driven AML compared with *IDH2*^{R140}-associated AML in recipients (**Figure 44C**). These results are in agreement with the study reported by Su and colleagues showing that D-2HG exerts a broad anti-leukemic activity *in vitro* and *in vivo* by inhibiting leukemia cell proliferation/viability[317].

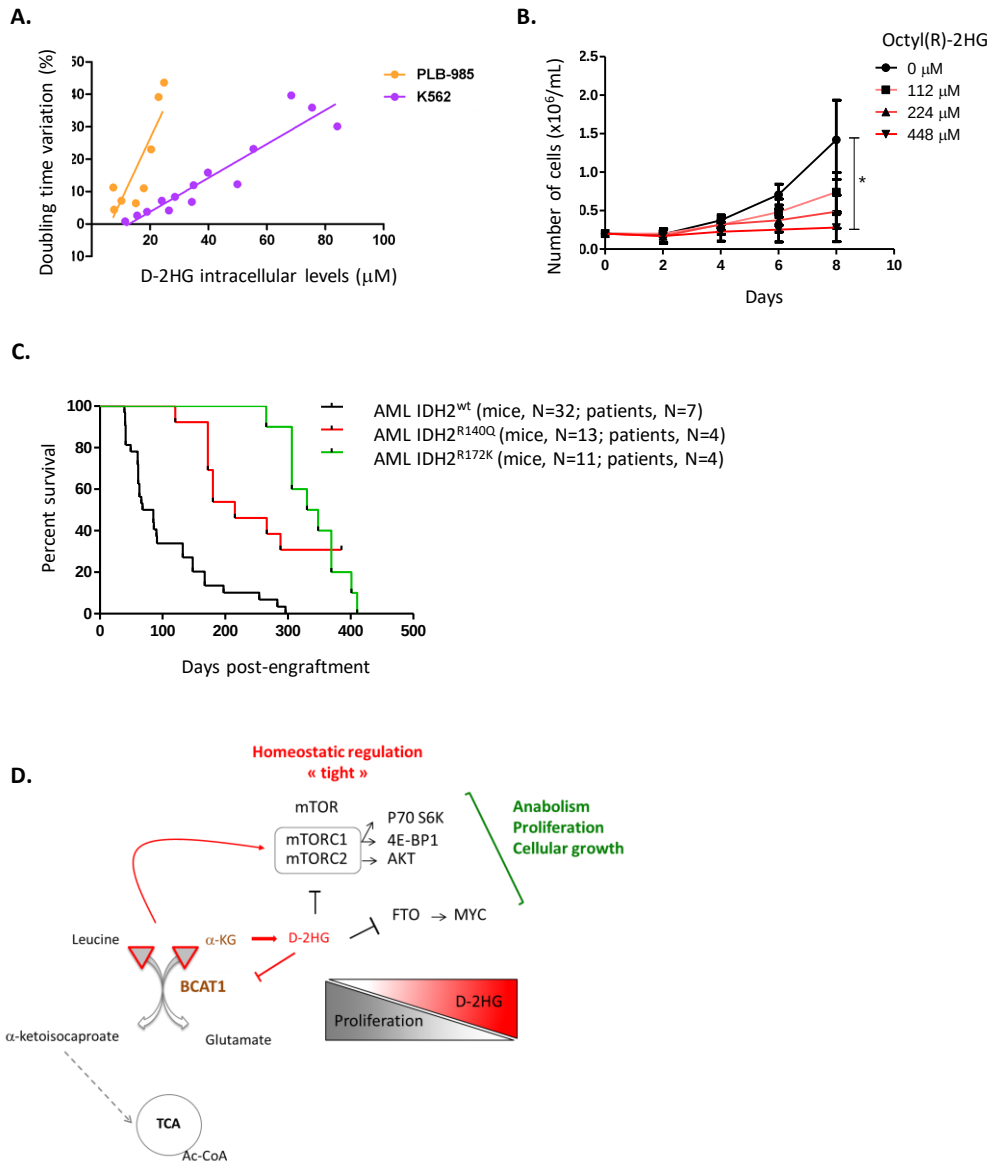

Figure 44: A) *Intracellular D-2HG levels of PLB-985 (orange) and K562 (purple) populations as a function of percentage increase in cell doubling time. B) Viability of wild type IDH2 AML cells treated with increasing doses of octyl(R)-2HG for 8 days. P-value was assessed by unpaired t-test. C) Overall survival of NSG mice engrafted with primary wild type IDH2 AML cells (N=7 samples; N=32 mice), IDH2^{R140Q} AML cells (N=4 samples; N=13 mice) and IDH2^{R172K} AML cells (N=4 samples N=11 mice). Mice were sacrificed at the time of clinical worsening or due to the presence of ≥ 80 % hCD45^{+} cells in the peripheral blood. Median time for engraftment was 1.3, 4.05 and 5.1 months for wild type IDH2, IDH2^{R140Q} and IDH2^{R172K} respectively (P<0.001). Median overall survival was 76.5, 215 and 339 days for*

wild type IDH2, IDH2^{R140Q} and IDH2^{R172K} respectively. D) Homeostatic regulation of BCAA metabolism in IDH2^{R140} AML cells.

Our findings with others[176,317] emphasize the notion that D2-HG shows growth-inhibitory effect in mutant *IDH* AML cells. Importantly, most of mutant *IDH* AML upregulate MYC to counteract the effect of D-2HG on proliferation[317] and *BCAT1* is a known MYC target gene ; in addition *BCAT1* overexpression is also able to activate MYC signaling[318]. A previous study identified a positive correlation between c-MYC overexpression and enhanced *BCAT1* transcript levels, which supported cell invasion in solid tumor[319].

It can be presumed that BCAT1 activity and accumulation of leucine might contribute, at least in part, to sustain mTORC1 activity otherwise inhibited by the accumulation of D-2HG (**Figure 44D**). On the other hand, intracellular accumulation of D-2HG is a process that needs to be finely controlled because excess of oncometabolite inhibits cell growth. Therefore, in mutant *IDH2* AML cells, leucine metabolism appears as a dynamic pathway, that take place in a regulatory loop to regulate the reactivation of mTORC1 but also to maintain an intracellular level of D-2HG below a threshold that would compromise cellular proliferation. BCAT1 enzymatic reaction overwhelmed as addition of octyl(R)-2HG inhibits its anabolic function in primary *IDH2^{R140Q}* AML cells (**not shown**). The BCAT1/leucine/mTORC1 pathway could thus be considered as an homeostatic regulatory loop (**Figure 44D**). Further characterization of BCAA metabolism will shed insight into how malignant hematopoietic cells handle metabolic demands for essential amino acids and how this can influence AML growth.

Summary points:

- We have identified a specific activity in the BCAA/leucine pathway distinguishing mutant *IDH* (leucine anabolism) from wild-type *IDH* (leucine catabolism) primary AML cells.

- Metabolic shift toward leucine production is associated to a strong upregulated expression of the α-KG-dependent *BCAT1* by breaking a H3K27me3-dependent negative regulatory mechanism.

- Primary mutant *IDH2*-expressing blasts are strictly dependent on BCAT1 activity for their growth and maintenance in culture and in a engrafted model. Knockdown of *BCAT1* expression or activity in mutant *IDH2* bulk AML cells results in proliferation arrest and substantial induction of cellular differentiation.

- Leucine anabolism appeared as a consequence of impaired mTOR activity due to 2-HG accumulation.

These findings reveal a metabolic feature of mutant *IDH2*-expressing AML cells that maintain cellular proliferation by running the BCAA pathway in reverse compared with wild-type *ID2H* AML, and point to a therapeutic strategy for targeting mutant *IDH* AML by exploiting the metabolic liability that comes with their increased reliance of dietary leucine.

6.2 PART II : MECHANISMS OF RESPONSE AND ACQUIRED OF RESISTANCE TO ENASIDENIB

6.2.1 Introduction

Differentiation arrest in AML can be successfully reversed and this can be exploited to cure AML.

Preclinical *in vitro* and *in vivo* studies have validated the proof of concept that targeted inhibition of *IDH* mutants resulted in normalization in a dose-dependent manner of D-2HG, reversal of histone and DNA hypermethylation and release of cellular differentiation block [289,320,321]. AGI-6780 is a small-molecule selective inhibitor of $IDH2^{R140Q}$ that normalized D-2HG, reversed histone and DNA hypermethylation and induced differentiation of $IDH2^{R140Q}$-mutant TF-1 erythroleukemia cells[322] but also of primary human AML cells harboring $IDH2^{R140Q}$ mutation[321].

The AG-221 compound is slow tight binder of the mutant IDH2 enzyme[287]. AG-221 allosterically stabilizes the open homodimer conformation, preventing the conformational change required for catalysis. AG-221 displayed higher potency against $IDH2^{R140}$ versus $IDH2^{R172}$. Therefore, this compound induced 99% reduction in intracellular D-2HG in $IDH2^{R140}$ cells at low concentrations (1µM) whereas $IDH2^{R172}$ required high concentrations (5µM) to achieve 99% reduction relative to vehicle-treated controls. *In vitro* treatment of primary $IDH2^{R140Q}$ AML cells with AG-221 resulted in normalization of D2-HG intracellular levels and alleviation of the cell differentiation block, which translated into engagement of leukemic blasts into differentiation along the mono- or granulocytic lineages, in primary AML cells treated *ex vivo* and in PDX mouse models[287]. Importantly, these differentiated cells were functional; $IDH2^{R140Q}$-mutant neutrophils obtained from primary $IDH2^{R140Q}$ -mutant blasts treated *ex vivo* with AG-221 demonstrated intact phagocytic activity, and exhibited granules colocalizing with lactoferrin, a canonical marker of secondary and tertiary granules of mature neutrophils[287].

These data prompted the launching in December 2013 of a clinical trial in the Gustave Roussy Institute and in several US Cancer Care Centers (phase 1/2 study, NCT01915498; AG-221/CC90007 (Enasidenib) first-in-human).

In the phase 1/2 study, 214 patients with mutant *IDH2* relapsed/refractory (R/R) AML (heavily pretreated population; median age: 68 years) received 100 mg per day; the safety

profile of the drug is very favorable (not cytotoxic) and the maximum tolerated dose in the phase 1/2 study has not been reached at daily doses up to 650 mg. Enasidenib produced an overall response rate (ORR) of 40.3%, a complete remission (CR) rate of 20.6%, and a median overall survival (OS) of 9.3 months in treated patients[290,291]. Median number of enasidenib treatment cycles was 5.0 (range, 1-38), median OS was 8.8 months (95% CI, 7.7-9.6), and median event-free survival (EFS) was 4.7 months (95% CI, 3.7-5.6). Estimated median OS was 22.9 months in 42 R/R AML patients who achieved CR, 10.6 months for patients who achieved a non-CR response, and 5.6 months for non-responders. Interestingly, median OS differed significantly between patients who had received 1, 2 or ≥3 prior AML treatments before study entry, 11.8 months (95% CI, 8.3-15.4), 7.8 months (95% CI, 5.8-9.1), and 7.0 months (95% CI, 4.9-8.8), respectively (P=0.001).

The recommended dose is 100 mg daily in continuous 28-day cycles because above 100 mg per day neither D-2HG suppression nor response rates were improved. As expected, patients with $IDH2^{R140Q}$ showed greater maximum D-2HG reductions from baseline (median, 92.9%) compared with $IDH2^{R172}$ patients (median, 47.4%) (P= 0.0004). However, there was no significant difference in ORR between R/R AML patients with $IDH2^{R140Q}$ (35.8%; 95% CI, 28.4-43.7) or $IDH2^{R172}$ (47.1%; 95% CI, 32.9-61.5) AML (P=0.187). In patients with $IDH2^{R140Q}$ AML, D-2HG was normalized in almost all cases and cannot act as a surrogate marker of efficacy. On the opposite, the magnitude of D-2HG reduction on-study was associated with CR in patients with $IDH2^{R172}$AML[264].

As epigenetic therapy, enasidenib acts slowly and median time to first response was 1.9 months (range, 0.5-9.4), and median time to best response was 3.7 months (0.6-14.7). In the absence of early response (before 90 days), patients were kept on drug (until overt progression). Even in the absence of significant marrow blast reduction, a subset of patients benefited from enasidenib as they became transfusion independent or/and produced neutrophils[264,265]. Terminally differentiated cells retained the *IDH2* mutation and were fully functional (at least neutrophils)[325].

Enasidenib induced differentiation of malignant cells, leading to a clinical *IDH* differentiation syndrome in 10% to 20% of patients[326], analogous to the differentiation syndrome seen in patients with acute promyelocytic leukemia (APL) treated with all-*trans* retinoic acid (ATRA)-based regimens. D-2HG is reduced in nearly all patients treated with enasidenib but does not predict clinical response (refractory, incomplete CR, CR)

indicating that although the drug shows an on-target therapeutic effect, mechanisms of primary resistance dictate the degree of clinical benefit.

In a minority of patients, enasidenib therapy induced molecular remission (assessed by digital PCR) associated with restoration of wild type terminal blood cell production and progenitor function from wild-type cells; molecular remission was seen in 12 % of the responders but there was no significant survival difference between these patients and patients in morphologic CR with detectable mutant *IDH2*. Clearance of mutant *IDH2* clones was associated with achievement of CR[323,264].

Thus, although the survival benefit provided by mutant IDH2 inhibition was clear, the drug was however not uniformly efficacious across patient populations. Notably, some patients failed to achieve meaningful or durable responses (> 6 months) and treatment-resistant diseases emerged during the course of the trial. Failure to achieve a response correlated with number (higher mutational burden) and nature of co-existing mutations, notably with mutations in genes related to RNA splicing and receptors/kinases/signaling (in particular *FLT3-ITD* or *TKD*) (P=0.007 and 0.005, respectively)[323,325]. In most patients treated in clinical trials, D-2HG remained suppressed at relapse, demonstrating that enasidenib remained on target and suggesting that relapsed clones were not dependent on mutant *IDH2*.

6.2.2 Results

In collaboration with Dr Lynn Quek and Pr Paresh Vyas (Oxford University, UK) and the Department of Clinical Hematology and the DITEP of Gustave Roussy (promoters of the phase I trials), the team has engaged a study on the molecular bases of response and acquired resistance to enasidenib on paired diagnosis/relapse samples obtained from the AG-221/CC90007/enasidenib clinical trial[291]. An average of 23 somatic mutations were detected per AML sample by whole-exome-sequencing (WES). Mapping of the clonal structure in leukemic cell population before therapy and during the course of treatment, evidenced that enasidenib promoted hematopoietic differentiation from AML clones showing variable differentiation arrest (i.e., progenitor-like or precursor-like stage); less frequently, treatment promoted differentiation of nonmutant cells. This study also showed that enasidenib caused a clone-specific differentiation response, either from

ancestral or terminal clones, thus leading to near normalization of the sizes and functionality of progenitor and precursor hematopoietic compartments with an altered clonal mix.

During my PhD, I aimed to validate somatic variant evolution between diagnosis (N=136) and relapse (N=148) in 12 samples by targeted PCR. I selected mutations for further validation by targeted re-sequencing, based on the following criteria: 1) known recurrent mutations in AML, 2) non-recurrent mutations in genes commonly mutated in AML. Mutations associated to a VAF that varied by at least 5% between sequential samples in the same patient were also analyzed, as these may be markers of clonal shifts. Specific primers were designed, amplicons were purified then pooled and sequenced (MiSeq, Illumina Technology, Gustave Roussy Genomic platform). Sequences were analyzed to validate the somatic nature of the variants.

Beside molecular abnormalities, del(7q) was the most frequent chromosomic alteration observed at relapse (N=4/12). Two patients developed isoform switching from *IDH2*$^{R140/R172}$ to *IDH1*^{R132} mutation, which was mutually exclusive from del(7q).IDH isoform switching has also been reported by others [327] and may occurred in 10-20% of cases at relapse. This pattern was associated with an increase in plasma 2HG[291,323,325] and DNA hypermethylation at relapse[328].

Other examples of genetic changes leading to enasidenib resistance included gain of function mutations in RTK signaling pathways (i.e. *FLT3*) and loss of or altered function in transcriptional regulators of hemopoiesis (i.e. *GATA2, CEBPA, RUNX1*) as reported few months later for ivosidenib secondary resistance[329].

We did not identify second-site mutations in *IDH2* at relapse on paired diagnosis/relapse samples although this situation has been reported by others[330]. Mutations in the IDH2 target, reported in few cases of acquired resistance, occurred in areas where enasidenib binds to the IDH2 dimer (e.g., Q316E and I319M substitutions); these in *trans* mutations are treatment-emergent under the selective therapeutic pressure of enasidenib therapy[330]. Thus, mechanisms underlying enasidenib resistance mostly rely on clonal evolution and bypass pathways acquisition. In AML, this phenomenon has been largely reported with other targeted therapies and may be explained, at least partially by clonal heterogeneity and highly dynamic plasticity of leukemic cells.

The phase 1, multicenter, open-label, dose-escalation and dose-expansion study using ivosidenib has been reported [331]. Remarkably, among patients who had a CR or CR with partial hematologic recovery, 21% had no residual detectable *IDH1* mutations on digital PCR (deep molecular remission). Rare acquisition of *TET2* mutations were also detected as a likely ivosidenib resistance mechanism; however, in contrast with the IDH switching, TET2-acquired cases showed continued suppression of plasma 2HG at relapse, while DNA hypomethylation did not occur[328]. Second site mutation in the IDH1 target occurred in larger number of cases, 10-20% at relapse[329,331]. IDH isoform switching was also observed and RTK signaling pathways mutations were present in 37% of relapsed cases, mostly associated to MAPKinase signaling pathways[329]. Liu and colleagues recently showed that STAT5 is a critical mediator of resistance to ivosidenib, especially in RTK pathway mutation, that could be overcome by STAT5 inhibitor such as pimozide[332].

6.2.3 Discussion

In this work we have studied at the single cell level the mutational landscape of mutant *IDH2* AML cells treated with the drug and identified mutations critical for enasidenib acquired resistance. We have identified mutation in hematopoietic differentiation transcription factors (*RUNX1, CEBPA, GATA2*). Since *RUNX* and *CEBPA* both encode essential transcription factors for myeloid differentiation, mutations in these genes likely abrogates differentiation signals induced by IDH inhibitors, thus contributing to the clinical resistance.

Mutations in the RAS-RTK pathway represent another major mechanism of the resistance. Mutations in *NRAS/KRAS* or in other MAPK pathway effectors (e.g., *tyrosine-protein phosphatase non-receptor type 11* (*PTPN11), NF1, FLT3*) and associated with acquired resistance to enasidenib, ivosidenib and FLT3 inhibitors[258, 259]. As they are enriched at baseline in refractory patients, they are likely mechanisms of resistance; primary resistance may be mediated through the expansion of preexisting resistant clones. Using a multigenomic analysis on longitudinally collected samples from the ivosidenib and enasidenib clinical trials, Wang and colleagues recently reported the molecular profiling of IDH inhibitors-treated AML samples and revealed that leukemia stemness plays major role in

primary resistance to the drugs[328]. Notably, non-responders to the drugs had a significantly higher 17-gene LSC score (LSC17, cf. [335]) compared with responders (**Figure 44**).

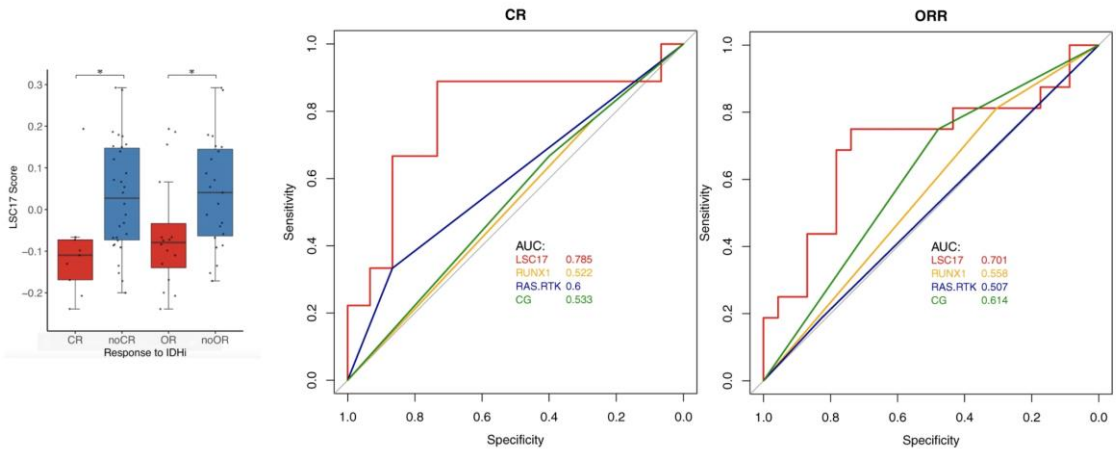

Figure 45: higher LSC17 score is the strongest predictor of response to IDH inhibitors. Data are from [328]).
*Left panel: LSC17 score calculated for each baseline sample and compared between patients achieving CR (N = 9) vs. not (N = 30) and OR (N = 16) vs. not (N = 23). *P < 0.05 (P = 0.011 for CR vs. non-CR; P = 0.037 for OR vs. non-OR). Box plot shows the minimum, first quartile (Q1), median, third quartile (Q3), and maximum.*
Right panel: Receiver operating curve (ROC) for predicting CR or OR with LSC17 score, RUNX1 mutation status, RAS-RTK mutation status, and ELN cytogenetic risk classification.
Legend: CR=complete response, OR=overall response, ORR = overall response rate.

6.2.4 Clinical update

In AML patients "fit" for intensive chemotherapy, IDH inhibitors are currently investigated frontline in a large randomized phase III trial (HOVON 156/AMLSG 28-18 (NCT04027309)). In newly diagnosed unfit AML patients, the phase III randomized AGILE trial has been recently reported. Ivosidenib + aza significantly EFS, OS, and clinical response, compared with placebo + aza[336]. Enasidenib + aza also showed promising clinical activity in a single-arm, phase 1b and randomized, phase 2 trials. Combination enasidenib + aza was well tolerated and significantly improved overall response rates compared with aza monotherapy[337,338].

There is also a strong rationale for the combination of IDH inhibitors with BCL2 inhibitors as accumulation of 2-HG caused by *IDH* mutations leads to the inhibition of cytochrome c oxidase activity, mimicking an oxygen-deprived state and decreasing the mitochondrial threshold for induction of apoptosis. Based on higher response rate in *IDH* mutant AML

patients treated with venetoclax-based combination, new treatment strategies have emerged. Lachoviez and colleagues recently reported preliminary results of ivosidenib, venetoclax and azacytidine combination in mutated *IDH1* myeloid malignancies. Composite CR (CRc: $CR^{+}CRi^{+}CRh$) was 84% including 92%, 63%, and 100% of patients with newly diagnosed AML, R/R-AML, or MDS respectively[249].

6.2.5 Published manuscript

Clonal heterogeneity of acute myeloid leukemia treated with the IDH2 inhibitor enasidenib

Lynn Quek[1,2,3,16*], Muriel D. David[4,16], Alison Kennedy[1,2], Marlen Metzner[1,2], Michael Amatangelo[5], Alan Shih[6], Bilyana Stoilova[1,2], Cyril Quivoron[4], Maël Heiblig[4], Christophe Willekens[4,7], Véronique Saada[4,7], Samar Alsafadi[8], M. S. Vijayabaskar[9], Andy Peniket[3], Oliver A. Bernard[4], Sam Agresta[10], Katharine Yen[10], Kyle MacBeth[5], Eytan Stein[6], George S. Vassiliou[9,11,12,13], Ross Levine[6,14,15], Stephane De Botton[4,7,17*], Anjan Thakurta[5,17*], Virginie Penard-Lacronique[4,17*] and Paresh Vyas[1,2,3,17*]

Mutations in the gene encoding isocitrate dehydrogenase 2 (*IDH2*) occur in several types of cancer, including acute myeloid leukemia (AML). In model systems, mutant IDH2 causes hematopoietic differentiation arrest. Enasidenib, a selective small-molecule inhibitor of mutant IDH2, produces a clinical response in 40% of treated patients with relapsed/refractory AML by promoting leukemic cell differentiation. Here, we studied the clonal basis of response and acquired resistance to enasidenib treatment. Using sequential patient samples, we determined the clonal structure of hematopoietic cell populations at different stages of differentiation. Before therapy, *IDH2*-mutant clones showed variable differentiation arrest. Enasidenib treatment promoted hematopoietic differentiation from either terminal or ancestral mutant clones; less frequently, treatment promoted differentiation of nonmutant cells. Analysis of paired diagnosis/relapse samples did not identify second-site mutations in *IDH2* at relapse. Instead, relapse arose by clonal evolution or selection of terminal or ancestral clones, thus highlighting multiple bypass pathways that could potentially be targeted to restore differentiation arrest. These results show how mapping of clonal structure in cell populations at different stages of differentiation can reveal the response and evolution of clones during treatment response and relapse.

Differentiation arrest is a common feature of many cancer cells. Although intratumoral clonal heterogeneity is well documented, a detailed understanding of how the complement of driver mutations within a clone contributes to differentiation arrest is lacking. Furthermore, although genetic and functional intratumoral heterogeneity clearly helps determine clinical outcomes in cancer therapy[1,2], few studies have investigated the relationship between clonal structure and therapy response, particularly for therapies targeting oncogenic epigenetic processes. With an average of 13 somatic mutations per patient, arranged in an limited number of clones[3], AML has a simpler genomic context than most cancers, thus providing a potential paradigm to answer these questions.

Somatic mutations in the conserved arginine residues R140 and R172 in isocitrate dehydrogenase 2 (IDH2) occur in 15–25% of patients with AML[4–6]. The mutant proteins have neomorphic activity producing (*R*)-2-hydroxyglutarate (2-HG), which competitively inhibits α-ketoglutarate-dependent enzymes including the TET family of 5-methylcytosine hydroxylases and Jumonji-C domain histone demethylases[7,8]. This inhibition leads to DNA hypermethylation[9], increased repressive histone methylation[8] and impaired hematopoietic differentiation, effects reversed by mutation-based IDH inhibition in model systems[8,10–12].

We have recently shown that enasidenib (AG-221/CC-90007), a first-in-class, allosteric inhibitor of mutant IDH2 (ref. [13]), decreases serum 2-HG, reverses DNA hypermethylation and promotes hematopoietic differentiation in preclinical models[13,14]. In a phase 1/2 clinical trial, enasidenib monotherapy produced a response rate of 40.3% in relapsed/refractory patients with AML[15]. In most of those responding patients, terminally mature blood cells were *IDH2* mutant, in agreement with a response due to enasidenib-induced differentiation of *IDH2*-mutant cells[16]. However, in 9/71 (12.6%) responding patients, *IDH2*-mutant cells were eliminated from peripheral blood cells[16]. A failure to respond to enasidenib was associated with a higher comutational burden and *NRAS* mutations[16]. Finally, most patients who initially responded eventually relapsed. These initial studies did not assess which clones differentiated in

[1]MRC Molecular Hematology Unit, WIMM, University of Oxford, Oxford, UK. [2]Haematology Theme, Oxford Biomedical Research Centre, Oxford University Hospitals NHS Foundation Trust, Oxford, UK. [3]Department of Hematology, Oxford University Hospitals NHS Foundation Trust, Oxford, UK. [4]INSERM U1170, Gustave Roussy, Université Paris-Saclay, Equipe Labellisée Ligue Nationale Contre le Cancer, Villejuif, France. [5]Celgene Corporation, Summit, NJ, USA. [6]Department of Medicine, Leukemia Service, Memorial Sloan Kettering Cancer Center, New York, NY, USA. [7]Département d'Hématologie, Gustave Roussy, Université Paris-Saclay, Villejuif, France. [8]Département de Recherche Translationnelle/INSERM U830, Institut Curie, Université Paris Sciences et Lettres, Paris, France. [9]Haematological Cancer Genetics, Wellcome Trust Sanger Institute, Hinxton, Cambridge, UK. [10]Agios Pharmaceuticals, Inc, Cambridge, MA, USA. [11]Department of Haematology, University of Cambridge, Cambridge, UK. [12]Department of Haematology, Cambridge University Hospitals NHS Trust, Cambridge, UK. [13]Cancer Research UK Cambridge Institute, University of Cambridge, Robinson Way, Cambridge, UK. [14]Center for Hematologic Malignancies, Memorial Sloan Kettering Cancer Center, New York, NY, USA. [15]Human Oncology and Pathogenesis Program, Memorial Sloan Kettering Cancer Center, New York, NY, USA. [16]These authors contributed equally: Lynn Quek, Muriel D. David. [17]These authors jointly supervised this work: Stephane De Botton, Anjan Thakurta, Virginie Penard-Lacronique, Paresh Vyas *e-mail: lynn.quek@imm.ox.ac.uk; stephane.debotton@gustaveroussy.fr; athakurta@celgene.com; virginie.penard-lacronique@inserm.fr; paresh.vyas@imm.ox.ac.uk

response to enasidenib or the clonal mechanism of acquired enasidenib resistance.

Here, we addressed these two questions by studying sequential samples from a subset of trial patients. We found marked variation in the degree of differentiation arrest of mutant *IDH2* clones. The restoration of differentiation by inhibition of mutant IDH2 was also clone dependent, varying among patients and arising from either ancestral or terminal clones. In a minority of patients, differentiation occurred from wild-type progenitor cells, in agreement with molecular remission in a subset of patients. Acquired resistance to enasidenib, leading to differentiation arrest and relapse, did not occur as a result of second-site mutations in *IDH2*. Instead, differentiation arrest was restored by multiple mechanisms through clonal evolution or clonal selection.

Results

Patient cohort studied. The trial enrolled 176 relapsed/refractory *IDH2*-mutant patients with AML[15]. Here, we studied a cytogenetically and genetically representative subset of 37 patients that was enriched in enasidenib responders (30/37 responders; Supplementary Fig. 1a–c). An extended mutational profile was determined in 33/37 patients through either whole-exome sequencing (WES) (16/36 patients at read depth of 19–843×, average 121× at loci where variants were called) or targeted resequencing (17/36 patients) (Supplementary Tables 1 and 2). Compared with the entire trial cohort, the patient cohort studied here had similar serum baseline 2-HG levels, and the mean level of 2-HG suppression was similar in the two cohorts (i.e., on-target response to enasidenib; Supplementary Fig. 1d,e).

Enasidenib rebalanced progenitor and precursor compartment sizes and restored progenitor function. In AML, there are two orthogonal potential hierarchies (Supplementary Fig. 2a). First, there is clonal hierarchy with an initiating clone, and transitional and terminal clones. We refer to all nonterminal clones as ancestral clones. These mutant clones exist in a second hierarchy, a hematopoietic cell hierarchy. AML-initiating mutations occur in stem cells or long-lived progenitor cells, but initiating clones are not usually arrested in differentiation[17–19]. However, with acquisition of additional transforming mutations and epigenetic alterations, clones do not complete maturation. In the fully transformed state, hemopoiesis in human AML is dominated by expansion of either progenitor-like cells, presumably because of a differentiation block between progenitor and downstream precursor cells[20], or, less commonly, precursor-like cells, presumably because of a differentiation block between precursor and mature cells[21]. In both cases, expanded leukemic progenitor-like or precursor-like populations have functional leukemic stem cell activity[20,21]. Thus, we set out to address three questions: (i) where are individual clones arrested in the hematopoietic hierarchy; (ii) which clones respond to mutant IDH2 inhibition by differentiating; and (iii) which clones are responsible for loss of response to enasidenib after an initial response, and through what mechanism?

The experimental approach is shown in Supplementary Fig. 2b. We first performed flow-cytometric quantification of hematopoietic stem/progenitor ($Lin^-CD34^+CD117^+$), precursor ($Lin^-CD34^-CD117^+$) and mature myeloid cell ($Lin^-CD34^-CD117^-$) populations[21] at trial entry in 15 patients (Fig. 1a,b and Supplementary Fig. 3a,b). The sizes of individual stem/progenitor populations within Lin^-CD34^+ cells were also quantified. 11/15 patients had abnormally expanded progenitor-like compartments (mainly lymphoid-primed multipotent progenitor (LMPP)-like and granulocyte-macrophage progenitor (GMP)-like populations; termed progenitor AML) and 4/15 abnormally large myeloid precursor–like populations (termed precursor AML). The ratio of progenitor to precursor AML was consistent with findings in previous studies[20,21].

Next, we analyzed the bone marrow (BM) stem/progenitor/precursor populations in five patients who achieved complete remission (CR) with enasidenib (Fig. 1b,c). In all five patients, there was near normalization of the sizes of the stem/progenitor compartments. Before treatment, two patients had pathologically expanded LMPP- and GMP-like progenitor populations (patients #201-023 and #201-011), and two patients had expanded myeloid precursor compartments (#201-010 and #203-002). Functionally, Lin^-CD34^+ progenitor cells from these five patients in CR formed myeloid–erythroid colonies nearly as efficiently as normal cells, in contrast to cells from patients who did not achieve CR (Fig. 1d and Supplementary Fig. 3c,d). Thus, enasidenib therapy rebalanced the sizes of hematopoietic stem/progenitor/precursor/mature populations at CR with reacquisition of normal myeloid progenitor function.

Wild-type hemopoiesis occurs occasionally with enasidenib therapy. Next, we investigated the clonal basis of differentiation. In principle, enasidenib could have directly or indirectly restored differentiation from wild-type cells, ancestral clones or terminal clones in a clonal hierarchy (Fig. 2a). We established the clonal basis of response in six patients by using samples taken at multiple time points before and through treatment, including relapse (Fig. 2b). We used WES and karyotyping of BM mononuclear cells (BMMNCs) to determine chromosomal copy number and mutational changes (Supplementary Tables 2 and 3). Next, we used WES data to design patient-specific mutation panels to test variant allele frequencies (VAFs) of mutations in unsorted BMMNCs and flow-cytometry-sorted hematopoietic stem/progenitor/precursor/mature cell populations and genotype flow-cytometry-sorted single cells and hematopoietic colonies derived from single cells (Supplementary Table 3). A combination of all these data was used to establish clonal structures. Details on setting false-positive and false-negative thresholds in single-cell genotyping (SCG) are presented in Methods.

In our initial study, 9/29 patients who achieved CR, for whom samples were available, had loss of mutant *IDH2* peripheral blood cells (complete molecular remission in peripheral blood[16]. However, it was unclear whether these differentiated blood cells were truly wild type or were from genetically mutant clones that lacked mutant *IDH2*. We studied this question in a patient who had mutations in *IDH2* (I), *PEX26* (P), *FEZ2* (S208T substitution; F), *DNMT3B* (D), *ZCCHC1* (official symbol *LIN28A*; Z), *NPM1* (N) and *ELMO3* (E) in AML blasts before enasidenib treatment (#201-022, Fig. 2c), and who achieved mutant *IDH2* molecular remission. Before therapy, imputation from VAF suggested the presence of wild-type cells and three possible mutant clones: a clone with *IDH2* mutation alone (I), a clone with genotype IPFDZN and a minor clone that was either IPFDZNE or IE (Supplementary Fig. 4a–c), although the exact clonal structure could not established unambiguously (Supplementary Fig. 4d–h). At CR, the VAF of all mutations was <1.6% (Fig. 2c and Supplementary Table 4 for depth of sequencing). Concordantly, at CR, most (94.6%) of the 111 individually genotyped hematopoietic colonies did not contain any mutations present pretherapy (Fig. 2d). Functionally, the colonies produced a normal ratio of myeloid to erythroid colonies, in agreement with a wild-type genotype (Fig. 2e). Thus, in a minority of patients, enasidenib therapy resulted in restoration of wild-type terminal blood cell production and progenitor function from wild-type cells.

Enasidenib restored differentiation from ancestral and terminal clones in a clone-dependent manner. In one patient, enasidenib promoted differentiation from an ancestral clone (#201-023, Fig. 3). WES and targeted resequencing of BMMNCs before enasidenib treatment detected mutations in *SRSF2* (S), *IDH2* (I), *ASXL1* (A) and *GATA2* (G), and two mutations in *RUNX1* (R and r) (Supplementary

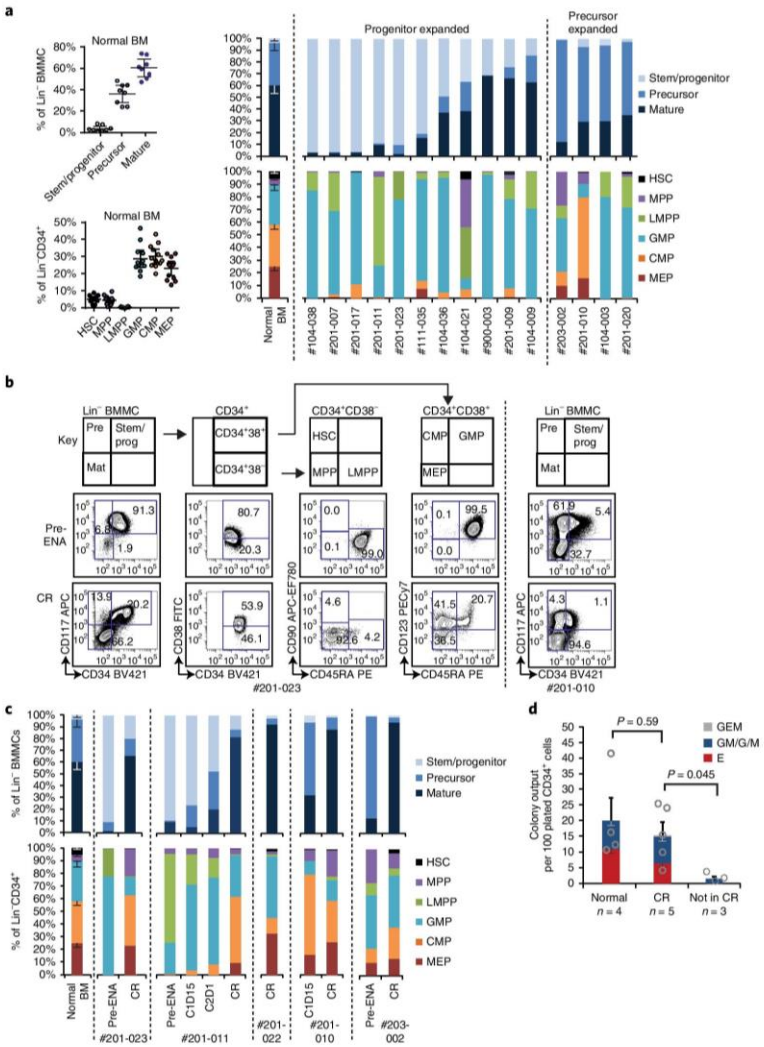

Fig. 1 | Enasidenib treatment induces differentiation of AML progenitor and precursor cell populations and restores progenitor function. a, Top right, immunophenotyping of hematopoietic stem/progenitor/precursor and mature cell populations in pretreatment AML BM) samples, showing expanded progenitor ($n = 11$ biologically independent samples) or precursor ($n = 4$ biologically independent samples) populations, and in normal BM ($n = 8$ biologically independent samples). Bottom right, detailed composition of stem/progenitor compartments in pretreatment AML BM samples ($n = 15$ biologically independent samples) and in normal BM ($n = 12$ biologically independent samples). Graphs with individual data points of normal BM are also shown. Error bars in normal BM, 95% confidence intervals. HSC, hematopoietic stem cell; MPP, multipotent progenitor; CMP, common myeloid progenitor; MEP, megakaryocyte–erythroid progenitor. **b**, Top, schematic representation of the flow-cytometric approach and sequential gates used to analyze samples in a. Lin⁻, lineage negative; stem/prog, stem/progenitor populations; pre, precursors; mat, mature. Bottom, examples of flow-cytometry plots from a representative sample before enasidenib treatment (pre-ENA) and at CR in patients with expanded progenitor-like populations (#201-023; left, experiment performed once) or expanded myeloid precursor-like population (#201-010; right, experiment performed once). Numbers shown within the gates indicate the percentages of the corresponding cell population compared with all cells in the plot. **c**, Top, immunophenotyping of hematopoietic cell populations in normal BM (as in a) and in pre-ENA BM samples from five patients (#201-023, #201-011, #201-022, #201-010 and #203-002) obtained at intermediate time points during treatment and at CR. Bottom, sizes of stem and progenitor compartments. Abbreviations and error bars in normal BM are as in **a**. C, cycle; D, day. **d**, Number of mixed erythroid–myeloid colonies (GEM), granulocyte–macrophage (GM), granulocyte (G), macrophage (M) and erythroid (E) colonies produced per 100 plated flow-cytometry-sorted CD34⁺ cells from normal BM ($n = 4$ biologically independent samples), enasidenib-treated patients in CR ($n = 5$ biologically independent samples) and enasidenib-treated patients not in CR ($n = 3$ biologically independent samples). Patient samples were plated with addition of enasidenib (1 μM) to semisolid medium. Error bars, s.e.m. *P* values were determined by two-sided Student's paired *t* test.

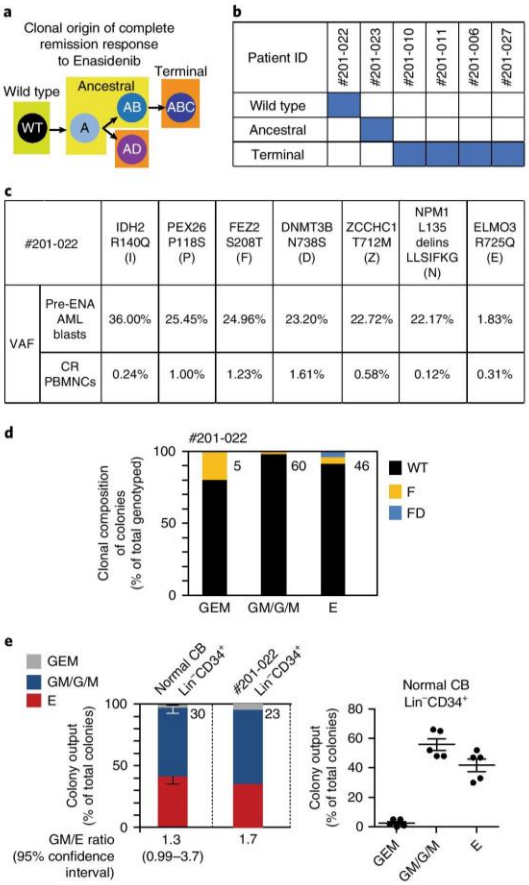

Fig. 2 | Differentiation response arising from wild-type cells in patients treated with enasidenib. a, Schematic representation of varying possible clonal responses to enasidenib. Four mutations (A–D) are present in four clones that are arranged in a branching structure. A differentiation response to enasidenib treatment could potentially occur either from wild-type cells or from ancestral or terminal clones. **b**, Summary of the types of differentiation responses (from wild-type cells or ancestral or terminal clones) in samples from six patients. **c**, VAFs of the indicated mutations in AML blasts of patient #201-022 before enasidenib treatment and in peripheral blood mononuclear cells (PBMNCs) at CR, as assessed through targeted resequencing. **d**, Clonal contribution to colony output from the CR sample from patient #201-022, shown as a percentage of all individually picked colonies genotyped. Clones were identified as wild type (WT), carrying the FEZ2 P118S mutation (F), or carrying the FEZ2 P118S and DNMT3B N738S mutations (FD). Lineage affiliations of the colonies are as in Fig. 1d. Numbers next to the bars indicate the numbers of colonies analyzed. **e**, Left, bar graph showing the lineage affiliation of colonies from normal cord blood (CB) Lin⁻CD34⁺ cells ($n = 5$ biologically independent samples) and CD34⁺ BM cells in the CR sample of patient #201-022. Graphs with individual data points of CB are also shown. Numbers next to the bars indicate average (CB) or actual (AML) number of colonies produced per 100 plated cells. The granulocyte-macrophage/erythroid (GM/E) ratio of colonies and the 95% confidence intervals for the GM/E ratio in normal BM are shown. Right, description.

Tables 2 and 3). Pretherapy imputation of clonal structure on the basis of VAF in unsorted BMMNCs by exome sequencing and targeted resequencing suggested initial acquisition of an *SRSF2* mutation (clone S) followed by an *IDH2* mutation (clone SI) followed by acquisition of *ASXL1* mutation, the two *RUNX1* mutations and *GATA2* mutation (Supplementary Fig. 5a and Supplementary Tables 2 and 3). At CR, only mutations *SRSF*, *IDH2* and *ASXL1* were detected in mature cells, thus supporting the existence of an SIA clone that preferentially completes terminal maturation in the presence of enasidenib (Supplementary Fig. 5a–c).

To clarify clonal structure, and to position clones within the hemopoietic hierarchy, we performed targeted resequencing for driver variants in 63 single cells and cell populations, from flow-cytometry-sorted progenitor and mature myeloid cell compartments, from both pretherapy and CR samples (Fig. 3a,b and Supplementary Table 3). The results confirmed a linear clonal-evolution pattern: clone SI preceded clone SIA and was followed by clones that sequentially acquired *RUNX1* mutations (clones SIAR and SIARr), and finally the terminal clone, which acquired a *GATA2* mutation (SIARrG). The mutational profiles in four single cells did not fit into this clonal-evolution pathway. We detected a single cell with an *ASXL1* mutation (clone A) and three single cells with both *ASXL1* and *SRSF2* mutations (clone AS). In three cells with genotype AS, we detected allele dropout (ADO) of the *IDH2* allele in two of three cells. Consequently, we were unable to determine the mutational state of *IDH2* in those two cells. In contrast, out of 12 cells of the SI clone, ADO of the *ASXL1* allele was detected in only three cells (Supplementary Fig. 12a). Thus, although our results do not exclude a rarer parallel clonal-evolution pathway in which clones A and AS exist and do not acquire mutations in the order shown in the main pathway, they also are consistent with these cells being part of the main clonal-evolution pathway.

Pretherapy, 90% of BMMNCs were progenitors (LMPP and GMP) (Figs. 1c and 3d), and 90–100% of these leukemic progenitors were SIARrG (Fig. 3c). Thus, the SIARrG clone is arrested in differentiation at the progenitor stage and expands to dominate the BM. Less than 10% of BMMNCs were mature myeloid cells (Figs. 1c and 3d). We were able to genotype only eight mature myeloid cells pretherapy (Fig. 3c), and they were composed of a mixture of wild-type cells and cells with genotypes A, SI, AS and SIA. At CR, the mature myeloid cell compartment comprised 60% of BMMNCs (Figs. 1c and 3d), and 85% of mature cells had the SIA genotype (Fig. 3d, Supplementary Fig. 5b and Supplementary Table 3).

The progenitor compartment made up only 20% of BMMNCs at CR (Figs. 1c and 3d) and was composed of mixed ancestral clones SI, SIA and SIAR, but not the terminal clone SIARrG. Concordantly, most colonies generated by progenitors at CR were SIA, and a minority had the SI or SIA genotype (Fig. 3e). The ratio of myeloid to erythroid colonies was within normal limits (Fig. 3f) Together, these data demonstrated a complex clone-dependent pattern of enasidenib-induced differentiation with production of mature myeloid cells sustained principally by a self-renewing ancestral SIA clone.

In four patients, differentiation of mature cells was principally seen from terminal clones (Fig. 2b). In patient #201-011, WES (Supplementary Table 2) and targeted resequencing of BMMNCs revealed two mutations in *DNMT3A* and mutations in *IDH2*, *ASXL1* and *XPO1* pretherapy that persisted at different VAFs at CR (Supplementary Table 3 and Supplementary Fig. 6a). However, it was not possible to impute the clonal structure from the VAF (Supplementary Fig. 6b). We genotyped 110 single cells, pretherapy and at CR (Fig. 4a). The results revealed an initiating *DNMT3A* clone (clone D) that acquired an *IDH2* mutation (clone DI) (Fig. 4b). Subsequently, there was a branching clonal structure with two terminal clones; one acquired an *XPO1* mutation (clone DIX), whereas the other acquired two mutations (a second *DNMT3A* mutation and an *ASXL1* mutation; clone DIdA). SCG suggested

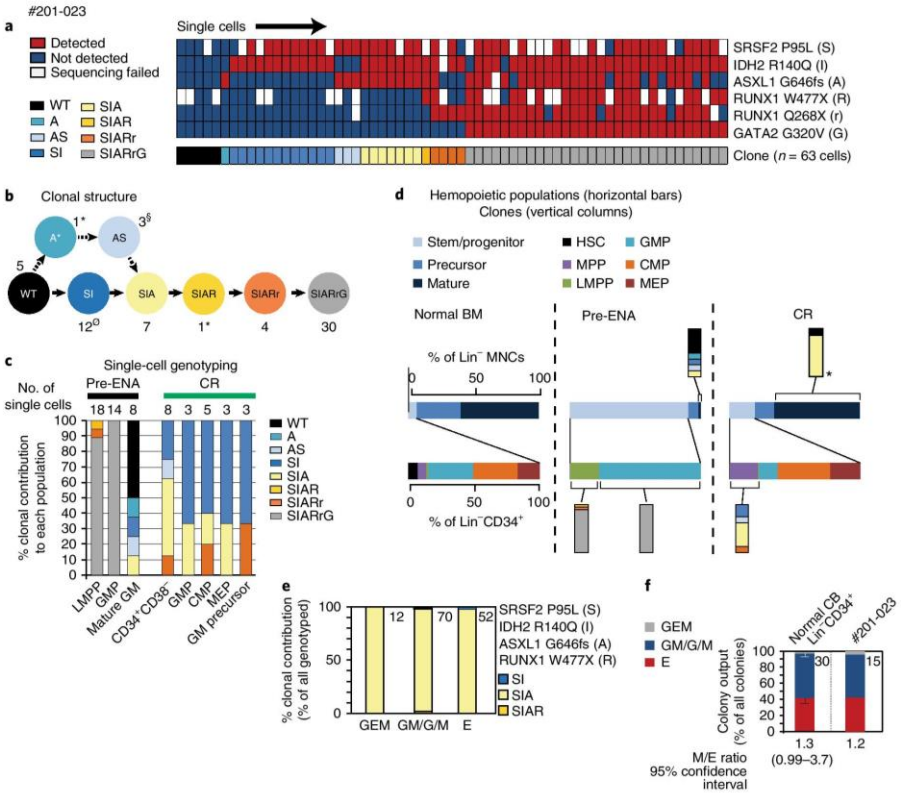

Fig. 3 | Enasidenib induces differentiation from an ancestral *IDH2*-mutant clone. All data shown refer to samples from patient #201-023. **a**, Heat map of targeted resequencing of mutations (rows) in single cells (columns, $n = 63$ cells) from flow-cytometry-sorted BM populations isolated either pretreatment or at CR (shown together). Clonal identification of each cell is shown below the heat map, and the key to mutations is denoted by letters on the right. **b**, Clonal structure of the AML sample, according to SCG. The number next to a given clone indicates the number of cells identified in that clone (data from **a**). The most likely clonal structure is shown in solid arrows, and alternatives are shown in dotted arrows. Asterisk indicates genotypes A or SIAR, which were each detected in only one cell. § indicates ADO of an *IDH2* allele occurring in two of three cells. Ø indicates ADO of the *ASXL1* allele occurring in 3 of 12 cells. Additional data in Supplementary Fig. 12a. **c**, Clonal composition in different immunophenotypic compartments in pre-ENA and CR samples. The number of cells studied is indicated. **d**, Clonal contribution (vertical bars) to immunophenotypic stem, progenitor, myeloid precursor and terminal mature granulocyte–macrophage populations in pre-ENA and CR patient samples (horizontal bars). Data are from SCG, except for the mature granulocyte–macrophage population in the CR sample, in which the flow-cytometry-sorted cell population was genotyped (asterisk). Normal BM is shown for comparison of immunophenotypic cell populations. **e**, Clonal contribution to colonies grown from the CR sample (percentage of genotyped, individually picked colonies). Key to mutations detected is as in **b**. Numbers next to the bars indicate the numbers of colonies analyzed. Lineage affiliations are as in Fig. 1d. **f**, Lineage affiliation of colonies from BM CD34+ cells purified from the CR sample, as compared with normal CB (as in Fig. 2e).

that the DIdA clone might have arisen through convergent evolution through intermediate DId and DIA clones. There is a caveat with this interpretation, because ADO was detected in six of seven DIA-clone cells (Supplementary Fig. 12c). In the DId cells, although there were no heterozygous germline single-nucleotide polymorphisms (SNPs) in the sequenced *ASXL1* gene, the estimated ADO frequency of the *ASXL1* allele was 12.1%. Thus, the DIdA clone might also have arisen through just one mutational pathway.

Before enasidenib treatment, 89% of BMMNCs were leukemic progenitors (LMPP and GMP) virtually exclusively composed of the DIX clone (Fig. 4c,d). A small mature myeloid population was present before enasidenib and was composed of the DIdA clone (Supplementary Fig. 6c). These observations suggest that the *IDH2* mutation in the context of the DIdA clone is not fully effective at imposing a complete differentiation block, whereas the same *IDH2* mutation in the context of the DIX clone fully arrests at a progenitor stage.

At CR, 82% of BMMNCs were composed of mature myeloid cells, 85% of which were a mix of two terminal branching clones—DIdA (54%) and DIX (31%)—thus suggesting that enasidenib promoted differentiation from both terminal clones (Fig. 4c,d and Supplementary Table 3). To address which progenitors contribute to mature cell output, we genotyped single flow-cytometry-sorted progenitors. The DIdA clone dominated mature GMP, CMP and MEP progenitor compartments (Fig. 4c,d). In contrast, clone DIX was detected only in the more immature LMPP progenitor compartment. GMP, CMP and MEP are more clonogenic than LMPP[20,22], and concordantly, ~95% of colonies had the DIdA

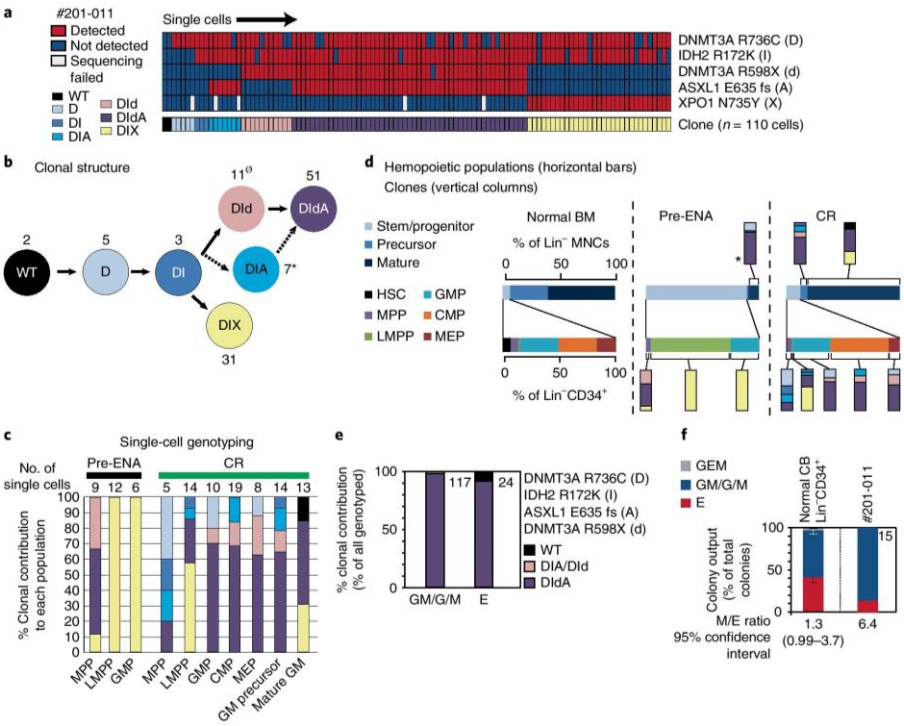

Fig. 4 | Enasidenib induces differentiation from a terminal *IDH2*-mutant clone. All data shown refer to samples from patient #201-011. **a**, Heat map of targeted resequencing of mutations (rows) in single cells (columns, $n = 110$ cells) from flow-cytometry-sorted BM populations isolated either pretreatment or at CR (shown together). The key is as in Fig. 3a. **b**, Clonal structure of the AML sample, according to SCG. The key is as in Fig. 3b. Asterisk indicates ADO for one of the two *DNMT3A* alleles, occurring in six of seven cells. Ø denotes the genotype DId. No heterozygous germline SNPs were available in the *ASXL1* gene. The estimated ADO frequency of the *ASXL1* allele was 12.1%. Additional data in Supplementary Fig. 12c. **c**, Clonal composition in different immunophenotypic compartments in pre-ENA and CR samples, as in Fig. 3c. **d**, Clonal contribution (vertical bars) to immunophenotypic BM hematopoietic populations in pre-ENA and CR patient samples (horizontal bars). Data are from SCG, except for the mature granulocyte–macrophage population in the pre-ENA samples, in which the flow-cytometry-sorted cell population was genotyped (asterisk). **e**, Clonal contribution to colonies grown from CR samples (percentage of genotyped, individually picked colonies), as in Fig. 3e. **f**, Lineage affiliation of colonies from BM CD34⁺ cells purified from the CR sample, as compared with normal CB (as in Fig. 2e).

genotype (Fig. 4e) and were myeloid biased (Fig. 4f). Interestingly, there was a substantial decrease in the size of the LMPP compartment at CR compared with pretherapy (Fig. 4d) (1,240-fold decrease within the Lin⁻ compartment and 81-fold decrease within the CD34⁺ compartment).

In three additional patients, the terminal clone contributed to mature myeloid cells at CR, on the basis of imputed clonal structures, genetic analysis of mature myeloid cells at CR (patient #201-010, Supplementary Fig. 6d,e) and genotyping of myeloid colonies at CR (patient #201-027, Supplementary Fig. 7a–d; patient #201-006, Supplementary Fig. 7e–h). The depth of coverage for each of the mutations in all three patients is shown in Supplementary Table 4.

In summary, enasidenib therapy provides relief of differentiation arrest at a progenitor-like or precursor-like stage, normalizing the sizes of these abnormally expanded compartments. The ability of mutant IDH2 to impose differentiation block is dependent on the context of coassociated mutations within a clone. Consequently, the efficacy of enasidenib-induced differentiation is also likely to depend on the mutational landscape within a clone.

Relapse of *IDH2*-mutant patients on enasidenib occurs through clonal selection/evolution and not second-site mutations in *IDH2*. Although responding patients have a median survival of 18–21 months, many patients relapse[15]. To study the mechanisms leading to relapse, we measured 2-HG levels in 16 patients at diagnosis and relapse, mutational profiles in 12 patients (by WES in 11 cases and by targeted sequencing in one case) and performed karyotype analysis in 11 subjects (Fig. 5a,b and Supplementary Table 5). We did not detect second-site *IDH2* mutations at relapse in any patient but instead documented seven patterns of clonal evolution/selection with acquisition of recurrent AML-associated genetic changes (Fig. 5a). These were recurrent missense mutations in myeloid malignancy, or nonsense and frameshift mutations in cancers, as documented in the COSMIC database (http://cancer.sanger.ac.uk/cosmic/). For patient #201-007, mutations were detected before relapse, but increased in frequency at relapse (Supplementary Table 3).

In 14/16 patients, 2-HG levels remained suppressed between best response (CR or PR) and relapse, thus suggesting that the drug was on target in suppressing neomorphic enzyme function (Fig. 5b). However, in two patients (#201-014 and #201-022) rising 2-HG

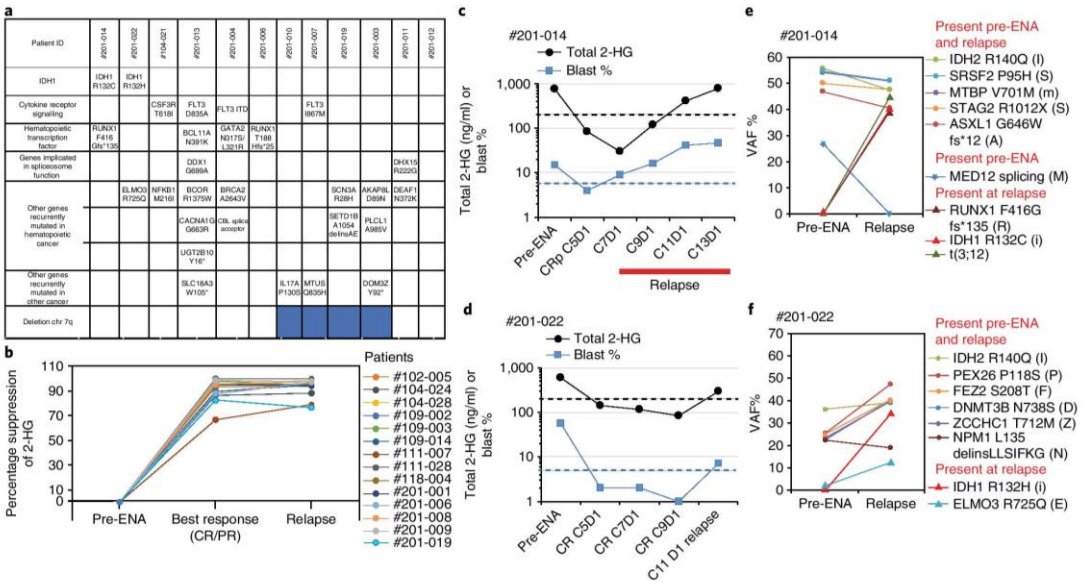

Fig. 5 | Mechanisms leading to relapse in enasidenib-treated patients. a, Summary of potential mechanisms (rows) leading to relapse in 12 patients (columns). Selected mutations or presence of monsomy 7 (indicated by blue box), detected at relapse by WES (all patients except #104-021) or by heme-panel bait-capture sequencing (#104-021) are each assigned to one of the potential mechanisms. **b**, Longitudinal analysis of the percentage suppression of serum 2-HG concentrations before enasidenib treatment, at best response (CR or PR) and at relapse in 14 patients with an *IDH2* codon mutation (affecting R140). **c**,**d**, Serum 2-HG levels and BM blast percentages in patients #201-014 (**c**) and #201-022 (**d**) before enasidenib treatment, at CR or complete remission without platelet recovery (CRp) during the course of treatment (C, cycle; D, day of treatment) and at relapse. **e**,**f**, Serial mutation analyses (VAF%) in flow-cytometry-sorted blasts obtained from patients #201-014 (**e**) and #201-022 (**f**) before enasidenib treatment and at relapse.

levels and BM leukemic cells (blasts) were seen (Fig. 5c,d). Exome sequencing revealed *IDH1* mutations encoding R132C or R132H, albeit accompanied by other genetic abnormalities, some of which are recurrent in AML (point mutations in *RUNX1* and *NPM1* and t(3;12)) (Fig. 5e,f). These *IDH1* mutations were previously undetectable by high-depth next-generation sequencing (NGS; 10,000×) before enasidenib therapy. Unexpectedly, in both cases, the VAF indicated that *IDH1* mutations were present in *IDH2*-mutant clones.

Relapse was also associated with increasing VAF of oncogenic gain-of-function mutations in two genes encoding cytokine receptors: *CSF3R* (#104-021, Supplementary Fig. 8a,b) and *FLT3* (#201-013 and #201-004, Supplementary Fig. 8c,d; #201-007, Supplementary Fig. 9f–h) and predicted loss-of-function mutation in *CBL*, encoding a negative regulator of cytokine signaling (#201-004, Supplementary Fig. 8d). For patient #104-021, we could not resolve the clonal structure from targeted resequencing of BMMNCs (Supplementary Fig. 8b and Supplementary Table 2), but genotyping of 214 single cells before enasidenib and at relapse (Fig. 6a) demonstrated an initiating *DNMT3A*/*IDH2*-mutant clone that spawned the major clone with a recurrent *U2AF1* mutation (DIU clone). A minor DIUF clone encoding a FLT3 D200E variant (not previously described in AML) was also present before enasidenib treatment. At relapse, the major clone in the expanded arrested LMPP and GMP compartments had acquired an oncogenic T618I mutation in *CSF3R*, which has been well described in myeloid leukemias[23] (DIUC clone). DIUC further evolved, acquiring a variant in *NFKB1* that has not been described previously in AML. Mutations in both *CSF3R* and *NFKB1* were detectable at the threshold of sensitivity before enasidenib (Supplementary Fig. 8a).

Relapse and reimposition of differentiation block were also associated with previously described mutations in hematopoietic transcription factors in myeloid cancers. These included frameshift mutations in *RUNX1* (Fig. 5e and Supplementary Fig. 8e, one of which has previously been described in AML (RUNX1 F416fs)[24]) and *BCORL1* (ref. [25]); nonsynonymous variants in the DNA- and protein-partner-binding N-terminal zinc finger of GATA2 (Supplementary Fig. 8d)[26,27] and in one of the zinc fingers of BCL11A[28] (Supplementary Fig. 8c). In all patients, these mutations were not detected before enasidenib treatment.

Deletion of all (monosomy 7) or part (del 7q) of chromosome 7 is common in myeloid malignancy[29]. Chromosomal abnormalities were present in 18% of the enasidenib cohort[15] and in 20% of the cohort studied here (Supplementary Fig. 1). Del 7q was detected in 4/12 patients who relapsed (#201-010, #201-007, #201-019 and #201-003) (Fig. 5a and Supplementary Table 5) but is not enriched in relapsed patients (M.A. and A.T., unpublished data). In all four patients, this deletion was detected either cytogenetically or by WES before enasidenib therapy (Supplementary Tables 2 and 5). In three of the four cases, the del 7q clone was selected at relapse (Supplementary Fig. 9a–e,k,l). In one case in which that clone was not selected, it was the dominant clone before therapy and at relapse (Supplementary Fig. 9g–j).

Clonal evolution at relapse also highlighted variants in genes less well studied in AML, including *NFKB1* (encoding M216I; Fig. 6a–d), *DDX1* (encoding G699A; Supplementary Fig. 8c), *MTUS1* (encoding Q781H; Supplementary Fig. 9f–i), *DHX15* (encoding R222G) and *DEAF1* (encoding N372K; Fig. 6e–h). Of these, the acquisition of the latter two variants by patient #201-011 at relapse was notable. Before enasidenib, the patient had expanded LMPP and GMP populations composed of an arrested DIX clone (Fig. 4b). At CR, the DIX clone was able to differentiate but persisted within only the LMPP com-

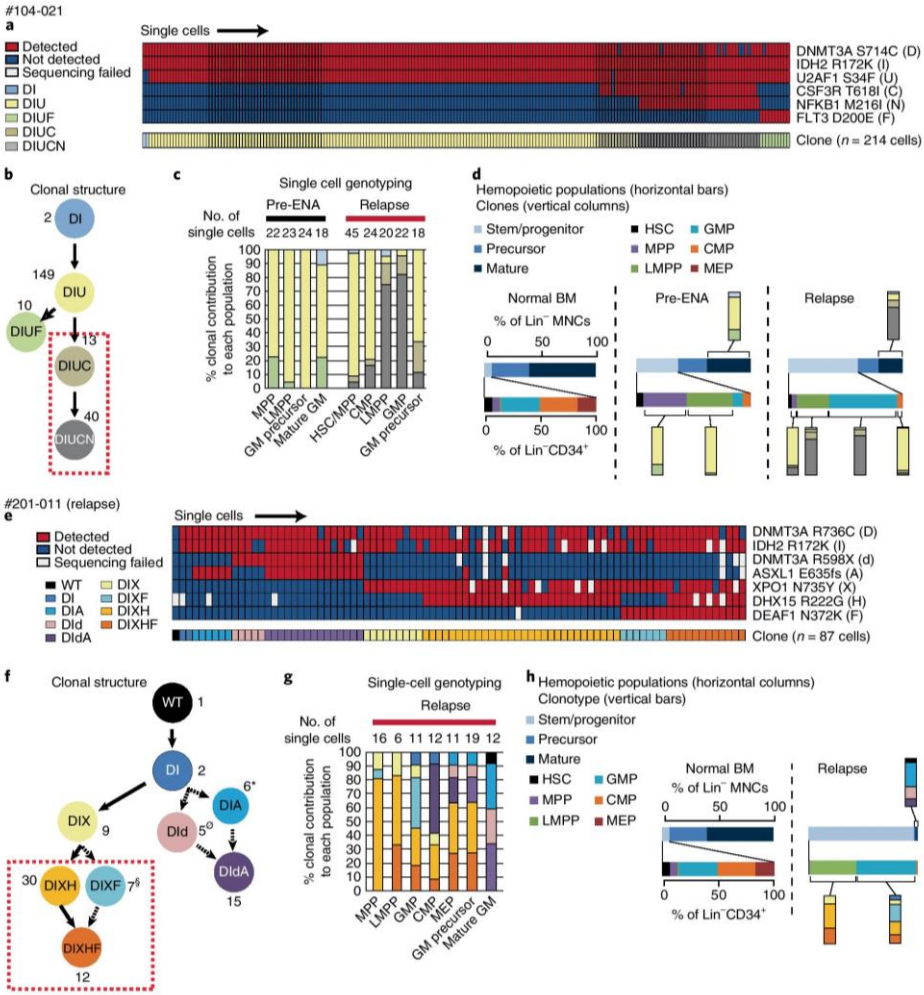

Fig. 6 | Relapse after enasidenib treatment occurs through clonal evolution/selection. Data shown for **a–d** and for **e–h** refer to samples from patients #104-021 and #201-011, respectively. **a**, Heat map of targeted resequencing of mutations (rows) in single cells ($n = 214$ cells, columns) from flow-cytometry-sorted BM populations isolated either pretreatment or at relapse (shown together). The key is as in Fig. 3a. **b**, Clonal structure, according to SCG. The key is as in Fig. 3b. Dotted red box highlights clones detected only at relapse. **c**, Clonal composition in different immunophenotypic compartments in the pre-ENA and relapse samples, as in Fig. 3c. **d**, Clonal contribution (vertical bars) to immunophenotypic BM hematopoietic populations in pre-ENA and relapse patient samples (horizontal bars). Data are from SCG. **e**, Heat map of targeted resequencing of mutations (rows) in single cells ($n = 87$ cells, columns) from flow-cytometry-sorted BM populations isolated at relapse. The key is as in Fig. 3a. **f**, Clonal structure at relapse. Asterisk indicates six cells with genotype DIA, in which we detected ADO in 4/5 cells in the *DNMT3A* allele. Ø denotes the genotype DId. The estimated ADO frequency of the mutant *ASXL1* allele was 12.1%. § indicates ADO of the *DHX15* mutant allele (encoding R222G) occurring in six of seven cells. Additional data in Supplementary Fig. 12c. Dotted red box is as in **b**. **g**, Clonal composition in different immunophenotypic compartments at relapse, as in Fig. 3c. **h**, Clonal contribution (vertical bars) to immunophenotypic BM hematopoietic populations in patient samples at relapse (horizontal bars). Data are from SCG.

partment (Fig. 4d). At relapse, we detected 30 cells with DIX mutations that acquired a missense mutation in the DExD/H-box helicase gene *DHX15* (encoding R222G; mutation H), seven cells with the DIX mutations that had acquired a variant in the transcription factor gene *DEAF1* (encoding N372L; variant F) and 12 cells with the DIXHF variants (Fig. 6e,f). However in six out of seven DIXF cells, there was ADO for the *DHX15* allele encoding the R222G mutation, and therefore we are unable to determine whether the R222G mutation was present in those cells (Supplementary Fig. 12c).

Acquisition of the additional *DHX15* and *DEAF1* mutations was associated with differentiation arrest and a reexpansion of LMPP and GMP progenitor compartments, comprising 89% of MNCs.

83% of LMPP cells were composed of the DIXH and DIXHF clones, whereas in the GMP-like compartment there was a more even contribution by the DIXHF, DIXH and DIXF clones (Fig. 6g,h).

Finally, both DHX15 and DDX1 regulate RNA splicing. Human DHX15 is structurally closely related to its yeast homolog, Prp43 (refs [30,31]). Both proteins have been shown to contribute to disassembly of splicesomes, efficient debranching and turnover of excised introns[32,33]. DHX15 R222G mutations have been previously described in AML[34,35]. To determine whether acquisition of DHX15 R222G results in altered splicing, we performed RNA-seq of AML blasts at relapse from patient #201-011 and compared splicing with that in AML cells from the same patient that were wild type for DHX15 at trial entry (Supplementary Fig. 8f). In cells expressing DHX15 R222G, compared with cells wild type for DHX15, there were alterations in exon skipping and intron retention. DDX1 is a DEAD-box RNA helicase with 5′ single-stranded RNA exonuclease activity that has been postulated to have multiple roles in RNA metabolism[36]. DDX1 G699A has not been previously described as a cancer-associated mutation nor has its effect on RNA splicing been studied. Our data show an increase in intron retention and use of alternative 5′ and 3′ splice sites, and a decrease in spliced exons in mutant compared with wild-type AML cells from the same patient (Supplementary Fig. 8g).

Discussion

This study of the clonal response and acquired resistance in sequential paired samples from patients with AML treated with an IDH2 inhibitor extends prior preclinical studies[13,14]. Before enasidenib treatment, there were complex patient- and clone-specific patterns of differentiation arrest. At CR, wild-type-dominated cellular reconstitution was less common but did occur. More commonly, enasidenib caused a clone-specific differentiation response, either from ancestral or terminal clones, thus leading to near normalization of the sizes and functionality of progenitor and precursor hematopoietic compartments with an altered clonal mix. Acquired resistance was never due to a second-site mutation in the same *IDH2* allele but instead was due to either clonal evolution or clonal selection. At least seven different mutational mechanisms led to reimposition of differentiation arrest (Supplementary Fig. 10).

In most patients, enasidenib was unable to promote terminal differentiation and eradication of *IDH2*-mutant clones; ancestral and/or terminal clones remained at CR. In patients with restitution of wild-type hemopoiesis, we infer that enasidenib probably promoted terminal differentiation of arrested self-renewing *IDH2*-mutant cells, thereby allowing normal cells to dominate hemopoiesis. Longer-term clinical follow-up of patients with molecular CR should indicate whether patients with molecular CR have better clinical outcomes and, if they relapse, the clonal origin of relapse. More generally, understanding the molecular mechanisms of relief from differentiation arrest by IDH2 inhibitors will require in-depth study of the changing patterns of epigenetic marks and transcriptional programs within highly purified and clone-specific hematopoietic stem, progenitor and precursor populations, before and after drug exposure, because transcriptional and epigenetic profiles are highly plastic through differentiation.

Drug resistance to targeted cancer therapy arises through multiple mechanisms. Resistance to kinase inhibitors in AML[37,38], chronic myeloid leukemia[39], chronic lymphoid leukemia[40] and lung cancer[41,42] often involves second-site mutations in the mutant allele modulating drug or substrate binding or copy-number changes in the mutant kinase. We did not observe such changes in enasidenib-treated patients.

Acquired resistance to IDH2 could arise through either epigenetic or genetic mechanisms or a combination thereof. In most patients, 2HG remained suppressed at relapse, thus suggesting that enasidenib remained on target, and relapsed clones were not dependent on mutant IDH2. In hematologic malignancies, genome-wide epigenetic variation (DNA methylation, for example) can be several orders more variable than genetic change[43–45]; moreover, this variation is somatically heritable and is subject to selection. Locus-specific DNA methylation (epiallele) variation shows dynamic changes in AML between diagnosis and relapse, and it can occur with distinct kinetics, such that some patients may have a high epiallele diversity and low somatic-mutation burden or vice versa[45]. In melanoma, resistance to a B-RAF inhibitor arises in rare cells through stochastic, transient variation in gene expression that is selected for by therapy[46]. This mechanism is consistent with prior findings on chromatin-mediated drug resistance in cancer cell lines[47].

Clones acquiring gene mutations, or gross genetic changes, have previously been reported in therapy-resistant chronic lymphocytic leukemia[48] and medulloblastoma[49]. Acquisition of an *IDH1* mutation in two patients is an example of how this resistance may occur. Here, AML propagation is likely to be highly dependent on high 2HG. 2HG addiction may be AML-cell autonomous, or alternatively the 2HG requirement may be in BM-niche supporting cells or other non-AML cell populations. AML clone-specific and non-AML cell-specific analysis of the effects of 2HG on epigenetic and transcriptional programs and metabolism of cells[50] is needed to understand this dependency. Other examples of genetic changes leading to enasidenib resistance include gain-of-function mutations in proliferative cytokine signaling pathways and loss of, or altered, function in transcriptional regulators of hemopoiesis. However, mutations in the RAS pathway that are correlated with a failure of initial response[16] were not associated with acquired resistance.

We also detected variants at relapse that were not previously well studied in AML. An example of this is the DHX15 R222G mutation, which has recently been described in *RUNX1–RUNXT1* AML[34]. The yeast homolog of DHX15, Prp43, regulates RNA splicing and ribosome biogenesis. Loss of wild-type DHX15 and overexpression of mutant DHX15 increases alternative splicing. In contrast, a role of DEAF1 has not been previously described in normal or malignant hemopoiesis. Interestingly, DEAF1 is a paralog of the transcription factor RUNXT1. DEAF1 is expressed throughout hemopoiesis but particularly in GMP and AML blasts[21]. In nonhemopoetic tissues, it binds LMO4, a member of the LMO transcriptional adaptor-protein family. In blood cells, LMO2, a closely related LMO family member, partners with transcription factors including GATA, E-box proteins and LDB1, thereby forming regulatory and oncogenic protein complexes. Thus, the role of DEAF1 in hemopoiesis and its interaction with DHX15 merits further study. More broadly, a deeper mechanistic understanding of how wild-type IDH2 promotes hematopoietic differentiation, which is currently poorly understood, should also increase understanding of how bypass pathways could reimpose differentiation block, for example by altering transcriptional programs, as seen in resistance to BET-inhibitor therapy[51].

Finally, this study demonstrates how any cancer therapy alters clonal structure across a fully transformed and premalignant cellular hierarchy. By defining clonal structures and mapping where clones were arrested across differentiation in purified hematopoietic compartments, we obtained a previously unavailable view of where different clones were arrested. These findings provide the necessary information to study why clones are arrested at different stages of differentiation. Furthermore, analysis of sequential samples through therapy shows how clones differentially respond to therapy. This information provides a basis to study clone-specific relief of IDH2 inhibition. More generally, our approach could be applied to any cancer therapy in which single-cell suspensions and purification of cells at different stages of differentiation are possible. This approach would then provide a clone-specific understanding of how therapy alters clonal structure through a cellular hierarchy.

Our approach also provides insights toward a rational basis for combination therapies to decrease drug resistance.

Methods

Methods, including statements of data availability and any associated accession codes and references, are available at https://doi.org/10.1038/s41591-018-0115-6.

Received: 5 November 2017; Accepted: 16 May 2018;
Published online: 16 July 2018

References

1. Abbosh, C. et al. Phylogenetic ctDNA analysis depicts early-stage lung cancer evolution. *Nature* **545**, 446–451 (2017).
2. Jamal-Hanjani, M. et al. Tracking the evolution of nonsmall-cell lung cancer. *N. Engl. J. Med.* **376**, 2109–2121 (2017).
3. Cancer Genome Atlas Research et al. Genomic and epigenomic landscapes of adult de novo acute myeloid leukemia. *N. Engl. J. Med.* **368**, 2059–2074 (2013).
4. Paschka, P. et al. IDH1 and IDH2 mutations are frequent genetic alterations in acute myeloid leukemia and confer adverse prognosis in cytogenetically normal acute myeloid leukemia with NPM1 mutation without FLT3 internal tandem duplication. *J. Clin. Oncol.* **28**, 3636–3643 (2010).
5. Green, C. L. et al. The prognostic significance of IDH2 mutations in AML depends on the location of the mutation. *Blood* **118**, 409–412 (2011).
6. Craddock, C. F. et al. Outcome of azacitidine therapy in acute myeloid leukemia is not improved by concurrent vorinostat therapy but is predicted by a diagnostic molecular signature. *Clin. Cancer Res.* **23**, 6430–6440 (2017).
7. Xu, W. et al. Oncometabolite 2-hydroxyglutarate is a competitive inhibitor of α-ketoglutarate-dependent dioxygenases. *Cancer Cell* **19**, 17–30 (2011).
8. Lu, C. et al. IDH mutation impairs histone demethylation and results in a block to cell differentiation. *Nature* **483**, 474–478 (2012).
9. Figueroa, M. E. et al. Leukemic IDH1 and IDH2 mutations result in a hypermethylation phenotype, disrupt TET2 function, and impair hematopoietic differentiation. *Cancer Cell* **18**, 553–567 (2010).
10. Losman, J. A. et al. (R)-2-hydroxyglutarate is sufficient to promote leukemogenesis and its effects are reversible. *Science* **339**, 1621–1625 (2013).
11. Wang, F. et al. Targeted inhibition of mutant IDH2 in leukemia cells induces cellular differentiation. *Science* **340**, 622–626 (2013).
12. Kats, L. M. et al. Proto-oncogenic role of mutant IDH2 in leukemia initiation and maintenance. *Cell Stem Cell* **14**, 329–341 (2014).
13. Yen, K. et al. AG-221, a first-in-class therapy targeting acute myeloid leukemia harboring oncogenic *IDH2* mutations. *Cancer Discov.* **7**, 478–493 (2017).
14. Shih, A. H. et al. Combination targeted therapy to disrupt aberrant oncogenic signaling and reverse epigenetic dysfunction in *IDH2*- and *TET2*-mutant acute myeloid leukemia. *Cancer Discov.* **7**, 494–505 (2017).
15. Stein, E. M. et al. Enasidenib in mutant *IDH2* relapsed or refractory acute myeloid leukemia. *Blood* **130**, 722–731 (2017).
16. Amatangelo, M. D. et al. Enasidenib induces acute myeloid leukemia cell differentiation to promote clinical response. *Blood* **130**, 732–741 (2017).
17. Jan, M. et al. Clonal evolution of preleukemic hematopoietic stem cells precedes human acute myeloid leukemia. *Sci. Transl. Med.* **4**, 149ra118 (2012).
18. Corces-Zimmerman, M. R., Hong, W. J., Weissman, I. L., Medeiros, B. C. & Majeti, R. Preleukemic mutations in human acute myeloid leukemia affect epigenetic regulators and persist in remission. *Proc. Natl Acad. Sci. USA* **111**, 2548–2553 (2014).
19. Shlush, L. I. et al. Identification of preleukaemic haematopoietic stem cells in acute leukaemia. *Nature* **506**, 328–333 (2014).
20. Goardon, N. et al. Coexistence of LMPP-like and GMP-like leukemia stem cells in acute myeloid leukemia. *Cancer Cell* **19**, 138–152 (2011).
21. Quek, L. et al. Genetically distinct leukemic stem cells in human CD34⁻ acute myeloid leukemia are arrested at a hemopoietic precursor-like stage. *J. Exp. Med.* **213**, 1513–1535 (2016).
22. Karamitros, D. et al. Single-cell analysis reveals the continuum of human lympho-myeloid progenitor cells. *Nat. Immunol.* **19**, 85–97 (2018).
23. Maxson, J. E. et al. Oncogenic CSF3R mutations in chronic neutrophilic leukemia and atypical CML. *N. Engl. J. Med.* **368**, 1781–1790 (2013).
24. Gaidzik, V. I. et al. RUNX1 mutations in acute myeloid leukemia: results from a comprehensive genetic and clinical analysis from the AML study group. *J. Clin. Oncol.* **29**, 1364–1372 (2011).
25. Li, M. et al. Somatic mutations in the transcriptional corepressor gene BCORL1 in adult acute myelogenous leukemia. *Blood* **118**, 5914–5917 (2011).
26. Papaemmanuil, E. et al. Genomic classification and prognosis in acute myeloid leukemia. *N. Engl. J. Med.* **374**, 2209–2221 (2016).
27. Fasan, A. et al. GATA2 mutations are frequent in intermediate-risk karyotype AML with biallelic CEBPA mutations and are associated with favorable prognosis. *Leukemia* **27**, 482–485 (2013).
28. Mason, C. C. et al. Age-related mutations and chronic myelomonocytic leukemia. *Leukemia* **30**, 906–913 (2016).
29. Grimwade, D. et al. Refinement of cytogenetic classification in acute myeloid leukemia: determination of prognostic significance of rare recurring chromosomal abnormalities among 5876 younger adult patients treated in the United Kingdom Medical Research Council trials. *Blood* **116**, 354–365 (2010).
30. Tauchert, M. J., Fourmann, J. B., Lührmann, R. & Ficner, R. Structural insights into the mechanism of the DEAH-box RNA helicase Prp43. *eLife* **6**, e21510 (2017).
31. Murakami, K., Nakano, K., Shimizu, T. & Ohto, U. The crystal structure of human DEAH-box RNA helicase 15 reveals a domain organization of the mammalian DEAH/RHA family. *Acta Crystallogr. F. Struct. Biol. Commun.* **73**, 347–355 (2017).
32. Arenas, J. E. & Abelson, J. N. Prp43: an RNA helicase-like factor involved in spliceosome disassembly. *Proc. Natl Acad. Sci. USA* **94**, 11798–11802 (1997).
33. Fourmann, J. B. et al. Dissection of the factor requirements for spliceosome disassembly and the elucidation of its dissociation products using a purified splicing system. *Genes Dev.* **27**, 413–428 (2013).
34. Faber, Z. J. et al. The genomic landscape of core-binding factor acute myeloid leukemias. *Nat. Genet.* **48**, 1551–1556 (2016).
35. Farrar, J. E. et al. Genomic profiling of pediatric acute myeloid leukemia reveals a changing mutational landscape from disease diagnosis to relapse. *Cancer Res.* **76**, 2197–2205 (2016).
36. Cordin, O., Banroques, J., Tanner, N. K. & Linder, P. The DEAD-box protein family of RNA helicases. *Gene* **367**, 17–37 (2006).
37. Cools, J. et al. Prediction of resistance to small molecule FLT3 inhibitors: implications for molecularly targeted therapy of acute leukemia. *Cancer Res.* **64**, 6385–6389 (2004).
38. Heidel, F. et al. Clinical resistance to the kinase inhibitor PKC412 in acute myeloid leukemia by mutation of Asn-676 in the FLT3 tyrosine kinase domain. *Blood* **107**, 293–300 (2006).
39. Shah, N. P. et al. Multiple BCR-ABL kinase domain mutations confer polyclonal resistance to the tyrosine kinase inhibitor imatinib (STI571) in chronic phase and blast crisis chronic myeloid leukemia. *Cancer Cell* **2**, 117–125 (2002).
40. Woyach, J. A. et al. Resistance mechanisms for the Bruton's tyrosine kinase inhibitor ibrutinib. *N. Engl. J. Med.* **370**, 2286–2294 (2014).
41. Kobayashi, S. et al. EGFR mutation and resistance of nonsmall-cell lung cancer to gefitinib. *N. Engl. J. Med.* **352**, 786–792 (2005).
42. Choi, Y. L. et al. EML4-ALK mutations in lung cancer that confer resistance to ALK inhibitors. *N. Engl. J. Med.* **363**, 1734–1739 (2010).
43. Figueroa, M. E. et al. DNA methylation signatures identify biologically distinct subtypes in acute myeloid leukemia. *Cancer Cell* **17**, 13–27 (2010).
44. Kulis, M. et al. Epigenomic analysis detects widespread gene-body DNA hypomethylation in chronic lymphocytic leukemia. *Nat. Genet.* **44**, 1236–1242 (2012).
45. Li, S. et al. Distinct evolution and dynamics of epigenetic and genetic heterogeneity in acute myeloid leukemia. *Nat. Med.* **22**, 792–799 (2016).
46. Shaffer, S. M. et al. Rare cell variability and drug-induced reprogramming as a mode of cancer drug resistance. *Nature* **546**, 431–435 (2017).
47. Sharma, S. V. et al. A chromatin-mediated reversible drug-tolerant state in cancer cell subpopulations. *Cell* **141**, 69–80 (2010).
48. Landau, D. A. et al. Evolution and impact of subclonal mutations in chronic lymphocytic leukemia. *Cell* **152**, 714–726 (2013).
49. Morrissy, A. S. et al. Divergent clonal selection dominates medulloblastoma at recurrence. *Nature* **529**, 351–357 (2016).
50. Raffel, S. et al. BCAT1 restricts αKG levels in AML stem cells leading to IDHmut-like DNA hypermethylation. *Nature* **551**, 384–388 (2017).
51. Rathert, P. et al. Transcriptional plasticity promotes primary and acquired resistance to BET inhibition. *Nature* **525**, 543–547 (2015).

Acknowledgements

We thank the patients and clinical staff for the samples studied. L.Q. was supported by an Oxford-Celgene Fellowship; P.V. acknowledges funding from the MRC Disease Team Awards (G1000729/94931 and MR/L008963/1), MRC Molecular Haematology Unit and the Oxford Partnership Comprehensive Biomedical Research Centre (NIHR BRC Funding scheme. oxfbrc-2012-1). V.P.-L. and S.D.B. acknowledge funding from the French National Institute of Health (INSERM-AVIESAN), the National Cancer Institute (INCa-DGOS-Inserm_6043 and INCa 2012-1-RT-09), SIRIC-SOCRATE 2.0 and the Fondation Association pour la Recherche sur le Cancer (ARC, Programme). M.D.D. is funded by a fellowship from the Institut National du Cancer (INCa-DGOS_5733). M.H. is supported as a fellow of the Fondation Philanthropia, Ecole des Sciences du Cancer, Gustave Roussy, Villejuif, France. We acknowledge the Core Flow Cytometry and Next Generation Sequencing Facilities at the WIMM; the Imaging, Cytometry and Integrated Biology platforms at Gustave Roussy (P. Rameau, Y. Lecluse, N. Droin, M. K. Diop and UMS AMMICa); the clinical departments at Gustave Roussy (J.-B. Micol for clinical

specimens; N. Auger for cytogenetic analyses; and C. Marzac and E. Leclercq for FLT3 genotyping) and Memorial Sloan Kettering. R.L.L. is supported by grants from the NIH, including R35 CA197594-01A1 and a Memorial Sloan Kettering Cancer Center Support Grant (NIH P30 CA008748, including a supplement to R.L.L.). The views expressed are those of the authors and not necessarily those of the NHS, the NIHR or the Department of Health.

Author contributions

L.Q. and M.D.D. designed and performed experiments, and analyzed data; A.K., M.M., M.A., B.S., C.Q., M.H., C.W., V.S. and S. Alsafadi performed experiments and analyzed data; M.S.V. and G.S.V. analyzed data; M.A., A.S., A.P., K.Y., S. Agresta, S.D.B., R.L., E.S., K.M. and A.T. provided reagents/samples/clinical data; O.A.B., S.D.B., A.T., R.L., V.P.-L. and P.V. designed the experiments and analyzed the data. L.Q. and P.V. wrote the manuscript. All authors edited the manuscript.

Competing interests

P.V. has received research grant support from Celgene and is on its speaker bureau. L.Q. has received research grant support from Celgene.

Additional information

Supplementary information is available for this paper at https://doi.org/10.1038/s41591-018-0115-6.

Reprints and permissions information is available at www.nature.com/reprints.

Correspondence and requests for materials should be addressed to P.V., L.Q., V.P.-L, S.D.B. or A.T.

Publisher's note: Springer Nature remains neutral with regard to jurisdictional claims in published maps and institutional affiliations.

Methods

Patient samples. BM or blood samples from normal donors and patients with AML were obtained with informed consent and collected by research ethics committee–approved biobanks: MDSBio Study (MREC 06/Q1606/110), Oxford Musculoskeletal Biobank (MREC 09/H0606/11; South Central Oxford C REC), Gustave Roussy (Department of Clinical Hematology and Drug Development Department (DITEP), Gustave Roussy, Villejuif, France) and MSKCC biobanks. Cytogenetic analyses were performed in clinical laboratories. Mononuclear cells (MNCs) were isolated with Ficoll density gradients. MNCs were viably frozen in 90% FCS/10% DMSO in liquid nitrogen.

Measurement and analysis of 2-hydroxyglutarate. Serum samples were collected within 28 d before the first dose of enasidenib ('screening') and/or predose on day 1 of each treatment cycle. 2-HG concentrations were determined by liquid chromatography and tandem mass spectrometry (Covance, according to the manufacturer's validated method). Baseline 2-HG was taken as the average value of the screening sample and predose cycle 1 sample, or the value of either sample if both were not available. Percentage suppression of 2-HG was determined by comparing the lowest level of 2-HG observed after treatment relative to baseline.

Hematopoietic cell immunophenotyping. Frozen BMMNCs from normal donors or AML samples were washed with Iscove's modified Dulbecco's medium (Thermo Fisher), 10% FBS (Sigma) and 1 mg/ml bovine pancreatic DNase I (Sigma). Cells were stained for flow cytometry with the antibodies listed in Supplementary Table 8. Analysis was carried out on either BD LSR Fortessa or BD FACSAria Fusion (Becton Dickinson) instruments. Antibodies used for the lineage (Lin) depletion were: anti-CD2, anti-CD3, anti-CD4, anti-CD8a, anti-CD10, anti-CD19, anti-CD20 and anti-CD235a (Supplementary Table 8). 7-aminoactinomycin-D (7AAD, Becton Dickinson) was used as a live/dead stain. Hematopoietic stem/progenitor cells were defined as subsets of Lin^-CD34^+, and myeloid precursor cells were defined as $Lin^-CD34^-CD117^+$, as previously described[21]. Terminally mature myeloid cells were defined as $Lin^-CD34^-CD117^-$.

Mutational analysis with FoundationOne heme panel. Analysis of samples in Fig. 1a with the FoundationOne heme panel was conducted by Foundation Medicine. Nucleic acid libraries were prepared from DNA and RNA extracted from fresh patient BM samples and captured with custom bait sets targeting 405 cancer-related genes by DNA-seq and 265 frequently rearranged genes by RNA-seq. Genes included in this analysis encode known or likely targets of therapies, either approved or in clinical trials, or are otherwise known drivers of oncogenesis described in the literature[52].

Mutational analysis with the Fluidigm Access Array. Selected samples from Fig. 1a and Supplementary Table 2 was analyzed with highly multiplexed PCR-based targeted resequencing with a custom panel of 373 amplicons covering areas of high-frequency AML mutations in 35 genes, by using the Fluidigm Access Array platform, as previously described[6].

Mutational analysis by whole-exome sequencing. Genomic DNA from flow-cytometry-sorted AML blasts or CD3-positive cells (germline control) was purified with Allprep DNA/RNA Mini or Micro Kits (Qiagen). After exome capture with a SureSelect V5 Mb All Exon kit (Agilent), paired-end 100-bp sequencing was performed on the HiSeq2000 (Illumina) platform. Read alignment to the hg19 reference genome was performed with the BWA algorithm (v0.7.10), with corrections with GATK (v3.3.0) after removal of PCR duplicates. Variant detection was carried out with VARSCAN (v2.3.7). Somatic variants (Supplementary Table 2) were selected with the following criteria: minimum depth 8×, VAF >10% in AML blasts and <10% in germline control, and $P < 0.001$. All variants were manually inspected with IGV (v2.3) software. Artifactual variants from DNA oxidation in which read-pair orientation bias was observed (i.e., predominant F2R1 orientation for C-to-A variations or F1R2 for G-to-T variations) were filtered out. The median depth at the positions reported in the Supplementary Table 2 was 121 (range 19–843).

Selection of mutations for targeted resequencing in populations and single cells. On average, 23 somatic mutations were detected per AML sample by WES. We selected mutations for further validation by targeted resequencing and SCG on the basis of the following criteria: (i) known recurrent mutations in AML and (ii) nonrecurrent mutations in genes commonly mutated in AML. In addition, mutations not meeting above criteria, but in which the VAF varied by at least 5% between sequential samples in the same patient, were of interest because these might be markers of clonal shifts. When multiple mutations had similar VAFs and showed similar patterns of change in VAFs in sequential samples, a representative mutation was selected. This procedure is illustrated in the example from patient #201-011 (Supplementary Fig. 11a). Mutations that were not validated by targeted resequencing were excluded in subsequent data analysis. Chromosomal loss of heterozygosity detected by WES (or by karyotyping) was examined on the basis of germline SNPs present in the affected chromosomal region.

Mutational analysis by targeted resequencing. Mutations detected by targeted resequencing in hematopoietic cell populations are shown in Supplementary Table 3. The average and range of read depth for each mutation are shown in Supplementary Table 4. DNA was extracted (DNeasy Blood and Tissue Extraction Kit, 69506, Qiagen) from bulk and flow-cytometry-sorted cells from patient samples. When material was limiting, whole-genome amplification (WGA; RepliG, Qiagen) was performed. Targeted PCR was performed with High-Fidelity Phusion Taq polymerase (NEB) or KAPA2G Multiplex DNA Polymerase (KAPA Biosystems) with 10 ng of gDNA. Primers used are listed in Supplementary Table 7. A second PCR reaction added Illumina barcodes and sequencing oligonucleotides before sample purification, quantification, pooling and library preparation for sequencing on the Illumina MiSeq platform. Raw data (average depth ~996×) were aligned with Stampy (v1.0.20)[53]. A minimum sequencing depth of 100 was set as the threshold for inclusion of data for analysis. >94% of reads had Phred scores > 30. VAF was obtained with the Unix 'grep' (globally search regular expression and print) command line.

Mutant *IDH2* variant-allele frequency determined by quantitative PCR. Mutant *IDH2* VAF was assessed in gDNA extracted from flow-cytometry-sorted patient blood $CD14^+$ monocytes, $CD16^+$ neutrophils or polymorphonuclear neutrophils (Ficoll gradient purification) at various time points during enasidenib treatment. Quantitative SNP assay PCR (12.5 ng DNA per test) was performed with TaqMan Universal PCR Master Mix (Applied Biosystems), TaqMan probes (specific for either IDH2 wild-type (FAM) or R140Q-mutant-encoding (VIC) alleles (rs121913502, Applied Biosystems)). PCR was performed on an ABI 7500 Fast Real-Time PCR analyzer (Applied Biosystems) with the following cycling conditions: initial 1 min at 60 °C; 10 min at 95 °C; 40 cycles of 15 s at 95 °C and 1 min at 60 °C; and 1 min at 60 °C.

Single-cell genotyping. Mutations interrogated by SCG are listed in Supplementary Table 3. Single cells were flow-cytometry-sorted into 96-well plates containing 2 µl of phosphate-buffered saline. WGA was carried out with a Single Cell RepliG Kit (Qiagen). Briefly, after cell lysis, alkali denaturation and neutralization, a master mix containing Phi29 polymerase, dNTPs and random oligonucleotide primers was added. WGA was carried out at 30 °C for 8 h and was followed by heat inactivation. Diluted (1:20) amplified DNA was used in single or multiplex PCR with primers relevant to the sample and High-Fidelity Phusion Taq polymerase (NEB) or KAPA2G Multiplex DNA Polymerase (KAPA Biosystems). Barcoding and sequencing oligonucleotides were added by PCR, and sequencing was performed on the Illumina MiSeq platform. ~94% of reads had Phred scores >30. A threshold of 50 reads was set for analysis inclusion. VAF thresholds for determining detection of mutations were determined by genotyping 48 single cells derived from normal BM, and were set at the 95% confidence level (mean ± 1.96× s.e.m.; i.e., <5% chance of false positive; Supplementary Table 6).

Imputation of clonal structures with bulk VAFs. The most common method used to impute clonal structure is based on the assumption that the most abundant mutation resides in the earliest-occurring ancestral clone. This method may be applicable to samples with linear clonal structures, but it may not be able to accurately resolve more complex or branching clonal structures. Longitudinal bulk genotyping data may offer additional information, particularly when there is evidence of clonal selection or evolution.

The putative clonal structure is first solved for each sample independently with the bulk VAF database according to the rules below. In samples for which there is no colony or SCG, longitudinal sampling (pre-ENA, best response and relapse) can provide additional information on the likely clonal structure of that patient. In the absence of colony or SCG data, bulk VAFs were used to estimate the size of the most likely clones in samples. In samples for which there was associated colony and/or SCG, the clonal structure was redrawn on the basis of these data, which provide a higher-confidence structure with some resolution of intermediate clones. After this clonal structure was solved, bulk VAF was used to estimate the sizes of clones in samples.

The sequence of acquisition of mutations can be imputed from bulk genotyping data, by using VAF as an estimate of clonal contribution (Supplementary Fig. 11b). Mutations are first ranked according to VAF: in these examples, V_A is highest, and V_D is lowest.

Factors that may cause data error and bias include limited cell-equivalent representation in extracted genomic DNA from small cell numbers, bias present in whole-genome-amplified material and PCR bias (including sequencing bias). Although we were unable to control for the first two factors, we were able to estimate the standard error of our sequencing data. We performed technical-replicate genotyping of 19 unsorted BMMC populations and obtained the s.e.m. from VAFs from each mutation. In total, 142 s.e.m. values were obtained, and the average s.e.m. was 1.9% (range 0.0–20.2%), with a 95%-confidence-interval upper limit of 2.47%. This procedure limited our ability to reliably distinguish between clones varying in VAF by ~2.5% (~5% of cells if mutations were heterozygous), and we were not able to impute the sequence of acquisition of mutations in population genotyping with a <2.5% difference in VAF between populations. When three or four mutations had VAF values within 2.5% of one another, the

average VAF of the cluster was taken as the VAF of all mutations in that cluster (Supplementary Fig. 11c).

Interpreting VAFs and cellular representation in the context of loss of heterozygosity or hemizygosity. We detected multiple occurrences of loss of heterozygosity (LoH, for example, copy-loss chromosomal deletions or copy-neutral uniparental disomy) and mutations, which were on the X chromosome in male patients (hemizygosity). There is complexity in interpreting bulk VAFs, owing to the potential mix of cells with or without LoH within a bulk population. Notwithstanding this caveat, we used the simple models described below to help interpret VAFs in different contexts. For somatic heterozygous variants (somatic mutation or germline polymorphism) in autosomal chromosomes, the estimated percentage of cellular representation was 2×VAF% (Supplementary Fig. 11d). Heterozygous variants and chromosomal deletion resulting in copy-loss LoH in autosomal chromosomes are illustrated in Supplementary Fig. 11e. Here, there was a nonlinear relationship between VAF and cellular representation (Supplementary Fig. 11f). The formula that we used to estimate cellular representation was as follows: % cellular representation = $[-2.777\times(\text{VAF ratio})^2] + (6.145\times\text{VAF ratio}) - 2.373$. In heterozygous variants and copy-neutral LoH (for example, uniparental disomy) in autosomal chromosomes, the percentage cellular representation was 100% −(2×VAF%) (Supplementary Fig. 11g). In X-linked variants in male subjects in sex chromosomes: the percentage cellular presentation was the same as the VAF% (Supplementary Fig. 11h).

Determination of clonal structures with single-cell genotyping. Each single cell was assessed for detection or nondetection of mutations in that patient sample through amplicon sequencing of DNA subjected to WGA. A minimum coverage of 30× across amplicons was required for an amplicon to be called. We assigned the most likely sequence of acquisition of mutations on the basis of the genotype identified in cells. For example, when mutations A, B, C, D and E were identified in a sample, discrete cells with genotypes A, AB, ABC, ABD, ABCD and AE might be called. In most cases, the sequence of acquisition, for example, A → AB, is clear. However, the sequence of acquisition of mutations during the transition, for example, from AB to ABCD, may not be clear because of ADO; i.e., the sequence of acquisition may be AB → ABC → ABCD or AB → ABD → ABCD. In such cases, intermediate genotypes represented by most cells may be more likely to be true. In all cases, models of clonal structures that require the least number of discrete mutational steps required are represented[54], although alternative structures, including ones in which the same mutation is acquired twice, are possible. After the most likely clonal structure is established, cells in which there was failure to amplify a locus that did not alter the assignment of a mutational complement (for example, an early mutation in the hierarchy) were included in the final analysis.

ADO estimation. ADO can be measured through two methods. First, ADO can be estimated by determining the phase of germline SNPs near mutations. For patients #201-023 and #201-011, we genotyped germline SNPs that were either in phase with (i.e., on the same allele as) a mutation or out of phase (i.e., on the opposite allele).

In-phase SNPs were rs6597996 and rs11246258, DEAF1 N372K mutation, patient #201-011. Out-of-phase SNPs were: (i) rs4911231, ASXL1 G646fs mutation, patient #201-023; (ii) rs2276598, DNMT3A R598X mutation, patient #201-011; (iii) rs7657364, DHX15 R222G mutation, patient #201-011. The SNPs were situated between 157 bases and 4 kb from the mutations. The threshold VAF for ascertaining dropout in these SNPs was <2% (homozygous reference) or >98% (homozygous variant).

In patient #201-023 (Fig. 3a,b) in two of three cells with the AS genotype, there was ADO of one of the *IDH2* alleles (Supplementary Fig. 12a, left) and in 2/12 cells with the genotype SI, there was ADO in the *ASXL1* allele (Supplementary Fig. 12a, right).

Our analysis also showed that in patient #201-011 the mutations encoding R598X and R736C are on different *DNMT3A* alleles, and the R736C-encoding mutation is in phase with rs2276598 (Supplementary Fig. 12b).

By studying both VAFs of the SNP rs2276598 and the R736C mutation in cells with genotype DIA in patient #201-011 in which ADO might have occurred, we determined that in six of seven cells at CR, ADO of the allele encoding the R598X mutation had occurred (Supplementary Fig. 12c left). When the SNP did not amplify, the VAF of the R736C mutation was informative. Similarly, in the same patient at relapse, five of six DIA cells at relapse had ADO of the R598X-encoding allele (Supplementary Fig. 12c center). We also determined that in six of seven cells with the DIXF genotype at relapse, there had been ADO of the *DHX15* allele encoding the R222G mutation (Supplementary Fig. 12c, right).

An alternate method to determine ADO more globally is to study the frequency with which a variant is called homozygous (either reference or alternative) when it should be heterozygous. We analyzed six SNPs in five genes (*ASXL1*, *IDH2*, *DNMT3A*, *DEAF1* and *DHX15*) in 402 single cells from two patients (#201-011 and #201-023) known to be heterozygous in the germ line (as confirmed by genotyping a population of flow-cytometry-sorted T cells from the patients). The mean VAF was 49.1% for all six SNPs, and there was a near-symmetrical distribution of VAFs across these single cells ranging from 0% to 100% (Supplementary Fig. 12d). The frequencies of homozygous-reference (VAF ≤1%) or variant calls in the 402 cells (VAF ≥99%; thresholds based on analysis of known homozygous SNPs in 237 cells) were 15.9% (64/402 cells) and 15.2% (61/402 cells), respectively (Supplementary Fig. 12d).

Next, if mutations in patients were assumed to be heterozygous (i.e., in cases with no data to support uniparental disomy or copy-number loss), we determined the frequency at which mutations were called homozygous (VAF ≥99%) (presumably because of ADO). Across the 23 mutations assessed with this method, the average ADO rate of the wild-type allele was 10.36% (s.d. 5.7%; Supplementary Fig. 12e). However, we found variation in ADO rates between different patients, even at the same mutation (for example, IDH2 R172K), thus suggesting that ADO is affected by factors in addition to that of the activity of the Phi21 polymerase. When possible, we used gene-specific germline SNPs or alternatively used sample- and mutation-specific ADO estimated by the 'homozygous mutant' method for our analyses.

Digital droplet PCR. We confirmed the VAFs detected by NGS with digital droplet PCR in 17 amplicons and 113 sorted multicell AML populations from five patients with the Bio-Rad platform, as previously described[21]. There was good correlation between the VAF values obtained with these two methods ($R^2 = 0.974$,). There was one AML variant (DHX15 R222G) in which NGS yielded an unexpectedly high VAF in single normal BMMNCs (in which the mutation was found to be absent in the bulk normal BM sample). Detection of this variant in normal and AML samples was therefore carried out with digital droplet PCR, which indicated the presence of the mutation in AML bulk and single cells but confirmed its absence in normal bulk and single cells.

Whole-transcriptome sequencing (RNA-seq) and analysis of alternative-splicing events. Copy DNA libraries were prepared with extracted RNA from AML blast cells flow-cytometry sorted from re- and postrelapse samples from patients #201-011 and #201-013. cDNA libraries were prepared for sequencing with tagmentation and indexing with an Illumina Nextera Sample Preparation Kit. RNA-seq data were generated as 75-bp paired-end unstranded Illumina reads. Reads were aligned with STAR(v2.4.0.1)[55] to the human genome (GRCh37) with default parameters. On average, the alignment was 96.7% (range 95.5–97.4%) with an average of 139×10^6 (range: 116×10^6 to 169×10^6) mapped reads per sample. Differentially spliced events for the wild type (prerelapse) and postrelapse with spliceosome gene mutations analyzed as paired samples were identified[56] with Mixture of Isoforms (MISO v0.5.4) with default parameters. An event was termed differentially spliced if Bayes factor ≥10, and $|\Delta PSI| > 0.2$, where PSI is the percentage spliced in, and the event is supported by ten or more reads. The classified differentially spliced events included skipped spliced exons, alternative 3′/5′ splice sites, mutually exclusive exons and retained introns.

Colony assays. 25–250 cells were plated in duplicate in 1.2 ml of MethoCult GFH4435 (StemCell Technologies). AML patient samples were assayed with added enasidenib (1 μM). The rest of the procedure was as previously described[20].

Statistical analysis. When applicable, statistical analyses were performed with GraphPad Prism software (v7.02). Statistical methods are noted in figure and table legends.

Reporting Summary. Further information on experimental design is available in the Nature Research Reporting Summary linked to this article.

Data availability. Exome sequencing data have been deposited in ArrayExpress under accession number E-MTAB-6299. RNA-sequencing data have been deposited in ArrayExpress under accession number E-MTAB-6660.

References

52. He, J. et al. Integrated genomic DNA/RNA profiling of hematologic malignancies in the clinical setting. *Blood* **127**, 3004–3014 (2016).
53. Lunter, G. & Goodson, M. Stampy: a statistical algorithm for sensitive and fast mapping of Illumina sequence reads. *Genome Res.* **21**, 936–939 (2011).
54. Potter, N. E. et al. Single-cell mutational profiling and clonal phylogeny in cancer. *Genome Res.* **23**, 2115–2125 (2013).
55. Dobin, A. et al. STAR: ultrafast universal RNA-seq aligner. *Bioinformatics* 29, (15–21 (2013).
56. Katz, Y., Wang, E. T., Airoldi, E. M. & Burge, C. B. Analysis and design of RNA sequencing experiments for identifying isoform regulation. *Nat. Methods* **7**, 1009–1015 (2010).

7 DISCUSSION

We have identified BCAT1 activity as limiting for mutant *IDH2* AML cell proliferation and found that this metabolic dependency could be selectively targeted for therapeutic gain. In mutant *IDH2* cells, BCAA anabolism correlates to *BCAT1* overexpression**.** Our study suggests that it is the *IDH2* genetic lesion, and/or the accumulation of D-2HG, that lies at the root of this metabolic feature. Indeed, our data converge mutant *IDH2* AML samples with metabolic similarity, despite their genetic heterogeneity, and indicate an unexpected directionality of the BCAT1-mediated reaction leading to leucine accumulation, that helps support mTOR activity and cellular growth.

We have analyzed the activity of the two alternative promoters from the *BCAT1* gene and identified a high activity level from both P1 and hypermethylated P2 promoters across mutant *IDH2* AML cells compared with wild type *IDH* AML samples. This result is consistent with previous findings of hypermethylation at P2 in mutant *IDH1* gliomas[283] suggesting that hypermethylation is associated with *IDH* genetic lesions. In mutant *IDH2* AML cells, DNA methylation level is negatively correlated with H3K27me^3 levels at hypermethylated sites in CGI, breaking a H3K27me^3-dependent negative regulatory mechanism. Little is known about how cancer-associated epigenetic marks influence *BCAT1* transcript variant expression. Recent works have proposed positive regulation of *BCAT1* expression in solids tumors through DOTL1-mediated methylation of histone 3 lysine 79 (H3K79)[339] or reduced activity of the euchromatic histone lysine methyltransferase 2 (EHMT2, also known as G9a) and suppressor of variegation 3-9 (Drosophila) homolog 1 (SUV39H1) H9K9 methyltransferases, resulting in decreased H3K9me2/me3 marks at P1[340]. Our findings, regarding the faint enrichment of the repressive mark H3K27me^3 at hypermethylated P2 in mutant *IDH2* AML cells compared with wild type *IDH2* cells, argue for a regulation of *BCAT1* expression by EZH2 ; these observations corroborate a murine experimental model of AML in which impaired EZH2-mediated H3K27me^3 deposit on both promoters is causative of *BCAT1* upregulation[277]. The repressive effect of D-2HG is not genome-wide in mutant *IDH2* AML cells; even the global level of H3K27me^3 is elevated in mutant *IDH2* leukemic blasts, the genomic distribution of this repressive mark seemingly promotes the transcription of a network of genes and/or account for the

expression of specific transcripts, rewiring transcriptional programs compared with wild type *IDH* AML (unpublished results). In line with our observations, in mutant *IDH1* glioma, altered H3K27me^3 dynamics is the main cause of transcriptional alteration, and genes highly expressed in healthy brain cells are more likely to be repressed by H3K27me^3 than by DNA methylation (5mC)[341]. Similarly, expression of *IDH2^{R172K}* in mesenchymal cells induces locus-specific histone hypermethylation and concentrates the effect of 2HG to regions that lose the repressive H3K9me2/3 mark[342]. However, as D-2HG itself inhibits BCAT1 activity[179], we cannot rule out the possibility that chronic *in vivo* D-2HG exposure in mutant IDH2 AML cells may lead to cell adaptation and selection of clones harboring high *BCAT1* expression level.

Over time after *BCAT1* ablation, a progressive clearance of mutant *IDH2* AML cells is observed in xenografted mice, that results from a proliferation arrest and differentiation induction, a dual mechanism that has also been reported in AML blasts upon inhibition of the *DHODH* involved in *de novo* pyrimidine synthesis pathway[343,344]. It has already been reported that BCAA availability plays a role in cell cycle regulation, through activation of the mTORC1 signaling by the CD98 heavy chain (CD98hc, encoded by *SLC3A2*)[310,345], a transmembrane protein required for adhesion and survival of AML cells[346]. CD98hc together with SLC7A5, forms the L-type amino acid transporter 1 (LAT1) that is an essential amino acid carrier. CRISPR-based screens of 14 human AML cell lines have identified SLC7A5 as an essential gene for cell survival[347]. siRNA-mediated silencing of *SLC7A5* in myelodysplastic syndromes (MDS)-derived cell lines leads to cell cycle arrest, reduced proliferation and the induction of apoptosis in these cells[348]. Interestingly, the LAT1 transmembrane complex is implicated in a tolerogenic phenotype via activation of the AhR signaling pathway in infiltrating monocytes-derived macrophages in human mutated *IDH1* gliomas ; this pathway also creates a metabolic vulnerability that can be targeted to restore a tumor microenvironment that is more responsive to immune-checkpoint therapy[163] (cf. **Figure 21**).

Small molecules that inhibit system L transport activity have been developed such as the leucine analog 2-aminobicyclo-(2,2,1)-heptane-2-carboxylic acid (BCH); BCH inhibits leucine import via LAT carriers and significantly slows the growth of the AML cell lines (HL60, NB4, K562) (**Figure 45**)[349]. BCH treatment leads to a reduction in phosphorylation of S6RP involved in the activation of the mTOR pathway in these cells[350]. In keeping, genetic or

pharmacological invalidation of LAT1 in different cancer cell lines results in a complete suppression of leucine transport, leading to a loss of amino acids homeostasis with activation of the eukaryotic translation initiation factor 2 alpha kinase 4 (EIF2AK4 also known as GCN2)-driven stress pathway, inhibition of mTORC1 and suppression of tumor growth [351].

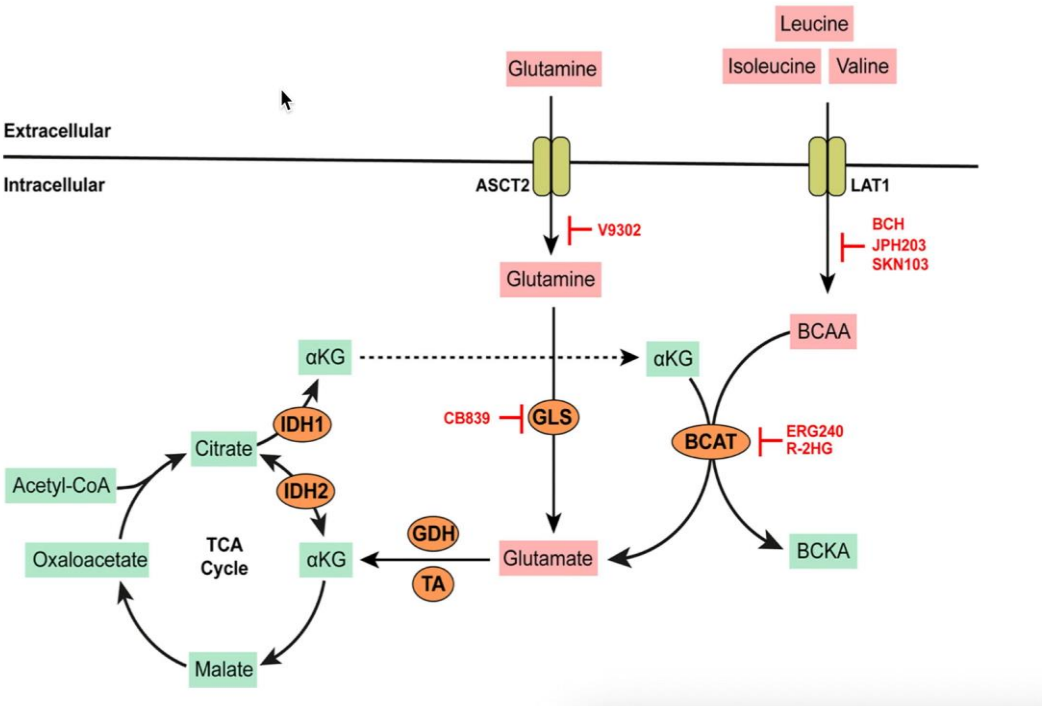

Figure 45: LAT1 mediates the reversible import of leucine in exchange for glutamine across the cell membrane (from [352]). BCAAs can fuel the TCA cycle through transamination and production of glutamate and respective α-ketoacids that can undergo decarboxylation to provide succinyl-CoA (valine metabolism) or acetyl-CoA (leucine or isoleucine metabolism). Enzyme inhibitors are indicated in red. ERG240, is a leucine analogue that inhibits BCAT1 activity[279]. As BCAT1 is an aKG-dependent enzyme, oncometabolite D-2HG blocks BCAT1 activity. 2-amino-3(4[methoxy]-3,5-dichlorophenyl) propanoic acid (JPH203, also known as KYT-0353) is a selective inhibitor of leucine transport via LAT1. (S)-2-amino-3-(4-((7-(3-aminophenyl)naphthalen-1-yl)methoxy)-3,5-dichlorophenyl)propanoic acid (SKN103) is a also a blocker of LAT1. SKN103 blocks leucine transport and mTOR activation in several cancer cell lines but has not yet been tested on myeloid cell lines. Mitochondrial glutaminase (GLS); glutamate dehydrogenase (GDH); amino acid transaminases (TAs); aspartate aminotransferase (AST); alanine transaminase (ALT).

BCAT1 also affects mitochondrial metabolism independently of leucine transamination. In macrophages *BCAT1* inhibition did not translate into major TCA cycle modification but leads to ROS imbalance and thus apoptosis; this indirect effect is associated with

activation of the transcription factor nuclear factor erythroid 2-related factor 2 (NRF2, also known as NFE2L2)[353]. Moreover, in mutant *IDH1* glioma, PI3K/mTOR inhibition leads to increased survival[354].

The anti-leukemic properties of BCAT1 inhibition are also associated to the promotion of differentiation. Both our *in vitro* (primary AML cells treated with gabapentin) and *in vivo* (PDX model) experiments have shown an increased expression of differentiation markers upon BCAT1 inhibition. Our data raised questions about the role of BCAA metabolism and BCAT1 activity in the bypass of differentiation block in AML cells but also in the induction of myeloid differentiation in physiological conditions. An important question is the contribution of BCAT1 in AML cells aberrant proliferation. From our data, BCAA metabolism provides a mechanism for regulating the levels of leucine which activates mTORC1. Numerous studies have demonstrated that mTORC1 and notably its target S6K1 are involved in aberrant HSC function such as the development of leukemia; the PI3K/Akt/mTOR signaling pathway is frequently hyperactivated in AML cells and potentially contributes to uncontrolled growth, proliferation, differentiation, metabolism, and survival (reviewed in [282, 283]). These observations must be mitigated by the fact that no clear evidence of clinical efficacy has been found by clinical trials of agents targeting mTOR in myeloid leukemia[357] (probably because adding mTOR inhibitor in glycolytic leukemic cells might induce a quick metabolic switch for OXPHOS and then promote cell survival[358]). mTORC1 promotes cell growth at least in part by enhancing RNA metabolism, including nucleotide synthesis, transcription, splicing, ribosome biogenesis, and translation[359].

Recently, a new mechanism emerges that links mTORC1 and the stimulation of the methylation of RNA at N6 of the adenosine base (N^6-methyladenosine, m^6A) that is one of the most common mRNA modifications that controls mRNA metabolism; increased mRNA methylation in turn promotes cell growth by enhancing mRNA degradation or translation (by reducing MXD2 expression and thereby enhancing MYC activity)[287, 288]. It will be interesting to investigate a possible correlation between m^6A RNA levels, mTORC1 activity and the growth of mutant *IDH2* AML cells and to determine whether mTORC1-mediated regulation of RNA methylation affects accumulation and/or translation of transcripts encoding effectors and/or regulators of cellular growth ; importantly, m^6A RNA levels are

regulated by the fat mass and obesity-associated protein (FTO), an RNA m^6A demethylase that is inhibited by excess of D-2HG in mutant *IDH* cells[317].

The anti-leukemic properties of BCAT1 inhibition are also associated to the promotion of partial differentiation. Both our *in vitro* (primary AML cells treated with gabapentin) and *in vivo* (PDX model) experiments have shown an increased expression of differentiation markers upon BCAT1 inhibition. Our data raised questions about the role of BCAA metabolism and BCAT1 activity in the bypass of differentiation block in AML cells but also in the induction of myeloid differentiation in physiological conditions. The mTORC1/S6K1/MYC pathway is a key check point in myeloid differentiation[362,363]; it has been shown that deletion of the mTORC1 component Raptor induces arrest of terminal differentiation ate the granulocyte-monocyte progenitor (GMP) state[364]; based on microarray gene expression analysis, leukemic populations are "GMP-like" cells[365]. Interestingly, the eukaryotic translation initiation factor eIF-4E (which activity is controlled by mTORC1) together with eI-F2a, control the expression of CEBPA[366]. In addition, m^6A causes reduced *CEBPA* transcript[317]. CEBPA instructs differentiation along the granulocytic lineage and is believed to be mediated by its ability to coordinate activation of a lineage-specific gene expression program with the withdrawal from the cell cycle (reviewed in [367]). CEBPA is required for AML development and several results point toward the importance of CEBPA for the leukemic activity of *IDH* mutations[225, 295]. It has been shown that CEBPA physically interacts with TET2[368] and that, in human AML, CEBPA interacts with the long splice isoform DNMT3A and inhibits its activity[369], suggesting that CEBPA may be an important part of epigenetic reprogramming in AML blasts. Both transcription and translation of *CEBPA* are regulated during myelopoiesis; in particular the *CEBPA* gene comprises a single exon with an internal translational start site, resulting in the full-length CEBPA (42 kDa; p42) and a shorter N-terminal–truncated isoform (30 kDa; p30) that lacks the first 117 amino acids including the transactivating domain 1 (TAD1) and exhibits lower transactivation potential. Interestingly, mTORC1 controls the translation of CEBPB isoforms through 4EBPs activity[370]. Whether in mutant *IDH2* blasts, mTORC1/CEBPA-driven molecular and cellular mechanisms participate to the dual mode of action of BCAT1 inhibition (i.e., growth arrest and induction of differentiation, as cell cycle exit is required for terminal differentiation) must be investigated.

Surprising is the observation that treatment of primary mutant *IDH2* AML cells with gabapentin led to a significant decrease of D-2HG. Ko and colleagues reported that inhibition of BCAT1with ERG240 in activated human macrophages induces a drastic reduction of the αKG pool but also 2-HG (mostly L-2HG)[353]. In contrast, in mutant *IDH1* glioma, inhibition of PI3K/mTOR signaling leads to a drop in 2-HG[354]. To understand the mechanism of action of the above processes, further experimental investigations are required. In the case of mutant *IDH2* AML cells, decrease in D-2HG level might contribute to the induction of differentiation through re-activation of histone- and DNA-modifying enzymes activity (including TET2), among others.

Altered BCAA metabolism has been involved in a broad spectrum of human cancers[371] as in drug resistance[340,372]. Interestingly, in human glioma *IDH1* mutation correlates with low levels of BCAT1 when compared to wild type controls[283]. In the brain, BCAA serve as nitrogen donors in the glutamine/glutamate cycle as well as sources for energetic and biosynthetic demands. Although low levels of *BCAT1* transcripts and proteins seemingly hallmark mutant *IDH1* gliomas compared with their wild type *IDH* counterparts[283], D-2HG affects the activity of BCAT1 leading to reduced growth and survival, and hyper-dependence on glutamate production[179]. It should be emphasized that *IDH1* mutations in gliomas are associated with a slower rate of disease progression and confer a significant survival advantage over wild type tumors. In the hematopoietic system, *BCAT1* aberrant overexpression and BCAA production are functionally required when *BCR-ABL*-driven CML evolves from a chronic phase to blast crisis, which is characterized by the rapid expansion of myeloid differentiation-arrested blasts[302]. Our results, together with the above-mentioned study, demonstrate that the overall flux of the BCAA metabolic pathway can be anabolic in AML, suggesting that targeting BCAT1 may be a way to benefit patients with CML or mutant *IDH2* AML. Leucine is involved in *MLL-AF9* AML development and progression in a xenografted model, as enhanced leukemic cell death induced by inhibition of the solute carrier family 1 member 5 (SLC1A5/ASCT2) responsible for taking up several amino acids is attributed to decreased leucine influx and inhibition of mTOR[373]. BCAT1 reactivation also cooperates with *NrasG12D* to enhance BCKA to BCAA in HSCP, during progression of MPN to AML in a mice model[277]. In human wild type *IDH* AML, *BCAT1* overexpression regulates BCAA catabolism in the critical LSC population[304],

again opening a path to develop therapeutic strategies to selectively eradicate LSC. In line, LSC harbor a high level of amino acids and are more sensitive to amino acid loss for OXPHOS and survival[374] compared with AML blasts, indicating a nutrient dependency not present in the non-LSC bulk. This LSC-specific metabolic property could explain the deep and durable responses observed in untreated patients with AML upon treatment with the selective inhibitor of BCL-2 venetoclax in combination with azacitidine[375 376], a situation that suppresses OXPHOS[376] but also decreases amino acids uptake and expression of amino acids transporters in LSC[374]. Likewise, our results show that BCAT1 serves as a regulatory checkpoint for leucine availability in mutant *IDH2* AML cells, suggesting that therapies that target BCAT1 as the leucine analogue ERG240[279] or that selectively deplete leucine, or even that inhibit aminopeptidase as tosedostat or bestatin which results in lowering the free amino acid levels (reviewed by [377]) could be useful approaches to target mutant *IDH2* AML, together with BCL-2 inhibition [178]. Our observations also highlight an underappreciated consequence of the presence of *IDH*2 mutation in AML bulk, in creating leucine dependency and mimicking an LSC-like metabolic activity for mutant *IDH2* AML cells. Importantly, *IDH2* mutations can be found in the pre-leukemic HSPC that are ancestral to the dominant AML clone and from which AML evolves [378,379,380,381]. Similar to LSC, these pre-malignant HSC are associated to induction chemotherapy survival and bone marrow persistence at remission [379]. Leucine dependency could also impacts the behavior of mutated *IDH* HSCP that undergo clonal expansion during ageing in healthy individuals who do not develop AML [382], or mutant *IDH* HSCP that could expand post-chemotherapy upon solid tumor treatment [150]. Whether similar metabolic dependency would manifest in these cellular subsets remains to be determined.

Identification of a metabolic flux that is amenable to therapeutic targeting in AML is an important observation stemming from this work. High *BCAT1* expression level predicts for poor response for patients with AML [302,304]. By analyzing AML data sets for whom follow-up information on survival was available (Beat AML [295]), we confirmed an elevated *BCAT1* RNA levels in AML samples associated with poor survival as reported[238,239], on a larger cohort (**Figure 46A**). In addition, overall survival result demonstrates a statistically significant survival benefit for the mutant *IDH* genotype (**Figure**

46B) that supports the main contribution of BCAT1 activity on the growth of mutant *IDH2* cells observed in our experiments.

Alternative molecular explanations are to be sought for wild type *IDH* AML since the activity of BCAT1 in these contexts is catabolic. It is possible that *BCAT1* expression varies according to AML mutational landscape and metabolic needs induced by the molecular context. Notably, core binding factor (CBF) AMLs show high expression of *BCAT1* compared to normal karyotype AMLs (**Figure 46E**). Beside their mutational landscape, CBF-AMLs are characterized by a specific transcriptomic signature [383,384]. *ZBTB7A* have been found to be recurrently mutated in CBF-AML and more specifically in RUNX1-RUNX1T1 AML[385,386]. ZBTB7A is a member of the POZ/BTB and Krüppel (POK) transcription repressor family that represses the transcription of critical glycolytic genes, including GLUT3, PFKP, and PKM [387]. ZBTB7A prevents RUNX1-RUNX1T1-dependent clonal expansion of HSC/LSC, suggesting that RUNX1-RUNX1T1 AMLs require specific metabolism environment to expand [388]. In mutated *NPM1* AML, which are usually associated with a good prognosis, we observed a trend toward a better outcome (median overall survival in "low" or "high BCAT1" groups is 28.9 or 14.5 months respectively), although it does not reach statistical significance (P=0.103) (**Figure 46C**). Altogether, these data suggest that combination of BCAT1 inhibitor with conventional induction chemotherapy might be of therapeutical interest. There is yet no specific clinical grade BCAT1 inhibitor.

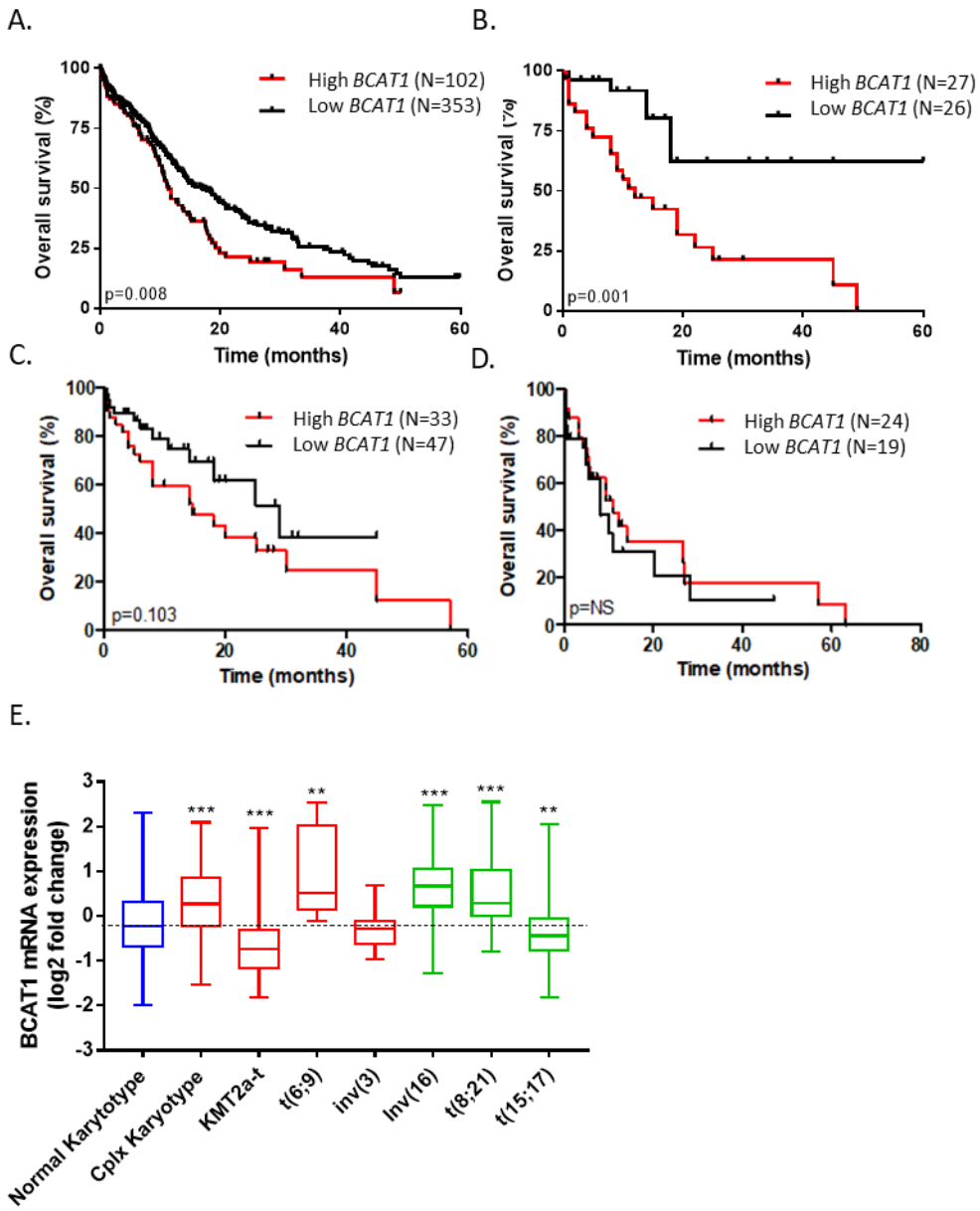

Figure 46: Influence of BCAT1 expression on overall survival (OS). A) Correlation of BCAT1 expression with OS of AML patients referenced in the BEAT AML database (Kaplan-Meier curves). Low or high BCAT1 expression indicates above or below the median expression respectively. B) Correlation of BCAT1 expression with OS of patients with AML harboring IDH (B) NPM1 (C) or TET2 (D) mutations. Statistical comparisons between groups are based on log-rank tests (P-values shown). E) BCAT1 expression in AML samples according to recurrent karyotype abnormalities (from GSE13159, GSE15434, GSE61804, GSE14468, and TCGA datasets; N=2077). P-values was assessed with two-sided unpaired t-test. All genotypes were compared to normal karyotype (blue box). Green boxes correspond to favorable cytogenetics. Red boxes correspond to unfavorable cytogenetics.

The question of how the level of BCAT1 expression affects the prognosis and response to chemotherapy in AML remains unresolved. In normal hematopoiesis, *BCAT1* as

PPM1K[276(p21)] and *BCKDHA* are upregulated in HSC and progressively downregulated throughout differentiation (**Figure 33**). In HSC, PPM1K promotes BCAA catabolism and maintains the glycolysis and quiescence of HSCs through the downregulation of CDC20-mediated ubiquitination of MEIS1 and p21. *BCAT1* expression might thus represent a consistent hallmark of HSC biology and/or stemness status. In AML, stemness features have been associated with lower response to conventional therapy, high risk of relapse and poor survival[335,389]. Ng and colleagues have identified a specific stemness transcriptomic signature based on 104 differentially expressed genes in human $CD34^+$ LSC[335]; whereas *BCAT1* was not part of these candidates genes, *MYCN* was one of the 17 most upregulated gene. Interestingly, MYC activates critical transporters, such as SLC7A5, SLC43A1, and SLC1A5, to promote essential amino acid transport and *BCAT1* is a downstream target of MYC (reviewed in [258]).

To further study a correlation between the prognosis value of *BCAT1* expression and the genotype, we have recently engaged analyses on datasets obtained from the ALFA0701 cohort. ALFA0701 is a prospective phase III study aiming to evaluate the efficacy of adding gemtuzumab ozogamycin, an anti-CD33 antibody coupled with calicheamicin, to classical intensive chemotherapy, in *de novo* AML adult patients. At 2 years, event free survival was estimated as 17.1% in the control group versus 40.8% in the gemtuzumab ozogamycin group (hazard ratio 0.58, P=0.0003) and the overall survival was 41.9% versus 53.2% respectively (HR=0.69, P=0.0368) [390]. RNA-sequencing was realized for most of the patients randomized in the study. As shown **Figure 46E**, *BCAT1* expression is heterogeneous among the different AML genotypes; yet we have not confirmed an overexpression of *BCAT1* in mutant *IDH* (N=40) compared to wild type *IDH AML* patients (**not shown**). However, expression of genes involved in the BCAA pathway distinguish patients with AML harboring *FLT3* abnormalities from patients with wild type *FLT3* AML (**Figure 47)**.

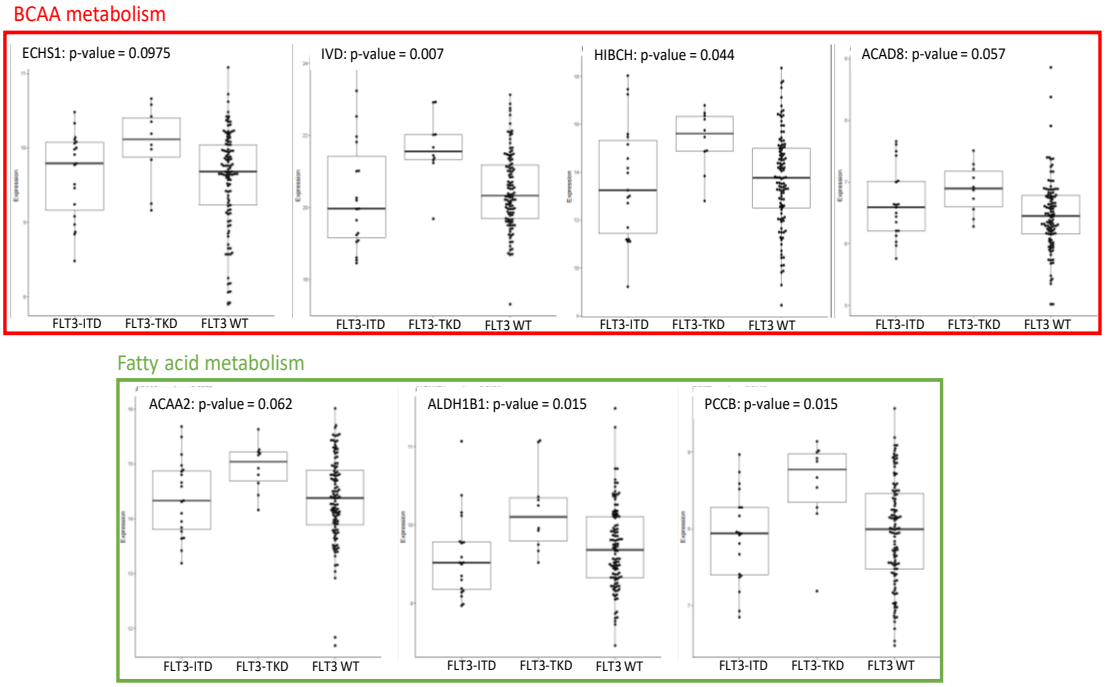

Figure 47: Expression of genes involved in the BCAA pathway and fatty acid metabolism in samples from AML patients with FLT3 genetic lesions (RMA normalized); data were obtained from the ALFA0701 trial dataset. enoyl coenzyme A hydratase, short chain, 1, mitochondrial (ECHS1); isovaleryl-CoA dehydrogenase (IVD); 3-hydroxyisobutyryl-CoA hydrolase (HIBCH); acyl-CoA dehydrogenase family member 8 (ACAD8); Acetyl-CoA acyltransferase 2 (ACAA2); aldehyde dehydrogenase 1 family member B1 (ALDH1B1); propionyl-CoA carboxylase subunit beta (PCCB).

8 CONCLUSION AND PERSPECTIVES

Our work brings new insights into the consequences of *IDH2* mutation on BCAA metabolism and identifies a metabolic vulnerability in mutated *IDH2* AML cells that could be of therapeutical interest. *BCAT1* expression is clearly regulated during hematopoietic differentiation; notably this expression is high in immature cells such as HSC and LSC, suggesting a major role of BCAT1 in the biology of those cells. These data raised questions about the role of BCAA metabolism and BCAT1 activity in myeloid commitment and differentiation in physiological conditions. BCAA metabolism contributes to hematopoietic system homeostasis; valine and leucine are required for HSCP maintenance in the bone marrow niche[391] and sustained uptake of leucine accompanies T cell differentiation [392]. Bcat1 is required to sustain the repopulation ability of HSCs in reconstitution experiment in mice, and BCAA catabolism maintains HSC quiescence [276]. Further studies targeting *BCAT1* in

myeloid diseases will improve our understanding of dietary amino acid and nutrient signal contribution to physiological and pathological myelopoiesis.

Moreover, as we observed that the BCAA-mTORC2 axis might be linked to BCKA levels, it would be of therapeutic interest to combine BCAT1 and mTORC2 inhibition in order to enhance antitumoral activity. This is even more reliable as mTORC2 has been associated with cell survival but also in metabolism sensing. Preliminary data on AML samples and obtained during my PhD support this hypothesis (**not shown**). It should also be of interest to use dual mTORC1/2 inhibitors, and/or dual PI3K/mTOR inhibitors that show greater activity in pre-clinical AML models [357]. Recently a specific inhibitor restricted to mTORC2 has been reported; Capivasertib, is an oral, potent, selective ATP-competitive pan-AKT kinase inhibitor, that has shown promising signs of antitumoral activity when combined with hormonotherapy in estrogen-receptor-positive (ER^+) mutated AKT breast cancer patients [393]. Indeed, the PI3K pathway is one of the most commonly activated signaling pathways in ER^+ breast cancer in an estimated 7% of ER+ breast cancers, pathway activation can occur through mutation in AKT that translate into constitutive AKT signaling pathway activation independently of PI3K [394] (PI3K/AKT inhibition is insufficient to induce apoptosis by itself but increase/reinduce chemosensitivity [395]). On a more fundamental point of view, it will be interesting to understand whether mTORC2 hyperactivity may influence the gene expression profiles observed in the leukemic cells. Indeed, Calejman and colleagues recently reported an important function of mTORC2 that is the control of the nuclear-cytoplasmic acetyl-CoA synthesis[396].

Our results unraveled a specific metabolic vulnerability in *IDH* mutant context. However, metabolism in AML remains largely unexplored. There is now growing evidences showing that leukemic bulk and LSC metabolism is highly dynamic and adaptive through therapeutic pressure. As this rapid metabolic adaptation may drive treatment resistance and relapse, understanding and targeting AML metabolism represent promising future direction in translational research.

9 REFERENCES

1. Hou S, Li Z, Zheng X, et al. Embryonic endothelial evolution towards first hematopoietic stem cells revealed by single-cell transcriptomic and functional analyses. *Cell Res*. 2020;30(5):376-392. doi:10.1038/s41422-020-0300-2

2. Dzierzak E, Bigas A. Blood Development: Hematopoietic Stem Cell Dependence and Independence. *Cell Stem Cell*. 2018;22(5):639-651. doi:10.1016/j.stem.2018.04.015

3. Bernitz JM, Kim HS, MacArthur B, Sieburg H, Moore K. Hematopoietic Stem Cells Count and Remember Self-Renewal Divisions. *Cell*. 2016;167(5):1296-1309.e10. doi:10.1016/j.cell.2016.10.022

4. Laurenti E, Göttgens B. From haematopoietic stem cells to complex differentiation landscapes. *Nature*. 2018;553(7689):418-426. doi:10.1038/nature25022

5. Velten L, Haas SF, Raffel S, et al. Human haematopoietic stem cell lineage commitment is a continuous process. *Nat Cell Biol*. 2017;19(4):271-281. doi:10.1038/ncb3493

6. Notta F, Zandi S, Takayama N, et al. Distinct routes of lineage development reshape the human blood hierarchy across ontogeny. *Science*. 2016;351(6269):aab2116. doi:10.1126/science.aab2116

7. Rodriguez-Fraticelli AE, Wolock SL, Weinreb CS, et al. Clonal analysis of lineage fate in native haematopoiesis. *Nature*. 2018;553(7687):212-216. doi:10.1038/nature25168

8. Hovorkova L, Zaliova M, Venn NC, et al. Monitoring of childhood ALL using BCR-ABL1 genomic breakpoints identifies a subgroup with CML-like biology. *Blood*. 2017;129(20):2771-2781. doi:10.1182/blood-2016-11-749978

9. Luo W, Hu H, Chang R, et al. Pyruvate kinase M2 is a PHD3-stimulated coactivator for hypoxia-inducible factor 1. *Cell*. 2011;145(5):732-744. doi:10.1016/j.cell.2011.03.054

10. Simsek T, Kocabas F, Zheng J, et al. The distinct metabolic profile of hematopoietic stem cells reflects their location in a hypoxic niche. *Cell Stem Cell*. 2010;7(3):380-390. doi:10.1016/j.stem.2010.07.011

11. Kocabas F, Zheng J, Thet S, et al. Meis1 regulates the metabolic phenotype and oxidant defense of hematopoietic stem cells. *Blood*. 2012;120(25):4963-4972. doi:10.1182/blood-2012-05-432260

12. Takubo K, Nagamatsu G, Kobayashi CI, et al. Regulation of glycolysis by Pdk functions as a metabolic checkpoint for cell cycle quiescence in hematopoietic stem cells. *Cell Stem Cell*. 2013;12(1):49-61. doi:10.1016/j.stem.2012.10.011

13. Hsieh WC, Sutter BM, Ruess H, Barnes SD, Malladi VS, Tu BP. Glucose starvation induces a switch in the histone acetylome for activation of gluconeogenic and fat metabolism genes. *Mol Cell*. 2022;82(1):60-74.e5. doi:10.1016/j.molcel.2021.12.015

14. Mews P, Donahue G, Drake AM, Luczak V, Abel T, Berger SL. Acetyl-CoA synthetase regulates histone acetylation and hippocampal memory. *Nature*. 2017;546(7658):381-386. doi:10.1038/nature22405

15. Li X, Yu W, Qian X, et al. Nucleus-Translocated ACSS2 Promotes Gene Transcription for Lysosomal Biogenesis and Autophagy. *Mol Cell*. 2017;66(5):684-697.e9. doi:10.1016/j.molcel.2017.04.026

16. Chandel NS. Evolution of Mitochondria as Signaling Organelles. *Cell Metab*. 2015;22(2):204-206. doi:10.1016/j.cmet.2015.05.013

17. Martínez-Reyes I, Chandel NS. Mitochondrial TCA cycle metabolites control physiology and disease. *Nat Commun*. 2020;11(1):102. doi:10.1038/s41467-019-13668-3

18. Xiao M, Yang H, Xu W, et al. Inhibition of α-KG-dependent histone and DNA demethylases by fumarate and succinate that are accumulated in mutations of FH and SDH tumor suppressors. *Genes Dev*. 2012;26(12):1326-1338. doi:10.1101/gad.191056.112

19. Halbrook CJ, Nwosu ZC, Lyssiotis CA. Fine-Tuning Mitochondrial Dysfunction and Reductive Carboxylation. *Trends Endocrinol Metab TEM*. 2018;29(9):599-602. doi:10.1016/j.tem.2018.04.002

20. Abla H, Sollazzo M, Gasparre G, Iommarini L, Porcelli AM. The multifaceted contribution of α-ketoglutarate to tumor progression: An opportunity to exploit? *Semin Cell Dev Biol*. 2020;98:26-33. doi:10.1016/j.semcdb.2019.05.031

21. Yu WM, Liu X, Shen J, et al. Metabolic Regulation by the Mitochondrial Phosphatase PTPMT1 Is Required for Hematopoietic Stem Cell Differentiation. *Cell Stem Cell*. 2013;12(1):62-74. doi:10.1016/j.stem.2012.11.022

22. Carey BW, Finley LWS, Cross JR, Allis CD, Thompson CB. Intracellular α-ketoglutarate maintains the pluripotency of embryonic stem cells. *Nature*. 2015;518(7539):413-416. doi:10.1038/nature13981

23. TeSlaa T, Chaikovsky AC, Lipchina I, et al. α-Ketoglutarate Accelerates the Initial Differentiation of Primed Human Pluripotent Stem Cells. *Cell Metab*. 2016;24(3):485-493. doi:10.1016/j.cmet.2016.07.002

24. Schvartzman JM, Thompson CB, Finley LWS. Metabolic regulation of chromatin modifications and gene expression. *J Cell Biol*. 2018;217(7):2247-2259. doi:10.1083/jcb.201803061

25. Jin G, Xu C, Zhang X, et al. Atad3a suppresses Pink1-dependent mitophagy to maintain homeostasis of hematopoietic progenitor cells. *Nat Immunol*.

2018;19(1):29-40. doi:10.1038/s41590-017-0002-1

26. Ananieva EA, Wilkinson AC. Branched-chain amino acid metabolism in cancer. *Curr Opin Clin Nutr Metab Care*. 2018;21(1):64-70. doi:10.1097/MCO.0000000000000430

27. Ito K, Carracedo A, Weiss D, et al. A PML–PPAR-δ pathway for fatty acid oxidation regulates hematopoietic stem cell maintenance. *Nat Med*. 2012;18(9):1350-1358. doi:10.1038/nm.2882

28. Ito K, Ito K. Hematopoietic stem cell fate through metabolic control. *Exp Hematol*. 2018;64:1-11. doi:10.1016/j.exphem.2018.05.005

29. Gan B, Hu J, Jiang S, et al. Lkb1 regulates quiescence and metabolic homeostasis of haematopoietic stem cells. *Nature*. 2010;468(7324):701-704. doi:10.1038/nature09595

30. Wu F, Chen Z, Liu J, Hou Y. The Akt–mTOR network at the interface of hematopoietic stem cell homeostasis. *Exp Hematol*. 2021;103:15-23. doi:10.1016/j.exphem.2021.08.009

31. Menon V, Ghaffari S. Transcription factors FOXO in the regulation of homeostatic hematopoiesis. *Curr Opin Hematol*. 2018;25(4):290-298. doi:10.1097/MOH.0000000000000441

32. Lee JY, Nakada D, Yilmaz OH, et al. mTOR Activation Induces Tumor Suppressors that Inhibit Leukemogenesis and Deplete Hematopoietic Stem Cells after Pten Deletion. *Cell Stem Cell*. 2010;7(5):593-605. doi:10.1016/j.stem.2010.09.015

33. Morrison SJ, Spradling AC. Stem cells and niches: mechanisms that promote stem cell maintenance throughout life. *Cell*. 2008;132(4):598-611. doi:10.1016/j.cell.2008.01.038

34. Wolfson RL, Chantranupong L, Saxton RA, et al. Sestrin2 is a leucine sensor for the mTORC1 pathway. *Science*. 2016;351(6268):43-48. doi:10.1126/science.aab2674

35. Saxton RA, Sabatini DM. mTOR Signaling in Growth, Metabolism, and Disease. *Cell*. 2017;168(6):960-976. doi:10.1016/j.cell.2017.02.004

36. Zhang T, Zhou Q, Ogmundsdottir MH, et al. Mitf is a master regulator of the v-ATPase, forming a control module for cellular homeostasis with v-ATPase and TORC1. *J Cell Sci*. 2015;128(15):2938-2950. doi:10.1242/jcs.173807

37. Chantranupong L, Scaria SM, Saxton RA, et al. The CASTOR Proteins Are Arginine Sensors for the mTORC1 Pathway. *Cell*. 2016;165(1):153-164. doi:10.1016/j.cell.2016.02.035

38. Han JM, Jeong SJ, Park MC, et al. Leucyl-tRNA synthetase is an intracellular leucine sensor for the mTORC1-signaling pathway. *Cell*. 2012;149(2):410-424. doi:10.1016/j.cell.2012.02.044

39. Liu L, Michowski W, Inuzuka H, et al. G1 cyclins link proliferation, pluripotency and differentiation of embryonic stem cells. *Nat Cell Biol*. 2017;19(3):177-188. doi:10.1038/ncb3474

40. Cupp JR, McAlister-Henn L. Cloning and characterization of the gene encoding the IDH1 subunit of NAD(+)-dependent isocitrate dehydrogenase from Saccharomyces cerevisiae. *J Biol Chem*. 1992;267(23):16417-16423. doi:10.1016/S0021-9258(18)42019-4

41. Panisko EA, McAlister-Henn L. Subunit interactions of yeast NAD+-specific isocitrate dehydrogenase. *J Biol Chem*. 2001;276(2):1204-1210. doi:10.1074/jbc.M005056200

42. Lin AP, McAlister-Henn L. Homologous Binding Sites in Yeast Isocitrate Dehydrogenase for Cofactor (NAD+) and Allosteric Activator (AMP) *. *J Biol Chem*. 2003;278(15):12864-12872. doi:10.1074/jbc.M300154200

43. Ma T, Peng Y, Huang W, Liu Y, Ding J. The β and γ subunits play distinct functional roles in the α2βγ heterotetramer of human NAD-dependent isocitrate dehydrogenase. *Sci Rep*. 2017;7(1):41882. doi:10.1038/srep41882

44. Xu Y, Liu L, Nakamura A, Someya S, Miyakawa T, Tanokura M. Studies on the regulatory mechanism of isocitrate dehydrogenase 2 using acetylation mimics. *Sci Rep*. 2017;7(1):9785. doi:10.1038/s41598-017-10337-7

45. Bruce-Brand C, Govender D. Gene of the month: IDH1. *J Clin Pathol*. 2020;73(10):611-615. doi:10.1136/jclinpath-2020-206813

46. Ramachandran N, Colman RF. Chemical characterization of distinct subunits of pig heart DPN-specific isocitrate dehydrogenase. *J Biol Chem*. 1980;255(18):8859-8864. doi:10.1016/S0021-9258(18)43581-8

47. Bzymek KP, Colman RF. Role of alpha-Asp181, beta-Asp192, and gamma-Asp190 in the distinctive subunits of human NAD-specific isocitrate dehydrogenase. *Biochemistry*. 2007;46(18):5391-5397. doi:10.1021/bi700061t

48. Gabriel JL, Zervos PR, Plaut GWE. Activity of purified NAD-specific isocitrate dehydrogenase at modulator and substrate concentrations approximating conditions in mitochondria. *Metabolism*. 1986;35(7):661-667. doi:10.1016/0026-0495(86)90175-7

49. Barnes LD, Kuehn GD, Atkinson DE. Yeast diphosphopyridine nucleotide specific isocitrate dehydrogenase. Purification and some properties. *Biochemistry*. 1971;10(21):3939-3944. doi:10.1021/bi00797a022

50. Fendt SM, Bell EL, Keibler MA, et al. Reductive glutamine metabolism is a function of the α-ketoglutarate to citrate ratio in cells. *Nat Commun*. 2013;4(1):2236. doi:10.1038/ncomms3236

51. Ronnebaum SM, Ilkayeva O, Burgess SC, et al. A pyruvate cycling pathway

involving cytosolic NADP-dependent isocitrate dehydrogenase regulates glucose-stimulated insulin secretion. *J Biol Chem*. 2006;281(41):30593-30602. doi:10.1074/jbc.M511908200

52. Joseph JW, Jensen MV, Ilkayeva O, et al. The Mitochondrial Citrate/Isocitrate Carrier Plays a Regulatory Role in Glucose-stimulated Insulin Secretion *. *J Biol Chem*. 2006;281(47):35624-35632. doi:10.1074/jbc.M602606200

53. Koh HJ, Lee SM, Son BG, et al. Cytosolic NADP+-dependent Isocitrate Dehydrogenase Plays a Key Role in Lipid Metabolism *. *J Biol Chem*. 2004;279(38):39968-39974. doi:10.1074/jbc.M402260200

54. Alzial G, Renoult O, Paris F, Gratas C, Clavreul A, Pecqueur C. Wild-type isocitrate dehydrogenase under the spotlight in glioblastoma. *Oncogene*. 2022;41(5):613-621. doi:10.1038/s41388-021-02056-1

55. Mullen AR, Wheaton WW, Jin ES, et al. Reductive carboxylation supports growth in tumour cells with defective mitochondria. *Nature*. 2012;481(7381):385-388. doi:10.1038/nature10642

56. Gaude E, Schmidt C, Gammage PA, et al. NADH Shuttling Couples Cytosolic Reductive Carboxylation of Glutamine with Glycolysis in Cells with Mitochondrial Dysfunction. *Mol Cell*. 2018;69(4):581-593.e7. doi:10.1016/j.molcel.2018.01.034

57. Mailloux RJ, Bériault R, Lemire J, et al. The Tricarboxylic Acid Cycle, an Ancient Metabolic Network with a Novel Twist. *PLOS ONE*. 2007;2(8):e690. doi:10.1371/journal.pone.0000690

58. Lee SM, Koh HJ, Park DC, Song BJ, Huh TL, Park JW. Cytosolic NADP(+)-dependent isocitrate dehydrogenase status modulates oxidative damage to cells. *Free Radic Biol Med*. 2002;32(11):1185-1196. doi:10.1016/s0891-5849(02)00815-8

59. Yang JH, Yang ES, Park JW. Inactivation of NADP+-dependent isocitrate dehydrogenase by lipid peroxidation products. *Free Radic Res*. 2004;38(3):241-249. doi:10.1080/10715760310001657712

60. Lee SM, Huh TL, Park JW. Inactivation of NADP(+)-dependent isocitrate dehydrogenase by reactive oxygen species. *Biochimie*. 2001;83(11-12):1057-1065. doi:10.1016/s0300-9084(01)01351-7

61. Shin SW, Oh CJ, Kil IS, Park JW. Glutathionylation regulates cytosolic NADP+-dependent isocitrate dehydrogenase activity. *Free Radic Res*. 2009;43(4):409-416. doi:10.1080/10715760902801525

62. Kil IS, Lee JH, Shin AH, Park JW. Glycation-induced inactivation of NADP(+)-dependent isocitrate dehydrogenase: implications for diabetes and aging. *Free Radic Biol Med*. 2004;37(11):1765-1778. doi:10.1016/j.freeradbiomed.2004.08.025

63. Bleeker FE, Atai NA, Lamba S, et al. The prognostic IDH1(R132) mutation is associated with reduced NADP+-dependent IDH activity in glioblastoma. *Acta*

Neuropathol (Berl). 2010;119(4):487-494. doi:10.1007/s00401-010-0645-6

64. Calvert AE, Chalastanis A, Wu Y, et al. Cancer-Associated IDH1 Promotes Growth and Resistance to Targeted Therapies in the Absence of Mutation. *Cell Rep*. 2017;19(9):1858-1873. doi:10.1016/j.celrep.2017.05.014

65. Shechter I, Dai P, Huo L, Guan G. IDH1 gene transcription is sterol regulated and activated by SREBP-1a and SREBP-2 in human hepatoma HepG2 cells: evidence that IDH1 may regulate lipogenesis in hepatic cells. *J Lipid Res*. 2003;44(11):2169-2180. doi:10.1194/jlr.M300285-JLR200

66. Gonthier K, Poluri RTK, Weidmann C, Tadros M, Audet-Walsh É. Reprogramming of Isocitrate Dehydrogenases Expression and Activity by the Androgen Receptor in Prostate Cancer. *Mol Cancer Res MCR*. 2019;17(8):1699-1709. doi:10.1158/1541-7786.MCR-19-0020

67. Garnak M, Reeves HC. Phosphorylation of Isocitrate Dehydrogenase of Escherichia coli. *Science*. Published online March 16, 1979. doi:10.1126/science.34215

68. Dean AM, Daniel E. Koshland J. Electrostatic and Steric Contributions to Regulation at the Active Site of Isocitrate Dehydrogenase. *Science*. Published online August 31, 1990. doi:10.1126/science.2204110

69. Xu X, Zhao J, Xu Z, et al. Structures of human cytosolic NADP-dependent isocitrate dehydrogenase reveal a novel self-regulatory mechanism of activity. *J Biol Chem*. 2004;279(32):33946-33957. doi:10.1074/jbc.M404298200

70. Chen D, Xia S, Wang M, et al. Mutant and Wild-Type Isocitrate Dehydrogenase 1 Share Enhancing Mechanisms Involving Distinct Tyrosine Kinase Cascades in Cancer. *Cancer Discov*. 2019;9(6):756-777. doi:10.1158/2159-8290.CD-18-1040

71. Zou X, Zhu Y, Park SH, et al. SIRT3-Mediated Dimerization of IDH2 Directs Cancer Cell Metabolism and Tumor Growth. *Cancer Res*. 2017;77(15):3990-3999. doi:10.1158/0008-5472.CAN-16-2393

72. Someya S, Yu W, Hallows WC, et al. Sirt3 mediates reduction of oxidative damage and prevention of age-related hearing loss under caloric restriction. *Cell*. 2010;143(5):802-812. doi:10.1016/j.cell.2010.10.002

73. Zhou L, Wang F, Sun R, et al. SIRT5 promotes IDH2 desuccinylation and G6PD deglutarylation to enhance cellular antioxidant defense. *EMBO Rep*. 2016;17(6):811-822. doi:10.15252/embr.201541643

74. Kil IS, Park JW. Regulation of Mitochondrial NADP+-dependent Isocitrate Dehydrogenase Activity by Glutathionylation. *J Biol Chem*. 2005;280(11):10846-10854. doi:10.1074/jbc.M411306200

75. Horton S, Huntly BJP. Kinase Networks Regulate Metabolism: I'D(H1) Never Have Guessed! *Cancer Discov*. 2019;9(6):699-701. doi:10.1158/2159-8290.CD-19-0373

76. Ho TT, Warr MR, Adelman ER, et al. Autophagy maintains the metabolism and function of young and old stem cells. *Nature*. 2017;543(7644):205-210. doi:10.1038/nature21388

77. Tran KA, Dillingham CM, Sridharan R. The role of α-ketoglutarate-dependent proteins in pluripotency acquisition and maintenance. *J Biol Chem*. 2019;294(14):5408-5419. doi:10.1074/jbc.TM118.000831

78. Lio CWJ, Rao A. TET Enzymes and 5hmC in Adaptive and Innate Immune Systems. *Front Immunol*. 2019;10:210. doi:10.3389/fimmu.2019.00210

79. Shi X, He BL, Ma ACH, et al. Functions of idh1 and its mutation in the regulation of developmental hematopoiesis in zebrafish. *Blood*. 2015;125(19):2974-2984. doi:10.1182/blood-2014-09-601187

80. INVS 2018. Estimations nationales de l'incidence et de la mortalité par cancer en France métropolitaine entre 1990 et 2018 - Hémopathies malignes : Étude à partir des registres des cancers du réseau Francim. Accessed February 6, 2022. https://www.santepubliquefrance.fr/import/estimations-nationales-de-l-incidence-et-de-la-mortalite-par-cancer-en-france-metropolitaine-entre-1990-et-2018-hemopathies-malignes-etude-a-pa

81. Mardis ER, Ding L, Dooling DJ, et al. Recurring mutations found by sequencing an acute myeloid leukemia genome. *N Engl J Med*. 2009;361(11):1058-1066. doi:10.1056/NEJMoa0903840

82. Papaemmanuil E, Gerstung M, Bullinger L, et al. Genomic Classification and Prognosis in Acute Myeloid Leukemia. *N Engl J Med*. 2016;374(23):2209-2221. doi:10.1056/NEJMoa1516192

83. Khwaja A, Bjorkholm M, Gale RE, et al. Acute myeloid leukaemia. *Nat Rev Dis Primer*. 2016;2:16010. doi:10.1038/nrdp.2016.10

84. Döhner H, Estey E, Grimwade D, et al. Diagnosis and management of AML in adults: 2017 ELN recommendations from an international expert panel. *Blood*. 2017;129(4):424-447. doi:10.1182/blood-2016-08-733196

85. Nagel G, Weber D, Fromm E, et al. Epidemiological, genetic, and clinical characterization by age of newly diagnosed acute myeloid leukemia based on an academic population-based registry study (AMLSG BiO). *Ann Hematol*. 2017;96(12):1993-2003. doi:10.1007/s00277-017-3150-3

86. Gardin C, Pautas C, Fournier E, et al. Added prognostic value of secondary AML-like gene mutations in ELN intermediate-risk older AML: ALFA-1200 study results. *Blood Adv*. 2020;4(9):1942-1949. doi:10.1182/bloodadvances.2019001349

87. Valk PJM, Verhaak RGW, Beijen MA, et al. Prognostically Useful Gene-Expression Profiles in Acute Myeloid Leukemia. *N Engl J Med*. 2004;350(16):1617-1628. doi:10.1056/NEJMoa040465

88. Burd A, Levine RL, Ruppert AS, et al. Precision medicine treatment in acute myeloid leukemia using prospective genomic profiling: feasibility and preliminary efficacy of the Beat AML Master Trial. *Nat Med*. 2020;26(12):1852-1858. doi:10.1038/s41591-020-1089-8

89. Pei S, Minhajuddin M, Adane B, et al. AMPK/FIS1-Mediated Mitophagy Is Required for Self-Renewal of Human AML Stem Cells. *Cell Stem Cell*. 2018;23(1):86-100.e6. doi:10.1016/j.stem.2018.05.021

90. Moujalled DM, Pomilio G, Ghiurau C, et al. Combining BH3-mimetics to target both BCL-2 and MCL1 has potent activity in pre-clinical models of acute myeloid leukemia. *Leukemia*. 2019;33(4):905-917. doi:10.1038/s41375-018-0261-3

91. Höckendorf U, Yabal M, Herold T, et al. RIPK3 Restricts Myeloid Leukemogenesis by Promoting Cell Death and Differentiation of Leukemia Initiating Cells. *Cancer Cell*. 2016;30(1):75-91. doi:10.1016/j.ccell.2016.06.002

92. Panina SB, Pei J, Kirienko NV. Mitochondrial metabolism as a target for acute myeloid leukemia treatment. *Cancer Metab*. 2021;9(1):17. doi:10.1186/s40170-021-00253-w

93. van Galen P, Hovestadt V, Wadsworth Ii MH, et al. Single-Cell RNA-Seq Reveals AML Hierarchies Relevant to Disease Progression and Immunity. *Cell*. 2019;176(6):1265-1281.e24. doi:10.1016/j.cell.2019.01.031

94. Farge T, Saland E, de Toni F, et al. Chemotherapy-Resistant Human Acute Myeloid Leukemia Cells Are Not Enriched for Leukemic Stem Cells but Require Oxidative Metabolism. *Cancer Discov*. 2017;7(7):716-735. doi:10.1158/2159-8290.CD-16-0441

95. Ishikawa F, Yoshida S, Saito Y, et al. Chemotherapy-resistant human AML stem cells home to and engraft within the bone-marrow endosteal region. *Nat Biotechnol*. 2007;25(11):1315-1321. doi:10.1038/nbt1350

96. Saito Y, Chapple RH, Lin A, Kitano A, Nakada D. AMPK Protects Leukemia-Initiating Cells in Myeloid Leukemias from Metabolic Stress in the Bone Marrow. *Cell Stem Cell*. 2015;17(5):585-596. doi:10.1016/j.stem.2015.08.019

97. Lagadinou ED, Sach A, Callahan K, et al. BCL-2 inhibition targets oxidative phosphorylation and selectively eradicates quiescent human leukemia stem cells. *Cell Stem Cell*. 2013;12(3):329-341. doi:10.1016/j.stem.2012.12.013

98. Zink F, Stacey SN, Norddahl GL, et al. Clonal hematopoiesis, with and without candidate driver mutations, is common in the elderly. *Blood*. 2017;130(6):742-752. doi:10.1182/blood-2017-02-769869

99. Feusier JE, Arunachalam S, Tashi T, et al. Large-scale Identification of Clonal Hematopoiesis and Mutations Recurrent in Blood Cancers. *Blood Cancer Discov*. 2021;2(3):226-237. doi:10.1158/2643-3230.BCD-20-0094

100. Yamashita M, Dellorusso PV, Olson OC, Passegué E. Dysregulated haematopoietic stem cell behaviour in myeloid leukaemogenesis. *Nat Rev Cancer*. 2020;20(7):365-382. doi:10.1038/s41568-020-0260-3

101. Shlush LI, Mitchell A, Heisler L, et al. Tracing the origins of relapse in acute myeloid leukaemia to stem cells. *Nature*. 2017;547(7661):104-108. doi:10.1038/nature22993

102. Jan M, Snyder TM, Corces-Zimmerman MR, et al. Clonal evolution of preleukemic hematopoietic stem cells precedes human acute myeloid leukemia. *Sci Transl Med*. 2012;4(149):149ra118. doi:10.1126/scitranslmed.3004315

103. Takahashi K, Wang F, Kantarjian H, et al. Preleukaemic clonal haemopoiesis and risk of therapy-related myeloid neoplasms: a case-control study. *Lancet Oncol*. 2017;18(1):100-111. doi:10.1016/S1470-2045(16)30626-X

104. Bolton KL, Gillis NK, Coombs CC, et al. Managing Clonal Hematopoiesis in Patients With Solid Tumors. *J Clin Oncol Off J Am Soc Clin Oncol*. 2019;37(1):7-11. doi:10.1200/JCO.18.00331

105. Wong TN, Ramsingh G, Young AL, et al. Role of TP53 mutations in the origin and evolution of therapy-related acute myeloid leukaemia. *Nature*. 2015;518(7540):552-555. doi:10.1038/nature13968

106. Wong TN, Miller CA, Jotte MRM, et al. Cellular stressors contribute to the expansion of hematopoietic clones of varying leukemic potential. *Nat Commun*. 2018;9(1):455. doi:10.1038/s41467-018-02858-0

107. Lindsley RC, Saber W, Mar BG, et al. Prognostic Mutations in Myelodysplastic Syndrome after Stem-Cell Transplantation. *N Engl J Med*. 2017;376(6):536-547. doi:10.1056/NEJMoa1611604

108. Genovese G, Kähler AK, Handsaker RE, et al. Clonal hematopoiesis and blood-cancer risk inferred from blood DNA sequence. *N Engl J Med*. 2014;371(26):2477-2487. doi:10.1056/NEJMoa1409405

109. Jaiswal S, Fontanillas P, Flannick J, et al. Age-related clonal hematopoiesis associated with adverse outcomes. *N Engl J Med*. 2014;371(26):2488-2498. doi:10.1056/NEJMoa1408617

110. Silver AJ, Jaiswal S. Clonal hematopoiesis: Pre-cancer PLUS. *Adv Cancer Res*. 2019;141:85-128. doi:10.1016/bs.acr.2018.12.003

111. Gao T, Ptashkin R, Bolton KL, et al. Interplay between chromosomal alterations and gene mutations shapes the evolutionary trajectory of clonal hematopoiesis. *Nat Commun*. 2021;12(1):338. doi:10.1038/s41467-020-20565-7

112. Niroula A, Sekar A, Murakami MA, et al. Distinction of lymphoid and myeloid clonal hematopoiesis. *Nat Med*. 2021;27(11):1921-1927. doi:10.1038/s41591-021-01521-4

113. Stauber J, Greally JM, Steidl U. Preleukemic and leukemic evolution at the stem cell level. *Blood*. 2021;137(8):1013-1018. doi:10.1182/blood.2019004397

114. Abelson S, Collord G, Ng SWK, et al. Prediction of acute myeloid leukaemia risk in healthy individuals. *Nature*. 2018;559(7714):400-404. doi:10.1038/s41586-018-0317-6

115. Desai P, Mencia-Trinchant N, Savenkov O, et al. Somatic mutations precede acute myeloid leukemia years before diagnosis. *Nat Med*. 2018;24(7):1015-1023. doi:10.1038/s41591-018-0081-z

116. Jongen-Lavrencic M, Grob T, Hanekamp D, et al. Molecular Minimal Residual Disease in Acute Myeloid Leukemia. *N Engl J Med*. 2018;378(13):1189-1199. doi:10.1056/NEJMoa1716863

117. Watson CJ, Papula AL, Poon GYP, et al. The evolutionary dynamics and fitness landscape of clonal hematopoiesis. *Science*. 2020;367(6485):1449-1454. doi:10.1126/science.aay9333

118. Single-cell multi-omics of human clonal hematopoiesis reveals that DNMT3A R882 mutations perturb early progenitor states through selective hypomethylation | bioRxiv. Accessed February 20, 2022. https://www.biorxiv.org/content/10.1101/2022.01.14.476225v1

119. Young AL, Challen GA, Birmann BM, Druley TE. Clonal haematopoiesis harbouring AML-associated mutations is ubiquitous in healthy adults. *Nat Commun*. 2016;7:12484. doi:10.1038/ncomms12484

120. Abegunde SO, Buckstein R, Wells RA, Rauh MJ. An inflammatory environment containing TNFα favors Tet2-mutant clonal hematopoiesis. *Exp Hematol*. 2018;59:60-65. doi:10.1016/j.exphem.2017.11.002

121. Hsu JI, Dayaram T, Tovy A, et al. PPM1D Mutations Drive Clonal Hematopoiesis in Response to Cytotoxic Chemotherapy. *Cell Stem Cell*. 2018;23(5):700-713.e6. doi:10.1016/j.stem.2018.10.004

122. Hérault A, Binnewies M, Leong S, et al. Myeloid progenitor cluster formation drives emergency and leukaemic myelopoiesis. *Nature*. 2017;544(7648):53-58. doi:10.1038/nature21693

123. Meisel M, Hinterleitner R, Pacis A, et al. Microbial signals drive pre-leukaemic myeloproliferation in a Tet2-deficient host. *Nature*. 2018;557(7706):580-584. doi:10.1038/s41586-018-0125-z

124. Bolton KL, Ptashkin RN, Gao T, et al. Cancer therapy shapes the fitness landscape of clonal hematopoiesis. *Nat Genet*. 2020;52(11):1219-1226. doi:10.1038/s41588-020-00710-0

125. Coombs CC, Zehir A, Devlin SM, et al. Therapy-Related Clonal Hematopoiesis in Patients with Non-hematologic Cancers Is Common and Associated with Adverse

Clinical Outcomes. *Cell Stem Cell*. 2017;21(3):374-382.e4. doi:10.1016/j.stem.2017.07.010

126. Gurnari C, Fabiani E, Falconi G, et al. From Clonal Hematopoiesis to Therapy-Related Myeloid Neoplasms: The Silent Way of Cancer Progression. *Biology*. 2021;10(2):128. doi:10.3390/biology10020128

127. Jaiswal S, Natarajan P, Silver AJ, et al. Clonal Hematopoiesis and Risk of Atherosclerotic Cardiovascular Disease. *N Engl J Med*. 2017;377(2):111-121. doi:10.1056/NEJMoa1701719

128. Sano S, Oshima K, Wang Y, Katanasaka Y, Sano M, Walsh K. CRISPR-Mediated Gene Editing to Assess the Roles of Tet2 and Dnmt3a in Clonal Hematopoiesis and Cardiovascular Disease. *Circ Res*. 2018;123(3):335-341. doi:10.1161/CIRCRESAHA.118.313225

129. Fuster JJ, MacLauchlan S, Zuriaga MA, et al. Clonal hematopoiesis associated with TET2 deficiency accelerates atherosclerosis development in mice. *Science*. 2017;355(6327):842-847. doi:10.1126/science.aag1381

130. Heyde A, Rohde D, McAlpine CS, et al. Increased stem cell proliferation in atherosclerosis accelerates clonal hematopoiesis. *Cell*. 2021;184(5):1348-1361.e22. doi:10.1016/j.cell.2021.01.049

131. Zhu YP, Hedrick CC, Gaddis DE. Hematopoietic stem cells gone rogue. *Science*. 2017;355(6327):798-799. doi:10.1126/science.aam7939

132. Lusis AJ. A vicious cycle in atherosclerosis. *Cell*. 2021;184(5):1139-1141. doi:10.1016/j.cell.2021.02.005

133. Ding L, Ley TJ, Larson DE, et al. Clonal evolution in relapsed acute myeloid leukaemia revealed by whole-genome sequencing. *Nature*. 2012;481(7382):506-510. doi:10.1038/nature10738

134. Silver AJ, Bick AG, Savona MR. Germline risk of clonal haematopoiesis. *Nat Rev Genet*. 2021;22(9):603-617. doi:10.1038/s41576-021-00356-6

135. Bick AG, Weinstock JS, Nandakumar SK, et al. Inherited causes of clonal haematopoiesis in 97,691 whole genomes. *Nature*. 2020;586(7831):763-768. doi:10.1038/s41586-020-2819-2

136. Méndez-Ferrer S, Bonnet D, Steensma DP, et al. Bone marrow niches in haematological malignancies. *Nat Rev Cancer*. 2020;20(5):285-298. doi:10.1038/s41568-020-0245-2

137. Caiado F, Pietras EM, Manz MG. Inflammation as a regulator of hematopoietic stem cell function in disease, aging, and clonal selection. *J Exp Med*. 2021;218(7):e20201541. doi:10.1084/jem.20201541

138. Hemmati S, Haque T, Gritsman K. Inflammatory Signaling Pathways in Preleukemic

and Leukemic Stem Cells. *Front Oncol*. 2017;7:265. doi:10.3389/fonc.2017.00265

139. Nam AS, Chaligne R, Landau DA. Integrating genetic and non-genetic determinants of cancer evolution by single-cell multi-omics. *Nat Rev Genet*. 2021;22(1):3-18. doi:10.1038/s41576-020-0265-5

140. Fennell KA, Vassiliadis D, Lam EYN, et al. Non-genetic determinants of malignant clonal fitness at single-cell resolution. *Nature*. 2022;601(7891):125-131. doi:10.1038/s41586-021-04206-7

141. Lindsley RC, Mar BG, Mazzola E, et al. Acute myeloid leukemia ontogeny is defined by distinct somatic mutations. *Blood*. 2015;125(9):1367-1376. doi:10.1182/blood-2014-11-610543

142. Gerstung M, Papaemmanuil E, Martincorena I, et al. Precision oncology for acute myeloid leukemia using a knowledge bank approach. *Nat Genet*. 2017;49(3):332-340. doi:10.1038/ng.3756

143. Patel SA, Litzow MR, Cerny J. Targeted and cytotoxic therapies as maintenance treatment for non-transplant eligible patients with acute myeloid leukemia. *Blood Rev*. 2021;50:100863. doi:10.1016/j.blre.2021.100863

144. Steensma DP, Bolton KL. What to tell your patient with clonal hematopoiesis and why: insights from 2 specialized clinics. *Blood*. 2020;136(14):1623-1631. doi:10.1182/blood.2019004291

145. Tommasini-Ghelfi S, Murnan K, Kouri FM, Mahajan AS, May JL, Stegh AH. Cancer-associated mutation and beyond: The emerging biology of isocitrate dehydrogenases in human disease. *Sci Adv*. 2019;5(5):eaaw4543. doi:10.1126/sciadv.aaw4543

146. Waitkus MS, Diplas BH, Yan H. Biological Role and Therapeutic Potential of IDH Mutations in Cancer. *Cancer Cell*. 2018;34(2):186-195. doi:10.1016/j.ccell.2018.04.011

147. Dang L, Yen K, Attar EC. IDH mutations in cancer and progress toward development of targeted therapeutics. *Ann Oncol Off J Eur Soc Med Oncol*. 2016;27(4):599-608. doi:10.1093/annonc/mdw013

148. Dang L, Su SSM. Isocitrate Dehydrogenase Mutation and (R)-2-Hydroxyglutarate: From Basic Discovery to Therapeutics Development. *Annu Rev Biochem*. 2017;86:305-331. doi:10.1146/annurev-biochem-061516-044732

149. Young AL, Tong RS, Birmann BM, Druley TE. Clonal hematopoiesis and risk of acute myeloid leukemia. *Haematologica*. 2019;104(12):2410-2417. doi:10.3324/haematol.2018.215269

150. Wiseman DH, Williams EL, Wilks DP, et al. Frequent reconstitution of IDH2(R140Q) mutant clonal multilineage hematopoiesis following chemotherapy for acute myeloid leukemia. *Leukemia*. 2016;30(9):1946-1950. doi:leu201693 [pii]

10.1038/leu.2016.93 [doi]

151. Kattih B, Shirvani A, Klement P, et al. IDH1/2 mutations in acute myeloid leukemia patients and risk of coronary artery disease and cardiac dysfunction-a retrospective propensity score analysis. *Leukemia*. 2021;35(5):1301-1316. doi:10.1038/s41375-020-01043-x

152. Mas-Peiro S, Hoffmann J, Fichtlscherer S, et al. Clonal haematopoiesis in patients with degenerative aortic valve stenosis undergoing transcatheter aortic valve implantation. *Eur Heart J*. 2020;41(8):933-939. doi:10.1093/eurheartj/ehz591

153. Janin M, Mylonas E, Saada V, et al. Serum 2-hydroxyglutarate production in IDH1- And IDH2-mutated de novo acute myeloid leukemia: A study by the acute leukemia french association group. *J Clin Oncol*. Published online 2014. doi:10.1200/JCO.2013.50.2047

154. Dang L, White DW, Gross S, et al. Cancer-associated IDH1 mutations produce 2-hydroxyglutarate. *Nature*. Published online 2009. doi:10.1038/nature08617

155. Willekens C, Renneville A, Broutin S, et al. Mutational profiling of isolated myeloid sarcomas and utility of serum 2HG as biomarker of IDH1/2 mutations. *Leukemia*. Published online 2018. doi:10.1038/s41375-018-0056-6

156. DiNardo CD, Propert KJ, Loren AW, et al. Serum 2-hydroxyglutarate levels predict isocitrate dehydrogenase mutations and clinical outcome in acute myeloid leukemia. *Blood*. 2013;121(24):4917-4924. doi:10.1182/blood-2013-03-493197

157. Zhao X, Fu J, Du J, Xu W. The Role of D-3-Phosphoglycerate Dehydrogenase in Cancer. *Int J Biol Sci*. 2020;16(9):1495-1506. doi:10.7150/ijbs.41051

158. Du X, Hu H. The Roles of 2-Hydroxyglutarate. *Front Cell Dev Biol*. 2021;9:651317. doi:10.3389/fcell.2021.651317

159. Thienpont B, Steinbacher J, Zhao H, et al. Tumour hypoxia causes DNA hypermethylation by reducing TET activity. *Nature*. 2016;537(7618):63-68. doi:10.1038/nature19081

160. Tyrakis PA, Palazon A, Macias D, et al. S-2-hydroxyglutarate regulates CD8+ T-lymphocyte fate. *Nature*. 2016;540(7632):236-241. doi:10.1038/nature20165

161. Xu T, Stewart KM, Wang X, et al. Metabolic control of TH17 and induced Treg cell balance by an epigenetic mechanism. *Nature*. 2017;548(7666):228-233. doi:10.1038/nature23475

162. Bunse L, Pusch S, Bunse T, et al. Suppression of antitumor T cell immunity by the oncometabolite (R)-2-hydroxyglutarate. *Nat Med*. 2018;24(8):1192-1203. doi:10.1038/s41591-018-0095-6

163. Friedrich M, Sankowski R, Bunse L, et al. Tryptophan metabolism drives dynamic immunosuppressive myeloid states in IDH-mutant gliomas. *Nat Cancer*.

2021;2(7):723-740. doi:10.1038/s43018-021-00201-z

164. Halaby MJ, McGaha TL. 2-HG modulates glioma macrophages via Trp metabolism. *Nat Cancer*. 2021;2(7):677-679. doi:10.1038/s43018-021-00231-7

165. Chen D, Xia S, Zhang R, et al. Lysine acetylation restricts mutant IDH2 activity to optimize transformation in AML cells. *Mol Cell*. 2021;81(18):3833-3847.e11. doi:10.1016/j.molcel.2021.06.027

166. Ye D, Guan KL, Xiong Y. Metabolism, Activity, and Targeting of D- and L-2-Hydroxyglutarates. *Trends Cancer*. 2018;4(2):151-165. doi:10.1016/j.trecan.2017.12.005

167. Sulkowski PL, Oeck S, Dow J, et al. Oncometabolites suppress DNA repair by disrupting local chromatin signalling. *Nature*. 2020;582(7813):586-591. doi:10.1038/s41586-020-2363-0

168. Sulkowski PL, Corso CD, Robinson ND, et al. 2-Hydroxyglutarate produced by neomorphic IDH mutations suppresses homologous recombination and induces PARP inhibitor sensitivity. *Sci Transl Med*. 2017;9(375):eaal2463. doi:10.1126/scitranslmed.aal2463

169. Izzo F, Lee SC, Poran A, et al. DNA methylation disruption reshapes the hematopoietic differentiation landscape. *Nat Genet*. 2020;52(4):378-387. doi:10.1038/s41588-020-0595-4

170. Zhang X, Wang X, Wang XQD, et al. Dnmt3a loss and Idh2 neomorphic mutations mutually potentiate malignant hematopoiesis. *Blood*. 2020;135(11):845-856. doi:10.1182/blood.2019003330

171. López-Moyado IF, Rao A. DNMT3A and TET2 mutations reshape hematopoiesis in opposing ways. *Nat Genet*. 2020;52(6):554-556. doi:10.1038/s41588-020-0641-2

172. Fu L, Guerrero CR, Zhong N, et al. Tet-mediated formation of 5-hydroxymethylcytosine in RNA. *J Am Chem Soc*. 2014;136(33):11582-11585. doi:10.1021/ja505305z

173. He C, Sidoli S, Warneford-Thomson R, et al. High-Resolution Mapping of RNA-Binding Regions in the Nuclear Proteome of Embryonic Stem Cells. *Mol Cell*. 2016;64(2):416-430. doi:10.1016/j.molcel.2016.09.034

174. Lan J, Rajan N, Bizet M, et al. Functional role of Tet-mediated RNA hydroxymethylcytosine in mouse ES cells and during differentiation. *Nat Commun*. 2020;11(1):4956. doi:10.1038/s41467-020-18729-6

175. Cheng JX, Chen L, Li Y, et al. RNA cytosine methylation and methyltransferases mediate chromatin organization and 5-azacytidine response and resistance in leukaemia. *Nat Commun*. 2018;9(1):1163. doi:10.1038/s41467-018-03513-4

176. Fu X, Chin RM, Vergnes L, et al. 2-Hydroxyglutarate Inhibits ATP Synthase and

mTOR Signaling. *Cell Metab*. 2015;22(3):508-515. doi:S1550-4131(15)00276-4 [pii] 10.1016/j.cmet.2015.06.009 [doi]

177. Li F, He X, Ye D, et al. NADP(+)-IDH Mutations Promote Hypersuccinylation that Impairs Mitochondria Respiration and Induces Apoptosis Resistance. *Mol Cell*. 2015;60(4):661-675. doi:S1097-2765(15)00808-4 [pii] 10.1016/j.molcel.2015.10.017 [doi]

178. Chan SM, Thomas D, Corces-Zimmerman MR, et al. Isocitrate dehydrogenase 1 and 2 mutations induce BCL-2 dependence in acute myeloid leukemia. *Nat Med*. 2015;21(2):178-184. doi:nm.3788 [pii] 10.1038/nm.3788 [doi]

179. McBrayer SK, Mayers JR, DiNatale GJ, et al. Transaminase Inhibition by 2-Hydroxyglutarate Impairs Glutamate Biosynthesis and Redox Homeostasis in Glioma. *Cell*. 2018;175(1):101-116.e25. doi:10.1016/j.cell.2018.08.038

180. Emadi A, Jun SA, Tsukamoto T, Fathi AT, Minden MD, Dang CV. Inhibition of glutaminase selectively suppresses the growth of primary acute myeloid leukemia cells with IDH mutations. *Exp Hematol*. 2014;42(4):247-251. doi:https://doi.org/10.1016/j.exphem.2013.12.001

181. Tateishi K, Wakimoto H, Iafrate AJ, et al. Extreme Vulnerability of IDH1 Mutant Cancers to NAD+ Depletion. *Cancer Cell*. 2015;28(6):773-784. doi:S1535-6108(15)00427-4 [pii] 10.1016/j.ccell.2015.11.006 [doi]

182. Su R, Dong L, Li C, et al. R-2HG Exhibits Anti-tumor Activity by Targeting FTO/m(6)A/MYC/CEBPA Signaling. *Cell*. 2018;172(1-2):90-105 e23. doi:S0092-8674(17)31382-X [pii] 10.1016/j.cell.2017.11.031 [doi]

183. Sabatier M, Boet E, Zaghdoudi S, et al. Activation of Vitamin D Receptor Pathway Enhances Differentiating Capacity in Acute Myeloid Leukemia with Isocitrate Dehydrogenase Mutations. *Cancers*. 2021;13(20):5243. doi:10.3390/cancers13205243

184. Boutzen H, Saland E, Larrue C, et al. Isocitrate dehydrogenase 1 mutations prime the all-trans retinoic acid myeloid differentiation pathway in acute myeloid leukemia. *J Exp Med*. 2016;213(4):483-497. doi:10.1084/jem.20150736

185. Stuani L, Sabatier M, Saland E, et al. Mitochondrial metabolism supports resistance to IDH mutant inhibitors in acute myeloid leukemia. *J Exp Med*. 2021;218(5):e20200924. doi:10.1084/jem.20200924

186. Cimmino L, Dolgalev I, Wang Y, et al. Restoration of TET2 Function Blocks Aberrant Self-Renewal and Leukemia Progression. *Cell*. 2017;170(6):1079-1095.e20. doi:10.1016/j.cell.2017.07.032

187. Agathocleous M, Meacham CE, Burgess RJ, et al. Ascorbate regulates haematopoietic stem cell function and leukaemogenesis. *Nature*. 2017;549(7673):476-481. doi:10.1038/nature23876

188. Hvinden IC, Cadoux-Hudson T, Schofield CJ, McCullagh JSO. Metabolic adaptations in cancers expressing isocitrate dehydrogenase mutations. *Cell Rep Med*. 2021;2(12):100469. doi:10.1016/j.xcrm.2021.100469

189. Chowdhry S, Zanca C, Rajkumar U, et al. NAD metabolic dependency in cancer is shaped by gene amplification and enhancer remodelling. *Nature*. 2019;569(7757):570-575. doi:10.1038/s41586-019-1150-2

190. Baccelli I, Gareau Y, Lehnertz B, et al. Mubritinib Targets the Electron Transport Chain Complex I and Reveals the Landscape of OXPHOS Dependency in Acute Myeloid Leukemia. *Cancer Cell*. 2019;36(1):84-99.e8. doi:10.1016/j.ccell.2019.06.003

191. Vander Heiden MG, Cantley LC, Thompson CB. Understanding the Warburg effect: the metabolic requirements of cell proliferation. *Science*. 2009;324(5930):1029-1033. doi:10.1126/science.1160809

192. Koppenol WH, Bounds PL, Dang CV. Otto Warburg's contributions to current concepts of cancer metabolism. *Nat Rev Cancer*. 2011;11(5):325-337. doi:10.1038/nrc3038

193. Woodford MR, Baker-Williams AJ, Sager RA, et al. The tumor suppressor folliculin inhibits lactate dehydrogenase A and regulates the Warburg effect. *Nat Struct Mol Biol*. 2021;28(8):662-670. doi:10.1038/s41594-021-00633-2

194. Engelman JA. Targeting PI3K signalling in cancer: opportunities, challenges and limitations. *Nat Rev Cancer*. 2009;9(8):550-562. doi:10.1038/nrc2664

195. Jin L, Zhou Y. Crucial role of the pentose phosphate pathway in malignant tumors. *Oncol Lett*. 2019;17(5):4213-4221. doi:10.3892/ol.2019.10112

196. Rashkovan M, Ferrando A. Metabolic dependencies and vulnerabilities in leukemia. *Genes Dev*. 2019;33(21-22):1460-1474. doi:10.1101/gad.326470.119

197. Tabe Y, Lorenzi PL, Konopleva M. Amino acid metabolism in hematologic malignancies and the era of targeted therapy. *Blood*. 2019;134(13):1014-1023. doi:10.1182/blood.2019001034

198. Stuani L, Sabatier M, Sarry JE. Exploiting metabolic vulnerabilities for personalized therapy in acute myeloid leukemia. *BMC Biol*. 2019;17(1):57. doi:10.1186/s12915-019-0670-4

199. Chapuis N, Poulain L, Birsen R, Tamburini J, Bouscary D. Rationale for Targeting Deregulated Metabolic Pathways as a Therapeutic Strategy in Acute Myeloid Leukemia. *Front Oncol*. 2019;9:405. doi:10.3389/fonc.2019.00405

200. Castro I, Sampaio-Marques B, Ludovico P. Targeting Metabolic Reprogramming in Acute Myeloid Leukemia. *Cells*. 2019;8(9):E967. doi:10.3390/cells8090967

201. Ohayon D, De Chiara A, Chapuis N, et al. Cytoplasmic proliferating cell nuclear

antigen connects glycolysis and cell survival in acute myeloid leukemia. *Sci Rep*. 2016;6:35561. doi:10.1038/srep35561

202. Watson AS, Riffelmacher T, Stranks A, et al. Autophagy limits proliferation and glycolytic metabolism in acute myeloid leukemia. *Cell Death Discov*. 2015;1:15008. doi:10.1038/cddiscovery.2015.8

203. Poulain L, Sujobert P, Zylbersztejn F, et al. High mTORC1 activity drives glycolysis addiction and sensitivity to G6PD inhibition in acute myeloid leukemia cells. *Leukemia*. 2017;31(11):2326-2335. doi:10.1038/leu.2017.81

204. Christofk HR, Vander Heiden MG, Harris MH, et al. The M2 splice isoform of pyruvate kinase is important for cancer metabolism and tumour growth. *Nature*. 2008;452(7184):230-233. doi:10.1038/nature06734

205. Wang YH, Israelsen WJ, Lee D, et al. Cell-state-specific metabolic dependency in hematopoiesis and leukemogenesis. *Cell*. 2014;158(6):1309-1323. doi:10.1016/j.cell.2014.07.048

206. Wang Y, Liu Y, Malek SN, Zheng P, Liu Y. Targeting HIF1α eliminates cancer stem cells in hematological malignancies. *Cell Stem Cell*. 2011;8(4):399-411. doi:10.1016/j.stem.2011.02.006

207. Zhao S, Lin Y, Xu W, et al. Glioma-derived mutations in IDH1 dominantly inhibit IDH1 catalytic activity and induce HIF-1alpha. *Science*. 2009;324(5924):261-265. doi:10.1126/science.1170944

208. Skrtić M, Sriskanthadevan S, Jhas B, et al. Inhibition of mitochondrial translation as a therapeutic strategy for human acute myeloid leukemia. *Cancer Cell*. 2011;20(5):674-688. doi:10.1016/j.ccr.2011.10.015

209. Sriskanthadevan S, Jeyaraju DV, Chung TE, et al. AML cells have low spare reserve capacity in their respiratory chain that renders them susceptible to oxidative metabolic stress. *Blood*. 2015;125(13):2120-2130. doi:10.1182/blood-2014-08-594408

210. Currie E, Schulze A, Zechner R, Walther TC, Farese RV. Cellular fatty acid metabolism and cancer. *Cell Metab*. 2013;18(2):153-161. doi:10.1016/j.cmet.2013.05.017

211. Tabe Y, Konopleva M, Andreeff M. Fatty Acid Metabolism, Bone Marrow Adipocytes, and AML. *Front Oncol*. 2020;10:155. doi:10.3389/fonc.2020.00155

212. Samudio I, Harmancey R, Fiegl M, et al. Pharmacologic inhibition of fatty acid oxidation sensitizes human leukemia cells to apoptosis induction. *J Clin Invest*. 2010;120(1):142-156. doi:10.1172/JCI38942

213. Tcheng M, Roma A, Ahmed N, et al. Very long chain fatty acid metabolism is required in acute myeloid leukemia. *Blood*. 2021;137(25):3518-3532. doi:10.1182/blood.2020008551

214. Behan JW, Yun JP, Proektor MP, et al. Adipocytes impair leukemia treatment in mice. *Cancer Res*. 2009;69(19):7867-7874. doi:10.1158/0008-5472.CAN-09-0800

215. Jeon SM, Chandel NS, Hay N. AMPK regulates NADPH homeostasis to promote tumour cell survival during energy stress. *Nature*. 2012;485(7400):661-665. doi:10.1038/nature11066

216. Ye H, Adane B, Khan N, et al. Leukemic Stem Cells Evade Chemotherapy by Metabolic Adaptation to an Adipose Tissue Niche. *Cell Stem Cell*. 2016;19(1):23-37. doi:10.1016/j.stem.2016.06.001

217. Lee EA, Angka L, Rota SG, et al. Targeting Mitochondria with Avocatin B Induces Selective Leukemia Cell Death. *Cancer Res*. 2015;75(12):2478-2488. doi:10.1158/0008-5472.CAN-14-2676

218. Tabe Y, Saitoh K, Yang H, et al. Inhibition of FAO in AML co-cultured with BM adipocytes: mechanisms of survival and chemosensitization to cytarabine. *Sci Rep*. 2018;8(1):16837. doi:10.1038/s41598-018-35198-6

219. Southam AD, Khanim FL, Hayden RE, et al. Drug Redeployment to Kill Leukemia and Lymphoma Cells by Disrupting SCD1-Mediated Synthesis of Monounsaturated Fatty Acids. *Cancer Res*. 2015;75(12):2530-2540. doi:10.1158/0008-5472.CAN-15-0202

220. Jacque N, Ronchetti AM, Larrue C, et al. Targeting glutaminolysis has antileukemic activity in acute myeloid leukemia and synergizes with BCL-2 inhibition. *Blood*. 2015;126(11):1346-1356. doi:10.1182/blood-2015-01-621870

221. Willems L, Jacque N, Jacquel A, et al. Inhibiting glutamine uptake represents an attractive new strategy for treating acute myeloid leukemia. *Blood*. 2013;122(20):3521-3532. doi:10.1182/blood-2013-03-493163

222. Kim E, Goraksha-Hicks P, Li L, Neufeld TP, Guan KL. Regulation of TORC1 by Rag GTPases in nutrient response. *Nat Cell Biol*. 2008;10(8):935-945. doi:10.1038/ncb1753

223. Miraki-Moud F, Ghazaly E, Ariza-McNaughton L, et al. Arginine deprivation using pegylated arginine deiminase has activity against primary acute myeloid leukemia cells in vivo. *Blood*. 2015;125(26):4060-4068. doi:10.1182/blood-2014-10-608133

224. Mussai F, Egan S, Higginbotham-Jones J, et al. Arginine dependence of acute myeloid leukemia blast proliferation: a novel therapeutic target. *Blood*. 2015;125(15):2386-2396. doi:10.1182/blood-2014-09-600643

225. Tsai HJ, Jiang SS, Hung WC, et al. A Phase II Study of Arginine Deiminase (ADI-PEG20) in Relapsed/Refractory or Poor-Risk Acute Myeloid Leukemia Patients. *Sci Rep*. 2017;7(1):11253. doi:10.1038/s41598-017-10542-4

226. Hattori A, Tsunoda M, Konuma T, et al. Cancer progression by reprogrammed BCAA metabolism in myeloid leukaemia. *Nature*. 2017;545(7655):500-504.

doi:10.1038/nature22314

227. Raffel S, Falcone M, Kneisel N, et al. BCAT1 restricts αKG levels in AML stem cells leading to IDHmut-like DNA hypermethylation. *Nature*. 2017;551(7680):384-388. doi:10.1038/nature24294

228. Jones CL, Stevens BM, D'Alessandro A, et al. Inhibition of Amino Acid Metabolism Selectively Targets Human Leukemia Stem Cells. *Cancer Cell*. 2018;34(5):724-740.e4. doi:10.1016/j.ccell.2018.10.005

229. Molina JR, Sun Y, Protopopova M, et al. An inhibitor of oxidative phosphorylation exploits cancer vulnerability. *Nat Med*. 2018;24(7):1036-1046. doi:10.1038/s41591-018-0052-4

230. Beuneu C, Auger R, Löffler M, Guissani A, Lemaire G, Lepoivre M. Indirect inhibition of mitochondrial dihydroorotate dehydrogenase activity by nitric oxide. *Free Radic Biol Med*. 2000;28(8):1206-1213. doi:10.1016/s0891-5849(00)00239-2

231. Sykes DB, Kfoury YS, Mercier FE, et al. Inhibition of Dihydroorotate Dehydrogenase Overcomes Differentiation Blockade in Acute Myeloid Leukemia. *Cell*. 2016;167(1):171-186.e15. doi:10.1016/j.cell.2016.08.057

232. Christian S, Merz C, Evans L, et al. The novel dihydroorotate dehydrogenase (DHODH) inhibitor BAY 2402234 triggers differentiation and is effective in the treatment of myeloid malignancies. *Leukemia*. 2019;33(10):2403-2415. doi:10.1038/s41375-019-0461-5

233. Jitkova Y, Gronda M, Hurren R, et al. A Novel Formulation of Tigecycline Has Enhanced Stability and Sustained Antibacterial and Antileukemic Activity. *PLoS ONE*. 2014;9(5):e95281. doi:10.1371/journal.pone.0095281

234. Stuart SD, Schauble A, Gupta S, et al. A strategically designed small molecule attacks alpha-ketoglutarate dehydrogenase in tumor cells through a redox process. *Cancer Metab*. 2014;2:4. doi:10.1186/2049-3002-2-4

235. Zachar Z, Marecek J, Maturo C, et al. Non-redox-active lipoate derivates disrupt cancer cell mitochondrial metabolism and are potent anticancer agents in vivo. *J Mol Med Berl Ger*. 2011;89(11):1137-1148. doi:10.1007/s00109-011-0785-8

236. Pardee TS, Anderson RG, Pladna KM, et al. A Phase I Study of CPI-613 in Combination with High-Dose Cytarabine and Mitoxantrone for Relapsed or Refractory Acute Myeloid Leukemia. *Clin Cancer Res Off J Am Assoc Cancer Res*. 2018;24(9):2060-2073. doi:10.1158/1078-0432.CCR-17-2282

237. Yan H, Wen L, Tan D, et al. Association of a cytarabine chemosensitivity related gene expression signature with survival in cytogenetically normal acute myeloid leukemia. *Oncotarget*. 2017;8(1):1529-1540. doi:10.18632/oncotarget.13650

238. Pollyea DA, Amaya M, Strati P, Konopleva MY. Venetoclax for AML: changing the treatment paradigm. *Blood Adv*. 2019;3(24):4326-4335.

doi:10.1182/bloodadvances.2019000937

239. Guerra VA, DiNardo C, Konopleva M. Venetoclax-based therapies for acute myeloid leukemia. *Best Pract Res Clin Haematol*. 2019;32(2):145-153. doi:10.1016/j.beha.2019.05.008

240. Konopleva M, Pollyea DA, Potluri J, et al. Efficacy and Biological Correlates of Response in a Phase II Study of Venetoclax Monotherapy in Patients with Acute Myelogenous Leukemia. *Cancer Discov*. 2016;6(10):1106-1117. doi:10.1158/2159-8290.CD-16-0313

241. Pollyea DA, Stevens BM, Jones CL, et al. Venetoclax with azacitidine disrupts energy metabolism and targets leukemia stem cells in patients with acute myeloid leukemia. *Nat Med*. 2018;24(12):1859-1866. doi:10.1038/s41591-018-0233-1

242. DiNardo CD, Pratz K, Pullarkat V, et al. Venetoclax combined with decitabine or azacitidine in treatment-naive, elderly patients with acute myeloid leukemia. *Blood*. 2019;133(1):7-17. doi:10.1182/blood-2018-08-868752

243. DiNardo CD, Jonas BA, Pullarkat V, et al. Azacitidine and Venetoclax in Previously Untreated Acute Myeloid Leukemia. *N Engl J Med*. 2020;383(7):617-629. doi:10.1056/NEJMoa2012971

244. Jones CL, Stevens BM, Culp-Hill R, et al. Inhibition of Fatty Acid Metabolism Re-Sensitizes Resistant Leukemia Stem Cells to Venetoclax with Azacitidine. *Blood*. 2019;134(Supplement_1):1272. doi:10.1182/blood-2019-125773

245. Jones CL, Stevens BM, Pollyea DA, et al. Nicotinamide Metabolism Mediates Resistance to Venetoclax in Relapsed Acute Myeloid Leukemia Stem Cells. *Cell Stem Cell*. 2020;27(5):748-764.e4. doi:10.1016/j.stem.2020.07.021

246. Bosc C, Saland E, Bousard A, et al. Mitochondrial inhibitors circumvent adaptive resistance to venetoclax and cytarabine combination therapy in acute myeloid leukemia. *Nat Cancer*. 2021;2(11):1204-1223. doi:10.1038/s43018-021-00264-y

247. Chan SM, Thomas D, Corces-Zimmerman MR, et al. Isocitrate dehydrogenase 1 and 2 mutations induce BCL-2 dependence in acute myeloid leukemia. *Nat Med*. 2015;21(2):178-184. doi:10.1038/nm.3788

248. Cathelin S, Sharon D, Subedi A, et al. Combination of Enasidenib and Venetoclax Shows Superior Anti-Leukemic Activity Against IDH2 Mutated AML in Patient-Derived Xenograft Models. *Blood*. 2018;132(Supplement 1):562. doi:10.1182/blood-2018-99-119688

249. Lachowiez et al. A PHASE IB/II STUDY OF IVOSIDENIB WITH VENETOCLAX +/- AZACITIDINE... by Curtis Lachowiez. Accessed February 6, 2022. https://library.ehaweb.org/eha/2021/eha2021-virtual-congress/324544/curtis.lachowiez.a.phase.ib.ii.study.of.ivosidenib.with.venetoclax.2B.-.html?f=listing%3D3%2Abrowseby%3D8%2Asortby%3D1%2Amedia%3D1

250. Nechiporuk T, Kurtz SE, Nikolova O, et al. The TP53 Apoptotic Network Is a Primary Mediator of Resistance to BCL2 Inhibition in AML Cells. *Cancer Discov*. 2019;9(7):910-925. doi:10.1158/2159-8290.CD-19-0125

251. Sharon D, Cathelin S, Mirali S, et al. Inhibition of mitochondrial translation overcomes venetoclax resistance in AML through activation of the integrated stress response. *Sci Transl Med*. 2019;11(516):eaax2863. doi:10.1126/scitranslmed.aax2863

252. Choi H, Na KJ. Pan-cancer analysis of tumor metabolic landscape associated with genomic alterations. *Mol Cancer*. 2018;17(1):150. doi:10.1186/s12943-018-0895-9

253. Huang A, Ju HQ, Liu K, et al. Metabolic alterations and drug sensitivity of tyrosine kinase inhibitor resistant leukemia cells with a FLT3/ITD mutation. *Cancer Lett*. 2016;377(2):149-157. doi:10.1016/j.canlet.2016.04.040

254. Gregory MA, D'Alessandro A, Alvarez-Calderon F, et al. ATM/G6PD-driven redox metabolism promotes FLT3 inhibitor resistance in acute myeloid leukemia. *Proc Natl Acad Sci U S A*. 2016;113(43):E6669-E6678. doi:10.1073/pnas.1603876113

255. Gallipoli P, Giotopoulos G, Tzelepis K, et al. Glutaminolysis is a metabolic dependency in FLT3ITD acute myeloid leukemia unmasked by FLT3 tyrosine kinase inhibition. *Blood*. 2018;131(15):1639-1653. doi:10.1182/blood-2017-12-820035

256. Kruiswijk F, Labuschagne CF, Vousden KH. p53 in survival, death and metabolic health: a lifeguard with a licence to kill. *Nat Rev Mol Cell Biol*. 2015;16(7):393-405. doi:10.1038/nrm4007

257. Stine ZE, Walton ZE, Altman BJ, Hsieh AL, Dang CV. MYC, Metabolism, and Cancer. *Cancer Discov*. 2015;5(10):1024-1039. doi:10.1158/2159-8290.CD-15-0507

258. Dong Y, Tu R, Liu H, Qing G. Regulation of cancer cell metabolism: oncogenic MYC in the driver's seat. *Signal Transduct Target Ther*. 2020;5(1):124. doi:10.1038/s41392-020-00235-2

259. Prochazka KT, Pregartner G, Rücker FG, et al. Clinical implications of subclonal TP53 mutations in acute myeloid leukemia. *Haematologica*. 2019;104(3):516-523. doi:10.3324/haematol.2018.205013

260. Eriksson M, Ambroise G, Ouchida AT, et al. Effect of Mutant p53 Proteins on Glycolysis and Mitochondrial Metabolism. *Mol Cell Biol*. 2017;37(24):e00328-17. doi:10.1128/MCB.00328-17

261. Rodrigues AS, Correia M, Gomes A, et al. Dichloroacetate, the Pyruvate Dehydrogenase Complex and the Modulation of mESC Pluripotency. *PloS One*. 2015;10(7):e0131663. doi:10.1371/journal.pone.0131663

262. Allende-Vega N, Krzywinska E, Orecchioni S, et al. The presence of wild type p53 in hematological cancers improves the efficacy of combinational therapy targeting metabolism. *Oncotarget*. 2015;6(22):19228-19245. doi:10.18632/oncotarget.4653

263. Freed-Pastor WA, Mizuno H, Zhao X, et al. Mutant p53 disrupts mammary tissue architecture via the mevalonate pathway. *Cell*. 2012;148(1-2):244-258. doi:10.1016/j.cell.2011.12.017

264. Zhou G, Wang J, Zhao M, et al. Gain-of-function mutant p53 promotes cell growth and cancer cell metabolism via inhibition of AMPK activation. *Mol Cell*. 2014;54(6):960-974. doi:10.1016/j.molcel.2014.04.024

265. Kollareddy M, Dimitrova E, Vallabhaneni KC, et al. Regulation of nucleotide metabolism by mutant p53 contributes to its gain-of-function activities. *Nat Commun*. 2015;6:7389. doi:10.1038/ncomms8389

266. Pippa R, Odero MD. The Role of MYC and PP2A in the Initiation and Progression of Myeloid Leukemias. *Cells*. 2020;9(3):E544. doi:10.3390/cells9030544

267. Liu J, Zhang C, Hu W, Feng Z. Tumor suppressor p53 and metabolism. *J Mol Cell Biol*. 2019;11(4):284-292. doi:10.1093/jmcb/mjy070

268. Shimomura Y, Murakami T, Nakai N, Nagasaki M, Harris RA. Exercise promotes BCAA catabolism: effects of BCAA supplementation on skeletal muscle during exercise. *J Nutr*. 2004;134(6 Suppl):1583S-1587S. doi:10.1093/jn/134.6.1583S

269. Zhen H, Kitaura Y, Kadota Y, et al. mTORC1 is involved in the regulation of branched-chain amino acid catabolism in mouse heart. *FEBS Open Bio*. 2016;6(1):43-49. doi:10.1002/2211-5463.12007

270. Lackey DE, Lynch CJ, Olson KC, et al. Regulation of adipose branched-chain amino acid catabolism enzyme expression and cross-adipose amino acid flux in human obesity. *Am J Physiol Endocrinol Metab*. 2013;304(11):E1175-1187. doi:10.1152/ajpendo.00630.2012

271. Gray S, Wang B, Orihuela Y, et al. Regulation of gluconeogenesis by Krüppel-like factor 15. *Cell Metab*. 2007;5(4):305-312. doi:10.1016/j.cmet.2007.03.002

272. Takeuchi Y, Yahagi N, Aita Y, et al. KLF15 Enables Rapid Switching between Lipogenesis and Gluconeogenesis during Fasting. *Cell Rep*. 2016;16(9):2373-2386. doi:10.1016/j.celrep.2016.07.069

273. Coles SJ, Hancock JT, Conway ME. Differential redox potential between the human cytosolic and mitochondrial branched-chain aminotransferase. *Acta Biochim Biophys Sin*. 2012;44(2):172-176. doi:10.1093/abbs/gmr103

274. Oyarzabal A, Martínez-Pardo M, Merinero B, et al. A novel regulatory defect in the branched-chain α-keto acid dehydrogenase complex due to a mutation in the PPM1K gene causes a mild variant phenotype of maple syrup urine disease. *Hum Mutat*. 2013;34(2):355-362. doi:10.1002/humu.22242

275. Harris RA, Joshi M, Jeoung NH, Obayashi M. Overview of the molecular and biochemical basis of branched-chain amino acid catabolism. *J Nutr*. 2005;135(6 Suppl):1527S-30S. doi:10.1093/jn/135.6.1527S

276. Liu X, Zhang F, Zhang Y, et al. PPM1K Regulates Hematopoiesis and Leukemogenesis through CDC20-Mediated Ubiquitination of MEIS1 and p21. *Cell Rep*. 2018;23(5):1461-1475. doi:10.1016/j.celrep.2018.03.140

277. Gu Z, Liu Y, Cai F, et al. Loss of EZH2 Reprograms BCAA Metabolism to Drive Leukemic Transformation. *Cancer Discov*. Published online June 12, 2019:candisc;2159-8290.CD-19-0152v3. doi:10.1158/2159-8290.CD-19-0152

278. Kakazu E, Ueno Y, Kondo Y, et al. Branched chain amino acids enhance the maturation and function of myeloid dendritic cells ex vivo in patients with advanced cirrhosis. *Hepatol Baltim Md*. 2009;50(6):1936-1945. doi:10.1002/hep.23248

279. Papathanassiu AE, Ko JH, Imprialou M, et al. BCAT1 controls metabolic reprogramming in activated human macrophages and is associated with inflammatory diseases. *Nat Commun*. 2017;8(1):16040. doi:10.1038/ncomms16040

280. Peng H, Wang Y, Luo W. Multifaceted role of branched-chain amino acid metabolism in cancer. *Oncogene*. 2020;39(44):6747-6756. doi:10.1038/s41388-020-01480-z

281. Wei Z, Liu X, Cheng C, Yu W, Yi P. Metabolism of Amino Acids in Cancer. *Front Cell Dev Biol*. 2020;8:603837. doi:10.3389/fcell.2020.603837

282. Jin J, Jin J, Pan J, et al. High Expression of BCAT1 promotes Acute Myeloid Leukemia Progression and Sensitize to PARP Inhibitor. *Blood*. 2019;134(Supplement_1):5041. doi:10.1182/blood-2019-125221

283. Tonjes M, Barbus S, Park YJ, et al. BCAT1 promotes cell proliferation through amino acid catabolism in gliomas carrying wild-type IDH1. *Nat Med*. 2013;19(7):901-908. doi:nm.3217 [pii] 10.1038/nm.3217 [doi]

284. Seltzer MJ, Bennett BD, Joshi AD, et al. Inhibition of glutaminase preferentially slows growth of glioma cells with mutant IDH1. *Cancer Res*. 2010;70(22):8981-8987. doi:10.1158/0008-5472.CAN-10-1666

285. Qing Y, Dong L, Gao L, et al. R-2-hydroxyglutarate attenuates aerobic glycolysis in leukemia by targeting the FTO/m6A/PFKP/LDHB axis. *Mol Cell*. 2021;81(5):922-939.e9. doi:10.1016/j.molcel.2020.12.026

286. McBrayer SK, Mayers JR, DiNatale GJ, et al. Transaminase Inhibition by 2-Hydroxyglutarate Impairs Glutamate Biosynthesis and Redox Homeostasis in Glioma. *Cell*. 2018;175(1):101-116.e25. doi:10.1016/j.cell.2018.08.038

287. Yen K, Travins J, Wang F, et al. AG-221, a First-in-Class Therapy Targeting Acute Myeloid Leukemia Harboring Oncogenic IDH2 Mutations. *Cancer Discov*. 2017;7(5):478-493. doi:10.1158/2159-8290.CD-16-1034

288. Rohle D, Popovici-Muller J, Palaskas N, et al. An inhibitor of mutant IDH1 delays growth and promotes differentiation of glioma cells. *Science*. 2013;340(6132):626-

630. doi:10.1126/science.1236062

289. Losman JA, Looper RE, Koivunen P, et al. (R)-2-hydroxyglutarate is sufficient to promote leukemogenesis and its effects are reversible. *Science*. 2013;339(6127):1621-1625. doi:10.1126/science.1231677

290. Stein EM, DiNardo CD, Fathi AT, et al. Molecular remission and response patterns in patients with mutant-IDH2 acute myeloid leukemia treated with enasidenib. *Blood*. 2019;133(7):676-687. doi:10.1182/blood-2018-08-869008

291. Stein EM, DiNardo CD, Pollyea DA, et al. Enasidenib in mutant IDH2 relapsed or refractory acute myeloid leukemia. *Blood*. 2017;130(6):722-731. doi:10.1182/blood-2017-04-779405

292. Poinsignon V, Mercier L, Nakabayashi K, et al. Quantitation of isocitrate dehydrogenase (IDH)-induced D and L enantiomers of 2-hydroxyglutaric acid in biological fluids by a fully validated liquid tandem mass spectrometry method, suitable for clinical applications. *J Chromatogr B Analyt Technol Biomed Life Sci*. 2016;1022:290-297. doi:10.1016/j.jchromb.2016.04.030

293. Tiberi G, Pekowska A, Oudin C, et al. PcG methylation of the HIST1 cluster defines an epigenetic marker of acute myeloid leukemia. *Leukemia*. 2015;29(5):1202-1206. doi:10.1038/leu.2014.339

294. Reitman ZJ, Jin G, Karoly ED, et al. Profiling the effects of isocitrate dehydrogenase 1 and 2 mutations on the cellular metabolome. *Proc Natl Acad Sci U A*. 2011;108(8):3270-3275. doi:1019393108 [pii] 10.1073/pnas.1019393108 [doi]

295. Tyner JW, Tognon CE, Bottomly D, et al. Functional genomic landscape of acute myeloid leukaemia. *Nature*. 2018;562(7728):526-531. doi:10.1038/s41586-018-0623-z

296. Xue P, Zeng F, Duan Q, et al. BCKDK of BCAA Catabolism Cross-talking With the MAPK Pathway Promotes Tumorigenesis of Colorectal Cancer. *EBioMedicine*. 2017;20:50-60. doi:10.1016/j.ebiom.2017.05.001

297. Chaturvedi A, Araujo Cruz MM, Jyotsana N, et al. Enantiomer-specific and paracrine leukemogenicity of mutant IDH metabolite 2-hydroxyglutarate. *Leukemia*. 2016;30(8):1708-1715. doi:10.1038/leu.2016.71

298. Oda M, Greally JM. The HELP assay. *Methods Mol Biol Clifton NJ*. 2009;507:77-87. doi:10.1007/978-1-59745-522-0_7

299. Laugesen A, Højfeldt JW, Helin K. Molecular Mechanisms Directing PRC2 Recruitment and H3K27 Methylation. *Mol Cell*. 2019;74(1):8-18. doi:10.1016/j.molcel.2019.03.011

300. Altevogt P, Sammar M, Hüser L, Kristiansen G. Novel insights into the function of CD24: A driving force in cancer. *Int J Cancer*. 2021;148(3):546-559. doi:10.1002/ijc.33249

301. Kim MH, Yang D, Kim M, Kim SY, Kim D, Kang SJ. A late-lineage murine neutrophil precursor population exhibits dynamic changes during demand-adapted granulopoiesis. *Sci Rep*. 2017;7:39804. doi:10.1038/srep39804

302. Hattori A, Tsunoda M, Konuma T, et al. Cancer progression by reprogrammed BCAA metabolism in myeloid leukaemia. *Nature*. 2017;545(7655):500-504. doi:nature22314 [pii] 10.1038/nature22314 [doi]

303. Hutson SM, Berkich D, Drown P, Xu B, Aschner M, LaNoue KF. Role of Branched-Chain Aminotransferase Isoenzymes and Gabapentin in Neurotransmitter Metabolism. *J Neurochem*. 2002;71(2):863-874. doi:10.1046/j.1471-4159.1998.71020863.x

304. Raffel S, Falcone M, Kneisel N, et al. BCAT1 restricts alphaKG levels in AML stem cells leading to IDHmut-like DNA hypermethylation. *Nature*. 2017;551(7680):384-388. doi:nature24294 [pii] 10.1038/nature24294 [doi]

305. Latini A, Scussiato K, Rosa RB, et al. D-2-hydroxyglutaric acid induces oxidative stress in cerebral cortex of young rats. *Eur J Neurosci*. 2003;17(10):2017-2022. doi:10.1046/j.1460-9568.2003.02639.x

306. Wang Y, Xiao J, Jiang W, et al. BCKDK alters the metabolism of non-small cell lung cancer. *Transl Lung Cancer Res*. 2021;10(12):4459-4476. doi:10.21037/tlcr-21-885

307. Bridi R, Braun CA, Zorzi GK, et al. alpha-keto acids accumulating in maple syrup urine disease stimulate lipid peroxidation and reduce antioxidant defences in cerebral cortex from young rats. *Metab Brain Dis*. 2005;20(2):155-167. doi:10.1007/s11011-005-4152-8

308. Maguolo A, Rodella G, Giorgetti A, et al. A Gain-of-Function Mutation on BCKDK Gene and Its Possible Pathogenic Role in Branched-Chain Amino Acid Metabolism. *Genes*. 2022;13(2):233. doi:10.3390/genes13020233

309. Nicklin P, Bergman P, Zhang B, et al. Bidirectional transport of amino acids regulates mTOR and autophagy. *Cell*. 2009;136(3):521-534. doi:10.1016/j.cell.2008.11.044

310. Nicklin P, Bergman P, Zhang B, et al. Bidirectional Transport of Amino Acids Regulates mTOR and Autophagy. *Cell*. 2009;136(3):521-534. doi:https://doi.org/10.1016/j.cell.2008.11.044

311. Wang X, Li W, Parra JL, Beugnet A, Proud CG. The C terminus of initiation factor 4E-binding protein 1 contains multiple regulatory features that influence its function and phosphorylation. *Mol Cell Biol*. 2003;23(5):1546-1557. doi:10.1128/MCB.23.5.1546-1557.2003

312. Gingras AC, Raught B, Gygi SP, et al. Hierarchical phosphorylation of the translation inhibitor 4E-BP1. *Genes Dev*. 2001;15(21):2852-2864. doi:10.1101/gad.912401

313. Feldman ME, Apsel B, Uotila A, et al. Active-Site Inhibitors of mTOR Target

Rapamycin-Resistant Outputs of mTORC1 and mTORC2. Hunter T, ed. *PLoS Biol*. 2009;7(2):e1000038. doi:10.1371/journal.pbio.1000038

314. Saxton RA, Sabatini DM. mTOR Signaling in Growth, Metabolism, and Disease. *Cell*. 2017;168(6):960-976. doi:10.1016/j.cell.2017.02.004

315. Inoki K, Zhu T, Guan KL. TSC2 Mediates Cellular Energy Response to Control Cell Growth and Survival. *Cell*. 2003;115(5):577-590. doi:10.1016/S0092-8674(03)00929-2

316. Fujiwara H, Tateishi K, Misumi K, et al. Mutant IDH1 confers resistance to energy stress in normal biliary cells through PFKP-induced aerobic glycolysis and AMPK activation. *Sci Rep*. 2019;9(1):18859. doi:10.1038/s41598-019-55211-w

317. Su R, Dong L, Li C, et al. R-2HG Exhibits Anti-tumor Activity by Targeting FTO/m6A/MYC/CEBPA Signaling. *Cell*. 2018;172(1-2):90-105.e23. doi:10.1016/j.cell.2017.11.031

318. Lin X, Tan S, Fu L, Dong Q. BCAT1 Overexpression Promotes Proliferation, Invasion, and Wnt Signaling in Non-Small Cell Lung Cancers. *OncoTargets Ther*. 2020;13:3583-3594. doi:10.2147/OTT.S237306

319. Zhou W, Feng X, Ren C, et al. Over-expression of BCAT1, a c-Myc target gene, induces cell proliferation, migration and invasion in nasopharyngeal carcinoma. *Mol Cancer*. 2013;12:53. doi:10.1186/1476-4598-12-53

320. Kats LM, Reschke M, Taulli R, et al. Proto-oncogenic role of mutant IDH2 in leukemia initiation and maintenance. *Cell Stem Cell*. 2014;14(3):329-341. doi:10.1016/j.stem.2013.12.016

321. Wang F, Travins J, DeLaBarre B, et al. Targeted inhibition of mutant IDH2 in leukemia cells induces cellular differentiation. *Science*. 2013;340(6132):622-626. doi:10.1126/science.1234769

322. Kernytsky A, Wang F, Hansen E, et al. IDH2 mutation-induced histone and DNA hypermethylation is progressively reversed by small-molecule inhibition. *Blood*. 2015;125(2):296-303. doi:10.1182/blood-2013-10-533604

323. Stein EM, DiNardo CD, Fathi AT, et al. Molecular remission and response patterns in patients with mutant-IDH2 acute myeloid leukemia treated with enasidenib. *Blood*. Published online 2019. doi:10.1182/blood-2018-08-869008

324. Stein EM, DiNardo CD, Pollyea DA, et al. Enasidenib in mutant IDH2 relapsed or refractory acute myeloid leukemia. *Blood*. Published online 2017. doi:10.1182/blood-2017-04-779405

325. Amatangelo MD, Quek L, Shih A, et al. Enasidenib induces acute myeloid leukemia cell differentiation to promote clinical response. *Blood*. 2017;130(6):732-741. doi:10.1182/blood-2017-04-779447

326. Fathi AT, DiNardo CD, Kline I, et al. Differentiation Syndrome Associated With Enasidenib, a Selective Inhibitor of Mutant Isocitrate Dehydrogenase 2: Analysis of a Phase 1/2 Study. *JAMA Oncol*. 2018;4(8):1106-1110. doi:10.1001/jamaoncol.2017.4695

327. Harding JJ, Lowery MA, Shih AH, et al. Isoform Switching as a Mechanism of Acquired Resistance to Mutant Isocitrate Dehydrogenase Inhibition. *Cancer Discov*. 2018;8(12):1540-1547. doi:10.1158/2159-8290.CD-18-0877

328. Wang F, Morita K, DiNardo CD, et al. Leukemia stemness and co-occurring mutations drive resistance to IDH inhibitors in acute myeloid leukemia. *Nat Commun*. 2021;12(1):2607. doi:10.1038/s41467-021-22874-x

329. Choe S, Wang H, DiNardo CD, et al. Molecular mechanisms mediating relapse following ivosidenib monotherapy in IDH1-mutant relapsed or refractory AML. *Blood Adv*. 2020;4(9):1894-1905. doi:10.1182/bloodadvances.2020001503

330. Intlekofer AM, Shih AH, Wang B, et al. Acquired resistance to IDH inhibition through trans or cis dimer-interface mutations. *Nature*. 2018;559(7712):125-129. doi:10.1038/s41586-018-0251-7

331. DiNardo CD, Stein EM, de Botton S, et al. Durable Remissions with Ivosidenib in IDH1-Mutated Relapsed or Refractory AML. *N Engl J Med*. 2018;378(25):2386-2398. doi:10.1056/NEJMoa1716984

332. Liu A. STAT5 Signaling Promotes Resistance to Ivosidenib in IDH1 Mutated AML. In: ASH; 2021. Accessed February 14, 2022. https://ash.confex.com/ash/2021/webprogram/Paper154278.html

333. Smith CC, Paguirigan A, Jeschke GR, et al. Heterogeneous resistance to quizartinib in acute myeloid leukemia revealed by single-cell analysis. *Blood*. 2017;130(1):48-58. doi:10.1182/blood-2016-04-711820

334. McMahon CM, Canaani J, Rea B, et al. Gilteritinib induces differentiation in relapsed and refractory FLT3-mutated acute myeloid leukemia. *Blood Adv*. 2019;3(10):1581-1585. doi:10.1182/bloodadvances.2018029496

335. Ng SWK, Mitchell A, Kennedy JA, et al. A 17-gene stemness score for rapid determination of risk in acute leukaemia. *Nature*. 2016;540(7633):433-437. doi:10.1038/nature20598

336. Döhner H. AGILE: A Global, Randomized, Double-Blind, Phase 3 Study of Ivosidenib + Azacitidine Versus Placebo + Azacitidine in Patients with Newly Diagnosed Acute Myeloid Leukemia with an IDH1</Em> Mutation. In: ASH; 2021. Accessed February 14, 2022. https://ash.confex.com/ash/2021/webprogram/Paper147805.html

337. DiNardo CD, Schuh AC, Stein EM, et al. Enasidenib plus azacitidine versus azacitidine alone in patients with newly diagnosed, mutant-IDH2 acute myeloid

leukaemia (AG221-AML-005): a single-arm, phase 1b and randomised, phase 2 trial. *Lancet Oncol*. 2021;22(11):1597-1608. doi:10.1016/S1470-2045(21)00494-0

338. Venugopal S, Takahashi K, Daver N, et al. Efficacy and safety of enasidenib and azacitidine combination in patients with IDH2 mutated acute myeloid leukemia and not eligible for intensive chemotherapy. *Blood Cancer J*. 2022;12(1):10. doi:10.1038/s41408-021-00604-2

339. Oktyabri D, Ishimura A, Tange S, Terashima M, Suzuki T. DOT1L histone methyltransferase regulates the expression of BCAT1 and is involved in sphere formation and cell migration of breast cancer cell lines. *Biochimie*. 2016;123:20-31. doi:10.1016/j.biochi.2016.01.005

340. Wang Y, Zhang J, Ren S, et al. Branched-Chain Amino Acid Metabolic Reprogramming Orchestrates Drug Resistance to EGFR Tyrosine Kinase Inhibitors. *Cell Rep*. 2019;28(2):512-525.e6. doi:10.1016/j.celrep.2019.06.026

341. Court F, Le Boiteux E, Fogli A, et al. Transcriptional alterations in glioma result primarily from DNA methylation-independent mechanisms. *Genome Res*. 2019;29(10):1605-1621. doi:10.1101/gr.249219.119

342. Schvartzman JM, Reuter VP, Koche RP, Thompson CB. 2-hydroxyglutarate inhibits MyoD-mediated differentiation by preventing H3K9 demethylation. *Proc Natl Acad Sci*. 2019;116(26):12851-12856. doi:10.1073/pnas.1817662116

343. Sykes DB, Kfoury YS, Mercier FE, et al. Inhibition of Dihydroorotate Dehydrogenase Overcomes Differentiation Blockade in Acute Myeloid Leukemia. *Cell*. 2016;167(1):171-186 e15. doi:S0092-8674(16)31154-0 [pii] 10.1016/j.cell.2016.08.057 [doi]

344. Christian S, Merz C, Evans L, et al. The novel dihydroorotate dehydrogenase (DHODH) inhibitor BAY 2402234 triggers differentiation and is effective in the treatment of myeloid malignancies. *Leukemia*. 2019;33(10):2403-2415. doi:10.1038/s41375-019-0461-5

345. Cano-Crespo S, Chillarón J, Junza A, et al. CD98hc (SLC3A2) sustains amino acid and nucleotide availability for cell cycle progression. *Sci Rep*. 2019;9(1):14065. doi:10.1038/s41598-019-50547-9

346. Bajaj J, Konuma T, Lytle NK, et al. CD98-Mediated Adhesive Signaling Enables the Establishment and Propagation of Acute Myelogenous Leukemia. *Cancer Cell*. 2016;30(5):792-805. doi:10.1016/j.ccell.2016.10.003

347. Wang T, Yu H, Hughes NW, et al. Gene Essentiality Profiling Reveals Gene Networks and Synthetic Lethal Interactions with Oncogenic Ras. *Cell*. 2017;168(5):890-903.e15. doi:10.1016/j.cell.2017.01.013

348. Ma Y, Song J, Chen B, Xu X, Lin G. SLC7A5 act as a potential leukemic transformation target gene in myelodysplastic syndrome. *Oncotarget*.

2016;7(6):6566-6575. doi:10.18632/oncotarget.6512

349. Xu SM, Tang K, Meng L, Tang Y. Suppression of amino acid transporter LAT3 expression on proliferation of K562 cells. *J Huazhong Univ Sci Technol Med Sci Hua Zhong Ke Ji Xue Xue Bao Yi Xue Ying Wen Ban Huazhong Keji Daxue Xuebao Yixue Yingdewen Ban*. 2013;33(5):632-635. doi:10.1007/s11596-013-1171-2

350. Oda K, Hosoda N, Endo H, et al. L-type amino acid transporter 1 inhibitors inhibit tumor cell growth. *Cancer Sci*. 2010;101(1):173-179. doi:10.1111/j.1349-7006.2009.01386.x

351. Cormerais Y, Giuliano S, LeFloch R, et al. Genetic Disruption of the Multifunctional CD98/LAT1 Complex Demonstrates the Key Role of Essential Amino Acid Transport in the Control of mTORC1 and Tumor Growth. *Cancer Res*. 2016;76(15):4481-4492. doi:10.1158/0008-5472.CAN-15-3376

352. Fultang L, Gneo L, De Santo C, Mussai FJ. Targeting Amino Acid Metabolic Vulnerabilities in Myeloid Malignancies. *Front Oncol*. 2021;11:674720. doi:10.3389/fonc.2021.674720

353. Ko JH, Olona A, Papathanassiu AE, et al. BCAT1 affects mitochondrial metabolism independently of leucine transamination in activated human macrophages. *J Cell Sci*. 2020;133(22):jcs247957. doi:10.1242/jcs.247957

354. Batsios G, Viswanath P, Subramani E, et al. PI3K/mTOR inhibition of IDH1 mutant glioma leads to reduced 2HG production that is associated with increased survival. *Sci Rep*. 2019;9(1):10521. doi:10.1038/s41598-019-47021-x

355. Meng D, Frank AR, Jewell JL. mTOR signaling in stem and progenitor cells. *Dev Camb Engl*. 2018;145(1):dev152595. doi:10.1242/dev.152595

356. Darici S, Alkhaldi H, Horne G, Jørgensen HG, Marmiroli S, Huang X. Targeting PI3K/Akt/mTOR in AML: Rationale and Clinical Evidence. *J Clin Med*. 2020;9(9):E2934. doi:10.3390/jcm9092934

357. Tabe Y, Tafuri A, Sekihara K, Yang H, Konopleva M. Inhibition of mTOR kinase as a therapeutic target for acute myeloid leukemia. *Expert Opin Ther Targets*. 2017;21(7):705-714. doi:10.1080/14728222.2017.1333600

358. Mirabilii S, Ricciardi MR, Tafuri A. mTOR Regulation of Metabolism in Hematologic Malignancies. *Cells*. 2020;9(2):E404. doi:10.3390/cells9020404

359. Tahmasebi S, Khoutorsky A, Mathews MB, Sonenberg N. Translation deregulation in human disease. *Nat Rev Mol Cell Biol*. 2018;19(12):791-807. doi:10.1038/s41580-018-0034-x

360. Cho S, Lee G, Pickering BF, et al. mTORC1 promotes cell growth via m6A-dependent mRNA degradation. *Mol Cell*. 2021;81(10):2064-2075.e8. doi:10.1016/j.molcel.2021.03.010

361. Villa E, Sahu U, O'Hara BP, et al. mTORC1 stimulates cell growth through SAM synthesis and m6A mRNA-dependent control of protein synthesis. *Mol Cell*. 2021;81(10):2076-2093.e9. doi:10.1016/j.molcel.2021.03.009

362. Karmaus PWF, Herrada AA, Guy C, et al. Critical roles of mTORC1 signaling and metabolic reprogramming for M-CSF-mediated myelopoiesis. *J Exp Med*. 2017;214(9):2629-2647. doi:10.1084/jem.20161855

363. Watson AR, Dai H, Zheng Y, et al. mTORC2 Deficiency Alters the Metabolic Profile of Conventional Dendritic Cells. *Front Immunol*. 2019;10:1451. doi:10.3389/fimmu.2019.01451

364. Lee PY, Sykes DB, Ameri S, et al. The metabolic regulator mTORC1 controls terminal myeloid differentiation. *Sci Immunol*. 2017;2(11):eaam6641. doi:10.1126/sciimmunol.aam6641

365. Majeti R, Weissman IL. Human acute myelogenous leukemia stem cells revisited: there's more than meets the eye. *Cancer Cell*. 2011;19(1):9-10. doi:10.1016/j.ccr.2011.01.007

366. Calkhoven CF, Müller C, Leutz A. Translational control of C/EBPalpha and C/EBPbeta isoform expression. *Genes Dev*. 2000;14(15):1920-1932.

367. Avellino R, Delwel R. Expression and regulation of C/EBPα in normal myelopoiesis and in malignant transformation. *Blood*. 2017;129(15):2083-2091. doi:10.1182/blood-2016-09-687822

368. Kallin EM, Rodríguez-Ubreva J, Christensen J, et al. Tet2 facilitates the derepression of myeloid target genes during CEBPα-induced transdifferentiation of pre-B cells. *Mol Cell*. 2012;48(2):266-276. doi:10.1016/j.molcel.2012.08.007

369. Chen X, Zhou W, Song RH, et al. Tumor suppressor CEBPA interacts with and inhibits DNMT3A activity. *Sci Adv*. 2022;8(4):eabl5220. doi:10.1126/sciadv.abl5220

370. Zidek LM, Ackermann T, Hartleben G, et al. Deficiency in mTORC1-controlled C/EBPβ-mRNA translation improves metabolic health in mice. *EMBO Rep*. 2015;16(8):1022-1036. doi:10.15252/embr.201439837

371. Ananieva EA, Wilkinson AC. Branched-chain amino acid metabolism in cancer: *Curr Opin Clin Nutr Metab Care*. 2018;21(1):64-70. doi:10.1097/MCO.0000000000000430

372. Thewes V, Simon R, Hlevnjak M, et al. The branched-chain amino acid transaminase 1 sustains growth of antiestrogen-resistant and ERα-negative breast cancer. *Oncogene*. 2017;36(29):4124-4134. doi:10.1038/onc.2017.32

373. Ni F, Yu WM, Li Z, et al. Critical role of ASCT2-mediated amino acid metabolism in promoting leukaemia development and progression. *Nat Metab*. 2019;1(3):390-403. doi:10.1038/s42255-019-0039-6

374. Jones CL, Stevens BM, D'Alessandro A, et al. Inhibition of Amino Acid Metabolism Selectively Targets Human Leukemia Stem Cells. *Cancer Cell*. 2018;34(5):724-740.e4. doi:https://doi.org/10.1016/j.ccell.2018.10.005

375. DiNardo CD, Pratz KW, Letai A, et al. Safety and preliminary efficacy of venetoclax with decitabine or azacitidine in elderly patients with previously untreated acute myeloid leukaemia: a non-randomised, open-label, phase 1b study. *Lancet Oncol*. 2018;19(2):216-228. doi:10.1016/S1470-2045(18)30010-X

376. Pollyea DA, Stevens BM, Jones CL, et al. Venetoclax with azacitidine disrupts energy metabolism and targets leukemia stem cells in patients with acute myeloid leukemia. *Nat Med*. 2018;24(12):1859-1866. doi:10.1038/s41591-018-0233-1

377. Hitzerd SM, Verbrugge SE, Ossenkoppele G, Jansen G, Peters GJ. Positioning of aminopeptidase inhibitors in next generation cancer therapy. *Amino Acids*. 2014;46(4):793-808. doi:10.1007/s00726-013-1648-0

378. Corces-Zimmerman MR, Hong WJ, Weissman IL, Medeiros BC, Majeti R. Preleukemic mutations in human acute myeloid leukemia affect epigenetic regulators and persist in remission. *Proc Natl Acad Sci U A*. 2014;111(7):2548-2553. doi:1324297111 [pii] 10.1073/pnas.1324297111 [doi]

379. Shlush LI, Zandi S, Mitchell A, et al. Identification of pre-leukaemic haematopoietic stem cells in acute leukaemia. *Nature*. 2014;506(7488):328-333. doi:nature13038 [pii] 10.1038/nature13038 [doi]

380. Shlush LI, Mitchell A, Heisler L, et al. Tracing the origins of relapse in acute myeloid leukaemia to stem cells. *Nature*. 2017;547(7661):104-108. doi:10.1038/nature22993

381. Abelson S, Collord G, Ng SWK, et al. Prediction of acute myeloid leukaemia risk in healthy individuals. *Nature*. 2018;559(7714):400-404. doi:10.1038/s41586-018-0317-6

382. Shlush LI. Age-related clonal hematopoiesis. *Blood*. 2018;131(5):496.

383. Hsu CH, Nguyen C, Yan C, et al. Transcriptome Profiling of Pediatric Core Binding Factor AML. *PloS One*. 2015;10(9):e0138782. doi:10.1371/journal.pone.0138782

384. Faber ZJ, Chen X, Gedman AL, et al. The genomic landscape of core-binding factor acute myeloid leukemias. *Nat Genet*. 2016;48(12):1551-1556. doi:10.1038/ng.3709

385. Hartmann L, Dutta S, Opatz S, et al. ZBTB7A mutations in acute myeloid leukaemia with t(8;21) translocation. *Nat Commun*. 2016;7:11733. doi:10.1038/ncomms11733

386. Lavallée VP, Lemieux S, Boucher G, et al. RNA-sequencing analysis of core binding factor AML identifies recurrent ZBTB7A mutations and defines RUNX1-CBFA2T3 fusion signature. *Blood*. 2016;127(20):2498-2501. doi:10.1182/blood-2016-03-703868

387. Liu XS, Haines JE, Mehanna EK, et al. ZBTB7A acts as a tumor suppressor through the transcriptional repression of glycolysis. *Genes Dev*. 2014;28(17):1917-1928. doi:10.1101/gad.245910.114

388. Redondo Monte E, Wilding A, Leubolt G, et al. ZBTB7A prevents RUNX1-RUNX1T1-dependent clonal expansion of human hematopoietic stem and progenitor cells. *Oncogene*. 2020;39(15):3195-3205. doi:10.1038/s41388-020-1209-4

389. Wang YH, Lin CC, Yao CY, et al. A 4-gene leukemic stem cell score can independently predict the prognosis of myelodysplastic syndrome patients. *Blood Adv*. 2020;4(4):644-654. doi:10.1182/bloodadvances.2019001185

390. Castaigne S, Pautas C, Terré C, et al. Effect of gemtuzumab ozogamicin on survival of adult patients with de-novo acute myeloid leukaemia (ALFA-0701): a randomised, open-label, phase 3 study. *Lancet Lond Engl*. 2012;379(9825):1508-1516. doi:10.1016/S0140-6736(12)60485-1

391. Taya Y, Ota Y, Wilkinson AC, et al. Depleting dietary valine permits nonmyeloablative mouse hematopoietic stem cell transplantation. *Science*. 2016;354(6316):1152-1155. doi:10.1126/science.aag3145

392. Sinclair LV, Rolf J, Emslie E, Shi YB, Taylor PM, Cantrell DA. Control of amino-acid transport by antigen receptors coordinates the metabolic reprogramming essential for T cell differentiation. *Nat Immunol*. 2013;14(5):500-508. doi:10.1038/ni.2556

393. Smyth LM, Tamura K, Oliveira M, et al. Capivasertib, an AKT Kinase Inhibitor, as Monotherapy or in Combination with Fulvestrant in Patients with AKT1 E17K-Mutant, ER-Positive Metastatic Breast Cancer. *Clin Cancer Res Off J Am Assoc Cancer Res*. 2020;26(15):3947-3957. doi:10.1158/1078-0432.CCR-19-3953

394. She QB, Chandarlapaty S, Ye Q, et al. Breast tumor cells with PI3K mutation or HER2 amplification are selectively addicted to Akt signaling. *PloS One*. 2008;3(8):e3065. doi:10.1371/journal.pone.0003065

395. Martelli AM, Evangelisti C, Chiarini F, McCubrey JA. The phosphatidylinositol 3-kinase/Akt/mTOR signaling network as a therapeutic target in acute myelogenous leukemia patients. *Oncotarget*. 2010;1(2):89-103. doi:10.18632/oncotarget.114

396. Martinez Calejman C, Trefely S, Entwisle SW, et al. mTORC2-AKT signaling to ATP-citrate lyase drives brown adipogenesis and de novo lipogenesis. *Nat Commun*. 2020;11(1):575. doi:10.1038/s41467-020-14430-w

Enasidenib for the treatment of relapsed or refractory acute myeloid leukemia with an isocitrate dehydrogenase 2 mutation

Mael Heiblig , Sabine Hachem-Khalife , Christophe Willekens , Jean-Baptiste Micol , Angelo Paci , Virginie Penard-Lacronique & Stéphane de Botton

To cite this article: Mael Heiblig , Sabine Hachem-Khalife , Christophe Willekens , Jean-Baptiste Micol , Angelo Paci , Virginie Penard-Lacronique & Stéphane de Botton (2020) Enasidenib for the treatment of relapsed or refractory acute myeloid leukemia with an isocitrate dehydrogenase 2 mutation, Expert Review of Precision Medicine and Drug Development, 5:6, 421-428, DOI: 10.1080/23808993.2020.1831909

To link to this article: https://doi.org/10.1080/23808993.2020.1831909

Published online: 25 Oct 2020.

Submit your article to this journal

Article views: 21

View related articles

View Crossmark data

Enasidenib for the treatment of relapsed or refractory acute myeloid leukemia with an isocitrate dehydrogenase 2 mutation

Mael Heiblig [a], Sabine Hachem-Khalife[b], Christophe Willekens [b], Jean-Baptiste Micol[b], Angelo Paci[c], Virginie Penard-Lacronique[a] and Stéphane de Botton[a,b,d,e]

[a]Inserm U1170, Gustave Roussy Cancer Campus, Université Paris-Sud, Villejuif, France; [b]Service d'Hématologie Clinique, Gustave Roussy Cancer Campus, Villejuif, France; [c]Service De Pharmacologie, Département De Biologie Et Pathologie Médicales, Gustave Roussy Cancer Campus Grand Paris, Villejuif, France; [d]Département d'Innovation Thérapeutique Et d'Essais Précoces (DITEP), Gustave Roussy, Université Paris-Saclay, Villejuif, France; [e]Faculté De Médecine Paris-Sud, Université Paris-Saclay, Kremlin-Bicêtre, France

ABSTRACT

Introduction: Isocitrate dehydrogenase 2 (IDH2) is a key metabolic enzyme that converts isocitrate to α-ketoglutarate (αKG). Somatic point mutations in *IDH2* confer a gain-of-function in blast cells resulting in overproduction of D-2-hydroxyglutarate (D-2HG). High intracellular concentrations of D-2HG inhibit α-ketoglutarate-dependent dioxygenases including histone, DNA and RNA demethylases, leading to histone, DNA and RNA hypermethylation, and cell differentiation blockade. *In vitro* and *in vivo* preclinical studies have demonstrated that inhibition of IDH2-mutant enzymes with enasidenib decrease intracellular D-2HG levels, reverse epigenetic dysregulation, and release the differentiation block. The US Food and Drug Administration (FDA) approved enasidenib, a mutant-IDH2 enzyme inhibitor for patients with relapsed or refractory (R/R) *IDH2*-mutated AML.

Areas covered: We review the biology and prognostic significance of *IDH2* mutations in AML and discuss the pharmacology, clinical efficacy, and toxicity profile of enasidenib. We highlight areas of ongoing preclinical and clinical research.

Expert opinion: Enasidenib was FDA approved due to high response rates, durability of the responses that translated into an impressive OS in that heavily pretreated population. Promising ongoing clinical trials are evaluating combination therapies with enasidenib frontline.

ARTICLE HISTORY
Received 24 February 2020
Accepted 30 September 2020

KEYWORDS
Tumor metabolism; epigenetic; oncogene; idh2; acute myeloid leukemia; 2-HG; targeted therapies; enasidenib

1. Introduction

Isocitrate dehydrogenase 2 (IDH2) is a metabolic enzyme catalyzing the conversion of isocitrate to α-ketoglutarate (αKG) while reducing NADP to NADPH. Point mutations in *IDH2* are present in 8–19% of AML [1–3]. Multiple preclinical models have demonstrated the oncogenic potential of *IDH2* mutations, which alter epigenetic regulation, cancer cell differentiation, and metabolism [4–12]. Depending on associated genomic aberrations and the cellular context, the oncogenic potential of *IDH2* mutation ranges from an initiating event – promoting transformation – to a secondary oncogenic event conferring selective advantage to cancer cells. *In vitro* and *in vivo* preclinical studies have demonstrated that inhibition of IDH2-mutant enzymes decreased intracellular D-2-hydroxyglutarate (D-2HG) levels, reverse epigenetic dysregulation and release the differentiation block [13–16]. Finally, phase 1/2 clinical trials demonstrated that inhibition of IDH1/2-mutant enzymes was highly effective in heavily pretreated AML patients with *IDH1/2* mutations [17–19].

2. Overview of the market

What are the unmet needs of currently available therapies?

IDH 2 R/R AML patients not eligible for intensive therapy and without remaining treatment options except for best supportive/palliative care

Which competitor compounds/classes of compounds are in the clinic/late development?

Co-occurring *FLT3-ITD* or *TKD* can be treated with gilteritinib, approved in R/R AML with a *FLT3* mutation

2.1. Normal functions of IDH enzymes

The IDH family of enzymes comprises three proteins located in the cytoplasm and peroxisomes (IDH1), and mitochondria (IDH2 and IDH3), involved in a number of cellular processes, including mitochondrial oxidative phosphorylation, glutamine metabolism, lipogenesis, glucose sensing, and regulation of cellular redox status [20–23]. IDH1 and IDH2 are highly similar enzymes, forming homodimers and catalyzing the reversible NADP+-dependent oxidative decarboxylation of isocitrate to αKG. NADPH is a key cellular reducing agent, required for detoxification processes through reduction of glutathione (GSH) and thioredoxins, and activation of catalase, which are all involved in the protection against the toxicity of reactive oxygen species (ROS) and oxidative DNA damage [24].

CONTACT Stéphane de Botton stephane.debotton@gustaveroussy.fr Service d'Hématologie Clinique, Gustave Roussy Cancer Campus, Villejuif 94805, France

2.2. *IDH2 mutants produce D-2HG and inhibit αKG-dependent dioxygenases*

IDH2 mutations are heterozygous, missense mutations leading to the substitution of the amino acids arginine 172 or 140 in *IDH2* [20,25]. These residues play key role in substrate binding in the enzyme active site. Initial functional studies of *IDH2*-mutant cells revealed that *IDH2* mutations decrease the ability of the mutant enzymes to convert isocitrate to αKG, and that IDH1-mutant enzyme inhibit wild-type activity in a dominant-negative manner. Further functional analysis demonstrated that IDH1/2-mutant enzymes gain neomorphic enzymatic activity, converting NADPH and αKG to NADP+ and D-2HG [26–28]. IDH2 mutant enzymes produce high levels of D-2HG in cells (50- to 100-fold higher than in normal tissues). 2HG is a chiral molecule that can exist in either the D-enantiomer or the L-enantiomer. IDH2 mutants exclusively produce D-2HG. Importantly *IDH*-mutant cells have normal αKG levels [26]. To date, D-2HG is not known to play any physiologic metabolic role (its intracellular concentration is controlled by the D-2-Hydroxyglutarate Dehydrogenase (D2HGDH) and remains low in physiological condition) and its production is poorly understood.

2.3. *IDH* mutations are associated with epigenetic reprogramming, altering cancer cells differentiation and DNA

D-2HG and αKG are highly similar molecules, differing only by the presence of a C2 hydroxyl group in D-2HG instead of the C2 carbonyl of αKG. D-2HG can occupy the same binding pocket as α-KG and acts as a weak competitive inhibitor of αKG dependent dioxygenases [29]. αKG as well as Fe2+ are used as cofactors of the activity of more than 60 αKG-dependent dioxygenases which are involved in a wide range of cellular processes such as hypoxia, angiogenesis, maturation of collagens of the extracellular matrix, DNA repair and regulation of epigenetics [30–34]. *In vitro* ectopic expression of IDH1/2 mutants produces high D-2HG levels that affect the activity of αKG-dependent dioxygenases including the DNA repair enzyme ALKBH [35], EGLN prolyl 4-hydroxylases [36], KDM4/JMJD2 and KDM2A/JHDM1A histone demethylases [5,29,37], the methyl-cytosine dioxygenases TET [6,29,38], and the first identified mRNA demethylase Fat mass and obesity-associated protein (FTO) [39,40]. The epigenetic deregulation induced by IDH2-mutant enzymes results in the impairment of key steps in histone, DNA and RNA demethylation and translates into chromatin and RNA hypermethylation. Such wide epigenetic modifications are associated with altered expression of genes involved in cellular differentiation, broad growth-suppressive activity in primary cells, or established cell lines [4,6,10,41,42] as in genetically engineering mouse models [8,9,15,43], thereby resulting in a block to cellular differentiation.

2.4. *IDH2* mutations in hematologic malignancies

IDH2 (R140, R172) mutations are found in myeloid malignancies, i.e. myelodysplastic syndromes (MDS), AML and myeloproliferative neoplasms (MPN) but also in the peripheral T-cell lymphomas AITL [1,2,44–46]. In myeloid malignancies, *IDH2* mutations are considered as an initiating event in 34% of the cases of *IDH2* mutations [47]. However, *IDH2* mutations are likely to be implicated in early stages of *de novo* AML as others are, i.e. *NPM1, DNMT3A, TET2* and *ASXL1* [48]. *IDH* mutations have been more recently associated to clonal hematopoiesis of indeterminate potential (CHIP, also known as age-related clonal hematopoiesis, ARCH; reviewed in [49]), defined as the clonal expansion of hematopoietic stem and progenitor cells carrying somatic mutation in the absence of other diagnostic features of MDS or AML [50,51].

IDH2 mutations (*IDH2 R140Q* and *IDH2 R172K*) are found in 8–19% of de novo AML [3] but in the largest series incidence ranged from 8 to 12% [46]. In *de novo* AML, *IDH2 R140Q* mutation is associated with older age, normal karyotype and *NPM1, SRSF2* and *DNMT3A* mutations [52]. *IDH2 R140Q, TET2* and *WT1* mutations are mutually exclusive [4,35,53]. On the opposite, *IDH2 R172K* and *NPM1* are mutually exclusive [52]. Among *IDH2* mutations, *IDH2 R140Q* mutation is the most frequent (75–80%) and *IDH2 R172K* mutation is found in 20–25% of the cases. Prognostic significance of each *IDH* 2 specific mutation analyzed with co-occurring mutations treated with intensive chemotherapy (IC) remains inconsistent. The prognostic impact of these mutations differs, depending of the mutational spectrum. *IDH2 R140Q* mutations has favorable or no impact on overall survival (OS) [1,46,47,54,55]. Among defined AML subgroups, *IDH2 R172K* mutation emerged as a new provisionally entity with a favorable outcome when treated with IC. However, due to the limited number of such AML patients (1%), prognosis of *IDH2 R172K* mutation remains largely unknown and earliest series reported a worse prognosis, with lower complete remission (CR) rates, higher relapse rates and lower OS [52,56,57].

IDH1/2 mutations are found in 4–12% of MDS cases, with a higher incidence (up to 23%) in high risk MDS. They are associated with an older age, *DNMT3A, ASXL1, SRSF2* mutations and higher rates of transformation to AML [46,58–61]. In MPN, the incidence of *IDH1/2* mutations is between 2 and 4%, rising up to 31% at AML transformation. They are associated with older age and *SRSF2* mutations. In patients with myelofibrosis, these mutations confer a worse prognosis [62].

2.5. D2HG as a predictive biomarker in *IDH*-mutant cancers

2HG release in the serum and/or urine by *IDH*-mutant cancer cells is a biomarker of *IDH1/2* mutations, reflecting the neomorphic enzymatic activity of the mutant enzymes. 2HG levels are of interest for both the diagnosis and monitoring of patients with *IDH*-mutant malignancies but are not used in routine clinical practice [17–19,63–72].

At diagnosis, 2HG is a biomarker predictive of the presence of IDH1/2 mutations in AML [69]. High total 2HG concentration is highly predictive of the presence of an *IDH1/2* mutation, although separation of the D and L enantiomers distinguished *IDH*-mutant and *IDH*-wild-type AML [68,69] or intrahepatic cholangiocarcinoma [65,73] with greater specificity. In isolated myeloid sarcomas, a situation in which molecular characterization is not routinely performed due to technical difficulties,

D-2HG elevation is also predictive of the presence of an *IDH1/2* mutation [64].

Prospective evaluation of D-2HG levels during treatment of newly diagnosed AML treated with standard chemotherapy revealed that failure to normalize 2HG levels is associated with treatment failure whereas elevated 2HG levels at CR are associated with poorer outcome suggesting that 2HG is a biomarker predictive of clinical response to intensive chemotherapy in AML patients with IDH1/2 mutations [68,69].

3. Targeting of *IDH2*-mutant tumors

The discovery of *IDH* mutations has resulted in a number of novel therapeutic approaches, that either restore normal IDH function or block production or downstream effects of D-2HG.

3.1. IDH-mutant enzymes inhibitors (preclinical studies)

Preclinical *in vitro* and *in vivo* studies have validated the proof of concept that targeted inhibition of IDH mutants resulted in normalization in a dose dependent manner of 2HG, reversal of histone and DNA hypermethylation and release of cellular differentiation block [7,9,13–16,42]. AGI-6780 is a small-molecule selective inhibitor of mutant *IDH2 R140Q* mutant. They normalized 2HG, reversed histone and DNA hypermethylation and induced differentiation of *IDH2 R140Q*-mutant TF-1 erythroleukemia cells but also of primary human AML cells harboring *IDH2 R140Q* mutation [10,13].

AG-221 (enasidenib) is a specific slow tight binder of the *IDH2 R140Q*-mutant enzyme (Figure 1). It targets selectively mutant/wild-type heterodimers and mutant homodimers over *IDH2*-wild-type homodimers, IDH1-wild-type homodimers and *IDH1 R132H*-mutant enzymes [16]. AG-221 allosterically stabilizes the open homodimer conformation, preventing the conformational change required for catalysis. Importantly, AG-221 displayed higher potency against R140Q versus R172K (Yen et al., 2017). Therefore, AG-221 induced 99% reduction in intracellular 2HG in R140Q at low concentrations (1 μM) whereas R172K required high concentrations (5 μM) to achieve 99% reduction relative to vehicle-treated controls [74]. AG-221 induced cellular differentiation in primary human *IDH2*-mutant AML cells treated *ex vivo* and in patient-derived xenograft (PDX) mouse models [14,74]. Importantly, these differentiated cells were functional; *IDH2 R140Q*-mutant neutrophils obtained from primary *IDH2 R140Q*-mutant blasts treated *ex vivo* with enasidenib demonstrated intact phagocytic activity, and exhibited granules colocalizing with lactoferrin, a canonical marker of secondary and tertiary granules of mature neutrophils [63,74]. AG-221 also provided a statistically significant survival benefit in an aggressive *IDH2 R140Q*-mutant AML xenograft mouse model [74].

3.2. CLINICAL EFFICACY: FDA approved mutant IDH2 enzyme inhibitor

3.2.1. AG-221/CC90007 (enasidenib)

was approved due to high response rates, durability of the responses that translated into an impressive OS in a heavily pretreated population. Furthermore, the safety profile of the drug is very favorable and the maximum tolerated dose in the phase 1/2 study (NCT01915498) has not been reached at daily doses up to 650 mg. The recommended dose is 100 mg daily in continuous 28-day cycles because above 100 mg per day neither 2HG suppression nor response rates were improved.

3.2.2. High response rates

In the phase 1/2 study, among 214 patients with mutant-*IDH2* relapsed/refractory (R/R) AML (median age: 68 years) who received 100 mg per day, 42 patients (19.6%) attained CR, overall response rate (ORR) was 38.8% (95% CI, 32.2–45.7). As epigenetic therapy, enasidenib acts slowly and median time to first response was 1.9 months (range, 0.5–9.4), and median time to best response was 3.7 months (0.6–14.7). Thus, in the absence of early response (before 90 days), patients must be kept on drug (probably until overt progression). Furthermore, even in the absence of significant marrow blast reduction, a subset of patients may benefit from enasidenib as they became transfusion independent or/and produced neutrophils [17,18].

Enasidenib was not cytotoxic, restored normal myeloid progenitor function but do not induce molecular remission in most of responders. Terminally differentiated cells retained

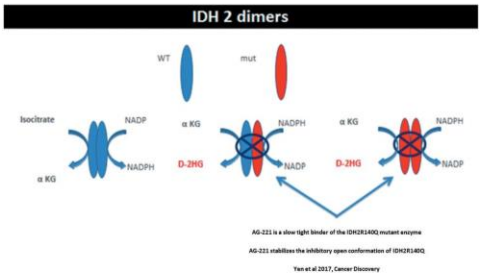

Figure 1. Mechanism of action of enasidenib AG-221 (enasidenib) is a specific slow tight binder of the IDH2 R140Q-mutant enzyme It targets selectively mutant/wild-type heterodimers and mutant homodimers over IDH2-wild-type homodimers, IDH1-wild-type homodimers and IDH1 R132H-mutant enzymes. AG-221 allosterically stabilizes the open homodimer conformation, preventing the conformational change required for catalysis. AG-221 induced 99% reduction in intracellular 2HG in R140Q even at low concentrations.

the *IDH2* mutation and are fully functional (at least neutrophils). In a minority of patients, enasidenib therapy induced molecular remission associated with restoration of wild-type terminal blood cell production and progenitor function from wild-type cells [63,75]. As expected, patients with *IDH2 R140* mutations showed significantly greater maximum 2HG reductions from baseline (median, −92.9%) compared with *IDH2 R172* patients (median, −47.4%) (P = .0004) [18,63]. In *IDH2 R172* patients, quantitation of enasidenib and its active metabolite, AGI-16,903 could be of interest to optimize enasidenib administration [76]. However, there was no significant difference in ORR between R/R AML patients with *IDH2 R140* mutations (35.8%; 95% CI, 28.4–43.7) or *IDH2 R172* mutations (47.1%; 95% CI, 32.9–61.5) (P= .187). In patients with *IDH2 R140* AML, 2HG was normalized in almost all cases and cannot act as a surrogate marker of efficacy. On the opposite, the magnitude of 2HG reduction on-study was associated with CR in patients with *IDH2 R172* AML [18]. Clearance of mutant *IDH2* clones was associated with achievement of CR [18]. Mapping of the clonal structure in leukemic cell population before therapy and during the course of treatment, evidenced that enasidenib promoted hematopoietic differentiation from AML clones showing variable differentiation arrest (i.e. progenitor-like or precursor-like stage); less frequently, treatment promoted differentiation of nonmutant cells [75,77]. Failure to achieve a response correlated with number (higher mutational burden) and nature of co-existing mutations, notably with mutations in genes related to the RNA splicing and the receptors/kinases/signaling (in particular FLT3 ITD or TKD) functional categories (P = .007 and .005, respectively) [18,63].

3.2.3. The responses are durable

Median number of enasidenib treatment cycles was 5.0 (range, 1–38). Median OS among 214 R/R AML patients who received 100 mg per day was also 8.8 months (95% CI, 7.7–9.6). Median event-free survival (EFS) was 4.7 months (95% CI, 3.7–5.6). Estimated median OS was 22.9 months in 42 R/R AML patients who achieved CR, 10.6 months for patients who achieved a non-CR response, and 5.6 months for nonresponders. Interestingly, median OS differed significantly between patients who had received 1, 2, or ≥3 prior AML treatments before study entry, 11.8 months (95% CI, 8.3–15.4), 7.8 months (95% CI, 5.8–9.1), and 7.0 months (95% CI, 4.9–8.8), respectively (P = .001) [18]. Mutant *IDH2* molecular remission, assessed by digital PCR, was seen in 12% of the responders but there was no significant survival difference between these patients and patients in morphologic CR with detectable mutant *IDH2*. In order to further demonstrate the efficacy of enasidenib, a phase 3 randomized trial is ongoing, comparing best supportive care, 5-azacytidine (5-AZA), or low- or intermediate-dose cytarabine in the R/R AML (> 60 years) with enasidenib alone.

In the phase 1/2 dose escalation study, frontline treatment with enasidenib alone has been assessed in 37 previously untreated elderly patients. Median age was 77 years (range 58–87); 62% of patients were aged ≥ 75 years. ORR was 37.8% (95%CI 22.5, 55.2) with 19% achieving CR. The median duration of CR was not reached (NR) (95%CI 3.7, NR) and median duration of any response was 12.2 months (2.9, NR). Median OS for responders and non-responders was 19.8 months and 5.4 months, respectively.

3.2.4. Relapse of responders *IDH2*-mutant patients on enasidenib

In most patients, 2HG remained suppressed at relapse, demonstrating that enasidenib remained on target. Therefore, relapsed clones were not dependent on mutant *IDH2*. Various patterns of clonal evolution/selection with acquisition of recurrent AML-associated genetic changes (new cytogenetic alterations along with new gene mutations) were seen in the context [75]. In several cases, 2HG elevation at relapse was associated with the appearance of *IDH1* mutations (subclones or in the same ancestral clone) [75,78] or a second-site mutation on the wild-type *IDH2* allele that can prevent binding of enasidenib [79].

3.2.5. A favorable safety profile

Importantly, enasidenib was very well tolerated (up to 650 mg per day). The most frequent treatment emergent adverse events (TEAEs) (any grade) occurring in ≥5% of patients [18] included hyperbilirubinemia (33%), nausea (28%), decreased appetite (19%), vomiting (17%), diarrhea (15%), fatigue (14%), IDH differentiation syndrome (16%), dysgeusia (10%), AST increased (9%), dyspnea (9%), leukocytosis (8%), anemia (7%), ALT increased (7%), rash (6%), and hyperuricemia (6%). The most frequent enasidenib-related grade 3 or 4 treatment-emergent adverse events were hyperbilirubinemia (10.4%), thrombocytopenia (6.7%), IDH differentiation syndrome (6.4%), and anemia (5.5%).

3.2.6. Hyperbilirubinemia

Enasidenib is known to inhibit UDP glucuronosyltransferase 1A1 (UGT1A1), and induced elevation of unconjugated bilirubin (up to 83% of the treated patients) [17,18] as in Gilbert's disease but with no serious consequences.

3.2.7. Differentiation syndrome (DS)

DS is a life-threatening complication of uncertain pathogenesis that can occur during the treatment of acute promyelocytic leukemia (APL) by ATRA and/or arsenic trioxide (ATO). In the absence of biological diagnostic criteria of DS, diagnosis of DS was made on clinical grounds. Signs were generally associated with increasing white blood cell (WBC) count and combined fever, weight gain, dyspnea, pleural effusion, and pulmonary infiltrates on chest radiograph and, in some patients, renal failure, hypotension, and pericardial effusion [80–84]. Pathophysiology is still elusive but is related to the process of blasts differentiation induced by ATO and/or ATRA. In CR no DS in APL has been described so far. Increased production of inflammatory cytokines, chemokines and expression of adhesion molecules on APL cells induced organ infiltration by differentiating cells (especially in the lung) and capillary-leak syndrome. Intensity of signs varied greatly, ranging from moderate pleural effusion discovered on chest x-ray film to major respiratory distress requiring mechanical ventilation.

It's prompt recognition and treatment with dexamethasone 10 mg twice daily until resolution of the DS rapidly ameliorate the picture. Discontinuation of ATRA is required and efficient (due to the short half-life of ATRA) in case of rapidly worsening situation

and/or severe presentation [84]. As differentiating agent, enasidenib was susceptible to induce DS and an independent differentiation syndrome review committee (DSRC) retrospectively reviewed possible cases of mutant-*IDH* inhibitor–associated DS (termed *IDH differentiation syndrome* [IDH-DS]). Among 281 patients enrolled in the phase 1/2 study at the time of the DSRC assessment, 11.7% of patients were identified as having experienced possible or probable DS. The most frequent clinical manifestations of IDH-DS were dyspnea, culture-negative fever, pulmonary infiltrates, hypoxia, renal failure and pleural effusion (Fathi et al., 2018). Median onset of enasidenib-induced DS was 30 days. As in APL, dexamethasone 10 mg twice daily was started in 85% of the cases and enasidenib was stopped in 45% of the cases. Hyperleukocytosis, was treated with hydroxyurea. At first suspicion of IDH-DS, dexamethasone, 10 mg twice daily, is recommended until signs and symptoms are significantly improved. If associated with severe pulmonary symptoms and/or renal dysfunction lasting more than 48 hours after corticosteroid treatment initiation, IVOSIDENIB therapy should be withheld until symptoms improve. Symptoms may not resolve immediately. Given the prolonged half-life of ENASIDENIB (137 hours), drug treatment interruption is not an alternative to corticosteroid use [85].

3.2.8. Leukocytosis

Leukocytosis occurred in 8% and can be related to disease progression but also due to enasidenib. Indeed, preclinical model demonstrated that *IDH2* mutants had proliferation upon drug exposure [13,74].

3.2.9. Tumor lysis syndrome (TLS)

Enasidenib based was associated with TLS 6% of the cases along with rising WBC counts. They can be lifethreatening (grade 3 or more) including a fatal case but enasidenib do not appear to induce TLS relative to similar R/R AML patients [18].

4. Frontline studies alone and in combination

4.1. Enasidenib alone in newly diagnosed mutant-*IDH2* AML and patients with mutant IDH2 MDS

In the phase 1/2 study (NCT01915498) older adults with newly diagnosed mutant-*IDH2* AML not candidates for cytotoxic regimens were also eligible to receive enasidenib. Among 39 patients with newly diagnosed mutant-*IDH2* AML (median age: 77 years), one patient received enasidenib 50 mg once daily, 29 patients received 100 mg per day and 9 patients received more than 100 mg per day. Median number of enasidenib treatment cycles was 6.0 (range 1–35). Seven patients (18%) attained CR, overall response rate (ORR) was 30.8% (95% CI, 17–45.6). As in R/R mutant-*IDH2* AML patients, median time to first response was 1.9 months, and median time to best response was 3.7 months. Median OS for all patients was 11.3 months (95% CI 5.7, 15.1), and was NR for responders. The favorable safety profile of enasidenib fitted for frailty of the population [86].

In the same phase 1/2 study (NCT01915498), 17 patients with R/R mutant *IDH2* MDS or who were not eligible for standard treatment received oral doses of enasidenib at 60–300 mg per day in repeated 28-day treatment cycles. An overall response was achieved in 9 patients (53%). Interestingly, among 13 patients who had received prior hypomethylating agent therapy, 6 (46%) responded. Median overall survival was 16.9 months (95% CI 1.5–32.3), and median event-free survival was 11.0 months (1.5–16.7). Median duration of response of 9.2 months (95% CI 1.0–not reached) [87].

4.2. In combination with intensive treatment

In an open-label, multicenter, phase 1 study (NCT02632708), eligible patients with newly diagnosed mutant-*IDH1* or mutant-*IDH2* AML are treated with induction therapy (daunorubicin 60 mg/m^2/day or idarubicin 12 mg/m^2/day × 3 days with cytarabine 200 mg/m^2/day × 7 days) in combination with either ivosidenib 500 mg once daily (for mutant-*IDH1*) or enasidenib 100 mg once daily (for mutant-*IDH2*). After induction, patients may receive ≤4 cycles of consolidation therapy while continuing the mutant *IDH* inhibitor. 134 patients had been treated: 47 with ivosidenib (median age 63 years, range 24–76) and 87 with enasidenib (median age 63 years, range 27–77). Secondary AML was present in 38% patients with mutant-*IDH2*. Among the 77 enasidenib-treated patients evaluable for efficacy, a response of CR, CRi, or complete remission with incomplete platelet recovery (CRp) was achieved in 33/45 (73%) patients with *de novo* AML and in 20/32 (63%) patients with AML. The combination was well tolerated and the most frequent grade ≥3 nonhematologic adverse events were febrile neutropenia (63%), hypertension (11%), colitis (8%), and maculopapular rash (8%) [88].

4.3. In combination with 5-AZA

A phase 1b study combined ivosidenib 500 mg daily (n = 23) or enasidenib 100 mg (n = 3) or 200 mg (n = 3) daily for patients with *IDH1* or *IDH2* mutations with 5-AZA in patients with newly diagnosed AML (NCT02677922). The combination is safe and most AEs were grade 1–2 GI events and ENA-related indirect bilirubin elevations. In the phase 2, patients were randomized in a 2:1 ratio to receive combination therapy with enasidenib (n = 68) or 5-AZA monotherapy (n = 33) in repeated 28-day cycles. Interim results showed significantly higher response rate with combination therapy compared to 5-AZA with overall response rates of 68% vs. 42%, respectively (P = 0.0155) and CR rates were 50% and 12%, respectively (P = 0.0002). However, median OS in the two groups was similar (22.0 months in the enasidenib + 5-AZA group vs. 22.3 months in the 5-AZA monotherapy group (HR 0.99 [95%CI 0.52, 1.87], P = 0.9686). A nonsignificant better median EFS was observed in the ENA + AZA group (17.2 months) vs. 10.8 months in the AZA Only group (HR 0.59 [95%CI 0.30, 1.17], P = 0.1278) [89,90].

5. Conclusions

Enasidenib monotherapy for AML patients with *IDH2* mutations induced high response rates, durability of the responses in a heavily pretreated population. Promising ongoing clinical trials are evaluating combination therapies with enasidenib frontline and included in Table 1.

Table 1. Ongoing trials incorporating enasidenib in AML/MDS.

NCT number	Phase	Disease	Treatment	Status
04203316	2	R/R AML pediatric patients	Enasidenib	Recruiting
03744390	1	R/R MDS, untreated MDS	Enasidenib ± AZA	Recruiting
03683433	2	R/R AML	Enasidenib +AZA	Recruiting
03383575	2	AML, HR MDS, CMML	Enasidenib + AZA	Recruiting
04092179	1	R/R AML	Enasidenib + venetoclax	not recruiting
03825796	1	R/R AML	Enasidenib + CPX-351	Recruiting
04075747	1	Untreated AML	Enasidenib + CPX-351	Recruiting
03839771	3	Untreated AML/EB2 MDS	Enasidenib vs. placebo + chemotherapy	Recruiting
03173248	3	Untreated AML (unfit)	Enasidenib vs. placebo + AZA with maintenance	Recruiting
03515512	1	AML	Maintenance post ACST	Recruiting
03728335	1	AM	Maintenance post ACST	Recruiting

6. Expert opinion

The discovery of *IDH2* mutations highlights the unique role of the 'oncometabolite' 2-HG in oncogenesis. Depending on associated genomic aberrations and the cellular context, the oncogenic potential of *IDH2* mutations range from an initiating event – promoting transformation – to a secondary oncogenic event conferring selective advantage to cancer cells. The druggable gain of function of the mutant enzymes led to the generation of a new class of drugs. The restoration of differentiation by inhibition of mutant IDH2 came from mutant clones and rarely from wild type progenitor cells, further demonstrating that Enasidenib is a true differentiating agent. Relevant preclinical models, and more importantly results of clinical trials in adults demonstrate that targeting IDH2 mutant enzymes is a valid strategy. The safety profile of the drug is very favorable and Enasidenib induces high response rate and durable responses. However, even in responders, most R/R AML patients treated with Enasidenib as single agent relapsed suggesting that enasidenib should be started upfront and in combination with current available therapies. Combination therapies suggest synergistic effect and are inducing high response rates that might translate into a significant improvement in EFS and possibly in OS.

Declaration of interest

Stephane de Botton declares consulting for and research funding from AGIOS; consulting for and a member of the speakers bureau of CELGENE; consulting for PIERRE FABRE; consulting for SERVIER; consulting for PFIZER; consulting for NOVARTIS; consulting for JANSSEN; consulting and researching funding from FORMA; consulting for SYROS; consulting for BAYER; consulting for ABBVIE; consulting for DAIICHI; consulting for ASTELLAS. The authors have no other relevant affiliations or financial involvement with any organization or entity with a financial interest in or financial conflict with the subject matter or materials discussed in the manuscript apart from those disclosed.

Reviewers disclosure

Peer reviewers on this manuscript have no relevant financial relationships or otherwise to disclose.

ORCID

Mael Heiblig http://orcid.org/0000-0003-1682-8657
Christophe Willekens http://orcid.org/0000-0001-9814-8537

References

Papers of special note have been highlighted as either of interest (•) or of considerable interest (••) to readers.

1. Mardis ER, Ding L, Dooling DJ, et al., Recurring mutations found by sequencing an acute myeloid leukemia genome. N Engl J Med. 2009;361(11):1058–1066.
   • **First detection of an *IDH1* mutation in AML.**
2. Kosmider O, Gelsi-Boyer V, Slama L, et al. Mutations of IDH1 and IDH2 genes in early and accelerated phases of myelodysplastic syndromes and MDS/myeloproliferative neoplasms. Leukemia. 2010. DOI:10.1038/leu.2010.52.
3. Döhner H, Weisdorf DJ, Bloomfield CD. Acute myeloid leukemia. N Engl J Med. 2015;373(12):1136–1152.
   •• **Areference review**
4. Figueroa ME, Abdel-Wahab O, Lu C, et al., Leukemic IDH1 and IDH2 mutations result in a hypermethylation phenotype, disrupt TET2 function, and impair hematopoietic differentiation. Cancer Cell. 2010; 18(6): 553–567.
   • **First demonstration that IDH2 mutations are associated with epigenetic reprogramming and block of differentiation.**
5. Lu C, Ward PS, Kapoor GS, et al., IDH mutation impairs histone demethylation and results in a block to cell differentiation. Nature. 2012;483(7390):474–478.
   • **Further demonstration that IDH2 mutations are associated with epigenetic reprogramming and block of differentiation.**
6. Turcan S, Rohle D, Goenka A, et al. IDH1 mutation is sufficient to establish the glioma hypermethylator phenotype. Nature. 2012. DOI:10.1038/nature10866.
7. Losman JA, Looper RE, Koivunen P, et al. (R)-2-hydroxyglutarate is sufficient to promote leukemogenesis and its effects are reversible. Science. 2013;339(6127):1621–1625.
8. Chen C, Liu Y, Lu C, et al. Cancer-associated IDH2 mutants drive an acute myeloid leukemia that is susceptible to Brd4 inhibition. Genes Dev. 2013. DOI:10.1101/gad.226613.113.
9. Kats LM, Reschke M, Taulli R, et al. Proto-oncogenic role of mutant IDH2 in leukemia initiation and maintenance. Cell Stem Cell. 2014. DOI:10.1016/j.stem.2013.12.016.
10. Kernytsky A, Wang F, Hansen E, et al. IDH2 mutation-induced histone and DNA hypermethylation is progressively reversed by small-molecule inhibition. Blood. 2015. DOI:10.1182/blood-2013-10-533604.
11. Fu X, Chin RM, Vergnes L, et al. 2-hydroxyglutarate inhibits ATP synthase and mTOR signaling. Cell Metab. 2015. DOI:10.1016/j.cmet.2015.06.009.
12. Chan SM, Thomas D, Corces-Zimmerman MR, et al. Isocitrate dehydrogenase 1 and 2 mutations induce BCL-2 dependence in acute myeloid leukemia. Nat Med. 2015. DOI:10.1038/nm.3788.
13. Wang F, Travins J, DeLaBarre B, et al., Targeted inhibition of mutant IDH2 in leukemia cells induces cellular differentiation. Science. 2013;340(80): 622–626.
   •• **First description of the mechanism of action of targeted inhibition of mutant IDH2.**
14. Kats LM, Vervoort SJ, Cole R, et al. A pharmacogenomic approach validates AG-221 as an effective and on-target therapy in IDH2 mutant AML. Leukemia. 2017;31(6):1466–1470.

15. Shih AH, Meydan C, Shank K, et al. Combination targeted therapy to disrupt aberrant oncogenic signaling and reverse epigenetic dysfunction in IDH2 and TET2 -mutant acute myeloid leukemia. Cancer Discov. 2017. DOI:10.1158/2159-8290.CD-16-1049.
16. Yen K, Travins J, Wang F, et al., AG-221, a First-in-class therapy targeting acute myeloid leukemia harboring oncogenic IDH2 mutations. Cancer Discov. 2017; 7(5): 478–493
•• **First description of the mechanism of action of ENASIDENIB.**
17. Stein EM, DiNardo CD, Pollyea DA, et al., Enasidenib in mutant IDH2 relapsed or refractory acute myeloid leukemia. Blood. 2017; 130(6): 722–731.
•• **First description of clinical efficacy of ENASIDENIB.**
18. Stein EM, DiNardo CD, Fathi AT, et al., Molecular remission and response patterns in patients with mutant-IDH2 acute myeloid leukemia treated with enasidenib. Blood. 2019; 133(7): 676–687.
•• **Final analyses of clinical efficacy of ENASIDENIB.**
19. DiNardo CD, Stein EM, De Botton S, et al., Durable remissions with ivosidenib in IDH1 -mutated relapsed or refractory AML. N Engl J Med. 2018; 378(25): 2386–2398.
•• **First description of clinical efficacy of IVOSIDENIB.**
20. Yen KE, Bittinger MA, Su SM, et al. Cancer-associated IDH mutations: biomarker and therapeutic opportunities. Oncogene. 2010;29 (49):6409–6417.
21. Cairns RA, Mak TW. Oncogenic isocitrate dehydrogenase mutations: mechanisms, models, and clinical opportunities. Cancer Discov. 2013;3(7):730–741.
22. Reitman ZJ, Yan H. Isocitrate dehydrogenase 1 and 2 mutations in cancer: alterations at a crossroads of cellular metabolism. J Natl Cancer Inst. 2010;102(13):932–941.
23. Dang L, Su -S-SM. Isocitrate dehydrogenase mutation and (R)-2-hydroxyglutarate: from basic discovery to therapeutics development. Annu Rev Biochem. 2017. DOI:10.1146/annurev-biochem-061516-044732
24. Lee SM, Koh HJ, Park DC, et al. Cytosolic NADP+-dependent isocitrate dehydrogenase status modulates oxidative damage to cells. Free Radic Biol Med. 2002. DOI:10.1016/S0891-5849(02)00815-8.
25. Paschka P, Schlenk RF, Gaidzik VI, et al. IDH1 and IDH2 mutations are frequent genetic alterations in acute myeloid leukemia and confer adverse prognosis in cytogenetically normal acute myeloid leukemia with NPM1 mutation without FLT3 internal tandem duplication. J Clin Oncol. 2010. DOI:10.1200/JCO.2010.28.3762.
26. Dang L, White DW, Gross S, et al., Cancer-associated IDH1 mutations produce 2-hydroxyglutarate. Nature. 2009;462(7274):739–744.
•• **First description of neomorphic activity of IDH mutants and 2HG production.**
27. Gross S, Cairns RA, Minden MD, et al. Cancer-associated metabolite 2-hydroxyglutarate accumulates in acute myelogenous leukemia with isocitrate dehydrogenase 1 and 2 mutations. J Exp Med. 2010. DOI:10.1084/jem.20092506.
28. Ward PS, Patel J, Wise DR, et al., The common feature of leukemia-associated IDH1 and IDH2 mutations is a neomorphic enzyme activity converting α-ketoglutarate to 2-hydroxyglutarate. Cancer Cell. 2010; 17(3): 225–234.
•• **First description of neomorphic activity of IDH mutants.**
29. Xu W, Yang H, Liu Y, et al., Oncometabolite 2-hydroxyglutarate is a competitive inhibitor of α-ketoglutarate-dependent dioxygenases. Cancer Cell. 2011;19(1):17–30.
•• **First description of neomorphic activity of IDH mutants leading to α-ketoglutarate-dependent dioxygenases inhibition.**
30. Loenarz C, Schofield CJ. Expanding chemical biology of 2-oxoglutarate oxygenases. Nat Chem Biol. 2008;4(3):152–156.
31. Tsukada YI, Fang J, Erdjument-Bromage H, et al. Histone demethylation by a family of JmjC domain-containing proteins. Nature. 2006;439(7078):811–816.
32. Kohli RM, Zhang Y. TET enzymes, TDG and the dynamics of DNA demethylation. Nature. 2013;502(7472):472–479.
33. demethylation and transcription. Nat Rev Mol Cell Biol. 2013.
34. Rasmussen KD, Helin K. Role of TET enzymes in DNA methylation, development, and cancer. Genes Dev. 2016;30(7):733–750.
35. Wang Y, Xiao M, Chen X, et al. WT1 recruits TET2 to regulate its target gene expression and suppress leukemia cell proliferation. Mol Cell. 2015 Feb 19;57(4):662–673.
36. Koivunen P, Lee S, Duncan CG, et al. Transformation by the (R)-enantiomer of 2-hydroxyglutarate linked to EGLN activation. Nature. 2012. DOI:10.1038/nature10898.
37. Chowdhury R, Yeoh KK, Tian YM, et al. The oncometabolite 2-hydroxyglutarate inhibits histone lysine demethylases. EMBO Rep. 2011. DOI:10.1038/embor.2011.43.
38. Figueroa ME, Abdel-Wahab O, Lu C, et al. Leukemic IDH1 and IDH2 mutations result in a hypermethylation phenotype, disrupt TET2 function, and impair hematopoietic differentiation. Cancer Cell. 2010. DOI:10.1016/j.ccr.2010.11.015.
39. Elkashef SM, Lin AP, Myers J, et al. IDH mutation, competitive inhibition of FTO, and RNA methylation. Cancer Cell. 2017;31(5):619–620.
40. Su R, Dong L, Li C, et al. R-2HG exhibits anti-tumor activity by targeting FTO/m6A/MYC/CEBPA signaling. Cell. 2018. DOI:10.1016/j.cell.2017.11.031.
41. Lu C, Venneti S, Akalin A, et al. Induction of sarcomas by mutant IDH2. Genes Dev. 2013. DOI:10.1101/gad.226753.113.
42. Rohle D, Popovici-Muller J, Palaskas N, et al. An inhibitor of mutant IDH1 delays growth and promotes differentiation of glioma cells. Science. 2013(80). DOI:10.1126/science.1236062.
43. Chaturvedi A, Araujo Cruz MM, Jyotsana N, et al. Mutant IDH1 promotes leukemogenesis in vivo and can be specifically targeted in human AML. Blood. 2013. DOI:10.1182/blood-2013-03-491571.
44. Cairns RA, Iqbal J, Lemonnier F, et al. IDH2 mutations are frequent in angioimmunoblastic T-cell lymphoma. Blood. 2012. DOI:10.1182/blood-2011-11-391748.
45. Marcucci G, Maharry K, Wu YZ, et al. IDH1 and IDH2 gene mutations identify novel molecular subsets within de novo cytogenetically normal acute myeloid leukemia: A cancer and leukemia group B study. J Clin Oncol. 2010. DOI:10.1200/JCO.2009.27.3730.
46. Im AP, Sehgal AR, Carroll MP, et al. DNMT3A and IDH mutations in acute myeloid leukemia and other myeloid malignancies: associations with prognosis and potential treatment strategies. Leukemia. 2014;28(9):1774–1783.
47. Molenaar RJ, Thota S, Nagata Y, et al., Clinical and biological implications of ancestral and non-ancestral IDH1 and IDH2 mutations in myeloid neoplasms. Leukemia. 2015; 29(11): 2134–2142.
• **to better refine the role of *IDH* mutations in leukemogenesis.**
48. Welch JS, Ley TJ, Link DC, et al. The origin and evolution of mutations in acute myeloid leukemia. Cell. 2012. DOI:10.1016/j.cell.2012.06.023.
49. Shlush LI. Age-related clonal hematopoiesis. Blood. 2018;131 (5):496–504.
50. Shlush LI, Zandi S, Mitchell A, et al. Identification of pre-leukaemic haematopoietic stem cells in acute leukaemia. Nature. 2014 Feb 20;506(7488):328–333.
51. Desai P, Mencia-Trinchant N, Savenkov O, et al. Somatic mutations precede acute myeloid leukemia years before diagnosis. Nat Med. 2018. DOI:10.1038/s41591-018-0081-z.
52. Papaemmanuil E, Gerstung M, Bullinger L, et al. Genomic classification and prognosis in acute myeloid leukemia. N Engl J Med. 2016. DOI:10.1056/NEJMoa1516192.
53. Rampal R, Alkalin A, Madzo J, et al. DNA hydroxymethylation profiling reveals that WT1 mutations result in loss of TET2 function in acute myeloid leukemia. Cell Rep. 2014. DOI:10.1016/j.celrep.2014.11.004.
54. Patel JP, Gönen M, Figueroa ME, et al. Prognostic relevance of integrated genetic profiling in acute myeloid leukemia. N Engl J Med. 2012. DOI:10.1056/NEJMoa1112304.
55. Abdel-Wahab O, Patel J, Levine RL. Clinical Implications of novel mutations in epigenetic modifiers in AML. Hematol Oncol Clin North Am. 2011;25(6):1119–1133.
56. Boissel N, Nibourel O, Renneville A, et al. Differential prognosis impact of IDH2 mutations in cytogenetically normal acute myeloid leukemia. Blood. 2011;117(13):3696–3697.
57. Green CL, Evans CM, Zhao L, et al. The prognostic significance of IDH2 mutations in AML depends on the location of the mutation. Blood. 2011. DOI:10.1182/blood-2010-12-322479.

58. Thol F, Damm F, Wagner K, et al. Prognostic impact of IDH2 mutations in cytogenetically normal acute myeloid leukemia. Blood. 2010. DOI:10.1182/blood-2010-03-272146.
59. Patnaik MM, Hanson CA, Hodnefield JM, et al. Differential prognostic effect of IDH1 versus IDH2 mutations in myelodysplastic syndromes: A mayo clinic study of 277 patients. Leukemia. 2012. DOI:10.1038/leu.2011.298.
60. Heiblig M, Elhamri M, Nicolini FE, et al. Effect of initial body mass index on survival outcome of patients with acute leukemia: a single-center retrospective study. Clin Lymphoma Myeloma Leuk. 2015;15.
61. Lin CC, Hou HA, Chou WC, et al. IDH mutations are closely associated with mutations of DNMT3A, ASXL1 and SRSF2 in patients with myelodysplastic syndromes and are stable during disease evolution. Am J Hematol. 2014. DOI:10.1002/ajh.23596.
62. Lasho TL, Jimma T, Finke CM, et al. SRSF2 mutations in primary myelofibrosis: significant clustering with IDH mutations and independent association with inferior overall and leukemia-free survival. Blood. 2012. DOI:10.1182/blood-2012-05-429696.
63. Amatangelo MD, Quek L, Shih A, et al. Enasidenib induces acute myeloid leukemia cell differentiation to promote clinical response. Blood. 2017. DOI:10.1182/blood-2017-04-779447.
64. Willekens C, Renneville A, Broutin S, et al. Mutational profiling of isolated myeloid sarcomas and utility of serum 2HG as biomarker of IDH1/2 mutations. Leukemia. 2018. DOI:10.1038/s41375-018-0056-6.
65. Delahousse J, Verlingue L, Broutin S, et al. Circulating oncometabolite D-2-hydroxyglutarate enantiomer is a surrogate marker of isocitrate dehydrogenase–mutated intrahepatic cholangiocarcinomas. Eur J Cancer. 2018;90:83–91.
66. Fathi AT, Sadrzadeh H, Borger DR, et al. Prospective serial evaluation of 2-hydroxyglutarate, during treatment of newly diagnosed acute myeloid leukemia, to assess disease activity and therapeutic response. Blood. 2012. DOI:10.1182/blood-2012-06-438267.
67. Pollyea DA, Kohrt HE, Zhang B, et al. 2-Hydroxyglutarate in IDH mutant acute myeloid leukemia: predicting patient responses, minimal residual disease and correlations with methylcytosine and hydroxymethylcytosine levels. Leuk Lymphoma. 2013;54(2):408–410.
68. DiNardo CD, Propert KJ, Loren AW, et al. Serum 2-hydroxyglutarate levels predict isocitrate dehydrogenase mutations and clinical outcome in acute myeloid leukemia. Blood. 2013. DOI:10.1182/blood-2013-03-493197.
69. Janin M, Mylonas E, Saada V, et al., Serum 2-hydroxyglutarate production in IDH1 and IDH2 -mutated de novo acute myeloid leukemia: a study by the acute leukemia french association group. J Clin Oncol. 2014; 32(4): 297–305.
•• **Descrription of serum 2-HG as a robust biomarker.**
70. Borger DR, Goyal L, Yau T, et al. Circulating oncometabolite 2-hydroxyglutarate is a potential surrogate biomarker in patients with isocitrate dehydrogenase-mutant intrahepatic cholangiocarcinoma. Clin Cancer Res. 2014. DOI:10.1158/1078-0432.CCR-13-2649.
71. Brunner AM, Neuberg DS, Wander SA, et al. Use of 2HG levels in the serum, urine, or bone marrow to predict IDH mutations in adults with acute myeloid leukemia. Blood. 2015. DOI:10.1182/blood.V126.23.2597.2597.
72. Lemonnier F, Cairns RA, Inoue S, et al. The IDH2 R172K mutation associated with angioimmunoblastic T-cell lymphoma produces 2HG in T cells and impacts lymphoid development. Proc Natl Acad Sci USA. 2016. DOI:10.1073/pnas.1617929114.
73. Poinsignon V, Mercier L, Nakabayashi K, et al. Quantitation of isocitrate dehydrogenase (IDH)-induced D and L enantiomers of 2-hydroxyglutaric acid in biological fluids by a fully validated liquid tandem mass spectrometry method, suitable for clinical applications. J Chromatogr B Anal Technol Biomed Life Sci. 2016. DOI:10.1016/j.jchromb.2016.04.030.
74. Yen K, Travins J, Wang F, et al. AG-221, a first-in-class therapy targeting acute myeloid leukemia harboring oncogenic IDH2 mutations. Cancer Discov. 2017;7(5):478–493.
75. Quek L, David MD, Kennedy A, et al., Clonal heterogeneity of acute myeloid leukemia treated with the IDH2 inhibitor enasidenib. Nat Med. 2018; 24(8): 1167–1177.
• • **First detailed description of acquired resistance to enasidenib inhibition.**
76. Dittakavi S, Jat RK, Mullangi R. Quantitative analysis of enasidenib in dried blood spots of mouse blood using an increased-sensitivity LC–MS/MS method: application to a pharmacokinetic study. Biomed Chromatogr. 2019. DOI:10.1002/bmc.4491
77. Dutta R, Zhang TY, Köhnke T, et al. Enasidenib drives human erythroid differentiation independently of isocitrate dehydrogenase 2. J Clin Invest. 2020 Apr 1;130(4):1843–1849. DOI:10.1172/JCI133344.
78. Harding JJ, Lowery MA, Shih AH, et al. Isoform switching as a mechanism of acquired resistance to mutant isocitrate dehydrogenase inhibition. Cancer Discov. 2018. DOI:10.1158/2159-8290.CD-18-0877.
79. Intlekofer AM, Shih AH, Wang B, et al., Acquired resistance to IDH inhibition through trans or cis dimer-interface mutations. Nature. 2018; 559(7712): 125–129.
• • **First description of acquired resistance to IDH inhibition through trans or cis dimer-interface mutations.**
80. Frankel SR, Eardley A, Lauwers G, et al. The "retinoic acid syndrome" in acute promyelocytic leukemia. Ann Intern Med. 1992. DOI:10.7326/0003-4819-117-4-292
•• **first descrition of ATRA syndrome.**
81. De Botton S, Dombret H, Sanz M, et al. Incidence, clinical features, and outcome of all trans-retinoic acid syndrome in 413 cases of newly diagnosed acute promyelocytic leukemia. Blood. 1998. DOI:10.1182/blood.V92.8.2712.
82. Tallman MS, Andersen JW, Schiffer CA, et al. Clinical description of 44 patients with acute promyelocytic leukemia who developed the retinoic acid syndrome. Blood. 2000 Jan 1;95(1):90–95.
83. Camacho LH, Soignet SL, Chanel S, et al. Leukocytosis and the retinoic acid syndrome in patients with acute promyelocytic leukemia treated with arsenic trioxide. J Clin Oncol. 2000. DOI:10.1200/JCO.2000.18.13.2620.
84. Montesinos P, Sanz MA. The differentiation syndrome in patients with acute promyelocytic leukemia: experience of the pethema group and review of the literature. Mediterr. J Hematol Infect Dis. 2011;3(1):e2011059.
85. Fathi AT, DiNardo CD, Kline I, et al., Differentiation syndrome associated with enasidenib, a selective inhibitor of mutant isocitrate dehydrogenase 2 analysis of a phase 1/2 study. JAMA Oncol. 2018; 4(8): 1106.
• • **First description of the Differentiation syndrome in AML patients with mutant IDH2 treated with Enasidenib.**
86. Pollyea DA, Tallman MS, de Botton S, et al., Enasidenib, an inhibitor of mutant IDH2 proteins, induces durable remissions in older patients with newly diagnosed acute myeloid leukemia. Leukemia. 2019; 33(11): 2575–2584.
• • **First description of the efficacy of Enasidenib in patients with mutant IDH2 and newly diagnosed acute myeloid leukemia.**
87. Stein EM, Fathi AT, DiNardo CD, et al., Enasidenib in patients with mutant IDH2 myelodysplastic syndromes: a phase 1 subgroup analysis of the multicentre, AG221-C-001 trial. Lancet Haematol. 2020; 7(4): e309-e319.
• **First description of the efficacy of Enasidenib in patients with mutant IDH2 myelodysplastic syndromes.**
88. Stein EM, DiNardo CD, Fathi AT, et al. Ivosidenib or enasidenib combined with induction and consolidation chemotherapy in patients with newly diagnosed AML with an IDH1 or IDH2 mutation is safe, effective, and leads to MRD-negative complete remissions. Blood. 2018. DOI:10.1182/blood-2018-99-110449.
89. DiNardo CD, Schuh AC, Stein EM, et al. Enasidenib plus azacitidine significantly improves complete remission and overall response compared with azacitidine alone in patients with newly diagnosed acute myeloid leukemia (AML) with isocitrate dehydrogenase 2 (IDH2) mutations: interim phase Ii res. Blood. 2019. DOI:10.1182/blood-2019-130362.
90. Dinardo CD, Stein AS, Stein EM, et al. Mutant IDH (mIDH) inhibitors, ivosidenib or enasidenib, with azacitidine (AZA) in patients with acute myeloid leukemia (AML). J Clin Oncol. 2018;36 (15_suppl):7042.